Permeation studies of hydrogen, deuterium and helium in aluminium, gold molybdenum and silver: the influence of phase boundary processes

Thesis

PERMEATION STUDIES OF HYDROGEN, DEUTERIUM AND HELIUM IN ALUMINIUM, GOLD, MOLYBDENUM AND SILVER: THE INFLUENCE OF PHASE BOUNDARY PROCESSES

A Thesis submitted for the degree of

Doctor of Philosophy of

The Open University

By

ESER FARAJ, B.A. (Oxon).

Oxford Research Unit

The Open University

September, 1981

Author's number: HDF 6681

Date of submission: 11-8-81

Date of award: 5-10-81

CONTENTS

LIST OF FIGURES

ACKNOWLEDGEMENTS

Thanks are due to:

The Science Research Council and the Open University for providing finance to keep both myself and my equipment in running order.

My colleques at the O.R.U., especially:

Derek Cummings and his philosophy of "PANIC!" in the face of flopping discs, Bob Reuben for his unquantifiable comradeship in times good and bad.

Chui (the exorcism worked).

The Technical Staff: Peter "SuperTech" Finnimore, Ted Beaver and Alan Knight for their potions, remedies, cures and curses.

The Secretarial Staff: Jill Uttley and Rosemary Loving for distracting the slave-driver.

David Blackburn: The slave-driver, who ruled O.K.

without all of whom this project would have been all work and no fun.

Special thanks are due to the typist, Mrs. Naran Gumush, for valour beyond the call of duty in the fourth chapter of this battle.

MR E. FARAJ PhD

To whom it may concern,

This is to certify that I the undersigned have no objection to my thesis being made available to readers or to being photocopied, subject to the discretion of the Librarian.

Eser Faraj.

ABSTRACT

The diffusivity of; hydrogen through aluminium, gold, molybdenum and silver; deuterium through gold, molybdenum and silver; helium through aluminium, gold and silver has been studied by a modified response time method using periodically modulated discharge and ion beam injection at the input surface.

Measurements consisted of the response time of pressure, across a metal membrane, in the detection chamber due to fluctuations at the input. The downstream vacuum chamber was continuously pumped.

The relationship between the time-lag of the downstream pressure relative to the upstream pressure yielded the diffusion coefficient.

The permeability of hydrogen and deuterium through molybdenum and gold were determined from separate time independent measurements of the flux through the membrane.

The relationships for the time-lags and steady rate fluxes were modified when account was taken of the possible importance of surface processes in permeation. The modified relations were found necessary when analysing the data of aluminium and gold.

CHAPTER ONE

INTRODUCTION

This thesis details an experimental study of light gas transmission through metal foils. Three gases and four metals were used. They were hydrogen, deuterium, helium and aluminium, gold, molybdenum and silver. These metals are all d block elements. Aluminium, gold and silver have f.c.c. crystal structure. Molybdenum has b.c.c. crystal structure.

The experimental arrangement separated two vacuum chambers by the experimental foils. Data was gathered on the response time of gas pressure changes in one chamber, caused by periodic changes of conditions in the other chamber. Gas entry to the foils was modulated by control of an electric discharge on one side of the foils, which raised the flow rate into the foils above that due to the simple process of solution.

An artificial method of gas injection was used in this experiment because it was intended to attempt measurement of helium diffusivity in metals. It is well know that helium has effectively zero solubility in metals and must be injected into experimental foils. It was also hoped this method of introducing gas into metals could be used to overcome temperature limits on diffusivity measurement, imposed by hydrogen solubility, especially for those metals with low hydrogen solubility constants e.g, gold.

For the data on the transmission of hydrogen and deuterium through molybdenum and silver, it proved possible to model the gas flow process as limited by diffusion alone and a series of diffusion coefficients were derived. For the other diffusion systems more complex models seem to be required; Work with aluminium showed clear evidence of surface reaction; Despite a sophisticated injection system and an extremely sensitive detector, helium was not shown to pass through any of the experimental foils.

There is a long history of study on the permeation of light gases in metals, spanning about a century and with most interest in hydrogen gas. More recently, interest in this field has been galvanised by the construction and development of conventional nuclear power stations and the design of the new fusion type reactors.

With respect to conventional power plants interest was raised because hydrogen is the best known moderator of thermal neutrons. Hydrogen also has a large solubility in many metals e.g. palladium, niobium, zirconium. Therefore if a hydrogen/metal system with good thermal and chemical stability could be found, it would be of considerable technological use.

With respect to the development of fusion-reactors, interest in the permeation constants for the hydrogen isotopes and helium is more direct. One of the fuel materials in the fusion-reactor is tritium, a gas which has two very unfortunate properties. It is an isotope of hydrogen and it is radioactive. Hydrogen is well known to dissolve and be very mobile in very many materials and the more so the more elevated the temperature. Therefore tritium is likely to leak out of any fusion-reactor system. This is undesirable because tritium is expensive, but more important, tritium can constitute a serious radiological hazard, since hydrogen is an important biological element. For these reasons tritium containment is an important requirement.

A second important requirement is that it is desirable to keep tritium concentrations in constructional materials as low as possible, because it and its helium decay product are deleterious to mechanical properties.

To achieve the above requirements choice must be made of processes and materials and designs of components which minimise the inventory of tritium and reduce its leakage rate. It is essential to show that adequate containment is possible before construction and operation of a fusion-reactor can even be licensed. For these reasons much time and money is being spent on measuring the permeation constants of hydrogen isotopes and helium, to estimate leakage rates etc.

There is a considerable body of data on the permeation constants of hydrogen in many metals. But similar data for tritium itself is very sparse. However, taken with the rather more plentiful measurements that have been made with deuterium, it is clear, at least at elevated temperatures, the isotope effect in the permeation constants is quite small. The heavier isotopes having slower diffusion and permeation rates and lower solubilities than hydrogen in the same material, but only by a factor that can be very roughly summarised as $\lesssim \frac{1}{2}m^{\frac{1}{2}}$, where m is the atomic mass. There is thus little avoidable error made in estimating tritium behaviour at elevated temperatures from hydrogen data.

There is very little data on the diffusivity of helium in metals. Since it is expected under plasma conditions in a fusion-reactor helium concentrations in a metal may reach several per cent, it is important to have some knowledge of its behaviour in metals. Therefore there is much interest in the measurement of helium diffusivities.

Amongst those metals for which interest is high include the possible constructional materials of reactors e.g. molybdenum, stainless steel, niobium and zirconium.

So far most attention has been given to the behaviour of hydrogen and its isotopes at elevated temperatures. Much work is now being done at below room temperatures. This is in part for theoretical reasons, but also because isotope effects seem to become more important, for example at $-125^{\circ}C$ $D_H/D_D \sim 6$ for vanadium, 20 for niobium and may be even larger for tantalum. These are the only three metals yet studied to such low temperatures so it is not known how widespread such giant effects might be. They suggest, though, the interesting possibility of using membranes of such materials for separation of hydrogen isotopes, especially as their diffusion coefficients are high and their solubilities are large and increase with decreasing temperature.

CHAPTER TWO

REVIEW: DIFFUSION OF LIGHT GASES IN METALS

The purpose of this chapter is to explain the choice of experimental field to be developed in the main body of the thesis and to relate it to current knowledge in the field. To this end the chapter deals first with accepted data on light gases in metals and continues with a review of the means used to gather this data and the theories used to structure it. The chapter ends with proposal for experimental work.

2.1 Some facts

Hydrogen is soluble in a large number of metals and depending on the metal and its thermodynamic history, very large equilibrium concentrations of hydrogen can occur. Figures 2.1 and 2.2 illustrate this for palladium and vanadium (1). As can be seen values for the atomic ratio, of hydrogen and the metal, as high as 0.6 are possible even with modest gas pressures. These figures also illustrate non-ideality, as demonstrated by the sharp rise in gradient for the isotherms at high atomic ratios.

Hydrogen, is comparatively mobile in metals and this is even true at low temperatures, because the diffusion coefficients are often characterised by relatively low activation energies. The activation energy has been measured for many metals and is almost always in the range 0.15 - 0.6 eV. These values are low compared to the activation energies of other solutes as is illustrated by Figure 2.3, which shows the logarithm of the diffusion coefficient versus T^{-1} for the three interstitial solutes hydrogen, nitrogen and oxygen in niobium. The gradients of the curves are a measure of the activation energy, these being $\sim$ 0.18 eV, $\sim$ 1eV and $\sim$ 0.9eV for hydrogen, nitrogen and oxygen respectively. The consequence is that the hydrogen diffusion coefficient is orders of magnitude larger than those of the other two solutes, for the entire temperature range over which measurements have been made. A similar situation would also be found if hydrogen diffusion rates were compared with those of substitutional solutes, which

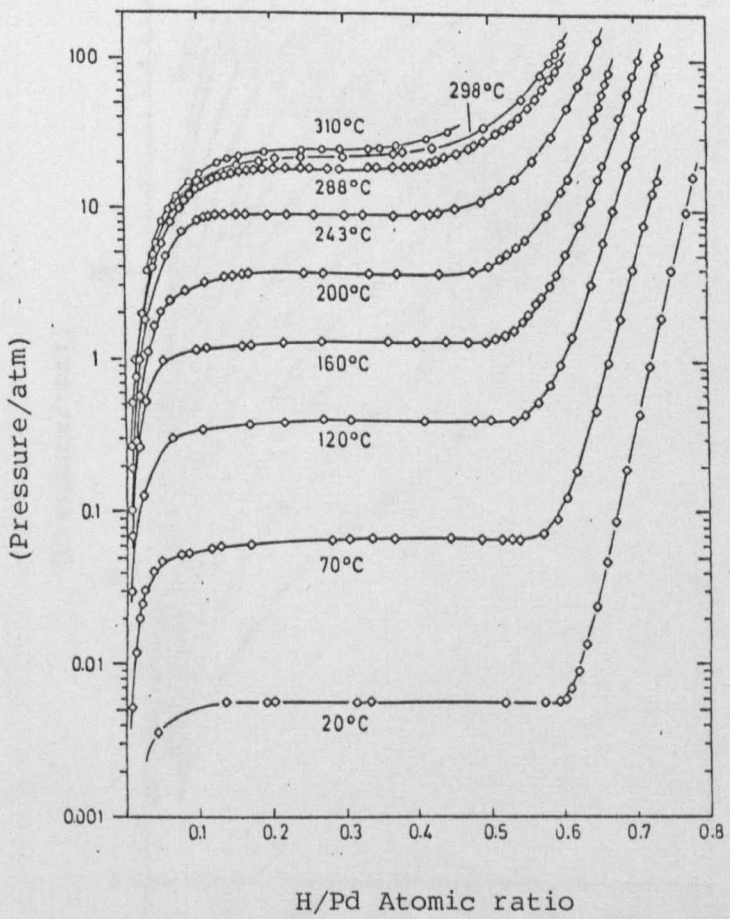

Fig. 2.1 Solubility isotherms for hydrogen in palladium

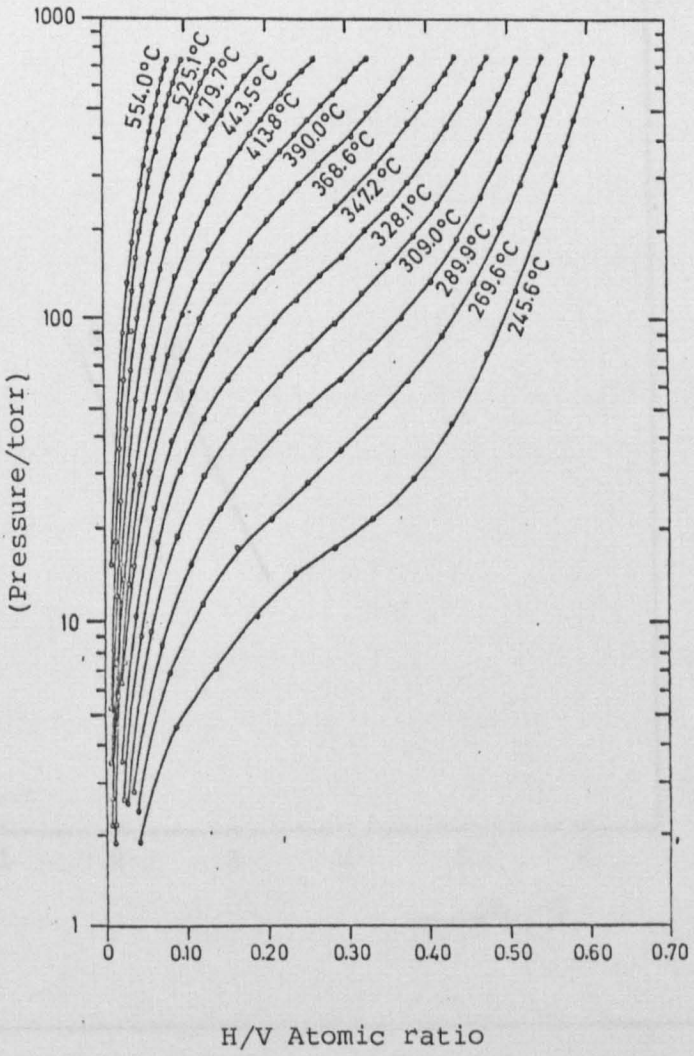

Fig. 2.2 Solubility isotherms for hydrogen in vanadium

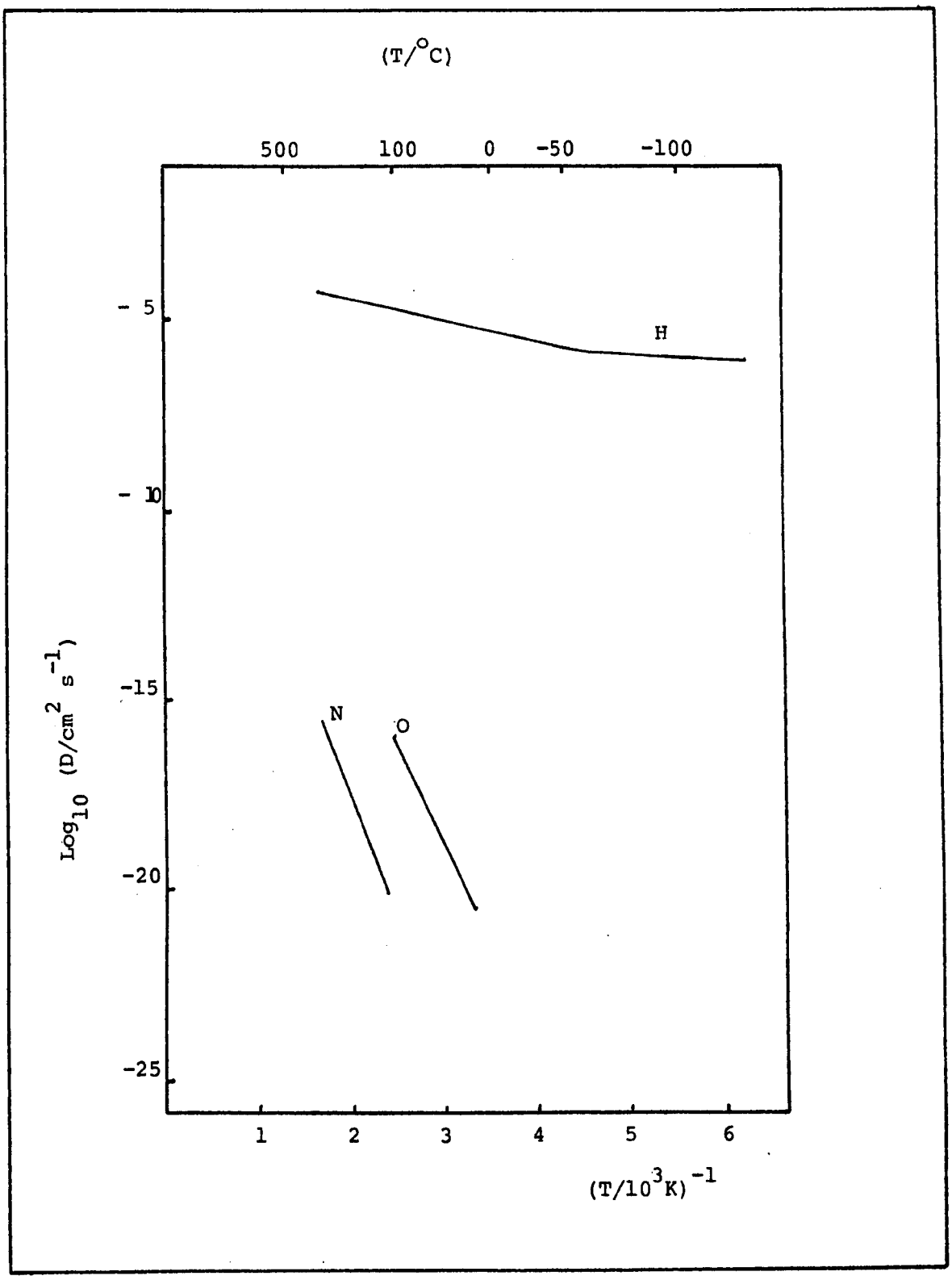

Fig, 2,3 $Log_{10}D$ v T^{-1} for ^{1}H, N and O in Nb

usually have activation energies in the range 1 - 5eV (2).

Not all hydrogen/metal systems have been investigated and most have only been examined over a restricted temperature range. The difficulty is often experimental, for example: cadmium rapidly evaporates at elevated temperatures and low pressures; lead has a very low solubility for hydrogen; aluminium has a tenacious and impervious surface oxide. These are extreme cases, the most usual difficulty is of solubility at low temperatures.

Some metals, however, have been extensively studied, over large ranges of temperature and diffusion coefficient, notably palladium, nickel and iron. The consistency of available data is rather variable. Data related to palladium and nickel for example is highly consistent. Palladium has been investigated over the temperature range 230 - 1000K and the diffusion coefficient range $2 \times 10^{-8} - 5 \times 10^{-4}$ cm^2 s^{-1}. The scatter of data amongst the various authors, approximately twenty e.g. (3) and (4), is seldom found to be more than 10%.

In nickel, measurements have been made over the temperature range 300 - 1300K and diffusion coefficient range $10^{-10} - 5 \times 10^{-4}$ cm^2 s^{-1}. The situation with respect to consistency amongst authors of diffusion coefficients is as with palladium, especially at temperatures above 400K, for example: (5), (6) and (7).

In contrast, to the two examples given above, the data for hydrogen diffusion in iron is remarkably inconsistent. Measurements have been made by about twenty authors, over the temperature range 50 - 1300K (with most data available above 250K) and the diffusion coefficient range $10^{-15} - 10^{-4}$ cm^2 s^{-1} (with most data available above 10^{-8} cm^2 s^{-1}).

Best consistency is found at temperatures above 400K, where data is scattered by less than an order of magnitude. Between 250K and 400K data is scattered over five orders of magnitude, and more recent work e.g. (8), using surface independent techniques below 250K have similar, if marginally improved, consistency.

The marked difference in the scatter of nickel and iron data is interesting because similar measurement techniques, over similar temperature and diffusion coefficient ranges, were used in both cases. These techniques were almost all surface dependent methods, because of hydrogens relatively low solubility in these metals. The opinion is if the scatter of data amongst authors was due mainly to volume effects brought about by impurities and crystal defects, then nickel and iron data should have comparable scatter, this they do not. This implies that the measurements depended mainly on surface behaviour. This opinion is supported by the improved, and good consistency, found amongst authors, when diffusion coefficients of hydrogen in niobium, tantalum and vanadium, measured by surface independent methods, only, are compared. A point of possible significance is that palladium and nickel are f.c.c. metals, whereas iron, niobium, tantalum and vanadium are b.c.c. metals, but this aspect has not yet been investigated in depth.

In contrast to work with hydrogen, experimentalists have experienced many difficulties in making measurements of helium diffusion rates in metals. This is because, in common with other inert gases, helium has an effective zero solubility in most metals.

Early work in noble gas diffusion was done by Le Claire and Rowe 1957 (9) with argon in silver. Since silver is virtually impermeable to all inert gases, argon was artificially introduced into silver by means of an

electric glow discharge. These experiments proved argon diffusivities in metals were finite. It was not long before this was shown to be true for other inert gases e.g. Tobin 1957 (10) with krypton and xenon in silver and Glyde and Mayne 1965 (11), (12) with argon and helium, in magnesium and aluminium.

Where data on inert gas diffusion in metals is available, it tends to confirm the view (11,12) that a substitutional mechanism operates. The most significant evidence for this is that the activation energies, for inert gas diffusion, are very close to those for self-diffusion of the metal itself.

2.2. Theories of diffusion for light gases in metals.

Current theories relate mainly to the diffusion of hydrogen, with little work specific to helium. What follows is a review showing the evolution of ideas on how to describe the diffusion of hydrogen in metals. The position with respect to helium is treated separately.

A general point to be noted in this work, is that diffusion rates are not yet predictable with any measure of reliability, for any metal.

2.2.1 Hydrogen diffusion; early attempts.

The temperature variation for the diffusion coefficient is found to be well describe by the relationship,

$$D = D_o \exp(-E_o/kT) \qquad (2.1)$$

where D_o is a constant pre-exponential factor, and E_o is the activation energy. Equation 2.1. seems to hold for all metals over almost all temperatures for which measurements have been made. Exceptions have been found, for example with niobium below room temperatures and nickel at extreme high temperatures. Due to this consistency of description, valid theoretical

models must compare with equation 2.1 at least in the high temperature limit.

One model used by early workers is based on chemical rate theory and is called absolute reaction rate theory. A notable author in this field was Eyring(13). According to this theory the reaction of reactant species A_r to form product species X_r

$$A_1 + \cdots + A_i \longrightarrow X_1 + \cdots + X_j$$

takes place in two steps. In the first step reactants are in equilibrium with an activated complex M according to the equation

$$A_1 + \cdots + A_i \rightleftharpoons M \qquad (2.2)$$

In the second step the activated complex decomposes to give the product species X_r. Eyring et.al. showed the rate of activated complex decomposition per unit volume is given by the expression

$$\frac{kT}{h} c_m \qquad (2.3)$$

where c_m is the number of complexes per unit volume. Using equation 2.3 the specific reaction rate constant K is then supposed (14) to be given by

$$K = \frac{kT}{h} \frac{g_1 \cdot g_2 \cdot \cdot g_i}{g_m} \left(\frac{V}{n}\right)^{i-1} \exp\left(-\Delta F^*/kT\right) \qquad (2.4)$$

where g_i are the activity coefficients for the reactant species ; ΔF^* is the difference in free energy between the activated complex and the reactants when each species is in its standard state at the temperature of the reaction; and (n/V) is the total number of particles per unit volume.

On applying chemical reaction rate theory to interstitial diffusion, equation 2.4 reduces to

$$K = \frac{kT}{h} \frac{g}{g_m} \exp\left(-\Delta F^*/kT\right) \qquad (2.5)$$

because there is only one reactant, i = 1, the solute atom in the interstitial site. The activated complex is a solute atom midway between two interstitial positions. The expression in the equation 2.5 is the "jump"

rate, therefore in an ideal solid solution

$$D \sim \frac{a^2}{S} \frac{g}{g_m} \frac{kT}{h} \exp\left(-\Delta F^*/kT\right) \qquad (2.6)$$

where a is the lattice constant and S^{-1} is the fraction of neighbouring interstitial sites available in the forward direction.

Comparison of equation 2.6 with 2.1 is not satisfactory. There is temperature dependence in the pre-exponential factor, but this may not matter since there is temperature dependence for ΔF^* also. Furthermore the activity coefficients, g_i, are not readily calculable, hence this theory is little used. The assumption $(g/g_m) \sim 1$ gives $D_o \sim 10^3$ at 500^oC which is orders of magnitude too large compared to measured D_o data.

A second model, used in early theoretical work is described as classical rate theory, (15), (16).

In basic terms the classical argument is to suppose that an atom will have sufficient thermal energy to pass over a potential barrier of height E_o only a fraction, $\exp(-E_o/kT)$, of the time. If ν is the characteristic vibrational frequency, then the probability, p, that sometime during one second the atom will have enough thermal energy to pass over the barrier is

$$p \sim \nu \exp(-E_o/kT)$$

This is the jump rate and leads to a diffusion coefficient

$$D = \frac{a^2}{S} \nu \exp(-E_o/kT) \qquad (2.7)$$

where a and S have the same meaning as in equation 2.6 .

Alternative approaches such as that of Vineyard (16), produce similar expressions, where ν now is a function of the normal mode frequencies of the lattice - plus - interstitial in the normal state and transition state.

The classical rate theory is superior to the absolute reaction rate theory in that equation 2.7 compares well with equation 2.1, and is more predictive. An order of magnitude calculation will illustrate this. Take ν to be the Einstein frequency of the interstitial in the site, ν_E. ν_E will be both host and interstitial dependent, i.e. the model is to some extent specific. For hydrogen take $\nu_E = 10^{14}$ Hz, and for the host, take the lattice constant a = 0.3 nm and S = 5, then $D_o = 1.8 \times 10^{-2}$ cm^2 s^{-1}. This value is actually a reasonable estimate, but the theory is not flexible enough to cover the three orders of magnitude span of most observed D_o. However, the main failure of classical theory is that for all hydrogen/metal systems there are significant deviations from its prediction for the isotope ratio:

$$\frac{D_1}{D_2} = \frac{\nu_1}{\nu_2} = \left(\frac{m_2}{m_1}\right)^{-\frac{1}{2}} \qquad (2.8)$$

This is not too unexpected in the light of the small mass and high Einstein temperatures of the hydrogen isotopes.

2.2.2 Hydrogen diffusion ; current position

Classical theory was based entirely on classical mechanics and failed, when applied to hydrogen. That wave mechanics could do better was best illustrated by the work of Le Claire, 1966 (17) and Ebisuzaki et.al, 1967 (18). They modified the classical theory of Vineyard (16), by substituting into the hydrogen/metal partition function, a discrete energy spectrum instead of the continuous energy spectrum of classical mechanics.

In Vineyards theory the hydrogen jump rate is

$$\Gamma = \nu'_q \frac{Z'}{Z} \qquad (2.9)$$

where ν'_q is a frequency associated with a coordinate passing through the saddle point between the initial and final interstitial sites and Z' and Z

are the total partition functions of the transition and normal state, respectively. Using the harmonic approximation and discrete energy levels

$$\Gamma = \left[\nu'_q \prod_i \left(\frac{\nu_i}{\nu'_i}\right) \exp(-E_o/kT) \right] \left\{ \prod_i (f(x_i)/f(x'_i)) \right\} \qquad (2.10)$$

where $f(x) = \sinh(x)/x$; $x = h\nu/2kT$; ν_i are the normal mode frequencies of the system. The jump rate in equation 2.10 is expressed in such a way, that the term in large square brackets corresponds to Vineyards original result, therefore the term in curly brackets is identified as the quantum correction. The isotope ratio then becomes

$$\frac{\Gamma_1}{\Gamma_2} = \left(\frac{m_2}{m_1}\right)^{\frac{1}{2}} \prod_i \left(\frac{f(x_{1i})\, f(x'_{2i})}{f(x_{2i})\, f(x'_{1i})}\right) \qquad (2.11)$$

suitable choice of x_{1i} and x'_{1i} can account for the observed deviations of isotope ratios from the classically expected result. This has been done, for instance, with nickel by Ebisuzaki et. al (18).

While the above theory is important, again it does not give quantitative results, since as with the Vineyard theory, it involves functions of the non-equilibrium transition state for which no calculations are available.

Other current theories are based mainly on the quantum mechanics of the double well e.g. (19), (20), (21). In principle such theories are specific and predictive, however in practise the necessary calculation of matrix elements becomes intractable. As a result most authors content themselves by making predictions concerning the temperature dependence of the transition rate. The concensus is that for high temperatures, $T \gg \Theta_D$ where Θ_D is the Debye temperature, the theories agree with equation 2.1. For low temperatures, the temperature dependence becomes a power law in temperature thus $D = \alpha T^n$ where n is usually a number between 1 and 7. Unfortunately experiments are not practical in the temperature regions where such power laws are expected.

The work of Flynn and Stoneham (20) is notable. They obtained expressions relating localized states, where the localization is increased by self trapping. Only ground states of the localized impurity were considered. There was no question of the representative point simply surmounting or penetrating a barrier in configuaration space, hence the saddle point plays no distinquishing role; only the exact Hamiltonian and the localized initial and final state wave functions are relevant; this approach does not allow calculation of transition probabilities for non tunnelling processes. Their distinquishing result at low temperatures, is a power law with n = 7.

Based on their model Flynn and Stoneham made an interesting distinction between b.c.c and f.c.c metals, a consequence of the self trapping. They argue that the activation energy

$$E_o = E_a + E_s$$

where E_a and E_s are due to modes which are antisymmetric and symmetric, respectively, about the midpoint of the jump path in real space. They then show that E_s is independent of impurity mass, whereas E_a is not. Furthermore due to the geometry of interstitial sites, they anticipate that in b.c.c solvents, E_a will contribute the major part of E_o, whereas this is not to be expected in f.c.c lattices. Therefore the ratio of diffusion coefficient activation energies for hydrogen and deuterium etc, in b.c.c metals should be greater than in f.c.c metals.

The treatment of the jump process, described in the above model was from an initial to a final wavefunction. An alternative treatment would be to consider the jump from an initial to a final localized ground state wavefunction, via a delocalised intermediate state. This latter model is used by Sussman (19) and the conclusions concerning the temperature dependence are very similar. The difference is that E_o, the activation energy is now identified as an effective barrier height.

2,2,3 Helium.

From the few available helium diffusion coefficients in metals(11), (12), it is supposed that helium is a substitutional solute, like the other inert gases. With respect to substitutional atoms, a successful theory has been developed by Lazarus (22), and elaborated by Le Claire (23), which accurately predicts differences in the diffusion activation energy between host and impurity atoms. In the theory of Lazarus this difference between activation energies, ΔE, is assumed to be the sum of two terms:

$$\Delta E = \delta E_f + \delta E_{m2} \qquad (2,12)$$

Where E_f is the heat of formation for an atom in a lattice site and the Thomas - Fermi potential is used to evaluate it, δE_{m2} is the accomodation energy of the lattice for an atom in a lattice site, and was supposed to be determined from the change in volume occupied by the impurity atom, using the elastic modulus, Lazarus found that

$$\Delta E = \frac{-Ze^2}{d} \exp\left(\frac{-d}{\rho}\right)\left(1 - \frac{1}{4}\left(\frac{d}{\rho}\right)^2 - \frac{5}{4}\left(\frac{d}{\rho}\right) - \frac{5}{4}\right) \qquad (2,13)$$

where d is the distance between atomic nuclei and $\rho = (h^2/(4me^2)) \times (\pi/(3n_e))^{1/3}$, with n_e equal to the number of electrons per unit volume. This result was not very accurate since it depends on the weak assumption made for evaluating E_{m2} and does not consider distortions of the electron cloud due to the defect nor does it allow for correlation effects.

Le Claire improved the agreement between theory and experiment by including an extra term in ΔE, i.e

$$\Delta E = \delta E_f + \delta E_{m2} - C \qquad (2,14)$$

where C is due to correlation; and by evaluating $\delta E_f + \delta E_{m2}$ from the calculations of Alfred and March:

$$\delta E_f + \delta E_{m2} = \frac{-Ze^2}{(11/16)d} \gamma \exp - \frac{11}{16}\frac{d}{\rho} \qquad (2,15)$$

Here d and ρ are as before and γ is a slowly varying term between 0,7 and 1 which corrects for electron cloud distortion.

Correlation effects are influenced by many considerations including the jump rates, of the host and impurity atoms, for which there is no reliable theory. For this reason C is an empirical term, usually determined from the temperature dependence of isotope effects. A readable account of determining correlation factors by the isotope effect method is given in (24).

That ΔE given by equations 2.14 and 2.15 compares well with experiment is shown by Table 2.1. There the difference between the diffusion activation energies, and the self-diffusion activation energy for silver, for various substitutional impurities are compared with theory. Note that the term due to correlation, plays an important role.

2.3 Experimental methods to measure hydrogen (and helium) diffusion rates.

Many measurements have been made of hydrogen diffusion rates in metals. There is a long history of experiment, mainly with successive refinements of a few basic methods, but also some dependent on more modern techniques.

Specifically there are two main approaches, microscopic (surface independent) and macroscopic (usually surface dependent). In the former atomic motion is followed, in the latter a bulk flow of material is detected.

For helium the position is different. The effectively zero solubility of helium in metals makes measurement difficult, so the possible techniques are limited.

2.3.1 Methods dependent on atomic motion.

Methods for detecting atomic motion include; nuclear magnetic resonance (N.M.R) (25); quasi-elastic neutron scattering (Q.N.S) (26) and

TABLE 2.1.

Comparison of theoretical and experimental ΔE (ΔE/kcal mole^{-1}) in Ag. Le Claire (23)

Element	Z	$\delta E_f + \delta E_{m2}$	ΔE theoretical	ΔE experimental
Cd	+1	- 4,30	- 2,45	- 2,57
In	+2	- 7,34	- 3,40	- 3,64
Sn	+3	- 9,80	- 4,65	- 4,97
Sb	+4	-11,92	- 5,70	- 5,95
Hg	+1	- 4,30	- 3,68	- 6,17
Tl	+2	- 7,34	- 4,66	- 6,37
Pb	+3	- 9,80	- 4,84	- 6,17
Zn	+1	- 4,30	- 2,24	- 2,57
Ge	+2	- 9,80	- 6,13	- 7,77
Ru	-3	+45,4	+45,4	+11,5
Fe	-0,7	+ 5,38	+ 4,76	+ 4,77

internal friction or the Snoek effect (27).

Internal friction is a familiar effect observed when any body is set in vibration. No matter how carefully a specimen is mounted the amplitude of oscillation decreases with time. This indicates the motion of the crystal lattice is not perfectly elastic. Instead the energy is dissipated by some form of internal frictional force. The damping arises from lattice interaction with impurities, defects etc.

In these experiments, so called internal friction 'peaks' are observed. The form of these peaks suggests they are due to some type of relaxation process with a characteristic time τ. Thus if a specimen is set into oscillation over a range of frequency there will be some frequencies at which energy is strongly absorbed. These are the internal friction peaks when, it is presummed, the period of the excitation is equal to the characteristic time, τ, of the friction process. When hydrogen is present, relaxation peaks may be observed whose amplitude sometimes can be shown to depend on hydrogen concentration. The effect is attributed to diffusion. For this case the relaxation time of the peaks is related to the mean time of stay of a hydrogen atom in a particular site. Unfortunately the effect is non-specific. It is not always possible to prove that the observed peaks are due to hydrogen relaxation processes, or that these processes have something to do with the individual steps leading to long range diffusion.

N.M.R. methods have been in use since the 1950's, (28), and several variations have been developed. A review of the method is given in (25). The procedure consists of measuring the longitudinal spin-lattice relaxation time T_1 and the transverse spin-spin relaxation time T_2. Temperature variation then give the activation energy for diffusion and knowledge of the diffusion mechanism allows calculation of the diffusion coefficient.

N.M.R. studies are limited by the high concentrations of hydrogen needed for detection. Hence few measurements have been made for hydrogen/metal α phases, (29). However, when applied to a metal with suitable solubility, the method has a large temperature range including the cryogenic region.

N.M.R. shares, in common with other microscopic methods, the disadvantage of having to assume a diffusion mechanism to derive the diffusion coefficient. Also measurements involving other processes can be mistaken for hydrogen motion e.g. the interaction with conduction electrons contributes to the spin-lattice relaxation time in niobium (30).

A fairly recent review on the application of quasineutron scattering (Q.N.S) can be found in (26). The experimental system uses a monoenergetic neutron beam which is passed through the metal specimen. Incoherent scattering by the protons in the metal broadens the energy spectrum of the emerging beam, from which it is possible to deduce the rate of diffusion. Small and large scattering angles contain different information. Small scattering angles correspond to small momentum transfer and almost elastic scattering. From the width at half maximum the diffusion coefficient is determined. From the line width at larger scattering angles, details such as the mean jump rate or mean jump distance can be obtained. This technique therefore can distinquish between octahedral - octahedral and tetrahedral - tetrahedral diffusion jump processes. The technique is limited by the resolution of the spectrometers and is useful for measurement of diffusion coefficients greater then about 10^{-7} cm^2 s^{-1}. It is also interesting to note that few diffusion coefficients measured by Q.N.S. are available above 700 K.

In conclusion the microscopic methods provide measures of diffusion rate without interference from surface processes. The methods are limited to high proton concentrations, but they can span a large temperature

range which includes temperatures well below 300K. Their main disadvantage is that diffusion coefficients must be interpreted indirectly from primary measurements, by assuming a diffusion mechanism.

2.3.2 Methods dependent on macroscopic flow.

Diffusion coefficients are defined by the macroscopic, phenomenological Fick equation (Ficks first law) which in one dimension is:

$$J = -D \frac{\partial N}{\partial x} \qquad (2,16)$$

J is the flux, D is the diffusion coefficient and N is the diffusant concentration per unit volume. If it is further assumed there are no sources or sinks for the diffusant in the solvent, then from the conservation of matter it follows that

$$\frac{\partial^2 N}{\partial x^2} = \frac{1}{D} \frac{\partial N}{\partial t} \qquad (2,17)$$

Equation 2,17 is known as the diffusion equation or Ficks second law. From these equations it may be seen that macroscopic methods for measurement of diffusion coefficients can be divided into two types; those that determine the diffusion coefficient from observations of the flux, into the metal, out of the metal, or through a metal membrane; those that determine the diffusion coefficient from observation of the concentration in the metal.

In the following short review examples of both types are given. Neutron radiography, resistivity relaxation and Gorsky effect, depend on concentration. The permeation methods depend on flux.

Neutron radiography is a relatively new method (31) and depends on the high attenuation of thermal neutrons by protons. Experimentally a large and non-equilibrium hydrogen distribution is set up in a sheet of metal and the relaxation with time is observed by measuring the optical density of the sheet to neutrons using neutron radiography. From the relaxation time the diffusion coefficient is determined.

The method has the advantage of being surface independent and is available for use at temperatures of about 300K, a region not always accessible to other methods. However, it cannot in general be used in the α phase.

Another relatively new method is resistivity relaxation (32). Resistivity is a property that can be measured very accurately and depends on both impurity concentration and temperature. Given accurate knowledge of the hydrogen concentration and temperature dependences of the resistivity for a metal, then it is possible to follow the relaxation of a non-equilibrium hydrogen distribution in a wire. The experimental procedure is to load one half of a metal wire uniformally with hydrogen, usually using an electrolytic method. The hydrogen concentration in that half of the wire is determined by making a resistivity measurement between two points along the loaded half of the wire. The wire is then held accurately at the experimental temperature and the change in hydrogen concentration, in the half of the wire which was not previously loaded with hydrogen, is monitored by measuring the resistivity between two points along this half of the wire. In this way the relaxation time to equilibrium is measured, from which the diffusion coefficient is determined.

The resistivity relaxation method can be used in the cryogenic region and typical working temperatures range from 200 to 350K. A disadvantage of the method is the need to reproduce temperatures to within 0.005K to differentiate hydrogen concentration effects from temperature effects on residual resistivity (33).

The Gorsky effect provides a well established method for the measurement of hydrogen diffusion rates. The topic is reviewed in (34). The Gorsky effect arises because hydrogen expands the lattice in which it dissolves. If a wire or foil having a uniform concentration of hydrogen is

bent the internal equilibrium will be perturbed. To relieve the stress hydrogen will tend to flow from the region of compression to the region of tension. This flow may be detected very sensitively and from the time required for diffusion across the sample diameter, the absolute value of the diffusion coefficient can be determined with no adjustable parameters, if the sample diameter is known.

The Gorsky method was used over a wide range of temperature, to measure the diffusivity of hydrogen in niobium. These measurements in niobium cover one of the widest T^{-1} ranges, for diffusion measurements, known. In common with the other relaxation methods, the Gorsky method also has the advantage that derived macroscopic diffusion coefficients are independent of surface processes.

In permeation experiments, fluxes of diffusant are measured. Measurement of diffusion coefficients in this way is less direct than by the macroscopic methods reviewed already, since the fluxes measured are outside the solid. The internal fluxes are derived by computation to give the diffusion coefficient. To do this calculation it is necessary to model the phase boundary between the solid and the surrounding gas. Most frequently this is done by supposing an equilibrium surface concentration. For hydrogen this is given by Sieverts law,

$$N = K_s p^{\frac{1}{2}} \qquad (2.18)$$

where N is the equilibrium hydrogen concentration in the metal, p is the gas pressure and K_s is Sieverts solubility constant. Clearly the precision of any diffusion coefficient measured depends on the particular feature of the interfaces involved.

The simplest, permeation, experimental regime uses steady rate permeation with two vacuum chambers separated by a membrane, the specimen. The hydrogen pressure is held constant on both sides of the membrane and the

downstream side is usually held at effectively zero pressure by continuous pumping. Under these conditions the solution to Ficks equations is:

$$J = \frac{D}{L}\left(N_{x=o} - N_{x=L}\right)$$

$$= \frac{D}{L} N_{x=o} \qquad (2,19)$$

On substituting from equation 2,18 into equation 2,19

$$J = \frac{DK_s}{L} p^{\frac{1}{2}} \qquad (2,20)$$

It is clear from equation 2,20 that, unless K_s is known, the diffusion coefficient cannot be determined from a steady state experiment. The product of D and K_s is called the permeation constant, P, and only this is directly determined by a steady state permeation experiment. Diffusion coefficients are sometimes determined from knowledge of P and K_s, but this is usually unsatisfactory because measurements of K_s are strongly influenced by surface conditions and lattice defects. To overcome this difficulty in determining reliable diffusion coefficients using a permeation method, led to the development of the "time lag" technique.

In time lag methods, the diffusion coefficient is obtained by making use of measurements during the transition between two steady states. Consider again equation 2,17

$$\frac{\partial^2 N}{\partial x^2} = \frac{1}{D}\frac{\partial N}{\partial t}$$

Substitution of the function $\exp\left(i(kx - \omega t)\right)$ for a propagating wave into this equation gives

$$-k^2 = \frac{\omega}{D} i \qquad (2,21)$$

where k is the magnitude of the wavevector for the wave and ω is its angular frequency. Equation 2,21 is called the dispersion relation for the diffusion equation. Dispersion relations characterize wave equations and from them the group velocities of the wave, described by the wave equation, can be derived:

$$\text{Group velocity} = \frac{d\omega}{dk} \qquad (2,22)$$

From equations 2.21 and 2.22 it is clear that the group velocity is independent of Sieverts constant. Hence the propagation time or "time lag" for a change in pressure, on one side of the membrane, to reach the other side of the membrane is independent of K_s, but dependent on D. Therefore from measurements of time lag, the diffusion coefficient can be determined with a permeation experiment.

Early time lag experiments (35) used a step function change in pressure as the disturbance. Such experiments are still performed, but in practise it is not possible to provide a perfect step function change in pressure. This problem is easily avoided because nothing in the above argument limits the disturbance to a particular form of pressure variation with time. This led to further development of the method.

The next development of the time lag method was to use a smooth periodic variation of pressure with time (36). In addition to overcoming the practical difficulties associated with a step function, the periodicity allows signal averaging so allowing an improvement in signal to noise ratio.

Permeation techniques are generally useful. They are simple, sensitive and cover a wide range of temperature, extending from about 400K upwards. The main criticism of these methods is that the interpretation of these experiments usually depend on the supposition that surface processes are very fast compared with the rate of diffusion inside the solid. This supposition is not universally justified.

In conclusion, from the above review of experimental methods, the method best used to determine a diffusion rate depend on the use to which the coefficient will be put, if it is to test a theory then the atomic methods are probably best. If it is for some technological application the macroscopic methods are probably to be preferred.

2,3,3. Helium diffusion

There are very few available diffusion coefficients for helium in metals because of the difficulty from its almost complete insolubility in metals, which precludes normal experiments. Even so, techniques have been developed which introduce helium into the metal and allow use of some of the above methods.

Helium is normally introduced into metals by bombarding foils with high energy (10 - 100 kev) helium ions. This produces a distribution like that in Figure 2,4. Ionic penetrations into metals are available in the literature (37).

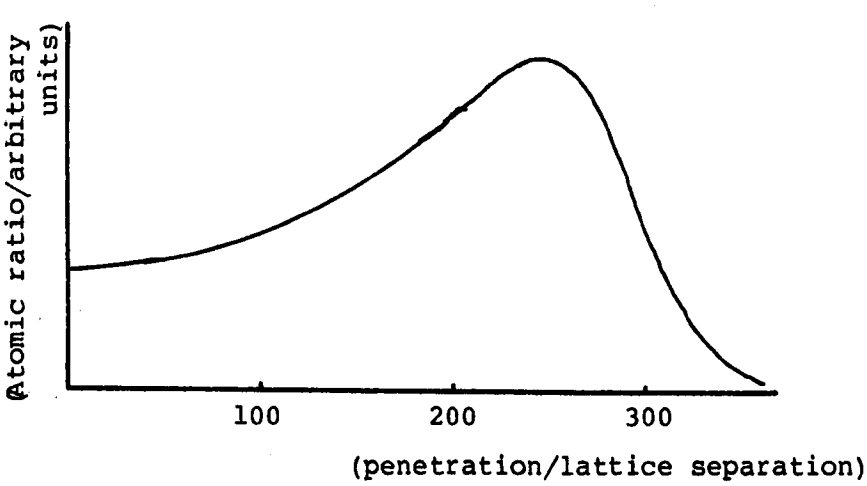

Fig. 2,4 Sketch of high energy helium penetration into metals

The depth at which the helium concentration is highest depends on both the beam energy and the host metal. To allow the measurement of the diffusion coefficient using such a helium distribution, foils are usually annealed and a gas release (desorption) experiment performed. An alternative expe - rimental technique is to use N,M,R with ^{3}He. (38).

Ion bombardment is not always a satisfactory method for introducing helium into metals because of the high local concentration. Except for conditions of very low concentration, inert gas atoms tend to form stable bubbles in the host lattice. This is known to occur with aluminium and

copper, but other metals seem not to suffer e.g. silver and magnesium, (39), (40). In their work with aluminium (and magnesium) Glyde and Mayne, (11) (12), overcame this problem by bombarding the specimen with 150 MeV protons, forming a uniform helium concentration in the specimen via the (p,α) reaction.

The results of inert gas diffusion measurements suggest that inert gases, including helium, diffuse as substitutional impurities in the host lattice. For example see Figure 2.5, which compares the diffusivity of helium in magnesium with magnesium self diffusion. The diffusion coefficient is much smaller than might be expected if helium diffused by an interstitial mechanism, like hydrogen.

2.4. Intentions

The first aim of the present work was to develop a technique for the measurement of hydrogen diffusion coefficients in metals, that might also be used with helium. The decision was made to work with hydrogen and some of the metals; silver, aluminium, niobium, zirconium, molybdenum and gold. It was hoped that the technique would have the sensitivity to provide data on low solubility materials that have been avoided in the past. If the method worked well attempts were to be made with helium.

A modified permeation method was chosen, using a double vacuum chamber, with foil specimen and time-lag form of analysis. Such a method is considered otherwise safe and assured. The modification favoured was to use a periodic sinusoidal input disturbance, because this increases sensitivity by allowing signal averaging. Also, worried by earlier work and the inability to pick out diffusion limited fluxes from fluxes limited by surface rates and traps, a pure sine wave (an eigenfunction of the diffusion equation time dependence) was used. This was thought to give some chance, (to be examined in the course of work) of picking out surface effects from bulk effects.

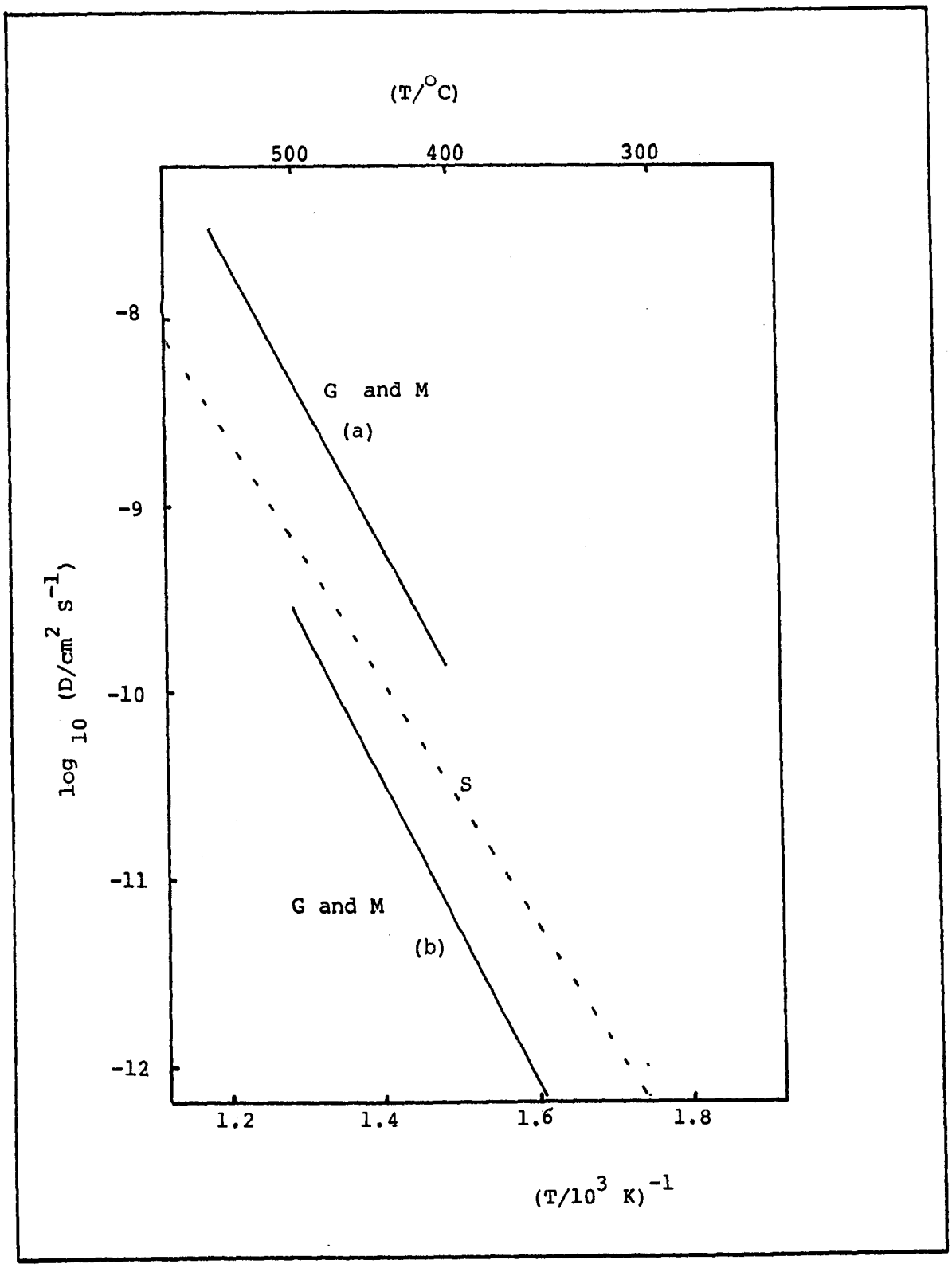

Fig. 2.5 ln D vT^{-1} for ^{4}He in Mg., G and M (11)

a) ^{4}He introduced by 1 MeV ion bombardment

b) ^{4}He introduced via (p, α) reaction using 150 MeV protons

S: Mg. self-diffusion (41)

Finally given the choice of using pressure modulation or a modulated gas discharge or ion beam as the disturbance, the electrical methods were opted for, since helium experiments then became possible.

The expected experimental window of the equipment was defined by:

$$100^{\circ}\,C \lesssim T \lesssim 900^{\circ}C$$

$$1\ \text{torr} \lesssim p \lesssim 15\ \text{torr}$$

$$0{,}01\ \text{cm} \lesssim L \lesssim 0{,}5\ \text{cm}$$

$$10^{-8}\ \text{cm}^2\ \text{s}^{-1} \lesssim D \lesssim 10^{-3}\ \text{cm}^2\ \text{s}^{-1}$$

$$10^{-9}\ \text{t,l,s}^{-1} \lesssim J \lesssim 10^{-3}\ \text{t,l,s}^{-1}$$

$$I \lesssim 200\ \mu\text{A}$$

$$E \lesssim 10\ \text{keV}$$

$$10^{5}\text{s} \lesssim \tau \lesssim 10\ \text{s.}$$

Where T = temperature; p = pressure; L = specimen thickness; D = diffusion coefficient; J = gas flux; I = ion beam current; E = ion beam energy ; τ = time lag.

SUMMARY

Diffusion rates are known for hydrogen in a wide range of metals and over a wide range of temperatures. In contrast data is very limited for helium in metals. Characteristic of hydrogen diffusion is a low activation energy $E_o \sim 0.5$ eV and pre-exponential factors $D_o \sim 10^{-2}$ cm^2 s^{-1}. The diffusion rates are well above those for heavy interstitials and for substitutional impurities. Hydrogen diffusion has been shown to be interstitial, whereas helium diffusion is much slower and believed to be substitutional.

Many theories for hydrogen diffusion have been proposed but they are of little use in practise; they are not predictive. Theorists are not helped by the uncertainties in the experimental data in a number of materials.

Helium diffusion rates are close to what might be expected from the Lazarus/Le Claire valence theory of substitutional impurities.

The widest used experimental technique observes the transit time for gas through a membrane. This technique is capable of refinement if periodic perturbations and signal averaging on the output are used.

An experiment of interest will be to use ion injection of gases in to foil specimens using a double vacuum chamber rig. Metals suitable for study in this way include Ag, Mo, Au, Al, Nb and Zr.

CHAPTER THREE

EXPERIMENTAL EQUIPMENT

For purposes of design the requirements on the experimental equipment were:

1) to support a foil specimen under conditions which would permit extensive experimental use without appreciable degradation.
2) to inject experimental gas at one side of the foil specimen
3) to detect small gas flows leaving the exit surface of the specimen and to do this with a short response time.
4) to provide correlation in time between the injection of an experimental gas and its emission from the far side of the experimental foil.

The specific design chosen called for a double vacuum system with both chambers capable of being out gassed to a pressure of about 10^{-8} torr. Detection of pressure fluctuations of order 10^{-10} torr was sought, but it was accepted that long integration times might be required to work at this level of sensitivity. Gas was to be injected using either a discharge or an ion gun and earlier trials (42) suggested that a discharge operating with about 3mA and 350V should be adequate to give detectable signals using specimens of thickness in the range of 0.1 - 1.0mm and reasonable temperatures.

Overall the system may be seen as comprising four components: double vacuum chamber; injection device; gas detection devices; and an electronic system to condition signals and correlate input with output. Figure 3.1 shows the chosen experimental arrangement in schematic form.

3.1. Experimental Chambers.

Diffusion was to be studied by the permeation of gas through a metal foil separating two vacuum chambers (see Fig. 3.2). Gas was to be injected into the specimen from one chamber at a rate subject to periodic, and defined, fluctuations. Detection of gas flow from the specimen was to be

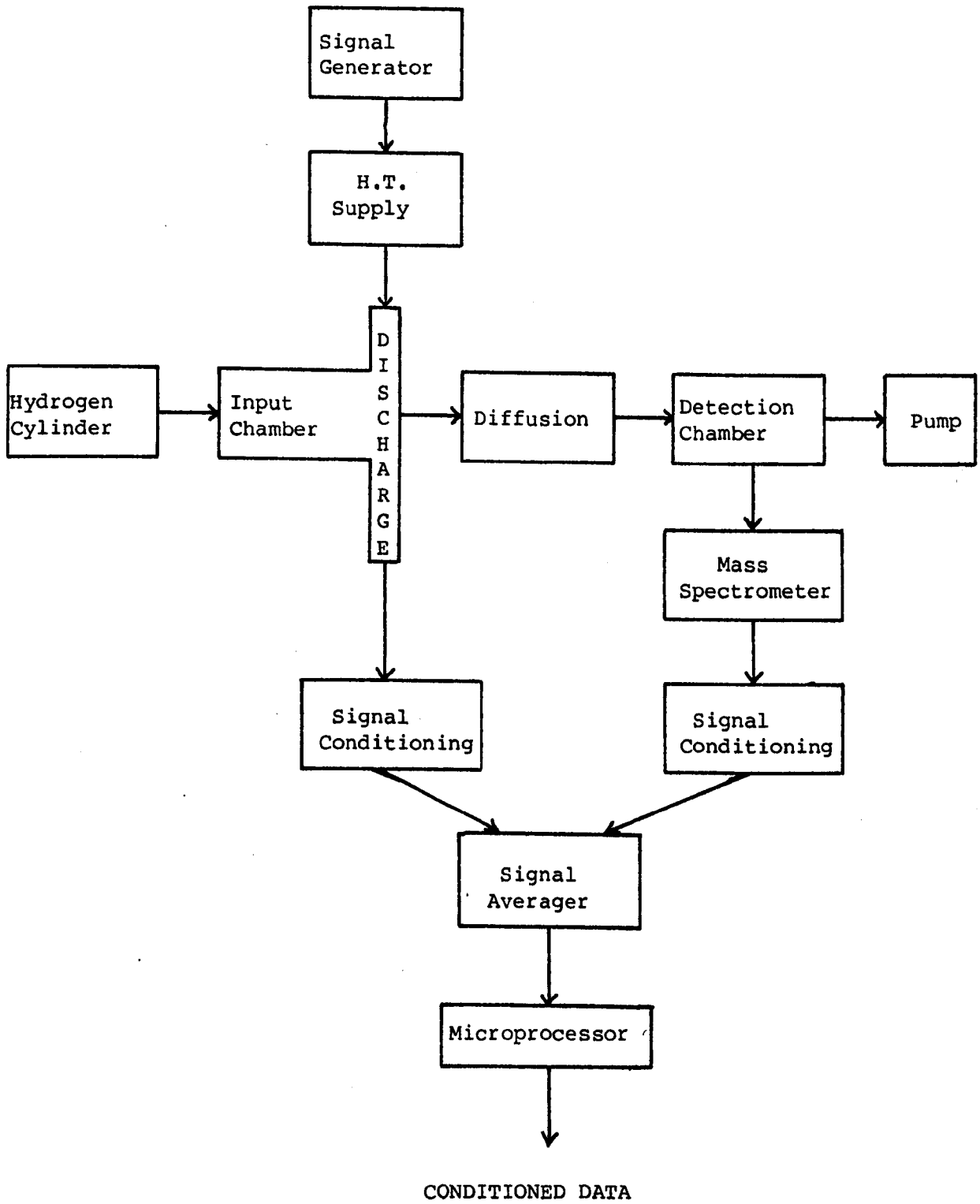

Fig . 3.1. Schematic diagram of data gathering process.
Horizontal arrows represent mass flow
Vertical arrows represent information flow

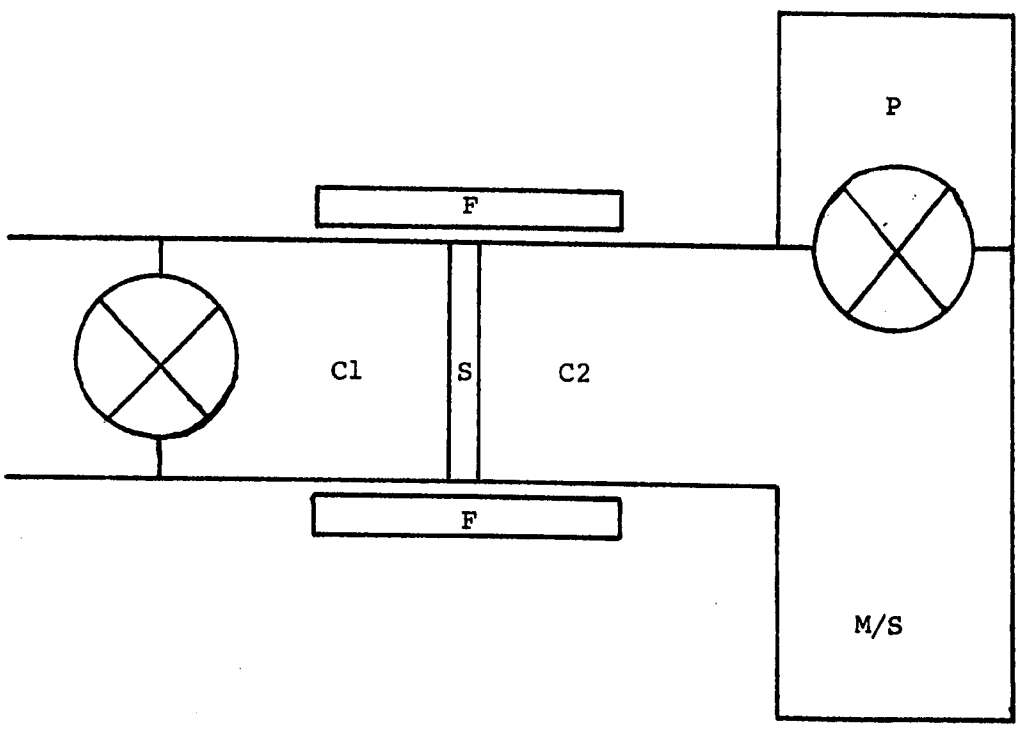

C1. Input Chamber
C2. Detection
F. Furnace
M/S. Mass Spectrometer
P. Pump
S. Specimen

Fig. 3.2 Schematic diagram of vacuum system

by measurement of the experimental gas partial pressure in the continuously pumped output chamber.

3.1.1. Detection Chamber

The flow rates of particular gases were to be examined and measurements would extend to the lowest flow rates possible. With such flow rates, the system would operate down to conditions where the outgas rate, for system components, was of the same order as the flow rates themselves.

An early design decision was to use a continuously pumped detection chamber. This is unusual in time lag work, but has the advantage of reducing pressure drift in the course of an experiment and of maintaining gas purity against the inevitable outgassing of the system walls. A disadvantage of the approach is that the data are a function of the pump characteristics; this point turns out not to be too important as will be shown later, section 3.3.

Detection targets for flux of 5×10^{-9} torr litres s^{-1}, that is 10^{10} molecules s^{-1}, and for pressure of $\sim 10^{-10}$ torr, were set. To achieve this the chamber was constructed as much as possible of stainless steel components. The Edwards range using gold ring seals was chosen, with an A.E.I P25 ion pump. The internal surface area of the detection chamber was about 10^3 cm^2, giving an expected rate of outgas $\sim 10^{-10}$ torr litres s^{-1}.

Use of the ion pump was in some degree fortuitous. These pumps are very constant in their pumping characteristics, whereas in a later modification of the chamber, for helium work, when an U.H.V. diffusion pump (10^{-11} torr capability) was used, there was evident variation in pump rate.

Pump rates vary with the gas in the vacuum system. Table 3.1 shows the pumping characteristics for the P25. Note that it has an appreciable

pumping rate even for helium.

Table 3.1

Relative pump rates of P25 ion pump for some gases

Nitrogen	100	($\sim$ 25 l s^{-1})
Hydrogen	200	
Water Vapour	100	
Helium	30	

In the course of experiments the vacuum chamber normally reached $\sim 10^{-8}$ torr when there was no flow through the specimen. The main contaminant of the system was then hydrogen, evolved by outgassing from the system components especially the heated stainless steel tubulation in the furnace region.

3.1.2. Input Chamber

The input chamber was similar in construction to the detection chamber. Principal differences were the addition of ion and discharge device mounts and a multiplicity of pumping devices to allow streaming of gas.

Once more a low outgassing rate was required for purposes of maintaining gas purity, which was supposed to be that of the tank. The general construction was of stainless steel tubulation with electrical insulators of glass and quartz.

3.1.3. Other requirements.

Specimens were expensive and needed careful preparation so a reliable mounting was needed. Flanges with gold ring seals were chosen because

of their simplicity, convenience and reliability compared with the alternative of a welded support. High purity gold wire was cut to length and the ends welded, in a propane flame, to make a ring. The rings were then annealed to make them soft and a pair, with carefully matched diameters, chosen. The specimen was then sandwiched between the rings. This arrangement was then bolted between the end flanges of the two vacuum chambers, (see Fig.3.3). Alignment of the gold rings was critical, particularly with the thinner specimens, but a high fraction of seals were successful.

To heat the specimen an external furnace was used, partly for convenience, partly because of system constraints. A furnace could not be put inside the input chamber because of the ion injection system and it could not be put in the output chamber as it would raise the outgassing rate. The furnace temperature was controlled from a thermocouple placed in the furnace region, by a Viscount, three - term controller, able to control temperature to $\sim$ 0.1K. To ensure temperature uniformity, nickel plated copper blocks, of the same diameter as the flanges, were mounted around the vacuum tubes leading to the specimen flanges. These provided a region of roughly uniform temperature extending to about 10cm each side of the specimen and ensured both that, a high fraction of the gas atoms colliding with the specimen and δ the radiation to which the specimen was exposed, came from surfaces at approximately specimen temperature.

Experimental temperatures were measured using two Chromel/Alumel thermocouples. One thermocouple was placed in contact with the flange holding the specimen, its cold junction being a hot cell held at 42.5 ^{o}C. Initially the second thermocouple was placed in contact with the specimen surface, inside the vacuum, and connected to a 0^{o} C cold junction (Delresister I cell) via chromel and alumel electrical feed throughs. During the course of experiment close agreement was observed between the measurements from these thermocouples (within 1 K). Thus for convenience of vacuum chamber construction,

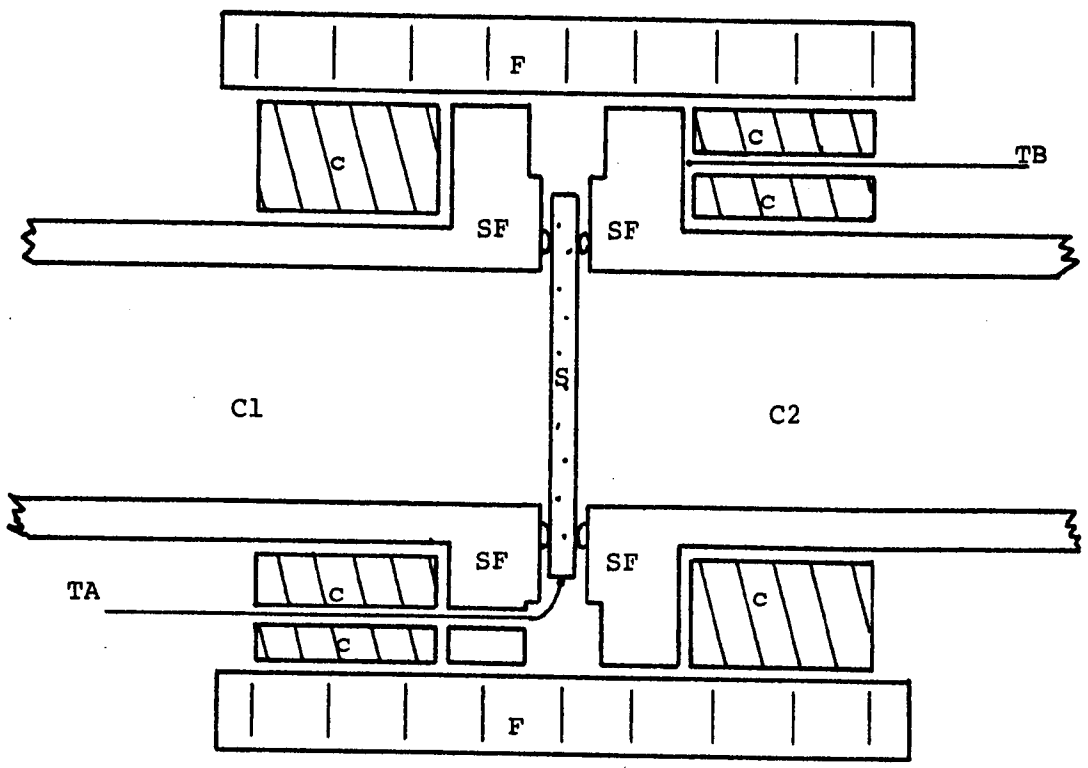

c. Copper Blocks
C1. Input Chamber
C2. Detection Chamber
F. Furnace element
SF. Stainless Steel flange.
TA. Thermocouple A
TB. Thermocouple B

Fig. 3.3 Sketch of: Specimen Mount,
Furnace Assembly and
Temperature measurement.

the second thermocouple was spot welded to the specimen surface just outside the gold ring seal in later work. Care was taken with temperature measurement and calibration checks of thermocouples were made regularly against a standard Pt/Pt Rh thermocouple. Precision of the temperature measurements varied with the voltmeter available. For most work a Solartron 3510 gave $\sim$ 0.1K precision but for some data uncertainties were $\sim$ 1K. Fortunately hydrogen diffusivities in metals have a low activation energy so uncertainties of this magnitude are not intolerable.

Rapid temperature changes were found, on occasion, to cause leaks at the gold vacuum seals. For this reason the temperature control system was provided with an electronic variable ramp generator which gave smooth temperature changes of about 25^{o}C per hour.

The maximum attainable temperature was limited by the materials properties of the specimen and sealing flanges. Although gold melts at 1300K and the softening of the stainless steel faces occurs in the range 1100K - 1700K, temperatures exceeding 1000K were never used. Infact with the specimen materials and thicknesses used, all experiments were performed at temperatures below 950K.

Ancillary equipment not used during the course of actual experiments involved: pirani and ion guages necessary in preparing for experiment; ultra high vacuum bakable valves, a fitted bake-out oven , not part of the chambers, but essential in establishing a vacuum with low levels of residual gas.

3.2. Gas Injection.

An early decision was to inject experimental gases into the specimens. For this purpose a series of discharges and ion guns was constructed. These injection devices were essential for work with helium and it was known

(42), that even the simple discharge devices could provide controllable gas input for experiments with hydrogen and deuterium. The gas flow induced by discharge injection through the specimen was typically a factor unity times the flow due to solution. This together with the low input gas pressures used, ~ 2 torr, meant that the experiments were performed with hydrogen/metal systems in the α phase. In α phase the concentration of hydrogen is low enough for hydrogen/hydrogen interactions to be neglected and the system can be treated as an ideal solid solution.

Initial experiments were with discharge devices; later ones used ion guns. The requirements on the ion gun were that a sufficient number of gas atoms traverse the specimen to give detection in the output chamber, and that the energy of the input beam be low enough not to heat the specimen surface to excess.

Figure 3.4 shows a typical discharge device. The simple construction, which led to initial use as an injection device, comprises a standard gold seal stainless steel flange with a glass envelope on one side through which passes, via a glass/metal seal, a single electrode. The electrode is supported by a quartz tube and to its end various anode designs may be connected. The widened tube at the tip of the discharge acted as a shroud directing the beam toward the specimen. The simplest anode used was a twist of wire, the most complicated involved a small stainless steel cup (~ 15 mm diameter) with holes in the bottom. All anodes were found to produce stable glow discharges in hydrogen, deuterium and helium under similar conditions of pressure, current and voltage. Using a specimen-anode separation of ~ 5mm, the working range was:

$$1 \text{ torr} \lesssim \text{pressure} \lesssim 15 \text{ torr}$$

$$1 \text{ mA} \lesssim \text{current} \lesssim 10 \text{ mA}$$

$$300 \text{ V} \lesssim \text{voltage} \lesssim 450 \text{ V}$$

Figure 3.5 illustrates the discharge characteristics at 2 and 5 torr

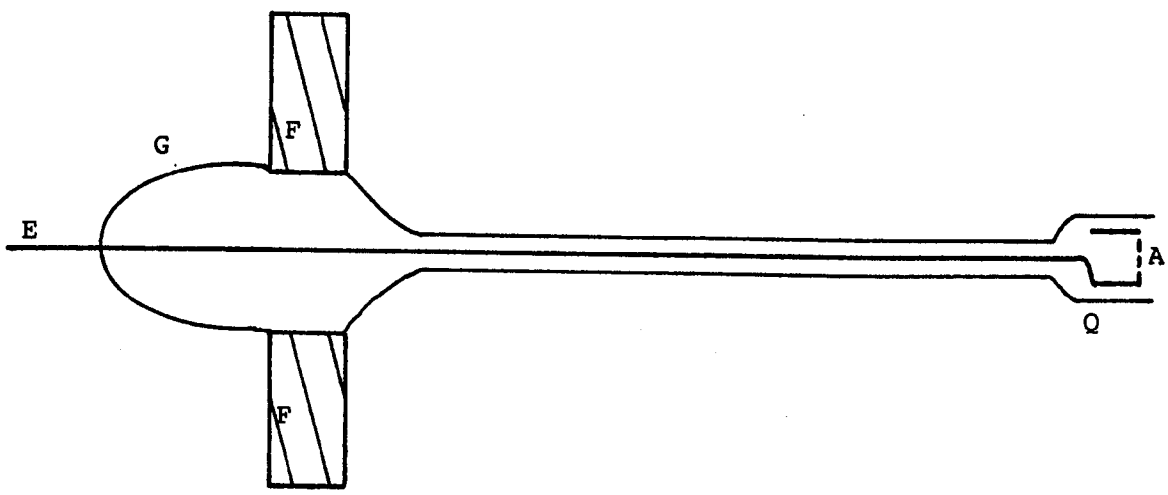

A. Anode
E. Electrical feedthrough
F. Flange
G. Glass envelope
Q. Quartz Shroud

Fig. 3.4 Discharge gun

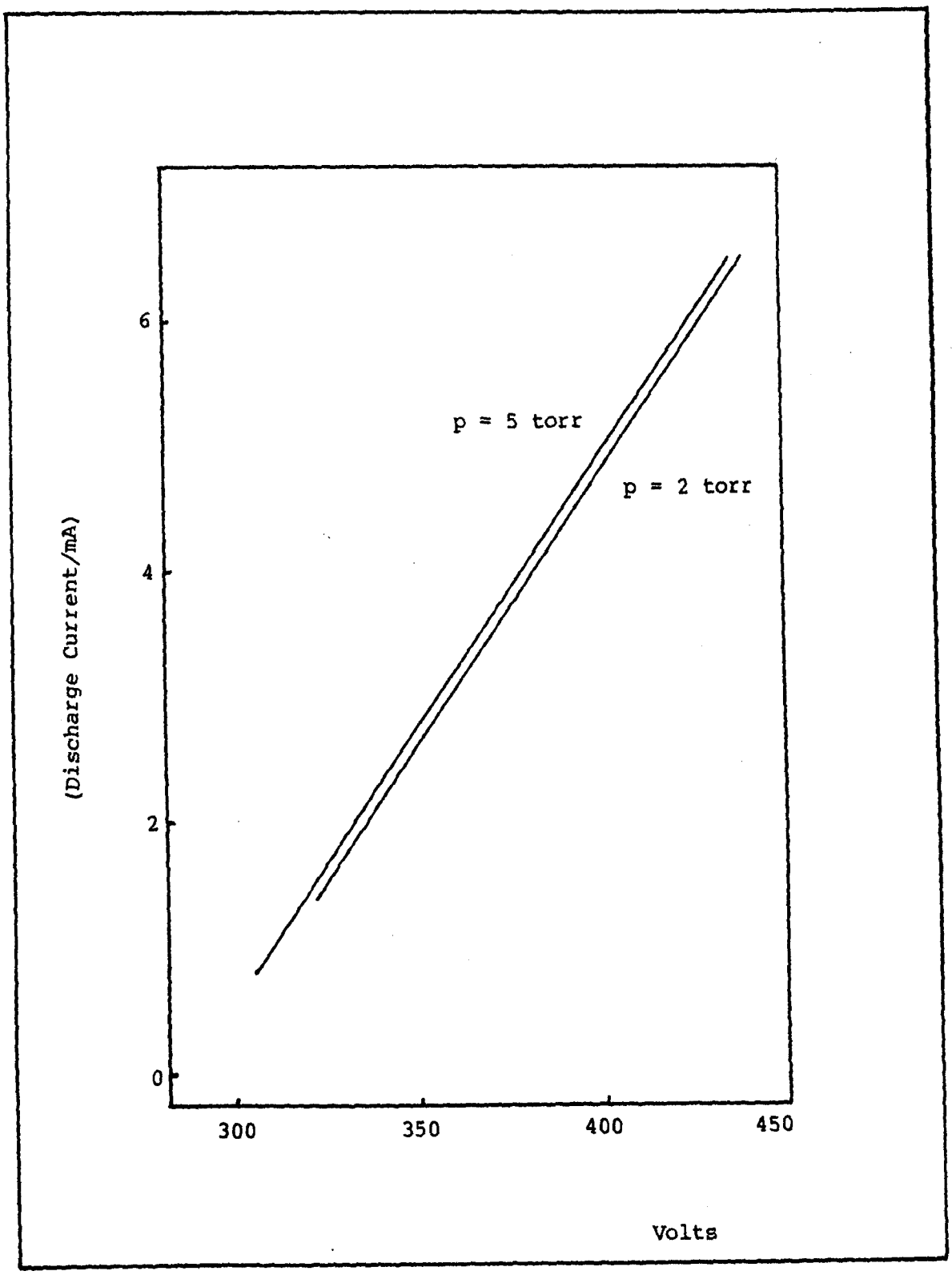

Fig. 3.5 Discharge gun characteristics at gas pressure 2 torr and 5 torr

Gas injection with a glow discharge was effective in experiments with hydrogen and deuterium, but it failed to satisfy the requirement of providing detection in the output chamber when used with helium. Numerous variations of operating conditions were used in the helium experiments, but any flow was consistently below the detection limit of $\sim 5 \times 10^{-9}$ torr litres s^{-1}.

The most reasonable explanation of the failure to observe helium flow seems to lie in the nature of the helium discharge. Even under the most advantageous operating conditions above, the mean free path between collisions for a particle in the discharge should be $\sim 2.5 \times 10^{-3}$cm. This particle moves in an electric field of upto ~ 900 V cm^{-1}. Thus a charged particle, such as an electron, can gain energy of only $\sim$ 2.25eV between collisions. Such modest energies can excite atoms and molecules but cannot ionize them; the first ionization energies of hydrogen and helium, for example, are $\sim$ 13eV and $\sim$ 24eV. Thus very few atoms will be ionized and those which are will have very little energy, perhaps 2eV, at impact. No more than monolayer penetration may be expected of them.

The helium glow discharge technique was not lightly abandoned. Several attempts were made to produce ions. Helium pressures were reduced to increase mean free paths; helium pressures well below that known to give stable discharge were used, in search of new pressure regions with discharge stability (such regions had been found for hydrogen). Next, the electric field strength was increased by reducing the specimen-anode separation.

For this purpose a stainless steel flexible bellows vacuum connection was used to support the discharge gun. By means of screws the specimen-anode separation could be adjusted, over the range 0 - 10mm, by known distances. In this way field strengths of ~ 9000 V cm^{-1} were set up, so with the given discharge conditions mean particle energies of $\sim$ 22.5eV

were anticipated. This is almost equal to the 24eV necessary for helium ionization, therefore ion production was expected.

No helium glow discharge ever produced a detectable output. Designs were therefore drawn up for the alternative injection device, the ion gun. Such a device permits direct measurement of the ion current and voltage, so input surface conditions are more tightly defined. The choice of input conditions is also much wider than with the discharge. In particular, energies of ~ 5keV, which are easily attainable, should give implantation to depths of 250-350 atomic layers below the metal surface,(37).

The design requirement for an ion gun are:

1) a vacuum giving mean free paths large relative to the gun-target separation.
2) a field geometry that will drive electrons along oscillatory paths long enough for electron/atom collision to be frequent and hence to give appreciable ion currents with a compact gun.
3) a confined region of major ion production leading to a restricted beam divergence and energy spectrum.
4) a device to allow measurement of ion currents.

and for the particular requirements of the present experiment.

5) a construction suitable for use at temperatures to 900K.

An early design consisted of three circular electrodes, an anode with two cathodes spaced symmetrically on either side. The anode had a central hole of ~ 5mm diameter, the cathodes had central holes of ~ 1mm diameter.

From the device symmetry, two equal ion beams were expected and requirement 4 could be satisfied by measuring the reverse beam ion current. Trials with this device showed it to be unstable at pressures low enough to give the required mean free paths. The ion beam currents, measured with a

Faraday cup collector, were also low ($\sim$ 1 μA) with acceleration potentials limited to $\sim$ 1keV.

Modifications of this design led eventually to a device similar to commercially available saddle field ion guns, Figure 3.6. This device satisfied the above specifications. With 1.5mm cathode aperture, it produced a divergent beam that would cover the specimen surface when mounted at a separation of $\sim$ 5cm. At this separation a gas pressure $\sim 10^{-3}$ torr was required to give an adequate mean free path and gas streaming had to be used to maintain gas purity. Streaming also cooled the gun, a consideration of some importance for sustained operation. Gun characteristics were:

gas pressure	$\sim 10^{-3}$ torr
minimum stable ion current, I_1	$\sim$ 20 μA
gun potential with I_1	$\sim$ 5.5kV
maximum sustainable ion current, I_2	$\sim$ 85 μA.
gun potential with I_2	$\sim$ 6.0kV

Overheating of the ion gun was a problem inherent to the experiment. The gun had to be operated at high temperatures and, because of the restricted geometry, it was of compact design. It had to be used furthermore in a vacuum. Actual power dissipation was modest, $\sim$ 15W for a beam of 140 μA at $\sim$ 7.2kV, but the local temperatures, especially for the anode, were high. Because standard high temperature ceramic insulators were not of suitable geometry, quartz tubing was used for electrical insulation. It proved adequate for sustained currents $\sim$ 100 μA but required periodic replacement.

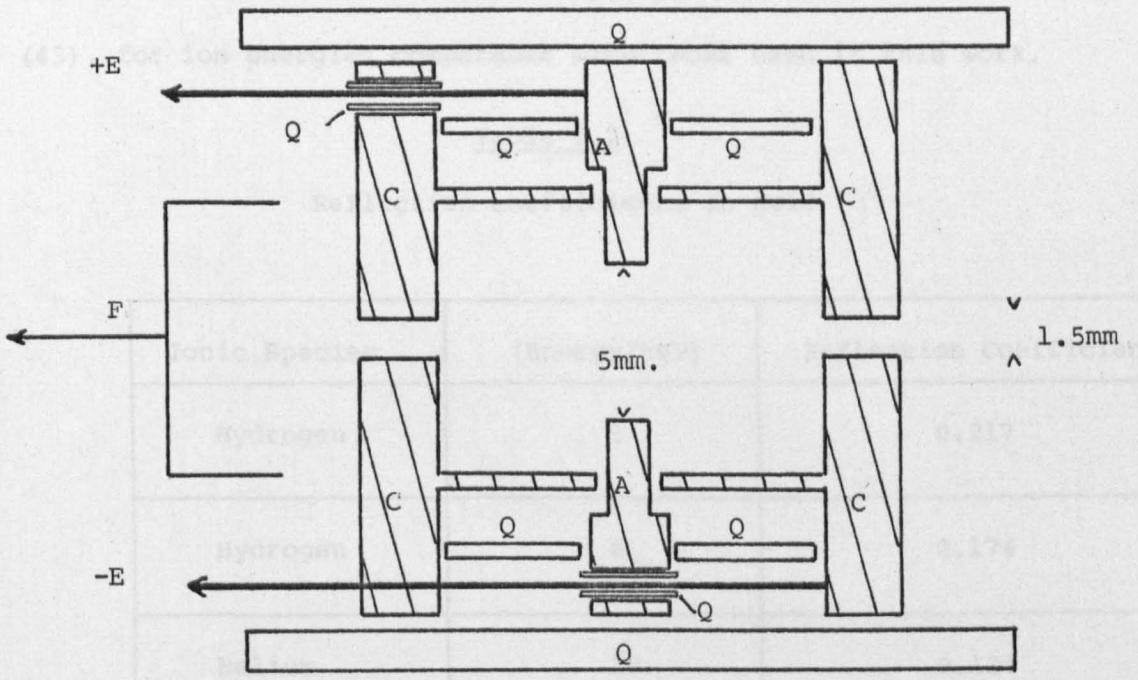

A. Anode
C. Cathode
-E. Negative electrical feed through
+E. Positive electrical feed through
F. Faraday Cup
Q. Quartz insulators

Fig. 3.6 Saddle field ion gun.

Although an ion beam current of ~ 100 μA was fired at the metal surface, notall of the ions in the beam were expected to penetrate. Table 3.2 gives the reflection coefficient of hydrogen and helium ions striking gold, (43), for ion energies comparable with those used in this work.

Table 3.2

Reflection coefficients in gold

Ionic Species	(Energy/keV)	Reflection Coefficient
Hydrogen	5	0.217
Hydrogen	8	0.174
Helium	10	0.134

Backscattering, at 5keV ion energies, is ~ 20% and hence not a major problem.

In conclusion the development of the ion gun extended the experimental possibilities for work with helium.

3.3. Detection systems

The requirement on the detection system was to allow comparison of two periodic fluctuations, one retarded relative to the other. The first fluctuation was produced by modulating the current of a H.T. supply, sinusoidally. This was measured directly from terminals on the supply unit and served as a reference signal since the gas injection rate was supposed proportional to the instantaneous discharge current. The second fluctuation was of gas flow and was measured indirectly by monitoring the gas pressure in the detection chamber. From knowledge of the time lag between the reference signal and the gas flow diffusion coefficients could be derived.

In some experiments ion gun injection was used, and ion currents were measured with the simple circuit shown in Figure 3.7. With this circuit the ion current corresponds to 10^4 μA per volt and was chosen as the reference signal.

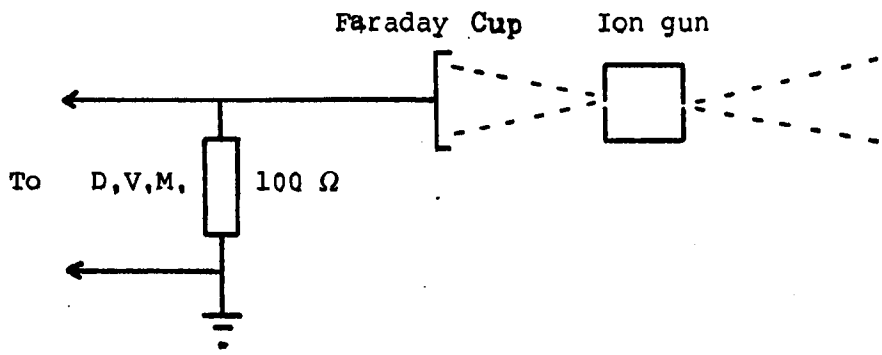

Fig. 3.7 Measurement of Ion current

Gas pressures in the detection chamber were measured with a V.G Micromass gas analyser with magnetic mass separation. A mass spectrometer was used because only experimental gas partial pressures were required, hence greater detection sensitivity was expected with this instrument. It had the following specifications:

Minimum detectable partial pressure	3×10^{-11} torr.
Maximum operating pressure	10^{-4} torr.
Selectable response time	0.3s or 2s.

To allow comparison of the two fluctuating signals it was necessary to measure their variation with time. The periodic nature of the signals simplified this requirement, and allowed signal averaging. The chosen method for following the signals in time used a multichannel averager, the Datalab DL 4000. This instrument had 1024 registers for data storage, with 12 bit precision in each register. Storage could be divided into 4, 256 register

channels, so that upto four inputs could be monitored at a time.

The Datalab DL4000 was restricted to inputs of $\pm$ 1V and had microsecond response, so the reference signal and mass spectrometer output had to be conditioned to suit the requirement of the instrument. A pair of matched amplifiers with d.c. offset capability and selectable integration times, in the range zero - 1s, were used.

Smoothing of the reference signal, which had a large high frequency noise component, was essential at this stage to avoid overload, so an integration time of $\sim$ 0.1s was used in this information line. It was matched in the mass spectrometer signal. Other unmatched contributions to the detection response time required correction.

Among these unmatched response times must be included the 300ms introduced by the mass spectrometer and already mentioned. Of possible greater significance, however, is the inherent response time of the detection chamber itself. This may be estimated as follows:

Consider the rate of change in the number of experimental gas molecules, N, in a detection chamber of volume V l. and pumped at the rate S l. s^{-1}, when the flux into the chamber is $J = J_o + J_1 e^{i\omega t}$

The equation relating time dependent terms is

$$\frac{dN}{dt} = J_1 e^{i\omega t} - S\frac{N}{V} \qquad (3.1)$$

Equation 3.1 solves to give for large t,

$$N = \frac{J_1 \exp\left(i(\omega t - \omega \frac{V}{S}) \right)}{\left| \frac{S}{V} + i\omega \right|} \qquad (3.2)$$

From equation 3.2 the response time is (V/S) s . With V $\sim$ 500cm^3 and

$S \sim 5 \times 10^4$ cm^3 s^{-1}, $(V/S) \sim 10^{-2}$s, which is small compared to the mass spectrometer contribution.

The flux/pressure measurement phase lag can be written as $\beta\omega$, where β represents the total response time of the detection system. Experimentally β may be evaluated by a pump down experiment.

To do this the valve, connecting the detection chamber to the pump, was shut allowing the chamber pressure to rise till a steady state was reached. Then the valve was suddenly opened and the change in detection chamber pressure was recorded on the multichannel averager, with the conditioning amplifier set to zero time constant.

Figure 3.8 shows the digital data, corresponding to detection chamber pressure, from the averager plotted as ln (pressure/arbitrary units) versus t. Only that portion of the pump down curve near the bottom is shown. From the figure it is clear the variation of pressure with time was not perfectly exponential. Near the bottom of the pump down curve, however, an exponential variation is a good approximation and $\beta \sim 0.3$s. As expected, the mass spectrometer response time dominated.

In experimental terms, β defines the effective upper limit of frequency that may be used. An estimate for this limit may be found as follows: suppose a typical measured phase is $\pi/6$, then if corrections due to response time are to be kept < 10%

$$\beta\omega \lesssim \pi/60$$

$$\therefore \quad \omega \lesssim 0.17 \text{ rad s}^{-1}$$

$$\therefore \quad \nu \lesssim \frac{0.17}{2\pi} = .028 \text{ Hz}$$

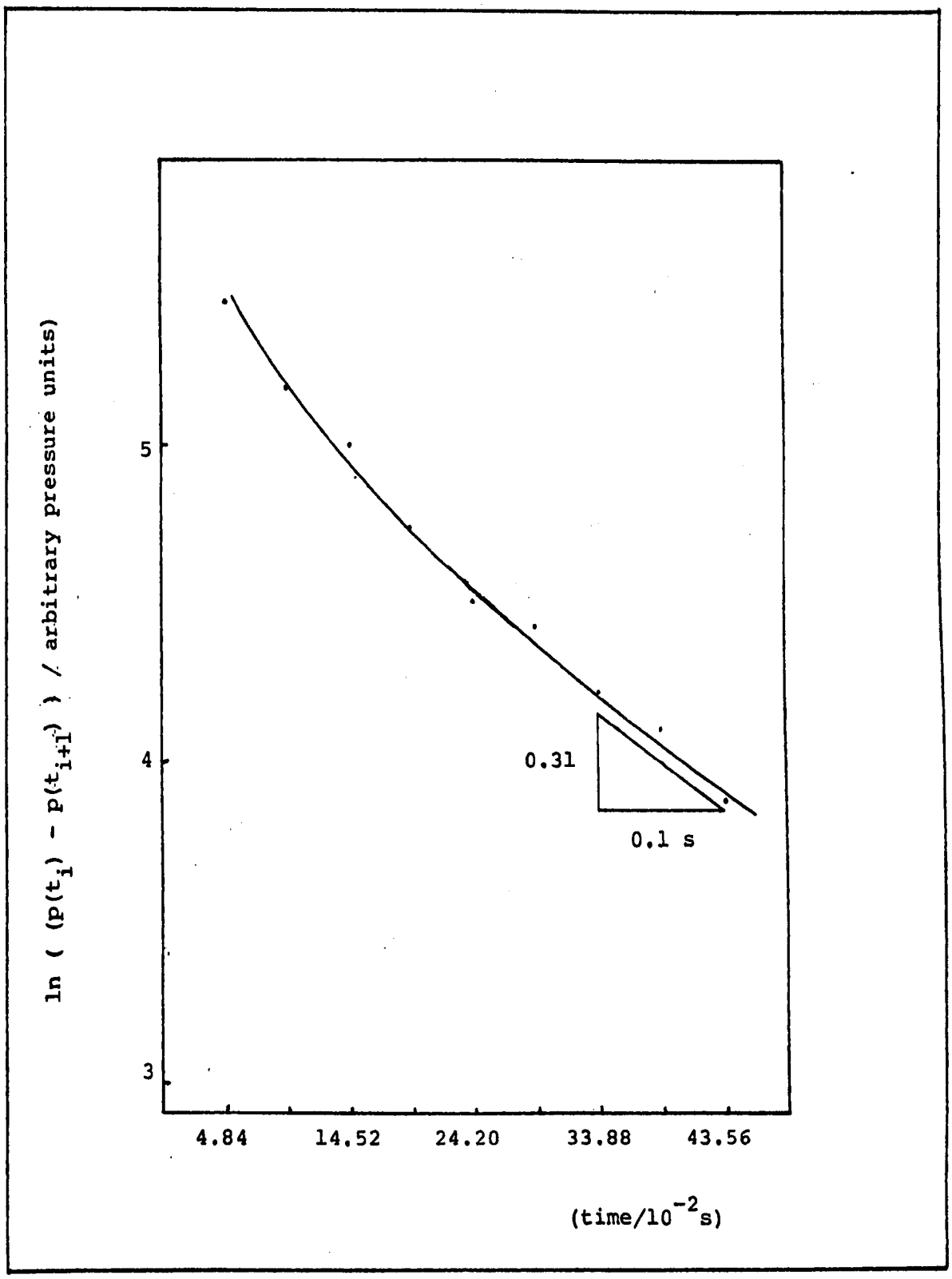

Fig. 3.8 Results of pump down experiment to evaluate β .

3.4. Experimental materials

Attempts were made to investigate six specimen materials, but details for only four of these will be discussed in this thesis. Problems with specimen mounting for the other two made experiments impossible. In consequence experiments were carried out using aluminium, gold, molybdenum and silver, but work on niobium and zirconium quickly dropped as possible experimental materials.

Specimen materials were supplied by Johnson - Matthey Ltd., and Goodfellow Metals Ltd.,. Those used were:

Silver: High Purity: Annealed: Grain Size ~ .1cm: Thickness 0.03cm to 0.06cm: Typical analysis: Cu 15 ppm, Pb 1 ppm.

Gold: High Purity: Annealed:
Thickness 0.025cm and 0.05cm: Typical Analysis: Ag 3 ppm, Pd 2ppm, (Cu, Fe, Mg) < 1 ppm.

Molybdenum: 99.9%: Annealed: Thickness 0.025cm: Typical analysis: Al 20ppm, Cu 20 ppm, Cr 50 ppm, Cu 20 ppm, Fe 50 ppm, K 2 ppm, Mg 20 ppm, Pb 30 ppm, Si 50 ppm, Ti 30 ppm, W 10 ppm, C 40 ppm, H 5 ppm, N 10 ppm, O 30 ppm.

Aluminium: 99.9%: Thickness 0.025 cm

Thicknesses were checked with a micrometer screwgauge and found not to vary significantly from the values quoted.

Mounting problems characterized the work with niobium and zirconium.

It was found with these metals that those areas of specimen surface outside the gold ring seals exposed to atmosphere, rapidly oxidized when heated. The oxidized region quickly extended, through the specimen, inside the gold rings causing a leak to atmosphere.

Aluminium also presented a problem to mount with gold rings, but it was found soft enough to seal between two flanges even without sealing rings.

With gold, molybdenum and silver, no particular mounting problems were experienced. In general the materials were prepared by first cutting out a circular specimen to the right size from a sheet. The specimen surfaces were then polished with 0.3 micron γ - Alumina on a Selvyt cloth washed in detergent, shaken ultrasonically in acetone and finally rinsed in distilled water, dried and immediately mounted in vacuum.

Aluminium was once again the exception. This was chemically polished with a solution of 5% concentrated nitric acid, 25% concentrated sulphuric acid and 70% concentrated orthophosphoric acid at 85^{o}C for 50 seconds. The percentages are by volume. The specimen was then rinsed in distilled water dried and immediately mounted in vacuum.

The experimental gases were hydrogen, deuterium and helium. All gases were research grade and supplied by B.O.C.

3.5. Data handling

In this experiment the central measurements were the time variations of injection current and output pressure. Ancillary measurements were also needed for setting up and maintaining experimental conditions. These included temperature and input and output chamber pressures.

The initial decision, to use periodic fluctuations, was made with the prospect of improved data handling by signal averaging on a signal of precisely known profile, giving improvement in signal to noise ratio. Sinusoidal fluctuations were chosen, because they are eigenfunctions of the diffusion equation time dependence and Fourier analysis could be used.

Data was pre-conditioned to match the ± 1V capability of the DL 4000 signal averager using matched amplifiers with selectable integration times, d.c. offsets, amplification in the range x1 - x1000. It was then fed to the averager in parallel streams.

In single channel operation, measurements taken sequentially at the input are stored in successive registers, the interval between successive measurements being set by clock pulses which may be generated either internally or externally. After completing a sequence of 1024 measurements the sequence begins again, new data for each register being added to the data already in that register. Both the time interval between measurements (down to 10^{-6}s) and the number of measurement sequences (2^{0} - 2^{20}) may be chosen. When read, the averager presents data in normalised form; that is, a full 12- bit register always shows as precisely ± 1V .

In the present work signals varied sinusoidally in time, so the averaging sequence was set to have the same period as the incoming signal. Because two signals were being compared however, the registers were split into four bands of 256, each connected to one of four inputs. In this mode of operation data for input 1 was stored in registers 1, 5, 9, ..., for input 2 in 2, 6, 10,....., and so on. The averaging sequence in other respects was similar to that for single channel operation.

Data extracted for analysis was subject to an inherent phase error equivalent to 1/256 of a cyle because of the sequential system of phase

measurement. Observations were not of sufficient precision to merit making the appropriate phase correction.

Information collected and stored by the signal averager was analysed to determine the signal phase with respect to a cosine function. This was done in a microprocessor using a Fourier analysis programe. The microprocessor used, a Triton micro-computor, was fast enough to allow analysis during data collection. It was possible therefore to determine when further averaging was pointless by tracing the computed phase value as the averaging sequence progressed.

As a measure of signal to noise ratio the computed amplitude of the fundamental component in the signal was compared with those of the first five harmonics. After averaging, the harmonics were found always to be $< 10\%$ of the fundamental and were normally $< 5\%$ in the mid-high temperature range of an experiment.

The accuracy of this data handling method was investigated at an early stage of this work, by feeding the data handling system with sinusoidal signals from a signal generator. Signal phases, in all four quadrants in the range $0-2\pi$, determined by the microprocessor, were compared with the phase determined by finding the channel number corresponding to a peak. The phases found using the two methods were within $\pm$ 0.01 radians which corresponds to the limit of accuracy for measurement made by finding the signal peak $\sim \pi/256$. Another test was made in which the averager was programmed to be triggered by a pulse from the signal generator. Signals stored in this way have zero or π phase. The measured phases were found to be within $\pm$ 0.005 rad. of zero and π.

A separate test was made to confirm that the analysis programme was proof against noise in the signal. A perfect sinusoidal signal was

degraded by the addition of first and second harmonics with amplitudes upto 25% of the fundamental. Noise from the mass spectrometer output was amplified to ~ 10% of the fundamental amplitude and also added. On analysis the difference in phase between the perfect and degraded signals was within ± 0.02 radians, therefore this represents the expected error in phase determination.

Amongst the ancillary measurements made, it was noted that the detection chamber background pressure drifted during the course of an experiment. Such a drift introduces a systematic error to phase measurement, so the phase analysis was programmed to determine the drift and correct for it. The slow rate of change of drifts meant they could be approximated by an apparent mean background pressure p varying linearly with time t:

$$p = a + bt \qquad (3.3)$$

To use this equation, the parameter, a, was determined from the mean of the signal averager data and b, by making a regressive least squares fit on the data for p = b×(register number - 128), after correction for a. When b had been evaluated it was used to correct the signal averager data for drift. The magnitude of b relative to signal amplitudes was monitored to ensure 256b less than 10% of the signal amplitude, hence keeping corrections small.

3.6 Operation

The experimental technique made data gathering and data handling simple, as the following step by step description should make clear.

3.6.1. Preparatory work

Routine preparation of the experimental chambers began with remachining of the flanges supporting the specimen, degreasing and baking.

Specimens were prepared as described in section 3.4. They were

then mounted, after the shortest possible interval, in the double vacuum rig.

Initial vacuum chamber residual gas pressures were rather high. The residual gas spectrum was routinely measured, Table 3.4 gives a typical prebake gas analysis.

Table 3.4

Typical prebake residual gas analysis

Mass	Partial Pressure/torr
2	1×10^{-7}
18	2×10^{-6}
28	4.5×10^{-7}
44	4×10^{-7}
56	2×10^{-7}

Masses 2, 18, 28, 44 and 56 correspond to hydrogen, water, nitrogen or carbon monoxide, carbon dioxide and pump oils (from initial rough pumping) respectively. The main vacuum contaminant at the prebake stage was normally water vapour.

Such a vacuum is not suitable for sensitive detection of small pressure fluctuations, nor is the contact of so much water vapour with a hot metal surface desirable. For these reasons the entire vacuum system was baked in a custom built aluminium box, the oven, using four electrical heating elements, each rated at 600W. The oven temperature was raised to 450K.

Sometimes it was necessary to bake the ion pumps as well. Then, both input and output vacuum systems were independently pumped by U.H.V. diffusion pumps. These pumps used modern low vapour pressure oils and were equipped with liquid nitrogen cold traps. Both pumps could produce a vacuum of $\sim 10^{-8}$ torr; with the one used to pump the detection chamber, pressures

of $\sim 10^{-10}$ torr were commonly observed.

Baking of the vacuum system initially caused a rise in pressure as the outgas rate from the chamber walls rose. The pressure remained high $\sim 10^{-5}$ torr, for several hours; this was followed by a gentle, exponential like drop. Outgassing was usually performed over a weekend, giving sufficient outgas time without wasting research time.

During outgas, the specimen temperature was raised, by use of the furnace, to the midway point of the expected working region. Molybdenum was an exception. The thermochemistry of its oxide is such that it sublimes above 970K (44). So molybdenum specimens were heated to $\sim$ 1000K and the temperature returned to the working range after outgas.

All temperature changes of specimens were performed gradually using a clock driven voltage ramp to control the temperature controller, giving temperature change rates of $\sim$ 100K per hour. Experience in early experiments with silver showed this to be a useful procedure in reducing the risk of specimen leaks due to differential expansion.

When outgas was over the oven was removed and the vacuum equipment left to cool before the plastic coated leads, mass spectrometer magnet etc., removed for their protection, were replaced. The mass spectrometer mass alignment was checked, adjusted and the detection chamber checked for leaks by monitoring mass four and squirting helium at the flanges. Another residual gas spectrum was then taken. Table 3.5 gives a typical post-bake gas analysis and may be seen that baking considerably improves vacuum.

Table 3.5

Typical post-bake detection chamber residual gas analysis

Mass	Partial Pressure/torr
2	1×10^{-8}
18	2×10^{-9}
28	3×10^{-9}
44	1×10^{-9}
56	2×10^{-9}

3.6.2. Running of experiments

A typical experiment usually began in the evening with the temperature clock set to ramp the temperature by about 25K over a period of an hour. Overnight any transients due to this change would decay.

The detection chamber was continuously pumped by an ion pump, which had the advantage over the diffusion pumps of not needing replenishment with liquid nitrogen.

An additional advantage, discovered during the course of experiment, was that ion pumps have a constant pump rate for hydrogen whereas the U.H.V. diffusion pumps available did not, giving instead almost periodic fluctuations (saw tooth $\sim 2 \times 10^{-9}$ torr amplitude, $\sim$ 1000s. period).

A fresh charge of experimental gas was used for each daily run. Overnight, the input chamber was ion pumped to a residual pressure of $\sim 10^{-7}$ torr, mostly hydrogen, while the inlet system was pumped with an U.H.V.

diffusion pump to a similar pressure. In the morning the pumps were isolated and gas allowed to stream into the inlet chamber until a stable discharge was established. The gas pressure was then ~ 1.8 torr. The input chamber was then isolated from the inlet system by shutting the U.H.V. valve. The inlet system was isolated from the cylinder and pumped down again.

Experimental gas now permeated, from the input chamber, through the metal specimen, into the detection chamber, by the two processes of solution and injection at the input surface of the metal. A typical discharge current would be 3mA plus 0.5mA amplitude, sinusoidal modulation, driven by a signal generator at a selected frequency of ~ 10^{-2}Hz.

The amplitude of the fluctuations in the detection chamber pressure due to the modulation at the input depends on; the amplitude of the discharge current modulation; the metal and the temperature. Therefore the most sensitive usable mass spectrometer scale was selected and the amplification and d.c. offset of the ancillary amplifiers adjusted to produce an output compatable with the required signal averager input.

The output from the H.T. supply corresponding to the discharge current was conditioned in a similar way. This signal was rather noisy so a 0.1s integration time was used to smooth it and improve signal to noise ratio. This integration time was matched in the mass spectrometer signal.

The two signals, due to modulation of discharge current at the input surface and the modulation of the flux at the output surface were fed into the signal averager. This machine was usually used in a mode where individual registers were timed by an internal clock but averaging sweeps were initiated by an external pulse coming from the signal generator driving the modulation.

The data in the signal averager memory was displayed in analog form on a C.R.O. so at all times the progress of the experiment was monitored visually. This provided a rapid and good check on the signal to noise ratio. A hard copy of events was also recorded on a chart recorder and pressure drifts and signal spikes due to external events like lightning storms etc., were observed. Drifts were approximated to linear gradients and their effect on measurement neutralised during phase analysis. Signal spikes were usually disastrous in their effect and the signal averager memory was cleared and the experiment started again.

From analysis of the data stored in the individual channels of the averager it was possible to evaluate the relative phase of the output flux with respect to the injection current and the signal amplitude. If an input pressure modulation experiment had been performed, rather than using gas injection, the amplitude data could have been used to determine solubilities. As it was, in the present experiment amplitudes were of little use. The analysis also provided a listing of the amplitude and phase for the first five harmonics. These were of small enough amplitude to neglect. Such measurements were repeated over a range of modulation frequencies, usually taking a day of experiment. It was therefore usual practise to reperform measurements made in the morning, later in the day to check for specimen degradation.

The final measurement made, was to check the temperature again. The experiment cycle would then begin once more.

From the phase lag versus frequency results the diffusion coefficient at the selected temperature was derived. This was done by performing, with the aid of the microcomputer, a regression fit of the observed with the theoretically expected results. This completed the experiment.

SUMMARY

In conclusion, equipment was designed and assembled that allowed the following to be done:

1) Support experimental foils of thickness 0.1mm - 1mm
2) Maintain temperatures in the range 300 - 1200K
3) Control experimental gas pressures in the ranges
   10^{-7}torr - tank pressure for the input
   10^{-10} - 10^{-4}torr for the output.
4) Modulate input of gas at the front surface at a range of frequencies down to 10^{-4} Hz.
5) Detect fluctuations in the output experimental gas partial pressure, down to $\sim 10^{-11}$ torr corresponding to a flux of $\sim 5 \times 10^{-10}$ torr litres s^{-1}
6) Signal average
7) Estimate relative phase, and to do this accurately for modulation frequencies upto $\sim 3 \times 10^{-2}$ Hz.

Hence it was expected that diffusion coefficient measurements could be made down to 10^{-8} cm^2 s^{-1}.

CHAPTER FOUR

MATHEMATICAL MODELS OF THE PERMEATION PROCESS

Chapter 3 describes a sensitive detection and data handling system. The data this system produces requires analysis in terms of a model for permeation through a metal foil. This model must have three facets to separate and deal with effects arising at the input surface, in the volume of the material and at the output surface.

Permeation flows have been described extensively, (45), but mainly in response to boundary conditions which are fixed or which suffer a step change and are fixed thereafter. In combination with these static boundary conditions, fluxes are often supposed rate limited entirely by the process of diffusion, surface processes being taken as extremely rapid. Attempts to treat surface process (46, 47) fully, add greatly to the complexity of the analysis.

For present purposes periodic boundary conditions are a central requirement. In what follows these conditions will be used in combination with particular suppositions for the surface conditions, the intention being to separate the overall process of permeation into the transfer of atoms between the input surface, volume and output surface.

The aim of the analysis which follows is two fold: to allow the interpretation of experimental periodic permeation fluxes in terms of diffusion coefficients: to explore the possibility of using such fluxes to describe surface behaviour.

4.1. The process of permeation

For a diatomic gas like hydrogen, Fast (48), (49), has proposed that permeation through a metal membrane generally consists of five fundamental processes. These are shown diagrammatically in Figure 4.1, which represents the spatial variation of the potential energy of a hydrogen atom as it moves from a molecular gas phase, in the input side, through the surface layer of a

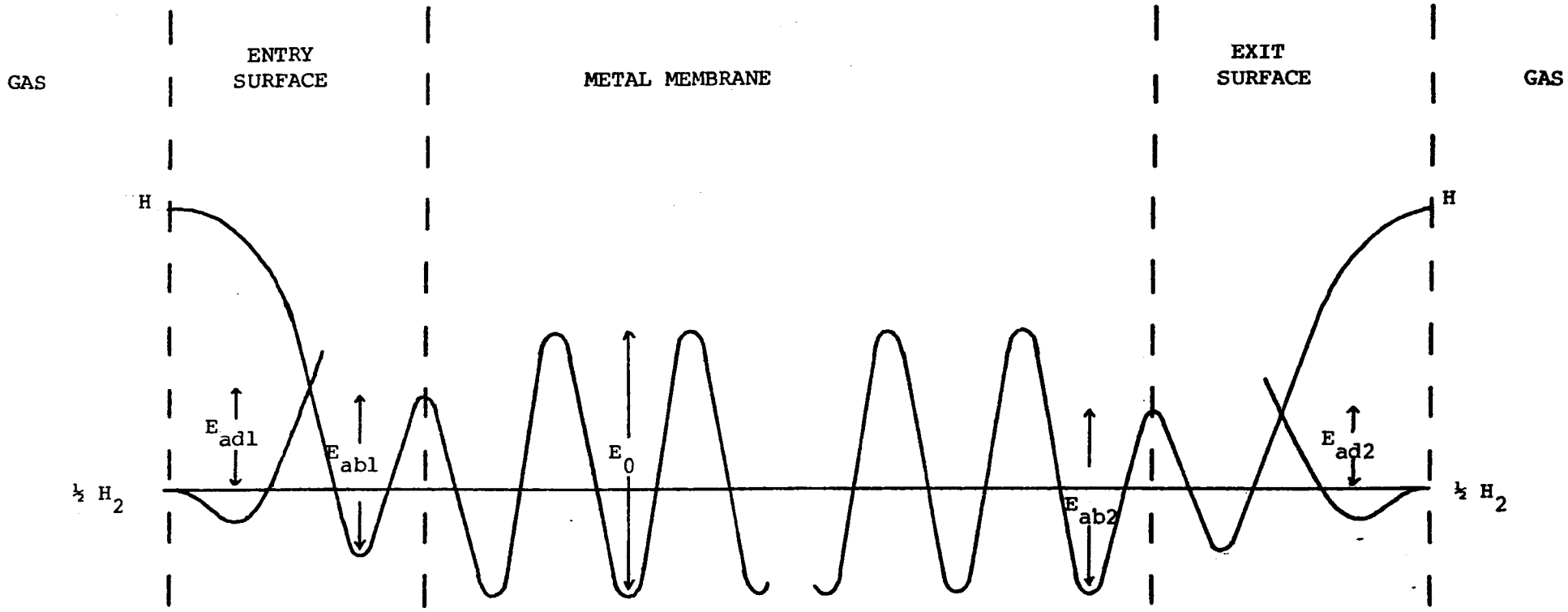

Fig. 4.1 Schematic representation of hydrogen atom interaction with a metal membrane by means of a potential curve. (Refer to text for details of the parameters).

metallic membrane, into the body and then out through another surface layer and into the gas phase in the output side.

The processes involved are:

1) adsorption; a hydrogen molecule impinging on the surface of entry becomes bound to it. Binding may be due to comparatively weak physical forces like molecular or van der Waals forces which retain molecular structure. Alternatively, it may be chemical in which case the molecule is split into two atoms each independently attached to the metal surface as an adatom by a chemical bond. Consequently, physical adsorption is a non-activated process while chemisorption requires an activation energy, denoted here by E_{adl}.

2) transition; hydrogen adatoms transfer from the adsorbed surface state to the absorbed state just inside the metal. This transition is described in the figure in terms of the activation energy E_{abl}.

3) diffusion; dissolved hydrogen atoms move through the metal lattice with a random or diffusive motion. Each step of this motion requires an activation energy, E_o. After many such steps permeating hydrogen atoms may finally come within the zone of influence of the exit surface.

4) reverse transition; dissolved hydrogen atoms just inside the exit surface undergo the inverse of 2) perhaps with a different activation energy E_{ab2}.

5) desorption; two hydrogen adatoms on the exit surface combine and desorb into the output side of the membrane with an

activation energy E_{ad2}. This energy can be taken as equal to E_{ad1} if the surface conditions of both the entry and exit surfaces are identical.

The above processes occur at rates which vary widely and differently with temperature. Except in complicated circumstances, where coupling among these processes occurs, the overall permeation rate can be seen as determined by the slowest of these five fundamental processes.

If diffusion is the rate controlling process, all the phase boundary processes above, are fast compared with that process. Consequently the concentration of dissolved hydrogen just inside the surface of the membrane will be close to equilibrium concentration appropriate to the gas pressure.

For present purposes the need is for macroscopic equations describing gas flow in a manner consistent with the above atomic model. Separate models will be used for the input surface, the volume and the output surface. Suitable defining equations will now be considered which trace the macroscopic flow of gas in its passage through the solid.

Flow will be supposed to take place through a membrane whose input surface is located in the plane $x = 0$ and exit surface in the plane $x = L$. Concentrations, atomic per unit volume in the solid, at x and time t, will be denoted by $N^*(x,t)$. Corresponding fluxes, atomic per unit area time, will be denoted $J^*(x,t)$.

$$N^*(x,t) = (\bar{N}(x) + N(x,t)) \text{ (atoms cm}^{-3})$$

$$J^*(x,t) = (\bar{J}(x) + J(x,t)) \text{ (atoms cm}^{-2}\text{ s}^{-1})$$

Here $\bar{N}(x)$ is the mean volume concentration, $N(x,t)$ the modulation of the volume concentration. $\bar{J}(x)$ is the mean flux in the volume and $J(x,t)$ is the modulation of the volume flux.

Associated with the volume flow will be input and exit flows, $J_i^*(t)$ and $J_e^*(t)$, and input and exit surface concentrations, $N_i^*(t)$ and $N_e^*(t)$. Thus,

$$N_i^*(t) = (\bar{N}_i + N_i(t)) \qquad \text{(atoms cm}^{-2}\text{)}$$

$$J_i^*(t) = (\bar{J}_i + J_i(t)) \qquad \text{(atoms cm}^{-2}\text{ s}^{-1}\text{)}$$

where $\bar{N}_i$ is the mean input surface concentration, $N_i(t)$ is the modulation of the input surface concentration. $\bar{J}_i$ is the mean input surface flux and $J_i(t)$ is the modulation of the input surface flux. Also,

$$N_e^*(t) = (\bar{N}_e + N_e(t)) \qquad \text{(atoms cm}^{-2}\text{)}$$

$$J_e^*(t) = (\bar{J}_e + J_e(t)) \qquad \text{(atoms cm}^{-2}\text{ s}^{-1}\text{)}$$

where $\bar{N}_e$ is the mean exit surface concentration, $N_e(t)$ is the modulation of the exit surface concentration. $\bar{J}_e$ is the mean exit surface flux and $J_e(t)$ is the modulation of the exit surface flux.

4.1.1. Input surface

At the input surface gas molecules arrive on the surface, adhere, split into atoms and then enter into solution. This will be modelled by introducing the additional surfaces $x = 0_-$ and $x = 0_+$ just outside and just inside the material.

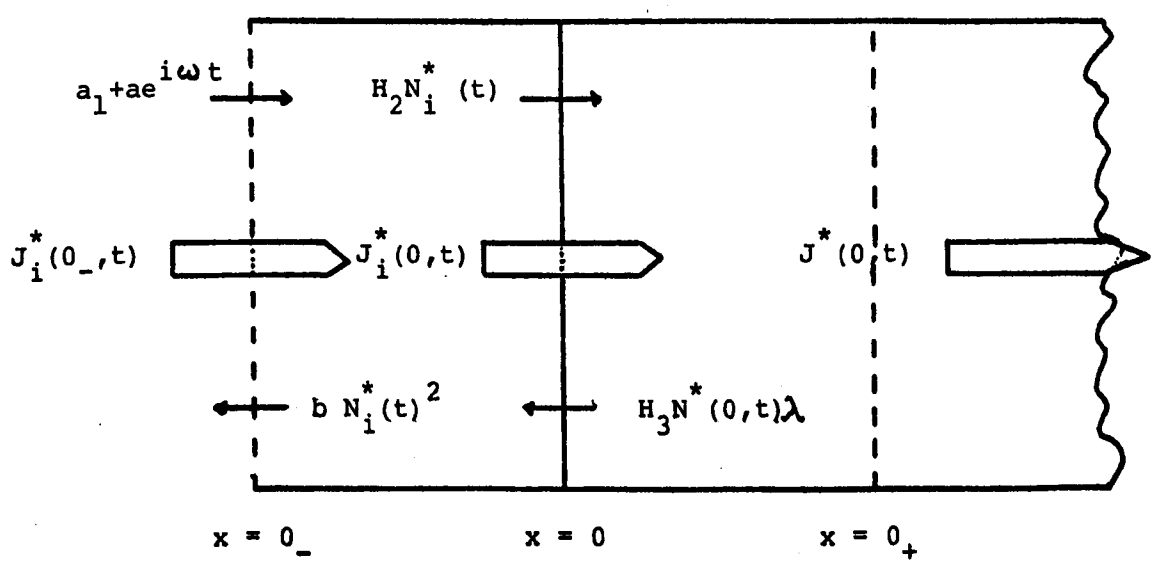

Fig. 4.2. Macroscopic model of the input surface.

Flows through these surfaces will be represented, as shown in Figure 4.2, in the following way:

1) at $x = 0_-$; the flow of gas molecules onto the surface and into a bound condition on it is represented by

$$a_1 + a\, e^{i\omega t} \qquad \text{(molecules cm}^{-2}\text{ s}^{-1}\text{)}$$

The reverse flow is represented by

$$b\, N_i^*(t)^2 \qquad \text{(molecules cm}^{-2}\text{ s}^{-1}\text{)}$$

(N.B. the reverse flow rate is taken as proportional to $N_1^*(t)^2$ in accordance with the chemical reaction:

$$H + H \longrightarrow H_2)$$

The net flow onto the surface is represented by

$$J_i^*(0_-,t) = (a_1 + ae^{i\omega t} - bN_i^*(t)^2) \text{ (molecules cm}^{-2}\text{ s}^{-1}\text{)} \qquad (4.1.)$$

2) at $x = 0$; the flow of gas atoms from the adsorbed surface state to the absorbed surface state just inside the metal surface is represented by

$$H_2 N_i^*(t) \qquad \text{(atoms cm}^{-2}\text{ s}^{-1}\text{)}$$

To model the reverse flow, first note that only atoms within a distance of order the lattice parameter inside the surface are available to move from the absorbed to the adsorbed state denote this distance λ. Then $N^*(0,t)\lambda$ atoms are available for the transition and such transitions take place at a rate such that the flow is

$$H_3 N^*(0)\lambda \qquad \text{(atoms cm}^{-2}\text{ s}^{-1}\text{)}$$

The net flow across the surface at $x = 0$ is then

$$J_i^*(0,t) = (H_2 N_i^*(t) - H_3 N^*(0,t)\lambda) \text{ (atoms cm}^{-2}\text{ s}^{-1}\text{)}$$

3) at $x = 0$; the net flow of atoms is represented by $J^*(0,t)$, the macroscopic flux $J^*(x,t)$, at $x = 0$, in the volume.

4.1.2. Solid volume

Atomic motion in a solid is commonly supposed to follow a random

path, (perhaps with the complication that particular lattice sites may act as traps for particular species). Macroscopically this motion is modelled by Ficks equation, which in one dimension, gives the flux as

$$J^*(x,t) = -D \frac{\partial N^*(x,t)}{\partial x} \qquad \text{(atoms cm}^{-2}\text{ s}^{-1}\text{)} \quad (4.3)$$

where D is the diffusion coefficient. For present purposes it will be supposed that this equation gives an adequate description of flow in the solid and the question of trapping will be ignored.

4.1.3. Output Surface

Flow at the output surface may be described as follows: Atoms in solution reach the output surface and there they are supposed to follow a random path until they eventually meet other atoms, recombine and leave the surface as gas molecules. This will be modelled by introducing the additional surfaces at $x = L_-$ and $x = L_+$, just inside and just outside the material.

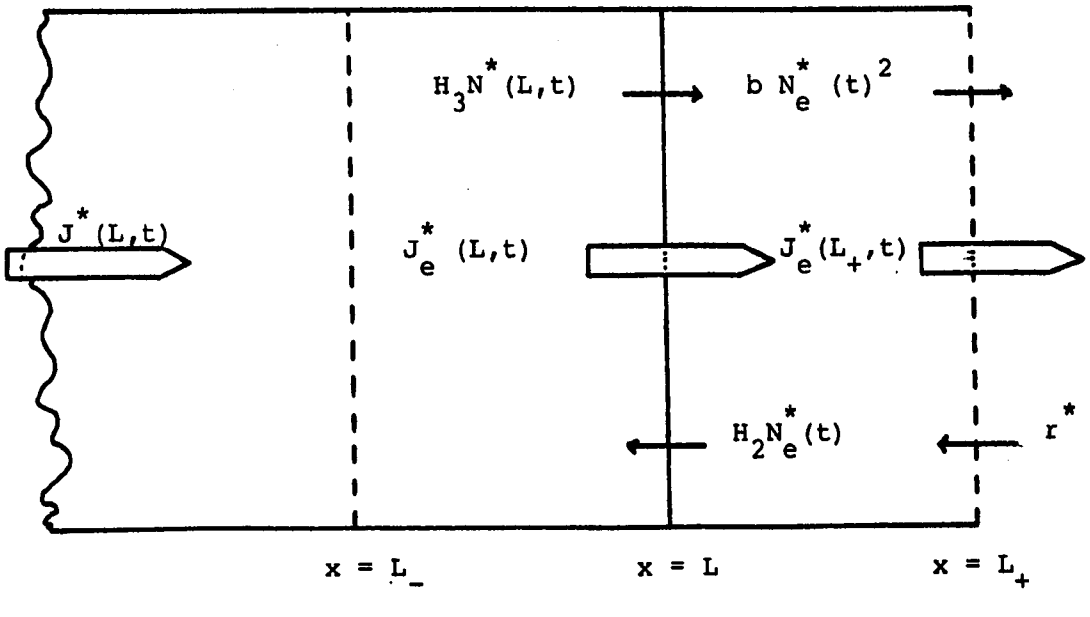

Fig. 4.3. Macroscopic model of the output surface.

Flows through the exit surface will be represented, as shown in Figure 4.3, in the following way:

1) at $x = L_-$, the net flow of atoms is represented by $J^*(L,t)$, the

macroscopic flux $J^*(x,t)$ at $x = L$, in the volume.

2) at $x = L$; the flow of gas atoms from the adsorbed surface state to the absorbed surface state just inside the metal, is represented by

$$H_2N_e^*(t) \qquad \text{(atoms cm}^{-2}\text{ s}^{-1}\text{)}$$

The reverse flow will be represented by

$$H_3N^*(L,t)\lambda \qquad \text{(atoms cm}^{-2}\text{ s}^{-1}\text{)}$$

where λ is the parameter of dimension length introduced in section 4.1.1. The net flow across the surface at $x = L$ is

$$J_e^*(L,t) = (H_3N^*(L,t)\lambda - H_2N_e^*(t)) \text{ (atoms cm}^{-2}\text{ s}^{-1}\text{)} \quad (4.4)$$

3) at $x = L_+$; the flow of gas molecules off the exit surface due to recombination is represented by

$$bN_e^*(t)^2 \qquad \text{(molecules cm}^{-2}\text{s}^{-1}\text{)}$$

The reverse flow of molecules onto the exit surface from the gas in the detection chamber is represented by

$$r^* \qquad \text{(molecules cm}^{-2}\text{s}^{-1}\text{)}$$

The net flow of molecules across the surface $x = L_+$ is

$$J_e^*(L_+,t) = (b\,N_e^*(t)^2 - r^*) \text{ (molecules cm}^{-2}\text{s}^{-1}\text{)} \quad (4.5)$$

Before proceeding with the calculation of flux into the detection chamber, based on the above model, it may be useful to list clearly the meaning of the symbols used so far, see Table 4.1.

Table 4.1.

Nomenclature

1) All concentrations are represented by the symbol N. The total concentration is written with an asterisk, the mean concentration is written with a bar and the modulation of the concentration is written simply as N. Therefore

$$N^* = \bar{N} + N$$

2) Surface concentrations are written with the suffixes e and i, so the total input and exit concentrations are written as $N_i^*(t)$ and $N_e^*(t)$ respectively

and have dimensions; atoms/(Length)^2. The total volume concentration is written as $N^*(x,t)$ and has dimensions; atoms /(Length)^3.

3) All net fluxes are represented by the symbol J and the same convention, introduced to describe concentrations, is used for total, mean and modulation parts. Thus the total net flux is

$$J^* = \bar{J} + J$$

4) For purposes of modelling, subsidiary surfaces are associated with the input and exit surfaces. The total net fluxes across the surfaces are written as

$J_i^*(0_-,t)$: total flux across the input surface at $x = 0_-$.

$J_i^*(0,t)$: total flux across the input surface at $x = 0$

$J_e^*(L,t)$: total flux across the exit surface at $x = L$

$J_e^*(L_+,t)$: total flux across the exit surface at $x = L_+$

5) The volume total flux is written as

$J^*(x,t)$

6) All rate constants are denoted by the symbol H and have dimensions; $(\text{time})^{-1}$.

4.2 Calculation of phases and amplitudes.

To determine the diffusion coefficients, the most important quantity in the analysis is the phase of the flux emerging from the exit surface, $J_e^*(L_+,t)$, relative to the driving variable. This is labelled ϕ_{Total}

$$\phi_{Total} = \phi_i + \phi_v + \phi_e$$

where the total phase has been reduced to the sum of three terms, the input surface, the volume and the exit surface phases. These terms will be investigated separately in the hope that the nature of surface behaviour may be revealed for the above permeation model.

4.2.1. The boundary conditions.

The equations governing permeation for the above model are derived

as follows:

1) Applying conservation of gas atoms to the region $0_- < x < 0$ gives

$$\frac{dN_i^*(t)}{dt} = J_i^*(0_-,t) - J_i^*(0,t)$$

so on substitution from equations 4.1 and 4.2

$$\frac{dN_i^*(t)}{dt} = a_1 + ae^{i\omega t} + H_3N^*(0,t)\lambda - bN_i^*(t)^2 - H_2N_i^*(t) \tag{4.6}$$

2) Applying conservation of gas atoms to the region $0 < x < 0_+$ gives

$$\frac{dN^*(0,t)\lambda}{dt} = J_i^*(0,t) - J^*(0,t)$$

so on substitution from equation 4.2

$$\frac{dN^*(0,t)\lambda}{dt} = H_2N_i^*(t) - H_3N^*(0,t)\lambda - J^*(0,t) \tag{4.7}$$

3) Applying conservation of gas atoms to the region $0_+ < x < L_-$

hence to equation 4.3, gives Ficks second equation

$$\frac{\partial^2 N^*(x,t)}{\partial t^2} = \frac{1}{D}\frac{\partial N^*(x,t)}{\partial t} \tag{4.8}$$

4) Applying conservation of gas atoms to the region $L_- < x < L$ gives

$$\frac{dN^*(L,t)\lambda}{dt} = J^*(L,t) - J_e^*(L,t)$$

so on substitution from equation 4.4

$$\frac{dN^*(L,t)\lambda}{dt} = J^*(L,t) + H_2N_e^*(t) - H_3N^*(L,t)\lambda \tag{4.9}$$

5) Applying conservation of gas atoms to the region $L < x < L_+$ gives

$$\frac{dN_e^*(t)}{dt} = J_e^*(L,t) - J_e^*(L_+,t)$$

so on substitution from equations 4.4 and 4.5

$$\frac{dN_e^*(t)}{dt} = H_3N^*(L,t)\lambda - bN_e^*(t)^2 - H_2N_e^*(t) \tag{4.10}$$

Gas pressures in the detection chamber are always extremely low with respect to those in the input chamber. For this reason r^* in equation 4.5 has been assigned the value zero.

The five equations; 4.6; 4.7; 4.8; 4.9 and 4.10 mathematically model

permeation as described in section 4.1.

A good place to start solving these equations is equation 4.8, which is a second order, partial differential equation in $N^*(x,t)$ only. Using the method of separation of variables :

Let

$$N^*(x,t) = X(x)\,T(t)$$

so on substitution into equation 4.8

$$\frac{1}{X}\frac{d^2X}{dx^2} = \frac{1}{D}\frac{1}{T}\frac{dT}{dt} \qquad (4.11)$$

The left hand side and right hand side of equation 4.11 are functions of independent variables, therefore let

$$\frac{d^2X}{dx^2} = mX$$

and

$$\frac{dT}{dt} = mDT$$

Therefore

$$\left.\begin{aligned} X_o &= c(L - x) + d \\ T_o &= \text{constant} \end{aligned}\right\} \; m = 0$$

$$\left.\begin{aligned} X_m &= A_m e^{-q(L - x)} + B_m e^{q(L - x)} \\ T_m &= C_m e^{mDt} \end{aligned}\right\} \; m \neq 0 \qquad (4.12)$$

where

$$q^2 = m$$

Since equation 4.8 is linear the general solution of $N^*(x,t)$ can be a linear combination of $X_m\,T_m$ for $m = 0, 1, 2, \ldots$. To find the particular solution requires the application of specific boundary conditions.

The boundary condition on T(t) can be expanded as a Fourier series in $e^{i\omega t}$ since it is supposed periodic in ω . Thus;

$$X_n\,T_n = (A_n e^{-q(L - x)} + B_n e^{q(L - x)})\, e^{in\omega t}, \text{ for } n=1,2,\ldots \qquad (4.13)$$

where

$$q^2 = m = in\omega/D$$

Therefore

$$N^*(x,t) = X_oT_o + X_1T_1 + \ldots\ldots + X_nT_n\ldots\ldots \qquad (4.14)$$

The functions $N_i^*(t)$ and $N_e^*(t)$ can be expanded in a similar way. Therefore, by collecting together terms in $e^{in\omega t}$, equations 4.6, 4.7, 4.9 and 4.10, become infinite sets of equations each involving terms in $e^{in\omega t}$ for each particular n. These equations can be solved independently.

In the calculations that follow, the equations involving the fundamental modulation, $e^{i\omega t}$, will be singled out for consideration. That this is acceptable is not immediately clear, because of the non-linearity introduced into the defining equations by the terms; $b\,N_i^*(t)^2$ and $bN_e^*(t)^2$. Fortunately however this non-linearity leaves the phase of the fundamental modulation term unaltered, as is demonstrated by expanding $N_i^*(t)$ and $N_e^*(t)$. Thus:

$$bN_i^*(t)^2 = (\bar{N}_i^2 + 2\bar{N}_i N_i(t) + N_i(t)^2)\, b$$

$$= (\bar{N}_i^2 + 2\bar{N}_i (N_i e^{i\omega t} + \ldots\ldots) + (N_i e^{i\omega t} + \ldots.)^2)\; b$$

The only term on the right hand side of this equation in $e^{i\omega t}$ is

$$2b\bar{N}_i N_i e^{i\omega t} = H_4 N_i e^{i\omega t}$$

Similarly for $bN_e^*(t)^2$

$$2b\bar{N}_e N_e e^{i\omega t} = H_5 N_e e^{i\omega t}$$

where H_4 and H_5 are rate constants, dependent on the mean surface concentrations at input and exit respectively.

Experimentally, the non-linearity presents no problems since the Fourier coefficients of the fundamental modulation are to be found.

Therefore, if the terms in $e^{i\omega t}$ are singled out from the set of equations 4.6, the relevant equation is:

$$\frac{dN_i(t)}{dt} = ae^{i\omega t} + H_3 N(0,t)\lambda - (H_2+H_4)\, N_i(t)$$

letting : $N_i(t) = N_i e^{i\omega t}$: $N(0,t) = N(0)e^{i\omega t}$: $N_e(t) = N_e e^{i\omega t}$, then:

$$(H_2 + H_4 + i\omega)\, N_i = a + H_3 N(0)\lambda \qquad (4.15)$$

Similarly with equation 4.7, giving:

$$(H_3+ i\omega)\ N(0)\lambda = H_2 N_i - J(0) \tag{4.16}$$

Similarly with equation 4.9, giving:

$$(H_3+ i\omega)\ N(L)\lambda = H_2\ N_e + J(L) \tag{4.17}$$

Similarly with equation 4.10, giving:

$$(H_2 + H_5 + i\omega)\ N_e = H_3\ N(L)\lambda \tag{4.18}$$

where the time dependence $e^{i\omega t}$, has been cancelled out from all the equations.

If now, N_i is eliminated from equations 4.15 and 4.16

$$((H_3 + i\omega)\ (H_2+ H_4+i\omega) - H_2\ H_3)\ N(0)\lambda = H_2 a - (H_2+ H_4+ i\omega)J(0) \tag{4.19}$$

Similarly if N_e is eliminated from equations 4.17 and 4.18

$$((H_3+ i\omega)\ (H_2+H_5+ i\omega) - H_2H_3)\ N(L)\lambda = (H_2+H_5+ i\omega)J(L) \tag{4.20}$$

on substituting

$$N(x) = X_1(x) = A_1 e^{-q(L-x)} + B_1 e^{q(L-x)}$$

and

$$J(x) = -D\frac{dN}{dx}(x) = -Dq\ (A_1 e^{-q(L-x)} - B_1 e^{q(L-x)})$$

into equations 4.19 and 4.20 gives a pair of simultaneous equations for A_1 & B_1

$$A_1\ R_4 e^{-qL} + B_1\ X_4 e^{qL} = H_2 a \tag{4.21}$$

$$A_1\ X_5 + B_1\ R_5 = 0 \tag{4.22}$$

where

$$\left.\begin{aligned} R_4 &= [(H_3+ i\omega)\ (H_2 +H_4+i\omega) - H_2\ H_3]\lambda - Dq(H_2+H_4+i\omega) \\ X_4 &= [(H_3+ i\omega)\ (H_2 +H_4+i\omega) - H_2\ H_3]\lambda + Dq(H_2+H_4+i\omega) \end{aligned}\right\} \tag{4.21a}$$

$$\left.\begin{aligned} X_5 &= [(H_3+ i\omega)\ (H_2 +H_5+i\omega) - H_2\ H_3]\lambda + Dq(H_2+H_5+i\omega) \\ R_5 &= [(H_3+ i\omega)\ (H_2 +H_5+i\omega) - H_2\ H_3]\lambda - Dq(H_2+H_5+i\omega) \end{aligned}\right\} \tag{4.22a}$$

Therefore equations 4.21 and 4.22 may be identified as the boundary conditions determing the particular solution N(x).

With N(x) and therefore J(x) determined, N_i and N_e may be solved for from equations 4.15, 4.16, 4.17, 4.18.

Before proceeding with the calculation of phases, consider the boundary conditions in the form given by equations 4.19 and 4.20. These conditions are called Cauchy or mixed boundary conditions because the function, N(x), and its derivative, J(x), are detailed at the surfaces x=0 and x=L.

The effective nature of the boundary condition will depend on the magnitude of the rate constants $H_{i=2-5}$. Also, choice of a particular model for surface behaviour will depend on these rate constants. Thus in order to reduce the available choice, it is useful to consider order of magnitude estimates, for $H_{i=2-5}$, here.

It may be expected that experimental fluxes will be in the range 10^{11} - 10^{15} atoms cm^{-2} s^{-1}. Therefore, typically

$$\bar{J}_e(L_+) = H_5 \bar{N}_e \sim 10^{13}$$

where equation 4.5 has been used. If $\bar{N}_e \sim$ 1 p.p.m ($\sim 10^9$ atoms cm^{-2}), then $H_5 \sim 10^4$ s^{-1}. The point demonstrated by this is that typically $H_{i=2-5} \gg 1$, are expected.

Consider now equation 4.19 with $H_{i=2-5} \gg 1$, therefore:

$$H_2 a \sim H_3 H_4 N(0) \lambda + (H_2+H_4) J(0)$$

$$\therefore \quad H_2 a \sim \left(\frac{(H_2+H_4)}{H_3 H_4 \lambda} \frac{J(0)}{N(0)} + 1 \right) H_3 H_4 N(0) \lambda \qquad (4.23)$$

Clearly, if in equation 4.23

$$\frac{(H_2+H_4)}{H_3 H_4 \lambda} \frac{|J(0)|}{|N(0)|} \sim 10^{-1} \qquad (4.24)$$

Then N(0) can no longer be considered to be in phase with the flow from the

gas. It is interesting to know if condition 4.24 can be true even with $H_{i=2-5} \gg 1$?

Suppose $|J(0)| \;/\; |N(0)| \sim D/L$, with $D \sim 10^{-5}\ cm^2\ s^{-1}$. $L \sim 5 \times 10^{-2}$cm and let $\lambda \sim 5 \times 10^{-8}$cm. Then

$$\frac{H_2+H_4}{H_3H_4} \sim 2.5 \times 10^{-5}$$

if it is supposed that the rate constants are characterized by some rate constant H, then $H \sim 8\times10^4\ s^{-1}$ i.e. $H \gg 1$.

Consider next equation 4.20 with $H_{i=2-5} \gg 1$, therefore:

$$H_3H_5\ N(L)\lambda \sim (H_2+H_5)\ J(L)$$

$$\therefore \quad N(L) \sim \frac{(H_2+H_5)\ J(L)}{H_3H_5\lambda} \qquad (4.25)$$

if it is supposed $|J(L)| \sim |J(0)| \sim \frac{D}{L}\ |N(0)|$ then

$$\left|\frac{N(L)}{N(0)}\right| \sim \frac{(H_2+H_5)}{H_3H_5}\ \frac{D}{L\lambda}$$

Substituting H, the characterizing rate constant, in to this equation gives

$$\left|\frac{N(L)}{N(0)}\right| \sim \frac{1}{H}\ \frac{D}{L\lambda}$$

clearly if H is not large enough, N(L) may no longer be negligible with respect to N(0). Consider the condition

$$\left|\frac{N(L)}{N(0)}\right| \sim \frac{1}{H}\ \frac{D}{L\lambda} \sim 10^{-1}$$

then using the same values for D, L and λ as above, $H \sim 8\times10^4\ s^{-1}$

From the above it is seen that permeation is governed by the competition between fluxes, both at the input and at the exit of the foil. If at the input surface the diffusion flux dominates over the reverse flow, $H_3N(0)\lambda$ in maintaining equilibrium with respect to the forward flow, then the input

concentration $N^*(o,t)$ may cease to be in continuous equilibrium with the gas. If at the exit, the removal of atoms from the exit is small relative to the diffusion flux, then a pile up of atoms may occur so that $|N(L)/N(0)|$ may cease to be negligible. In both cases, such behaviour will add to the phase lag of the flux into the detection chamber.

4.2.2 The phase lag ϕ_i due to the input surface.

The conclusion drawn in the last paragraph is particularly relevant in calculating ϕ_i. A decision has to be made with regard to defining ϕ_i. The usual supposition made in time lag analyses, is that the input concentration is at all times in equilibrium with the input gas. Therefore the phase of $N^*(0,t)$ relative to the flow of gas molecules onto the input surface, $a_1+ae^{i\omega t}$, is chosen as ϕ_i.

$$\frac{a}{N(0)} = \left|\frac{a}{N(0)}\right| e^{i\phi_i}$$

Using equation 4.19 and substituting $J(0)= \left|\frac{J(0)}{N(0)}\right| N(0)\, e^{i\Delta}$ where Δ is the phase between J(0) and N(0), gives

$$H_2 a = \left((H_3+ \left|\frac{J(0)}{N(0)}\right|\frac{e^{i\Delta}}{\lambda} + i\omega\right)(H_2+H_4+ i\omega) - H_2H_3\Big)\ N(0)\lambda$$

$$\tan\phi_i = \left[\frac{(H_2+H_4)\left|\frac{J(0)}{N(0)}\right|\frac{\sin\Delta}{\lambda} + \omega\left(H_2+H_3+H_4+\left|\frac{J(0)}{N(0)}\right|\frac{\cos\Delta}{\lambda}\right)}{(H_2+H_4)\left|\frac{J(0)}{N(0)}\right|\frac{\cos\Delta}{\lambda} + H_3H_4 - \omega\left(\omega+\left|\frac{J(0)}{N(0)}\right|\frac{\sin\Delta}{\lambda}\right)}\right] \qquad (4.26)$$

4.2.3 The volume phase lag ϕ_v

The difference in phase between the input concentration just inside the entry surface, N(0), and the net flux just inside the exit surface, J(L) is defined as ϕ_v

$$\therefore \quad \frac{N(0)}{J(L)} = \left|\frac{N(0)}{J(L)}\right| e^{i\phi_v}$$

This phase lag will be left undetermined for reasons that will become clear later.

4.2.4 The phase lag ϕ_e due to the exit surface.

The difference in phase between the net flux just inside the exit surface, J(L) and the net flux of gas from the exit surface, $J_e(L_+)$, is defined as ϕ_e.

To evaluate ϕ_e, the starting point is equation 4.5

$$J_e^* (L_+, t) = (b N_e^{*2} - r^*) \qquad (4.5)$$

Letting $r^* = 0$ and singling out the equation for the fundamental modulation.

$$J_e(L_+) = H_5 N_e \qquad (4.27)$$

$$\therefore \quad \frac{J(L)}{J_e(L_+)} = \left|\frac{J(L)}{J_e(L_+)}\right| e^{i\phi_e} = \frac{1}{H_5} \left|\frac{J(L)}{N_e}\right| e^{i\phi_e} = \frac{J(L)}{N_e} \frac{1}{H_5}$$

From equations 4.17 and 4.18

$$(H_3 + i\omega) N(L)\lambda = H_2 N_e + J(L) \qquad (4.17)$$

$$(H_2 + H_5 + i\omega) N_e = H_3 N(L)\lambda \qquad (4.18)$$

On eliminating $N(L)\lambda$

$$H_3 J(L) = \left((H_3 + i\omega)(H_2 + H_5 + i\omega) - H_2 H_3\right) N_e \qquad (4.28)$$

Therefore

$$\tan \phi_e = \left[\frac{\omega(H_2 + H_3 + H_5)}{H_3 H_5 - \omega^2}\right] \qquad (4.29)$$

4.2.5. Surface behaviour

It is worth investigating the behaviour of ϕ_i and ϕ_e. As discussed at the end of section 4.2.1, it is expected, if fluxes are to be detected, that the rate constants $H_{i = 2-5} \gg 1$. Therefore from equation 4.29 $\phi_e \sim 0$ i.e. it is expected to be below the limit of experimental detection. From equation 4.26

$$\tan \phi_i = \left[\frac{\frac{(H_2+H_4)}{H_3 H_4} \left|\frac{J(0)}{N(0)}\right| \frac{\sin\Delta}{\lambda} + \omega\left(\frac{(H_2+H_3+H_4)}{H_3 H_4} + \left|\frac{J(0)}{N(0)}\right| \frac{\cos\Delta}{H_3 H_4 \lambda}\right)}{\frac{(H_2+H_4)}{H_3 H_4} \left|\frac{J(0)}{N(0)}\right| \frac{\cos\Delta}{\lambda} + 1 - \omega\left(\frac{\omega}{H_3 H_4} + \left|\frac{J(0)}{N(0)}\right| \frac{\sin\Delta}{H_3 H_4 \lambda}\right)} \right]$$

Therefore if $H_{i=2-5} \gg 1$ (4.26)

$$\tan \phi_i \sim \left[\frac{\frac{(H_2+H_4)}{H_3 H_4 \lambda} \left|\frac{J(0)}{N(0)}\right| \sin\Delta}{\frac{(H_2+H_4)}{H_3 H_4 \lambda} \left|\frac{J(0)}{N(0)}\right| \cos\Delta + 1} \right]$$

But from equation 4.24 it may be seen that even when condition $H_{i=2-5} \gg 1$ is satisfied it is possible it is still true that:

$$\tan \phi_i \sim \left[\frac{\frac{(H_2+H_4)}{H_3 H_4 \lambda} \left|\frac{J(0)}{N(0)}\right| \sin\Delta}{\frac{(H_2+H_4)}{H_3 H_4 \lambda} \left|\frac{J(0)}{N(0)}\right| \cos\Delta} \right] = \tan\Delta$$

Therefore under the conditions

$$H_{i=2-5} \gg 1$$

$$\frac{(H_2+H_4)}{H_3 H_4 \lambda} \left|\frac{J(0)}{N(0)}\right| \cos\Delta > 1$$

the total phase lag is

$$\phi_{Total} \sim \Delta + \phi_v$$

Thus ϕ_{Total} is just the difference between the phases of J(L) and J(0). This statement is important since it implies that even under conditions of diffusion limited permeation computed phases hence time lags, may differ from the values expected under the supposition of input concentrations in continuous equilibrium with the gas.

4.2.6 The phase of J(L)

In section 4.2.5 it was concluded that the relative phase, between

the flow from the gas onto the input surface and the flow from the exit surface into the detection chamber, had negligible contributions due to characteristic delay times from atoms to traverse the input and exit surfaces. For this reason it seems pointless to reduce the total phase into the sum of so called surface and volume parts, each specified by complicated equations. Instead in what follows ϕ_{Total} is defined as the phase of J(L), the flux just inside the exit surface.

Using $N(x) = A_1 e^{-q(L-x)} + B_1 e^{q(L-x)}$

and $J(x) = - D \frac{dN(x)}{dx}$

$$J(L) = - Dq (A_1 - B_1) \qquad (4.30)$$

Substituting for A_1 and B_1 from equations 4.21 and 4.22 gives

$$J(L) = Dk H_2 a (1+i) (X_4 X_5 e^{qL} - R_4 R_5 e^{-qL})^{-1} (R_5 + X_5) \qquad (4.31)$$

Let $V = Dk H_2 a \left| X_4 X_5 e^{qL} - \bar{R}_4 \bar{R}_5 e^{-\bar{q}L} \right|^2$

$$\therefore \quad \frac{J(L)}{V} = (1+i) (\bar{X}_4 \bar{X}_5 e^{\bar{q}L} - \bar{R}_4 \bar{R}_5 e^{-\bar{q}L}) (R_5 + X_5)$$

where a bar over a function means the complex conjugate.

$$\frac{J(L)}{V} = \frac{E}{2} (e^{\bar{q}L} + e^{-\bar{q}L}) + \frac{F}{2} (e^{\bar{q}L} - e^{-\bar{q}L})$$

$$= E \cosh \bar{q}L + F \sinh \bar{q}L$$

where $E = (1+i) (R_5 + X_5) (\bar{X}_4 \bar{X}_5 - \bar{R}_4 \bar{R}_5) = E_1 + E_2 i \qquad (4.32)$

and $F = (1+i) (R_5 + X_5) (\bar{X}_4 \bar{X}_5 + \bar{R}_4 \bar{R}_5) = F_1 + F_2 i \qquad (4.33)$

Therefore $\frac{J(L)}{V} = (E_1 + E_2 i) \cosh \bar{q}L + (F_1 + F_2 i) \sinh \bar{q}L$

$$= \Big((E_1 + E_2 i) (\cosh kL \cos kL - i \sinh kL \sin kL) +$$

$$+ (F_1 + F_2 i) (\sinh kL \cos kL - i \cosh kL \sin kL) \Big)$$

$$= i \Big(E_2 \cosh kL \cos kL - E_1 \sinh kL \sin kL +$$

$$+ F_2 \sinh kL \cos kL - F_i \cosh kL \sin kL \Big) +$$

$$\Big(E_1 \cosh kL \cos kL + E_2 \sinh kL \sin kL +$$

$$+ F_1 \sinh kL \cos kL + F_2 \cosh kL \sin kL \Big)$$

Therefore since ϕ_{Total} is defined as the phase lag of J(L)

$$\tan \phi_{Total} = - \frac{\text{Imaginary } (J(L))}{\text{Real } (J(L))}$$

Thus after dividing throughout $\tan \phi_{Total}$ by cosh kL cos kL

$$\tan \phi_{Total} = \frac{F_1 \tan kL - F_2 \tanh kL - E_2 + E_1 \tan kL \tanh kL}{F_2 \tan kL + F_1 \tanh kL + E_1 + E_2 \tan kL \tanh kL} \quad (4.34)$$

This completes the phase analysis, but particular permeation models will be discussed later in the chapter.

4.2.7 Amplitudes

The modulation amplitude for the rate·gas molecules leave the exit surface is defined as $J_e(L_+)$ Z, with Z the exit surface area. Using equations 4.27 and 4.28

$$\left|J_e(L_+)\right| Z = \frac{H_3 H_5 \left|J(L)\right| Z}{(H_3+i\omega)(H_2+H_5+i\omega)-H_2H_3}$$

Substituting from equation 4.31 for J(L) gives

$$\left|J_e(L_+)\right| Z = \frac{Za\, H_2H_3H_5 (D\omega)^{\frac{1}{2}}}{\left[(H_3H_5 - \omega^2)^2 + \omega^2 (H_2+H_3+H_5)^2\right]^{\frac{1}{2}}} \times \frac{\left|R_5 + X_5\right|}{\left|e^{qL}X_4X_5 - R_4R_5e^{-qL}\right|} \quad (4.35)$$

In the present experimental method, fluxes are detected indirectly from the detection chamber gas pressures. The magnitude of pressure modulations, p, due to a flux into a volume V, pumped at the rate S was found to be given by equation 3.2. Therefore on substituting $\left|J_e(L_+)\right| Z$ into equation 3.2 for the flux,

$$p = \frac{\left|J_e(L_+)\right| Z}{\left((S/V)^2 + \omega^2\right)^{\frac{1}{2}}} \frac{kT}{V}$$

4.3 Characteristics of particular permeation models.

The equations in section 4.2 define a series of relationships between amplitude, phase and frequency. These equations involve a large number of parameters which make it difficult to see how particular parameter choices modify the phase/frequency behaviour. Thus difficulty may be expected if an attempt is made to find a unique set of parameters matching a given experimental curve.

For purposes of analysis it is useful to examine a few curves and search for their characteristics.

4.3.1. The case of very large rate constants, ($H_{i=2-5} \gg 1$).

Consider the parameters R_4 and R_5 defined by equations 4.21 (a) and 4.22(a). For large rate constants these parameters reduce to

$$R_4 \sim H_3H_4\lambda - Dq\,(H_2+H_4)$$

and

$$R_5 \sim H_3H_5\lambda - Dq\,(H_2+H_5)$$

On substituting into these equation $q = (\omega/2D)^{\frac{1}{2}}(1+i)$

$$R_4 \quad (1 - (D/2)^{\frac{1}{2}} \frac{(H_2+H_4)}{H_3H_4\lambda}\,(1+i)\,\omega^{\frac{1}{2}})\,H_3H_4\lambda \qquad (4.36a)$$

$$R_5 \quad (1 - (D/2)^{\frac{1}{2}} \frac{(H_2+H_5)}{H_3H_5\lambda}\,(1+i)\,\omega^{\frac{1}{2}})\,H_3H_5\lambda \qquad (4.36b)$$

From equations 4.36 (a) and 4.36(b) the condition of very large rate constants may be defined as when

$$(D/2)^{\frac{1}{2}} \frac{(H_2+H_4)}{H_3\,H_4\lambda} \ll 1$$

and

$$(D/2)^{\frac{1}{2}} \frac{(H_2+H_5)}{H_3H_5\lambda} \ll 1$$

Then with these conditions $R_4 \sim H_3H_4\lambda$, $R_5 \sim H_3H_5\lambda$, $X_4 \sim H_3H_4\lambda$ and $X_5 \sim H_3H_5\lambda$. Substituting these expressions into equations 4.32 and 4.33 gives

$$E_1 = E_2 = 0$$

$$F_1 = F_2 = 4\ (H_3H_4\lambda)\ (H_3H_5\lambda)^2$$

Therefore, from equation 4.35

$$\lim_{H_{i=2-5} \to \infty} \phi_{Total} \to \phi_{Classical} = \arctan\left[\frac{\tan kL - \tanh kL}{\tan kL + \tanh kL}\right] \qquad (4.37)$$

From the arguments at the end of section 4.2.1, $\phi_{Classical}$ corresponds to when N(0) is continuously in equilibrium with the gas, and $\frac{N(L)}{N(0)}$ tends to zero.

Figure 4.5. shows typical plots of $\phi_{Classical}$ versus $\nu^{\frac{1}{2}}$, where ν is the modulation frequency and has units Hz.. The curves show the following characteristics:

1) they depend only on the specimen parameters; D, the diffusion coefficient and, L, the specimen thickness.

2) they pass through the origin.

3) they have asymptotes given by

$$\lim_{kL \to \infty} \phi_{Classical} = \arctan \frac{\tanh kL - 1}{\tanh kL + 1}$$

$$= \arctan\ (\tan(kL - \pi/4))$$

$$= (\pi L^2/D)^{\frac{1}{2}}\ \nu^{\frac{1}{2}} - \pi/4 \qquad (4.38)$$

4) the asymptotes intercept the phase axis at $-\pi/4$

5) for small values of kL

$$\lim_{kL \to 0} \phi_{Classical} = \frac{2\pi L^2}{D}\ \nu \qquad (4.39)$$

The corresponding relationship for the amplitude, $A_{Classical}$, is from equation 4.35;

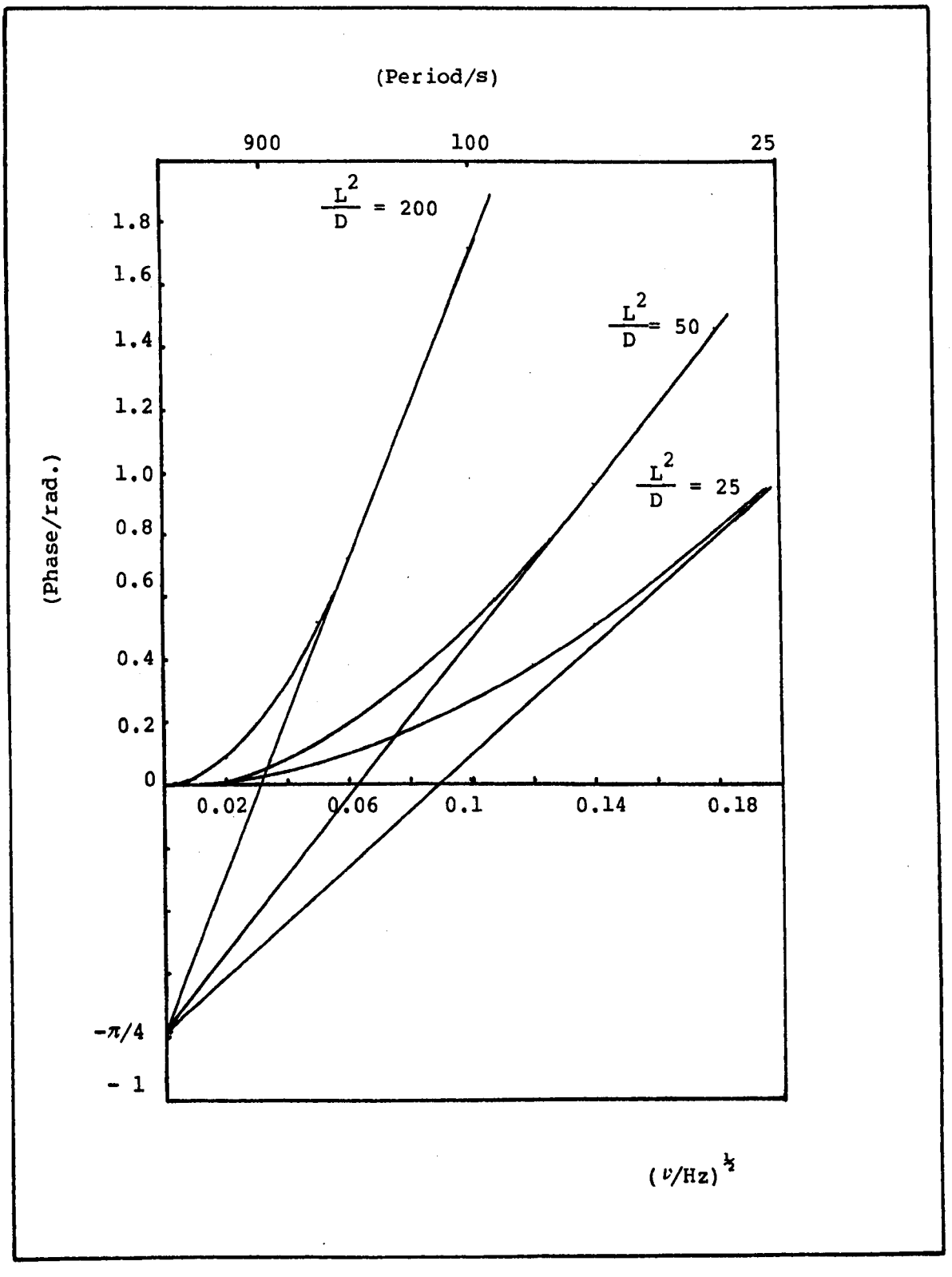

Fig. 4.5 $\phi_{\text{Classical}}$ v $\nu^{\frac{1}{2}}$

$$A_{Classical} = \text{Const.} \times \left(\frac{\omega}{\text{Sinh}^2 kL + \text{Sin}^2 kL} \right)^{\frac{1}{2}}$$

Figure 4.6 shows a typical $A_{Classical}$ versus $\nu^{\frac{1}{2}}$ plot. The curve is S shaped with no strong characteristics; it is not very interesting for the analysis of data.

Because of the strong characteristics for $\phi_{Classical}$, especially the asymptotic intercept, experimental data was always first compared with this model.

4.3.2 The case of large rate constants, $(H_{i=2-5} >> 1)$.

When in equations 4.36 (a) and 4.36 (b)

$$(D/2)^{\frac{1}{2}} \frac{(H_2+H_4)}{H_3 H_4 \lambda} \sim 1 \qquad (4.41a)$$

and

$$(D/2)^{\frac{1}{2}} \frac{(H_2+H_5)}{H_3 H_5 \lambda} \sim 1 \qquad (4.41b)$$

then it is expected that $\phi_{Classical}$ will no longer be a good approximation for ϕ_{Total}. If $D \sim 10^{-5}$ $cm^2 s^{-1}$ and $\lambda \sim 5 \times 10^{-8}$cm, the characterizing rate constant is $H \sim 9 \times 10^4$ s^{-1}. Comparison shows that this value is consistent with those estimated from the conditions given by equations 4.24 and 4.25. This implies that the concentration just inside the input surface, $N^*(0)$, may have ceased to be continuously in equilibrium with the gas, and that $N^*(L)$ may no longer be entirely negligible when compared to $N^*(0)$.

Unfortunately it cannot be determined, by inspection of equations 4.41 (a) and 4.41(b), if the changes at the input and exit occur simultaneously or not. However since by definition $H_4 > H_5$, it is likely that if they are not simultaneous, then the changes at the exit will proceed those at the input.

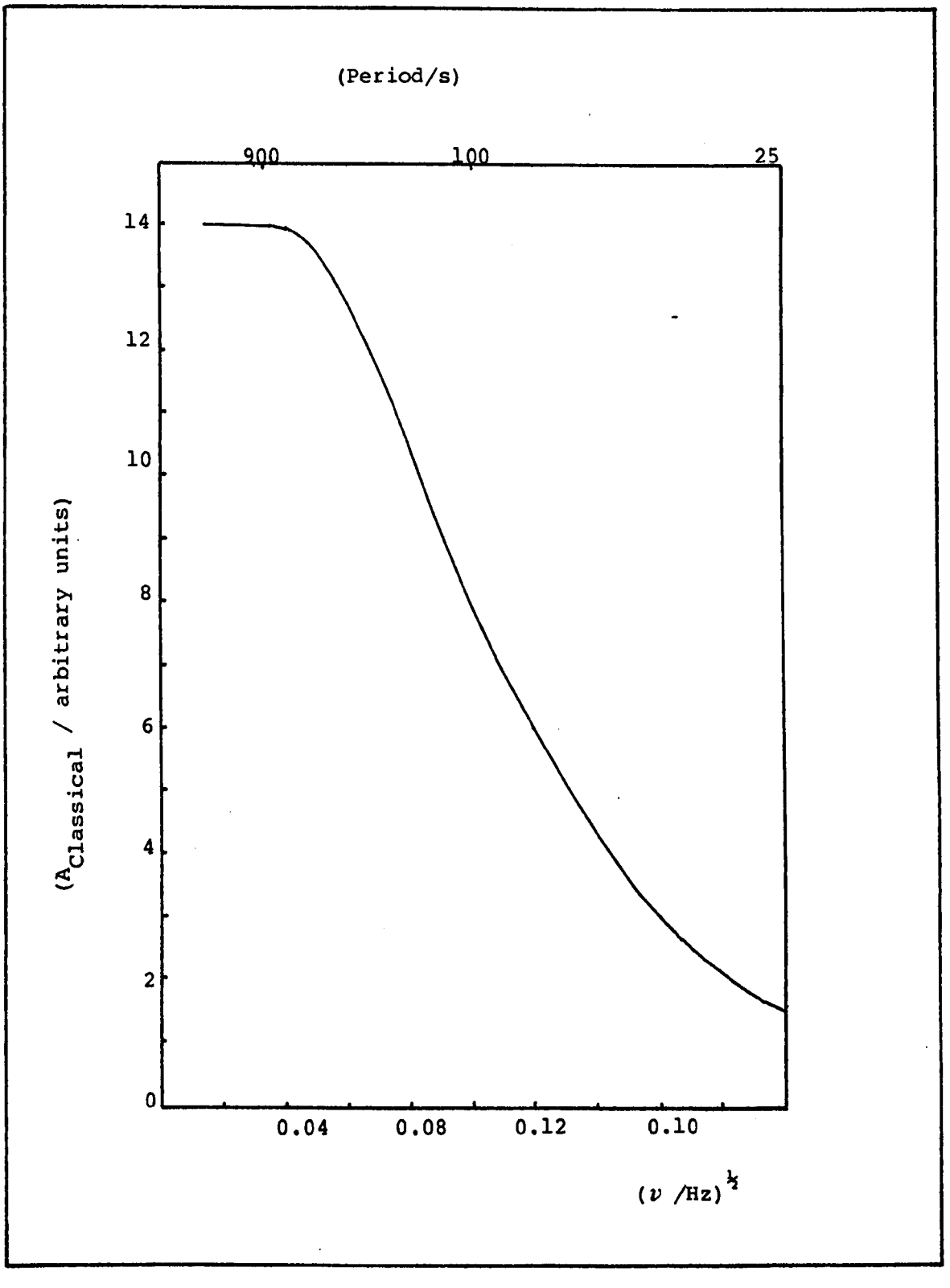

Fig. 4.6 $A_{Classical}$ v $\nu^{\frac{1}{2}}$. ($(L^2/D) = 200$)

If now R_4 and R_5 as given by equations 4.36 (a) and 4.36 (b) and the corresponding expressions for X_4 and X_5 are substituted into equations 4.32 and 4.33, then:

$$E_1 = 4\ (c_4\ \omega^{\frac{1}{2}} + c_5\ \omega^{\frac{1}{2}})\ f\ (H_{i=2-5})$$

$$E_2 = 0$$

$$F_1 = (1 + 2c_4c_5\omega)\ f\ (H_{i=2-5})$$

$$F_2 = (1 - 2c_4c_5\omega)\ f\ (H_{i=2-5})$$

where $f\ (H_{i=2-5})$ is function of the rate constants and

$$c_4 = (D/2)^{\frac{1}{2}}\ \frac{(H_2 + H_4)}{H_3\ H_4\ \lambda}$$

$$c_5 = (D/2)^{\frac{1}{2}}\ \frac{(H_2 + H_5)}{H_3\ H_5\ \lambda}$$

Substituting the expressions for E_1, F_1 and F_2 into equation 4.35 gives

$$\phi_{Total} \sim \phi_{H \gg 1}$$

where

$$\phi_{H \gg 1} = \arctan \left[\frac{(1 + 2c_4c_5\omega)\ \tan kL - (1 - 2c_4c_5\omega)\ \tanh kL + 4\ (c_4 + c_5)\ \omega^{\frac{1}{2}}\ \tan kL\ \tanh kL}{(1 - 2c_4c_5\omega)\ \tan kL + (1 + 2c_4c_5\omega)\ \tanh kL + 4\ (c_4 + c_5)\ \omega^{\frac{1}{2}}} \right] \qquad (4.42)$$

Equation 4.42 is somewhat more complicated than equation 4.37 and for this reason $\phi_{H \gg 1}$ does not show characteristics as strong as those for ϕ Classical.

Typical $\phi_{H \gg 1}$ v $\nu^{\frac{1}{2}}$ behaviour is illustrated by the curves in Figures 4.7, 4.8 and 4.9. The value $(L^2/D)=25$ was chosen for all the curves shown and the parameters c_4 and c_5 were varied. In Figure 4.7, the ratio $(c_4/c_5)=0.01$ was held constant, whilst c_5 was variously assigned the values:

0; 0.5; 5; 100. In Figure 4.8, c_5=1, was held constant and the ratio (c_4/c_5) variously assigned the valued: 0.001; 0.5; 1. In Figure 4.9, $\phi_{H \gg 1}$ is shown with (L^2/D)=25, c_5=250 and (c_4/c_5)=1, phase/frequency curves of this type may be expected when permeation is under the extreme influence of input and exit processes.

It is clear from these curves that $\phi_{H \gg 1}$ is strongly influenced by all three parameters, D, c_4 and c_5. For this reason it is not expected that $\phi_{H \gg 1}$ will have any strong characteristics for any particular set of these parameters. However, the curves do have characteristics which may be used to identify $\phi_{H \gg 1}$ behaviour during experiment:

1) they have linear regions which extrapolated back to the phase axis have intercepts $\gtrsim -\pi/4$
2) they depend on the input gas pressure or the mean discharge current which, by definition, govern H_4 and H_5 and hence c_4 and c_5.
3) they are always above the $\phi_{Classical}$ curve $(c_5=0)$ for identical values of diffusion coefficient, D.
4) they have asymptotes

$$\lim_{kL \to \infty} \phi_{H \gg 1} = \arctan \frac{\tan kL + 1}{1 - \tan kL}$$

$$= \arctan (\tan kL + \pi/4)$$

$$= \left(\pi \frac{L^2}{D}\right)^{\frac{1}{2}} \nu^{\frac{1}{2}} + \pi/4$$

5) the behaviour of the asymptote ensures that $\phi_{H \gg 1} \gtrsim \phi_{Classical}$ under all circumstances.

4.4. The steady rate flux and the pressure power law.

So far attention in this chapter has been in the modulated parts of

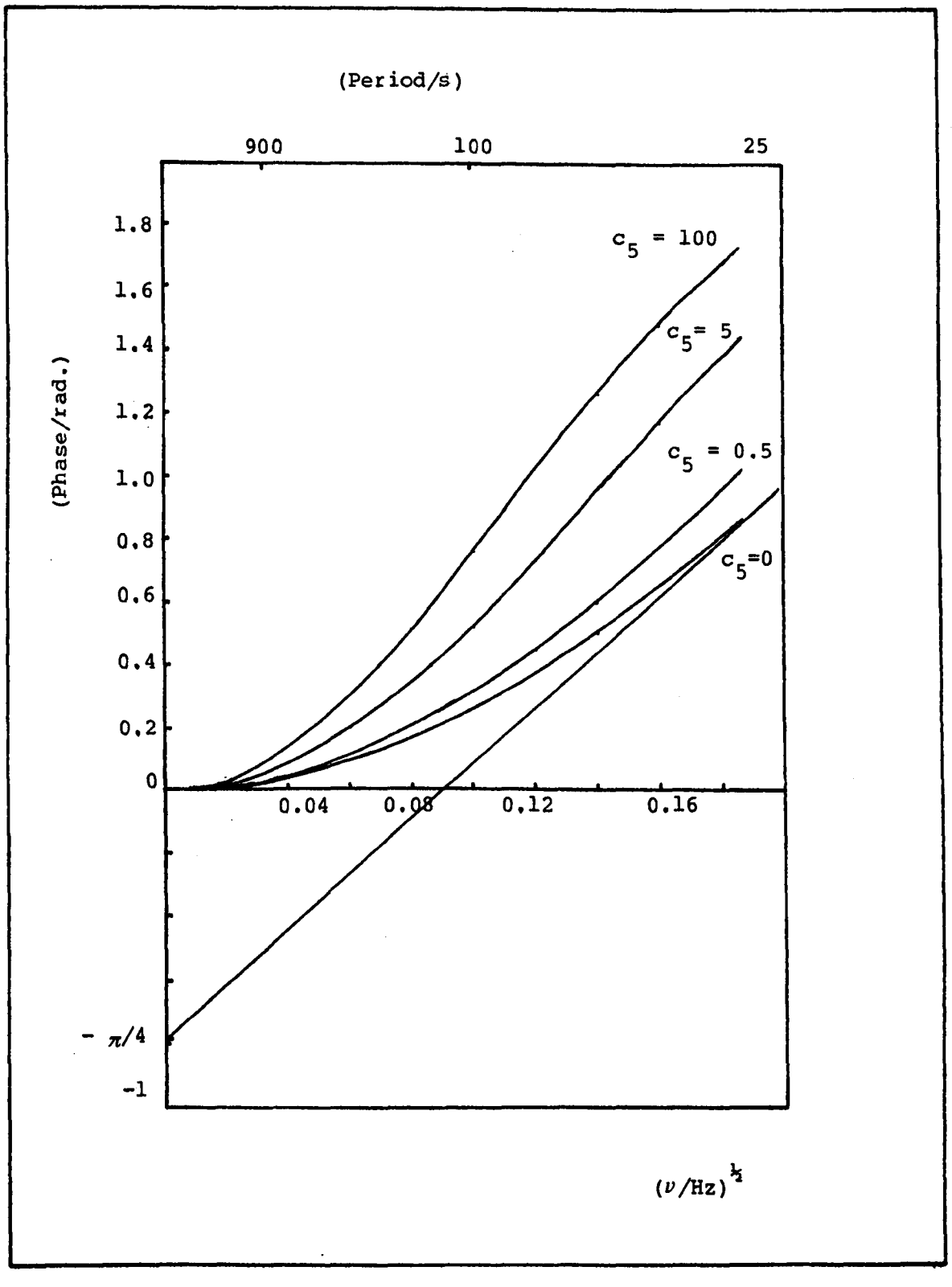

Fig. 4.7 $\phi_{H >> 1}$ v $\nu^{\frac{1}{2}}$: $(L^2/D) = 25$: $c_4 / c_5 = 0.01$

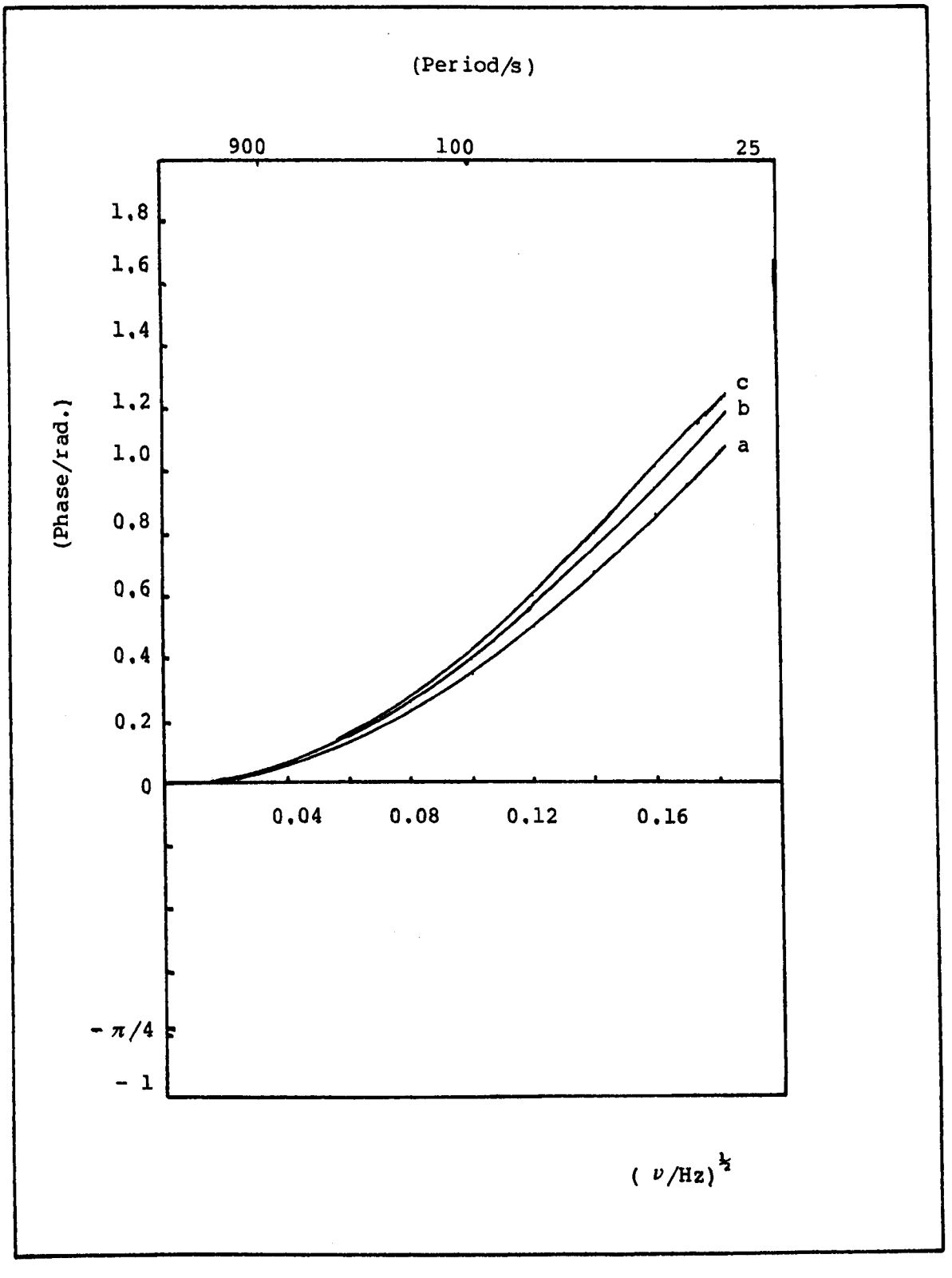

Fig. 4.8 $\varphi_H >> 1$ v $\nu^{\frac{1}{2}}$: $\frac{L^2}{D}$ = 25: c_5 = 1

a) c_4/c_5 =0.001

b) c_4/c_5 =0.05

c) c_4/c_5 =1

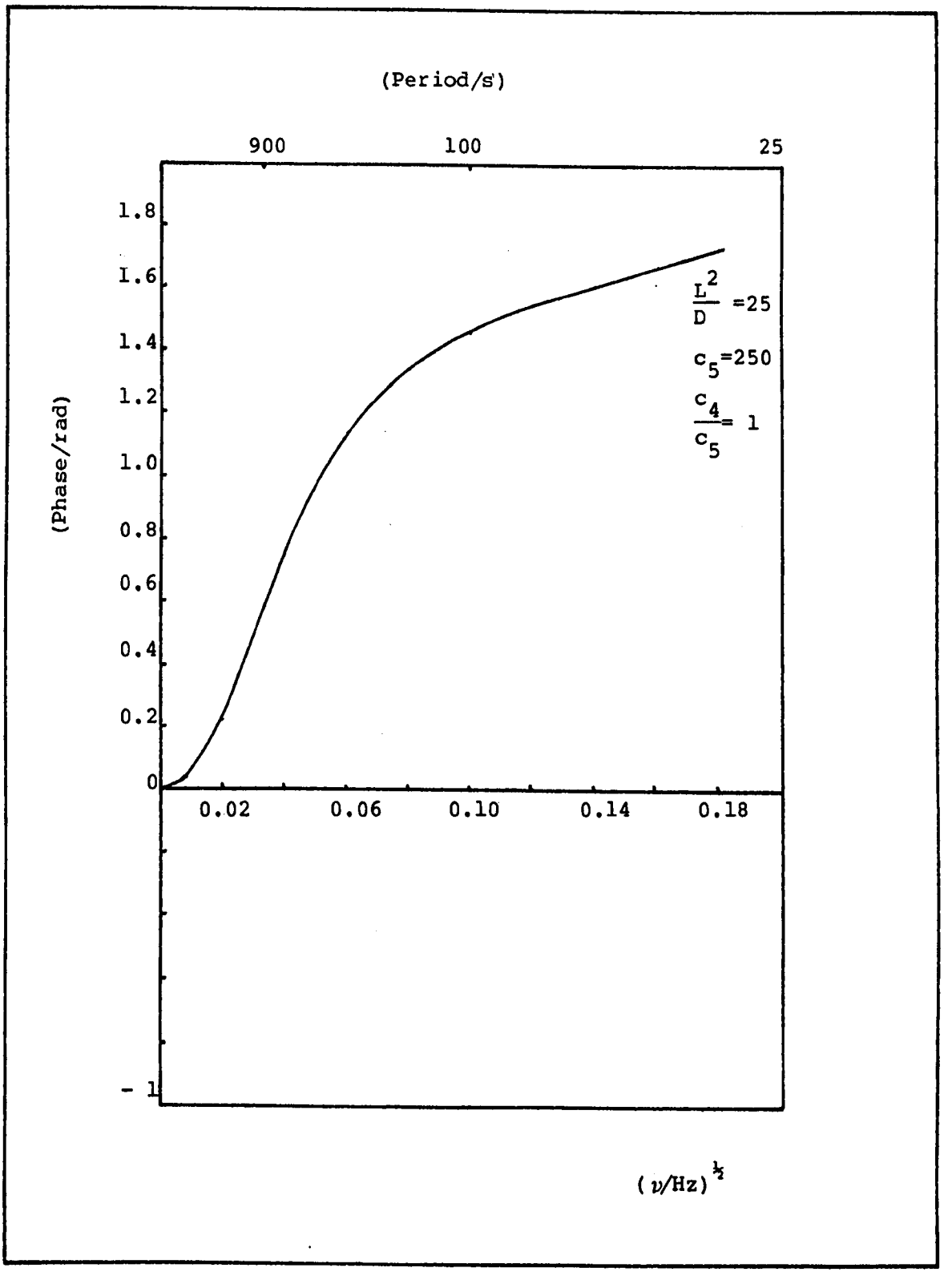

Fig. 4.9 $\phi_{H >> 1}$ v $\nu^{\frac{1}{2}}$: an extreme case.

the fluxes and concentrations. In particular to the fundamental modulation, for instance in equation 4.14 the general solution for the volume concentration,

$$N^*(x,t) = X_o T_o + X_1 T_1 + \ldots\ldots \qquad (4.14)$$

$X_1 T_1$ has been singled out. In this section the steady rate parts, for instance $X_o T_o$, are investigated, in particular the steady rate flux, $\bar{J}$.

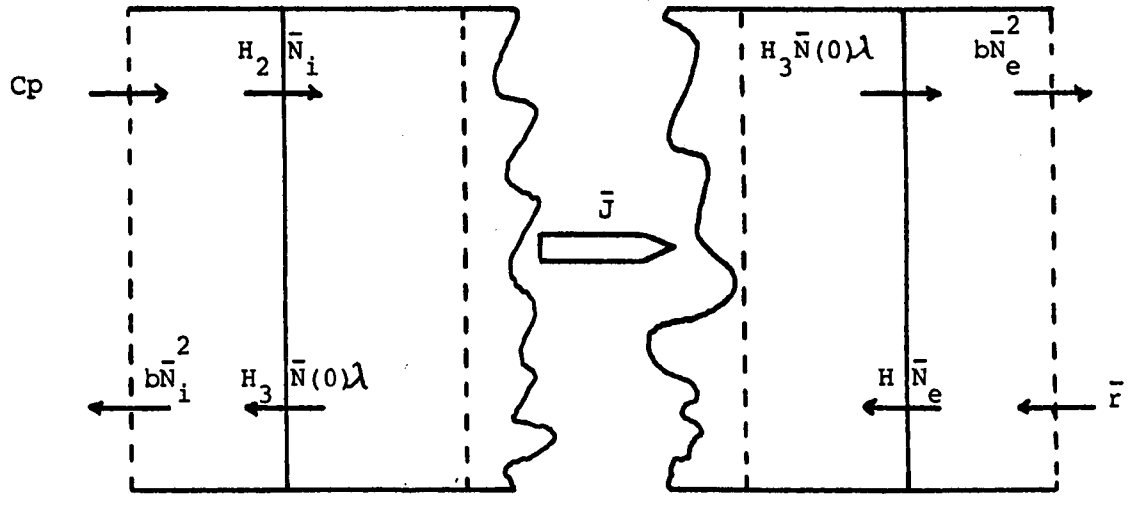

Fig. 4. 10 Steady rate permeation

Figure 4.10 sketches steady rate permeation for the present model. Comparing this with Figures 4.2 and 4.3 it is found

1) that only the steady rate parts of the total fluxes and concentrations have been retained.

2) that there is no multipicity of fluxes, $\bar{J}$ is the same at all the surfaces

3) that the steady rate flow of gas onto the surface, a_1, has been replaced by C_p, because $\bar{J}$ is assumed to arise only by the dissolution of gas at the surface. It is supposed that the rate of gas flow onto the surface and into a bound state is proportional to the number gas of atoms striking the surface, hence proportional to the pressure, p. The proportionality constant will depend on the "sticking coefficient" and so may

3) depend on the condition of the surface.

If from the sets of equations 4.6, 4.7, 4.9 and 4.10, those equations relating to the time independent parts are selected it is found: From equation 4.6 that

$$H_3\bar{N}(0)\lambda + Cp = b\bar{N}_i^2 + H_2\bar{N}_i \tag{4.43}$$

where a_1 has been replaced by Cp. From equation 4.7 that

$$H_3\bar{N}(0)\lambda + \bar{J} = H_2\bar{N}_i \tag{4.44}$$

From equation 4.9 that

$$H_3\bar{N}(L)\lambda - \bar{J} = H_2\bar{N}_e \tag{4.45}$$

From equation 4.10 that

$$\bar{J} = b\bar{N}_e^2 \tag{4.46}$$

From Ficks first law and equation 4.12 with m = o, that

$$\bar{J} = \frac{D}{L}\left(\bar{N}(0) - \bar{N}(L)\right) \tag{4.47}$$

Using equations 4.45 and 4.46

$$H_3\bar{N}(L)\lambda = \bar{J} + (H_2^2/b)^{\frac{1}{2}}\bar{J}^{\frac{1}{2}} \tag{4.48}$$

Substituting for N(L) in equation 4.47 from equation 4.48 gives

$$H_3\left(\bar{N}(0)\lambda - \frac{\lambda L}{D}\bar{J}\right) = \bar{J} + (H_2^2/b)^{\frac{1}{2}}\bar{J}^{\frac{1}{2}}$$

$$\therefore \quad H_3\bar{N}(0)\lambda = \bar{J}\left(1 + \frac{H_3L\lambda}{D}\right) + (H_2^2/b)^{\frac{1}{2}}\bar{J}^{\frac{1}{2}} \tag{4.49}$$

Using equations 4.43 and 4.44 gives

$$Cp = \left(\frac{b}{H_2^2}\right)(H_3\bar{N}(0)\lambda + \bar{J})^2 + \bar{J} \tag{4.50}$$

Therefore on substitution from equation 4.49 into equation 4.50 for $H_3\bar{N}(0)\lambda$

$$Cp = \left(\frac{b}{H_2^2}\right)\left(2 + \frac{H_3L\lambda}{D}\right)^2\bar{J}^2 + 2\left(2 + \frac{H_3L\lambda}{D}\right)\left(\frac{b}{H_2^2}\right)^{\frac{1}{2}}\bar{J} + 2\bar{J} \tag{4.51}$$

Equation 4.51 relates the macroscopic flow, $\bar{J}$, through a metal foil, to the input gas pressure p.

From equation 4.51 a characteristic flux, j, may be defined.

$$j = H_2^2/b\ (2 + H_3 L \lambda /D)^2 \qquad (4.52)$$

therefore equation 4.51 becomes

$$Cp = \frac{\bar{J}}{j}^2 + \frac{\bar{J}^{3/2}}{j^{1/2}} + 2J \qquad (4.53)$$

Dividing equation 4.53 by j, gives the dimensionless equation

$$x = y\ (y + 2y^{\frac{1}{2}} + 2) \qquad (4.54)$$

where $x = (Cp/j)$ and $y = (J/j)$.

An interesting experimental parameter is the gradient of a plot of ln $\bar{J}$ v. ln p. Using the dimensionless quantities in equation 4.54, this parameter is equal to the gradient of ln y v. ln x.

$$\frac{d \ln y}{d \ln x} = \frac{x}{y}\frac{dy}{dx}$$

Letting $g = (d \ln y/d \ln x)$, then

$$g = \frac{(y + 2y^{\frac{1}{2}} + 1)}{(2y + 3y^{\frac{1}{2}} + 2)} \qquad (4.55)$$

Consider now the limit of large y, then

$$\lim_{y \to \infty} g = 0.5$$

or

$$\bar{J} \to \infty$$

This result is equivalent to Sieverts supposition i.e.

$$\bar{J} = K_s\ p^{\frac{1}{2}}$$

Consider now the limit of small y, then

$$\lim_{y \to 0} g = 1$$

or

$$\bar{J} \to 0$$

This result implies that $\bar{J}$ is proportional to pressure and from equation 4.51 that $\bar{J}$ is independent of (D/L) a consequence of input behaviour. For this and

for technological reasons interest has currently grown in low pressure steady rate permeation.

For present purposes if g is supposed to be a slowly varying function, then it may be assumed to be constant over an experimental range of flux. Therefore using equation 4.55 to solve for y in terms of g, it is found

$$y^{\frac{1}{2}} = \frac{(2 - 3g) + (12g - 7g^2 - 4)^{\frac{1}{2}}}{2\,(2g - 1)} \qquad (4.56)$$

Hence if g, is known over some interval of measured flux, equation 4.56 may be used to determine

$$y = \bar{J}/j \qquad (4.57)$$

Thus if the mean value of the steady rate flux over the interval is substituted into equation 4.57, then an estimate for j, the characteristic flux for hydrogen through the metal, may be determined.

4.5 Models incorporating other physical effects.

A model much referred to when anomalous experimental results are observed is that in which diffusant atoms enter traps. Traps are sites in the lattice, usually supposed to be defects, which have characteristic times of occupancy longer than those for normal sites. Two types of traps are usually considered; reversible traps, with characteristic times short compared with the time for signals to traverse an experimental specimen; irreversible traps, with characteristic times long compared with the time for signals to traverse an experimental specimen.

Trapping is usually modelled using the McNabb and Foster equations, (50), which are a pair of simultaneous differential equations that in general must be solved by numerical methods.

Analytic solution is possible however in the limit of low trapping

concentrations, as shown by Cummings (51). In this limit Cummings anticipates experimental curves of the type shown in Figure 4.11. These curves show a characteristic hump, which is similar to a resonance.

The curves in Figure 4.11 are characterised by the parameters; p the probability that an occupied trap will release its captive in one second; k, the probability of an atom becoming trapped; N, the number of traps per unit volume.

In the present work, the trapping model has not been considered, for two reasons; (a) the specimens used were all high purity metals: (b) the curves in Figure 4.10 show a disturbing feature for this trapping model. The trapping curves are found to cross the $\emptyset_{Classical}$ curve for the same ratio of (L^2/D). This is surprising because the conditions appropriate to the $\emptyset_{Classical}$ model correspond to the most rapid propagation of signals.

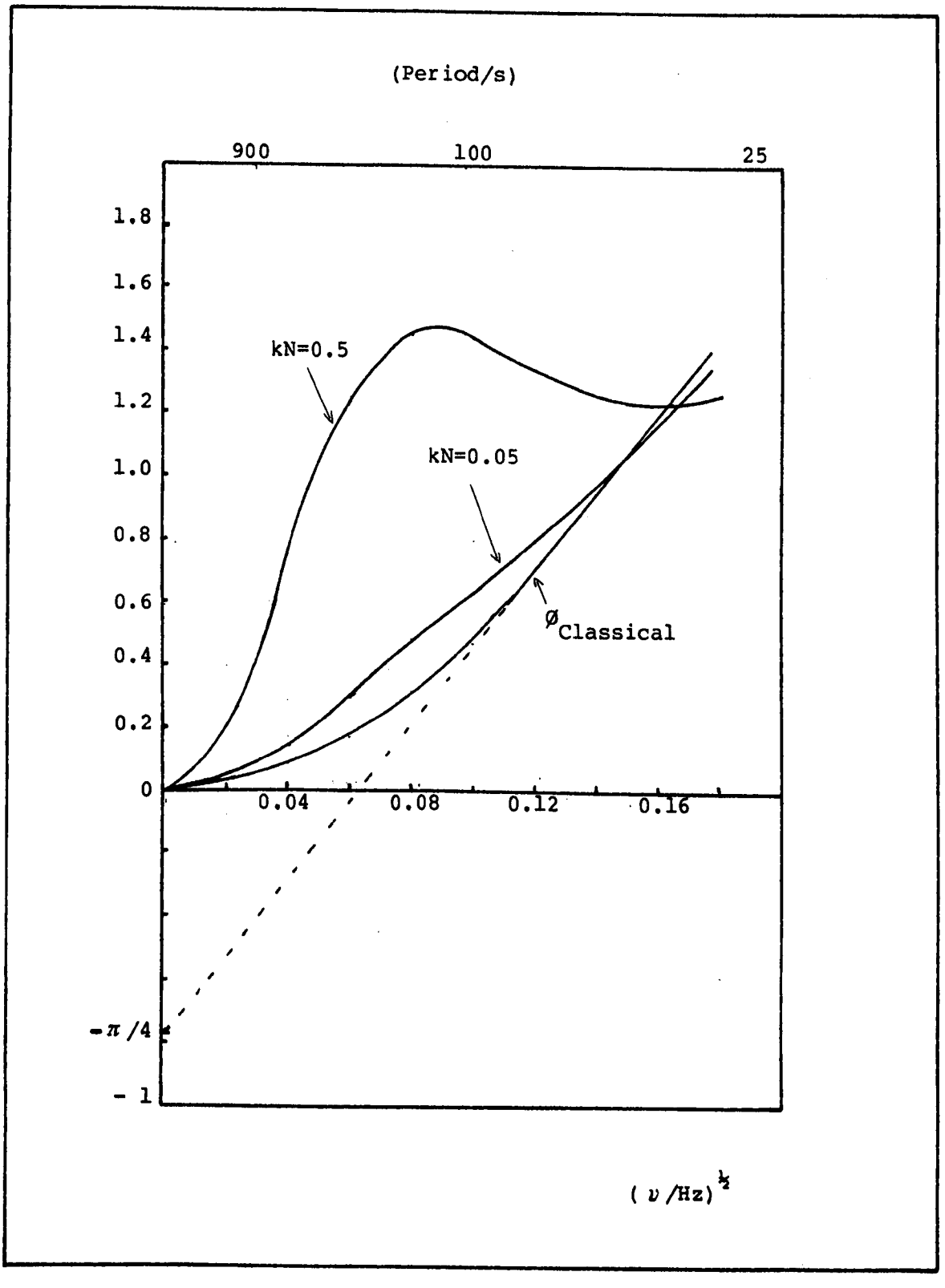

Fig. 4.11 ϕ v $\nu^{\frac{1}{2}}$ for trapping model:
$(L^2/D) = 50$: $p = 0.05$

SUMMARY

A generalized model of permeation has been developed which is characterised by four rate constants, $H_{i=2-5}$. By applying reasonable physical constraints to these rate constants, a particular model was chosen with which to analyse data collected by the modulation technique. This model is diffusion limited, in the sense that propagation times for transient events at the input to traverse the specimen are wholly due to the specimen volume. This corresponds to the rate constants $H_{i=2-5}$ being large and the phase lag for this model was denoted by $\phi_{H \gg 1}$.

A limiting case of $\phi_{H \gg 1}$ was investigated in which the rate constants were supposed to tend to infinity. The phase for this case was denoted by $\phi_{Classical}$. Under these conditions it was found that the input concentration $N^*(0)$ was continuously in equilibrium with the input gas and the exit concentration $N^*(L)$ could be neglected compared to $N^*(0)$.

In all other cases of $\phi_{H \gg 1}$ it was expected that $N^*(0)$, would no longer be in equilibrium with the gas and $N^*(L)$ could no longer be neglected with respect to $N^*(0)$. It was found that these changes at the input and exit were governed by the magnitudes of the competing fluxes at x = o and x = L.

Some typical phase/frequency curves were plotted for $\phi_{Classical}$ and $\phi_{H \gg 1}$. It was found that the curves for $\phi_{Classical}$ showed strong characteristics which may be useful, when analysing experimental data, to make particular choice of parameters. Amongst these characteristics are asymptotes with phase axis intercepts of $-\pi/4$, and independence of the mean flow of atoms onto the input surface. In general $\phi_{H \gg 1}$ is dependent on the mean flow of gas through a foil, by virtue of its dependence on H_4 and H_5.

An investigation was also made of steady rate fluxes and a characteristic flux, j, was identified which was a function of the rate parameters. It was found that the ratio of the steady rate flux $\bar{J}$ and j controlled the power law dependence of the flux on input pressure. When $(\bar{J}/j) \gg 1$ it was found

$$J \propto p^{\frac{1}{2}}$$

and when $(\bar{J}/j) \ll 1$ it was found

$$J \propto p^{1}.$$

CHAPTER FIVE

RESULTS

This chapter details an experimental study of light gas transmission through metal foils. Three gases, hydrogen, deuterium and helium and four metals, molybdenum, silver, gold and aluminium were used.

For the data on the transmission of hydrogen and deuterium in molybdenum and silver it proved possible to model gas flow using one parameter alone, the diffusion coefficient D, values for which were derived by finding the best least squares fit of $\phi_{Classical}$, defined by equation 4.37, on the data. A more complicated model, $\phi_{H \gg 1}$ defined by equation 4.42, with three parameters including the diffusion coefficient, was required to analyse the data for gold. Again a series of diffusion coefficients were derivd. Aluminium also showed behaviour conforming to the $\phi_{H \gg 1}$ model, however this data continuously changed even as it was gathered so no analysis was possible.

Despite a sophisticated injection system and an extremely sensitive detector, helium was not shown to pass through any of the experimental foils.

5.1. Materials with permeation data broadly conforming to the $\phi_{Classical}$ model.

When at the input the volume concentration, $N^*(0,t)$ is continuously in equilibrium with the gas and $N^*(0,t)$ is much greater than $N^*(L,t)$ the volume concentration at the exit, then the response time of fluctuations in the detection chamber due to fluctuations at the input should follow the pattern described in section 4.3.1. There it was shown that the phase, under these conditions, may be described by equation 4.37, which defines $\phi_{Classical}$, and depends on the diffusion coefficient and specimen thickness alone.

Phases of this class were found experimentally and investigated over a range of frequency. The following data which relates to molybdenum and silver concerns an experimental space limited in the following ways:

1) temperatures > 600K otherwise signal to noise ratio became

intolerably low or the experiments must be performed using low frequencies. In either case the rate of data gathering was reduced to an unacceptably low level.

2) temperatures < 950K, otherwise phase lags became too small at modulation frequencies within the limits set by the instrument response times.

3) ratios of (L^2/D) > 11s. Beyond this limit phase lags became too small.

4) ratios of (L^2/D) < 2×10^3s. Beyond this limit time lags became too long.

5) modulation frequencies < 3×10^{-2} Hz. Beyond this limit instrumental response times became important.

6) modulation frequencies greater than 2×10^{-4} Hz. Beyond this limit the rate of data gathering became too slow.

The experimental volume defined by these limits is sketched in Figure 5.1.

5.1.1. Molybdenum

Figure 5.2 shows plots of phase lag, ϕ, versus the square root of frequency, $\nu^{\frac{1}{2}}$, for hydrogen in molybdenum specimens of 0.025 cms thickness. The data at three temperatures, 695°K, 808°K 922°K are shown. Injection currents of 3mA with modulation amplitudes of 0.6mA were used. The data at 808°K and 922°K are for the same specimen. The detection chamber conditions for these experiments were: 2.25×10^{-8} torr with a modulation amplitude of about 2×10^{-9} torr: 1.25×10^{-7} torr with a modulation amplitude of about 7×10^{-9} torr: 7.5×10^{-7} torr with a modulation amplitude of about 4×10^{-8} torr respectively.

Characteristic of the data on molybdenum is that extrapolation of the high frequency data back to the phase axis gives an intercept of $-\pi/4$. For the data shown in Figure 5.2 the actual value of the intercepts are

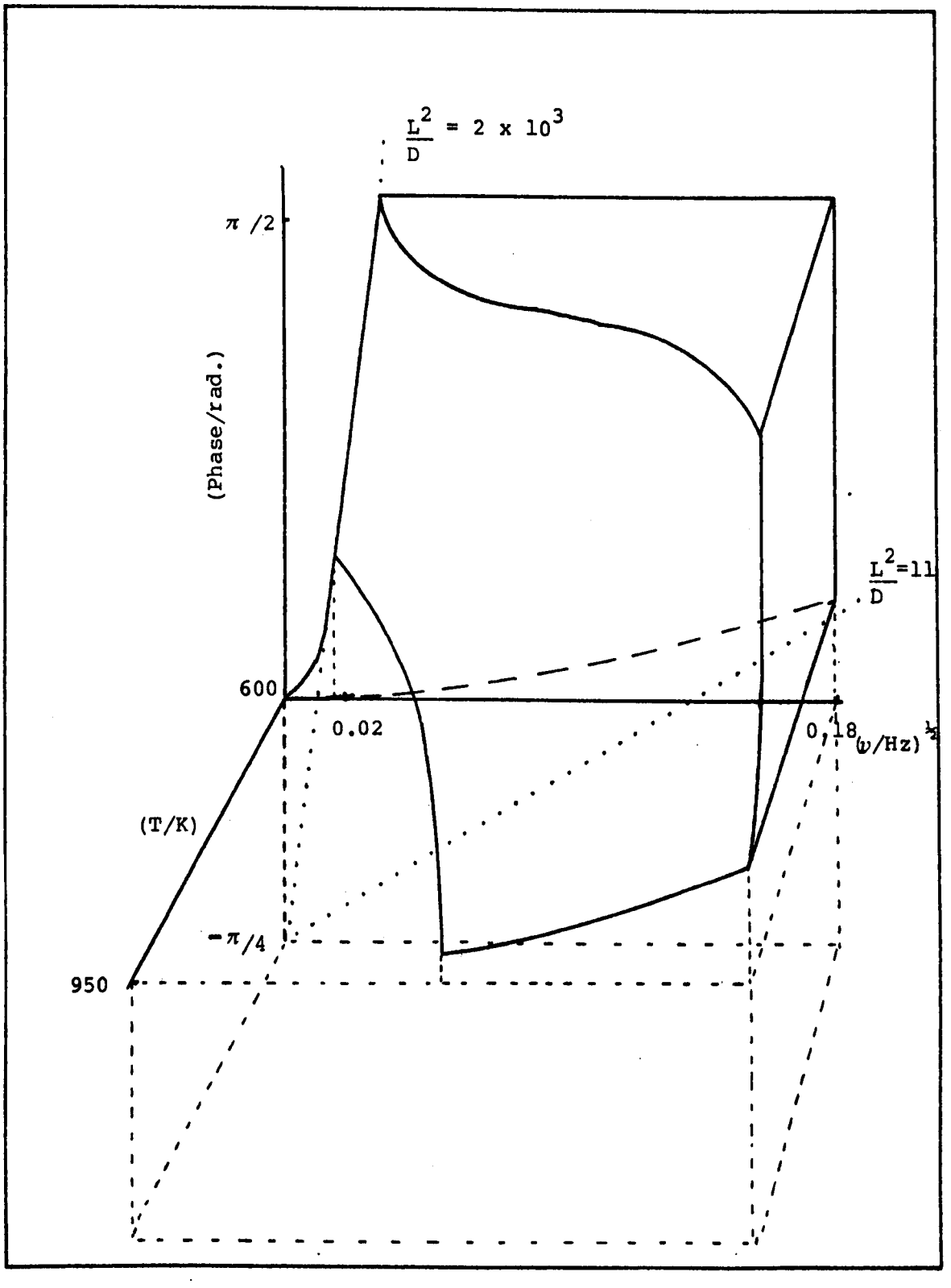

Fig. 5.1. The experimental volume. (See text)

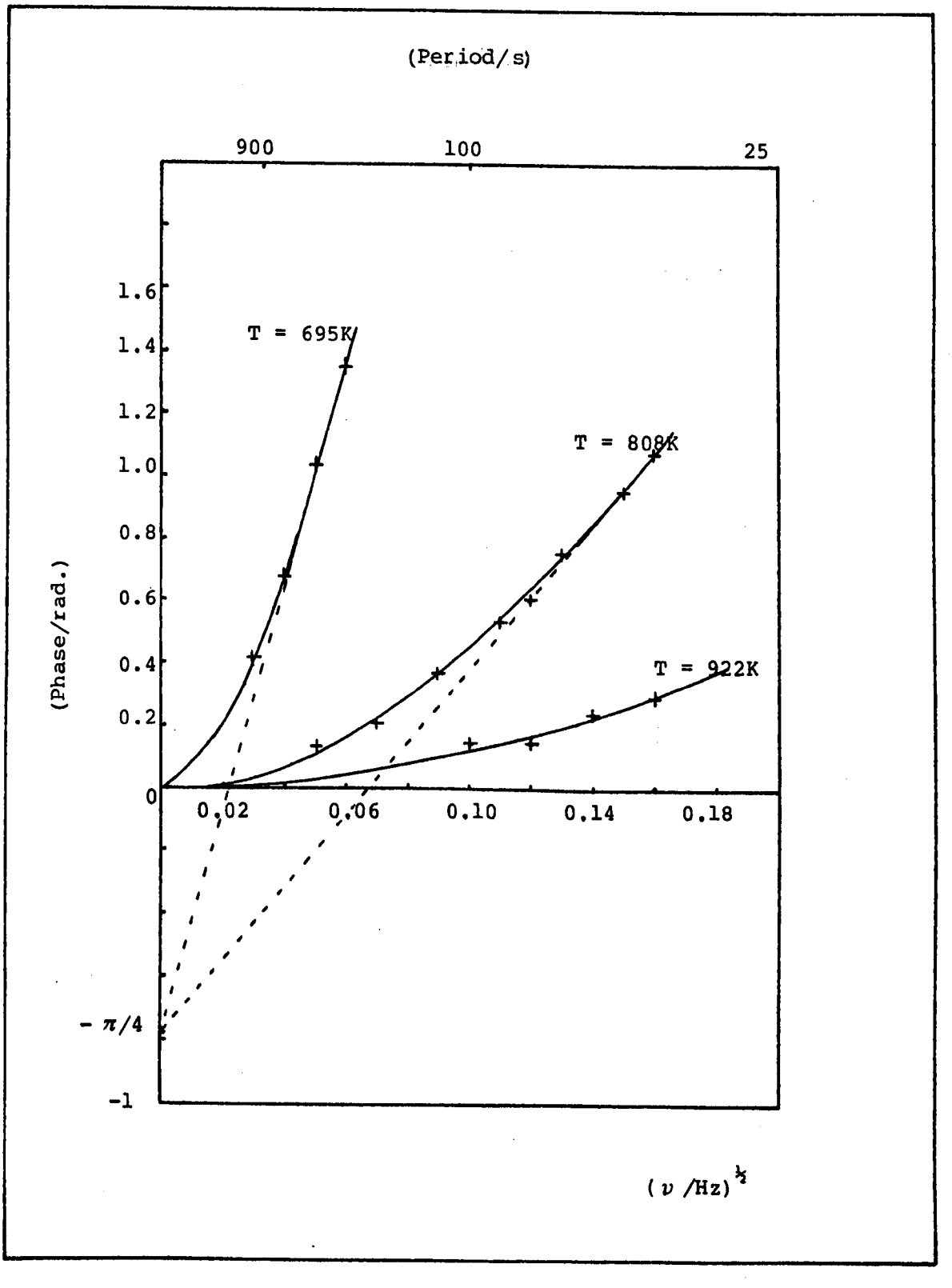

Fig. 5.2 Typical plots of Ø v $\nu^{\frac{1}{2}}$ for hydrogen in 0.025cm thick molybdenum at the temperatures: 695°K, 808°K, and 922°K.

-0.76 ± 0.03 radians, -0.75 ± 0.04 radians, which comfortably include the expected intercept of $-\pi/4$ and is indicative of the overall precision of the data. Note the actual intercepts are slightly greater than $-\pi/4$, this probably reflects that the data extends insufficiently into the linear region. Certainly the data at $922^{\circ}K$ is not in the linear region so no value of the intercept is given.

Figure 5.3 shows another plot, for the same specimen as used for the $695^{\circ}K$ data referred to above, but at a temperature of $638^{\circ}K$ and the same injection current. The detection chamber conditions were 1.9×10^{-8} torr with a modulation of $\sim 3 \times 10^{-10}$ torr. In this case the signal to noise ratio is lower. The actual intercept is now -0.62 ± 0.12 radians so the expected intercept, of $-\pi/4$, is just beyond this range. This may, to some extent, be due to specimen degradation.

Curves of the above character were found regularly using specimens of molybdenum and the reproducibility of the intercept of the extrapolation from high frequencies, came to be seen as an indicator of $\phi_{Classical}$ behaviour. To test the consistency of the data a number of experiments were performed using different injection conditions. The mean injection current was varied over the range 1mA - 8mA and had no appreciable effect on the phase lags. This is illustrated by Figure 5.4 which is for the experiment at $808^{\circ}K$ detailed above. The consistency of output with variations in the amplitude of the modulation of the injection current is exemplified in Figure 5.5 which shows data for almost the same experimental conditions, except the mean injection current was 6mA.

In molybdenum and in silver, as will be reported later, phase data proved to be stable, against variations in injection current. At no time were phase lags seen to vary with the mean injection current or with the amplitude of the modulation of that current. Strongly characteristic of almost all data

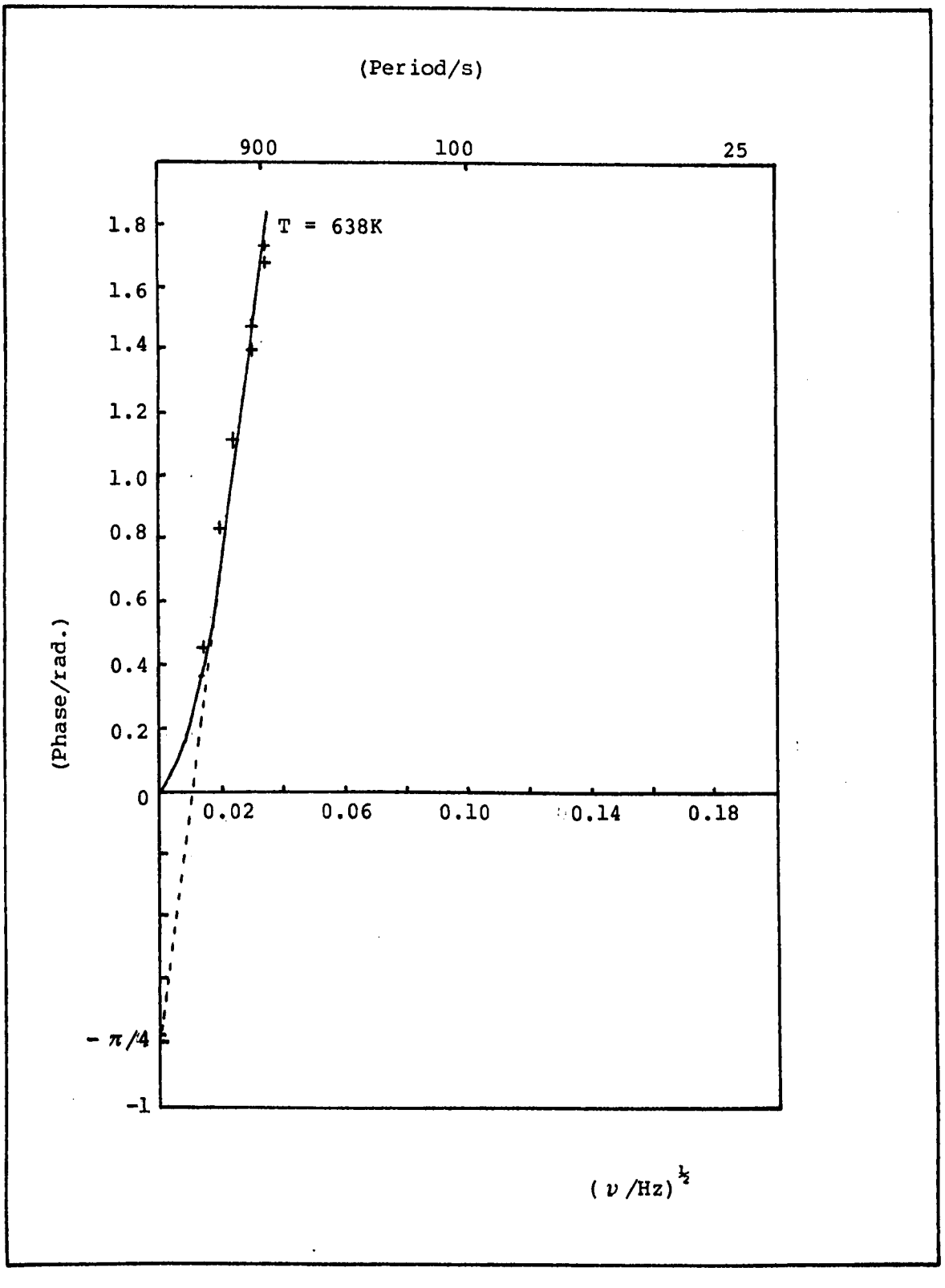

Fig. 5.3 Plot of ϕ v $\nu^{\frac{1}{2}}$ for hydrogen in molybdenum at 638°K showing poor signal to noise ratio.

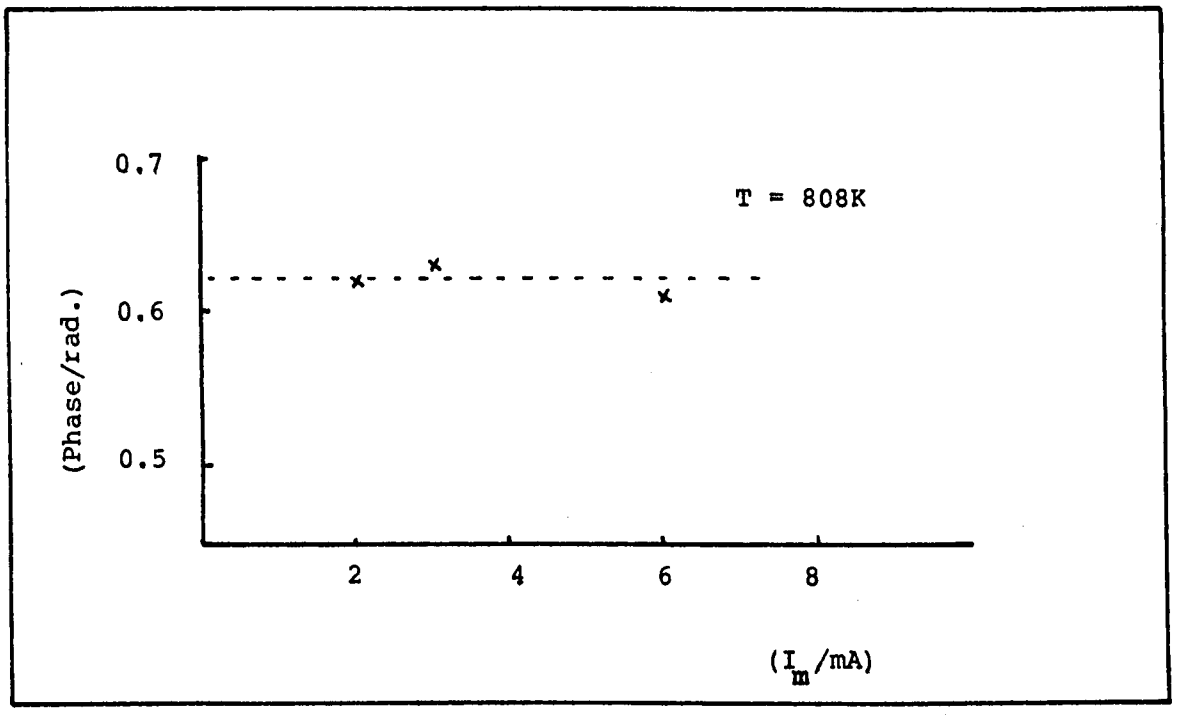

Fig. 5.4 Phase v mean discharge current at ν =0.0144 Hz, demonstrating phase invariance with mean discharge current.

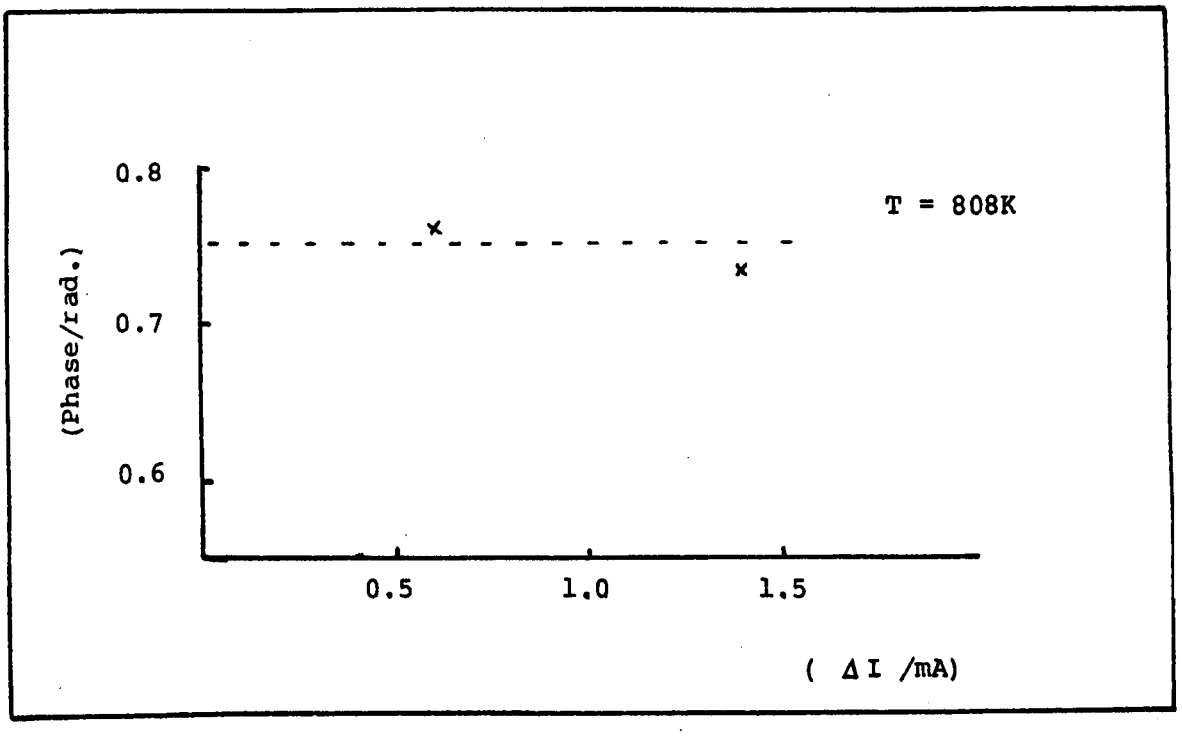

Fig. 5.5 Phase v modulation amplitude at ν =0.0169 Hz, demonstrating phase invariance with modulation amplitude of discharge current.

was the precision with which high frequency data extrapolated back to the intercept of $-\pi/4$ with the phase axis. For these reasons it was possible with some confidence, to use equation 4.37 for the evaluation of diffusion coefficients.

In a number of experiments attempts were made to use data in the amplitude of the pressure modulations found in the detection chamber. Figure 5.6 shows amplitudes of pressure modulations in the detection chamber versus the square root of frequency, at 875°K and a mean discharge current of 3mA with a modulation of 0.6mA. The detection chamber conditions were 4×10^{-7} torr, with a modulation amplitude of about 3×10^{-8} torr. Such a curve is to be interpreted using equation 4.35. This is shown in Figure 5.7 in which the same amplitudes are plotted versus $(\nu/(\sinh^2 kL + \sin^2 kL))^{\frac{1}{2}}$, the function defined in equation 4.40.

The diffusion coefficient from phase measurements has been used in $k = (\omega/2D)^{\frac{1}{2}}$ to evaluate the function. Diffusion coefficients are derivable from the amplitudes of pressure modulations in the detection chamber. But as the data in Figures 5.6 and 5.7 show, this is not a generally satisfactory method, even in less extreme cases because of the signal to noise ratio. For these reasons this mode of data evaluation was not pursued further.

In Figure 5.8 is shown the collected data for the diffusion of hydrogen in molybdenum. Each diffusion coefficient was calculated using a least squares fit on equation 4.37. All the phase/frequency data was used in the least square fit, not merely the high frequency data of the linear part to the curve. The collected diffusion coefficient data are given in Table 5.1. A least squares fit to this data gives as the diffusion coefficient of hydrogen in molybdenum:

$$D_H = (7.8 \pm 4.1) \times \exp[-(0.93 \pm 0.03)\ eV/kT]\ cm^2 s^{-1} \quad (5.1.)$$

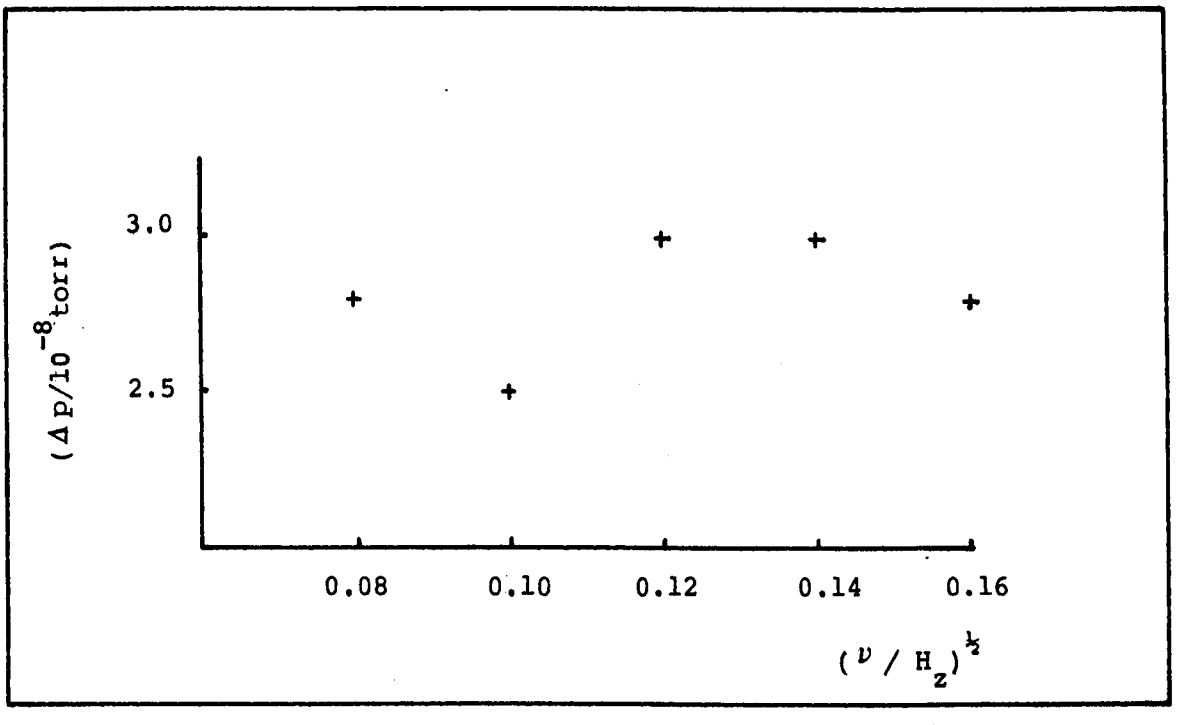

Fig. 5.6 Showing amplitude of detection chamber pressure modulations v $\nu^{\frac{1}{2}}$ at T= 875K.

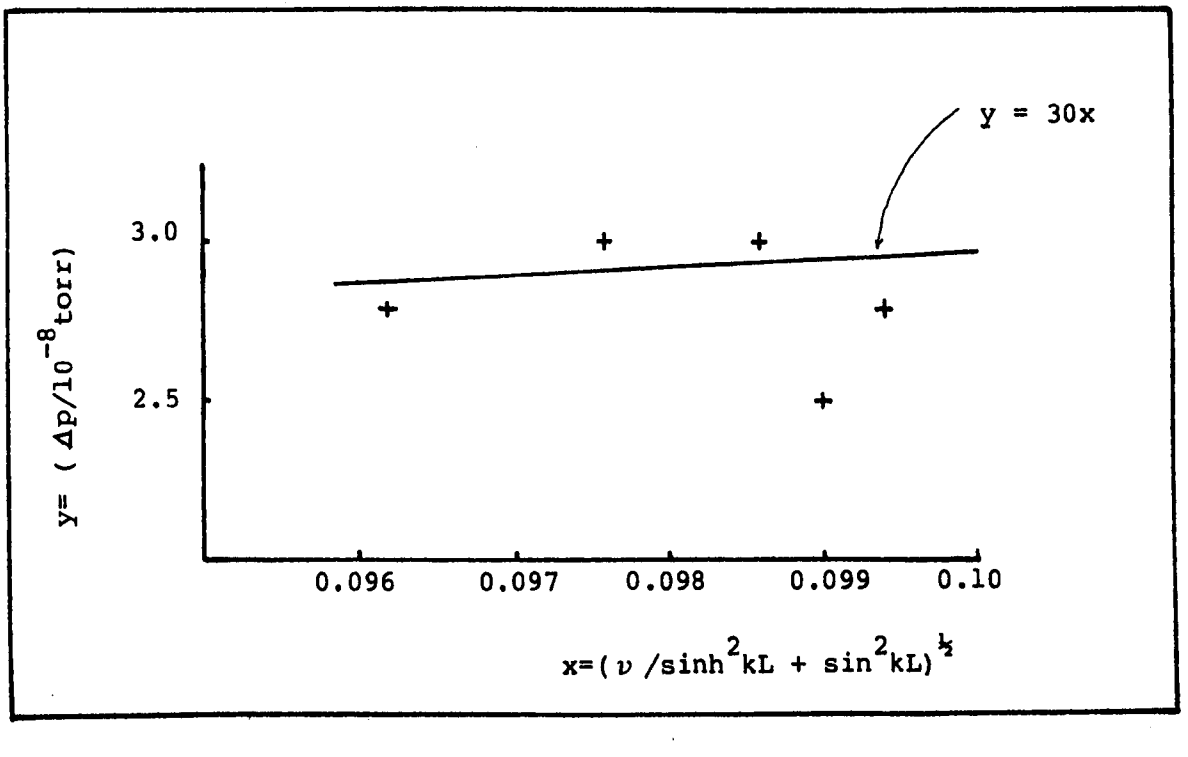

Fig. 5.7 Showing amplitudes of detection chamber pressure modulations v $(\nu /\sinh^2 kL + \sin^2 kL)$ at T= 875K with L^2/D = 50.35

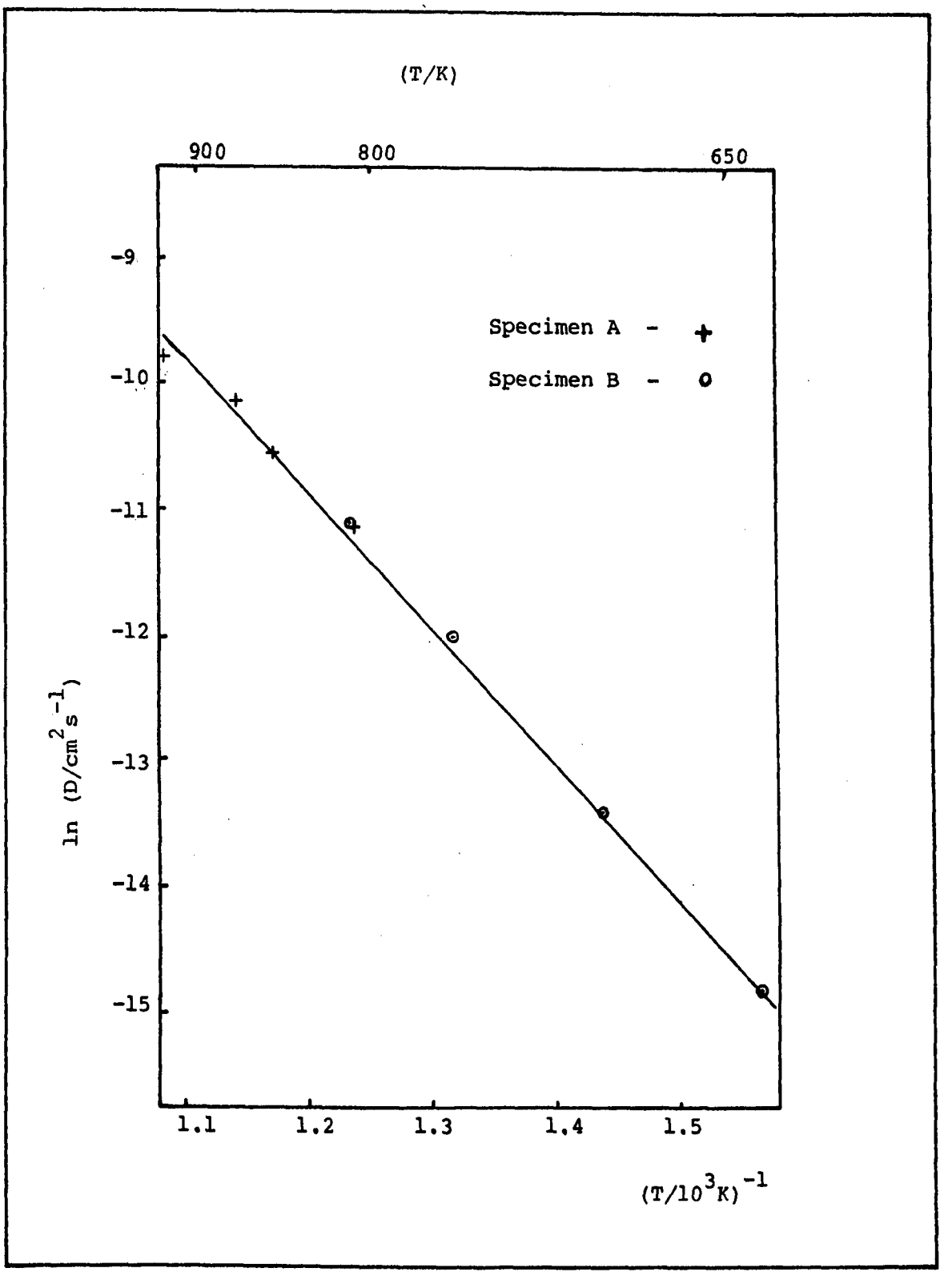

Fig. 5.8 ln D v T^{-1} for hydrogen in molybdenum.

Table 5.1

The collected diffusion coefficients of hydrogen in Molybdenum

(T/K)	$(T/10^3 K)^{-1}$	$(D/cm^2 s^{-1}$	$\pm(\Delta D/D)$ %	$\ln(D/cm^2 s^{-1})$	Specimen	Thickness
922	1.085	5.57×10^{-5}	7	- 9.796	A	0.025
875	1.143	3.90×10^{-5}	4.5	-10.152	A	0.025
853	1.172	2.75×10^{-5}	6	-10.501	A	0.025
808	1.238	1.43×10^{-5}	2.5	-11.155	A	0.025
810	1.235	1.40×10^{-5}	1.5	-11.118	B	0.025
759	1.317	5.97×10^{-6}	3.5	-12.029	B	0.025
695	1.439	1.49×10^{-6}	3	-13.417	B	0.025
638	1.567	3.62×10^{-7}	7.5	-14.832	B	0.025

Using the same specimens and working at the same experimental conditions almost idential experiments were performed using deuterium as the experimental gas. Figure 5.9 shows a plot of phase lag ϕ, versus the square root of frequency $\nu^{\frac{1}{2}}$, at $808^{\circ}K$. The detection chamber conditions were 1.15×10^{-7} torr with a modulation amplitude of about 5×10^{-9} torr. Also shown as a dotted curve, in Figure 5.9 is the hydrogen curve at this temperature for comparison.

Characteristic of the data on molybdenum, in the temperature range investigated, was that deuterium phase lags were always greater then the equivalent hydrogen data. This implies that deuterium diffusion coefficients are smaller than hydrogen diffusion coefficients in this range. Apart from this the data collected for deuterium showed the same behaviour as that from hydrogen. Specifically the data shows precise extrapolation of high frequency information to an intercept at $-\pi/4$ on the phase axis. For the curve in Figure 5.9 this intercept is actually -0.77 ± 0.02 radians. Also the consistency of data with variations of mean discharge and the amplitude of discharge current modulation. Hence deuterium diffusion coefficients were also evaluated using equation 4.37.

Figure 5.10 illustrates the collected data for the diffusion of deuterium in molybdenum, these diffusion coefficients are listed in Table 5.2. A least squares fit to this data gives as the diffusion coefficient of deuterium in molybdenum

$$D_D = (5.3 \pm 4.1) \exp\left[-(0.91 \pm .03)\,eV/kT\right] \quad cm^2 s^{-1} \qquad (5.2)$$

Comparing D_H and D_D from equations 5.1 and 5.2 it is found that the ratio of the pre-exponential factors is

$$\frac{D_O^H}{D_O^D} = 1.36 \pm 1.9$$

$$= (0.96 \pm 1.34)\sqrt{2}$$

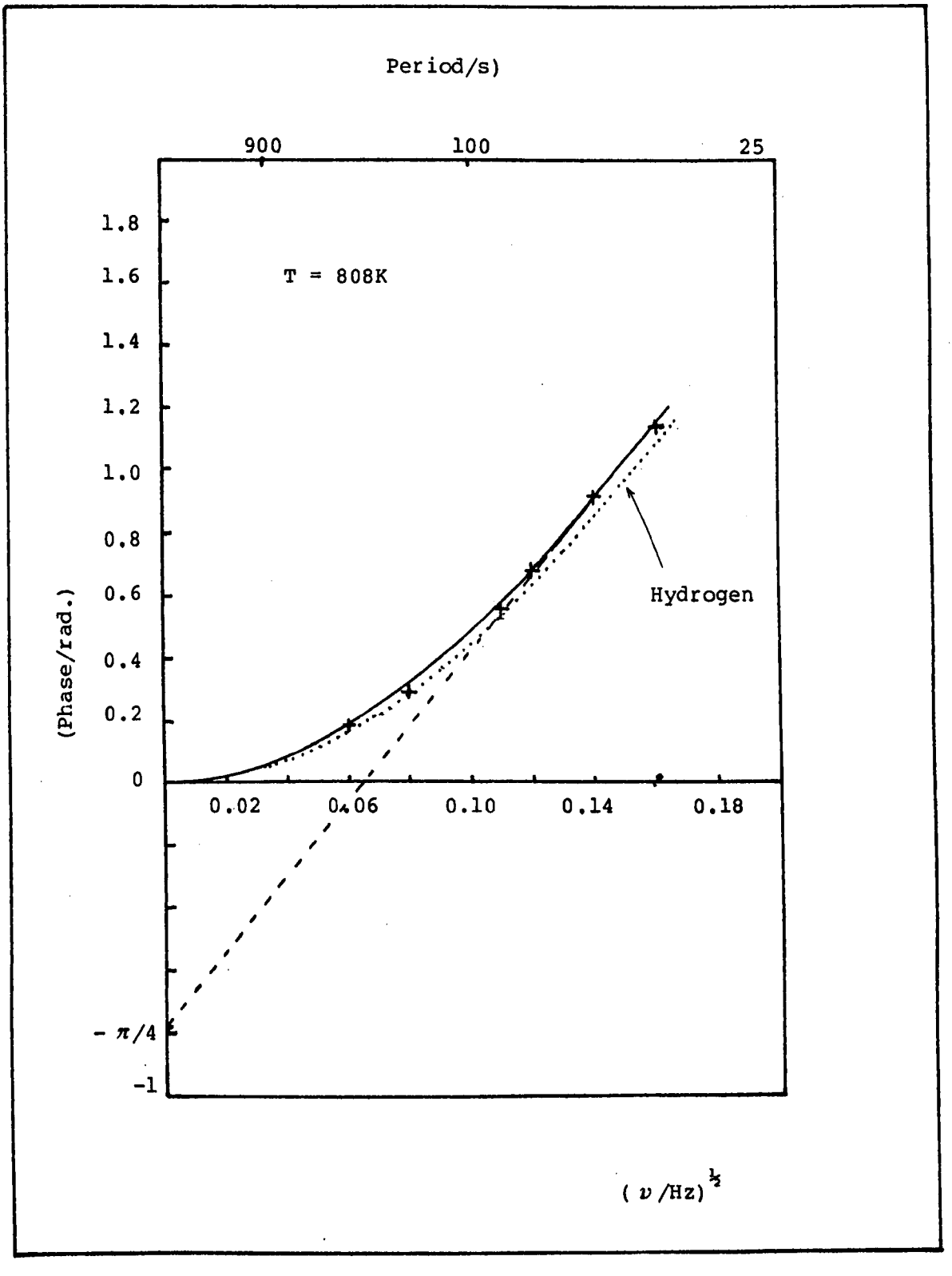

Fig. 5.9 ϕ v $\nu^{\frac{1}{2}}$ for deuterium in 0.025cm thick molybdenum at 808K. Also shown as a dotted line is the hydrogen phase/frequency curve at 808K, for comparison.

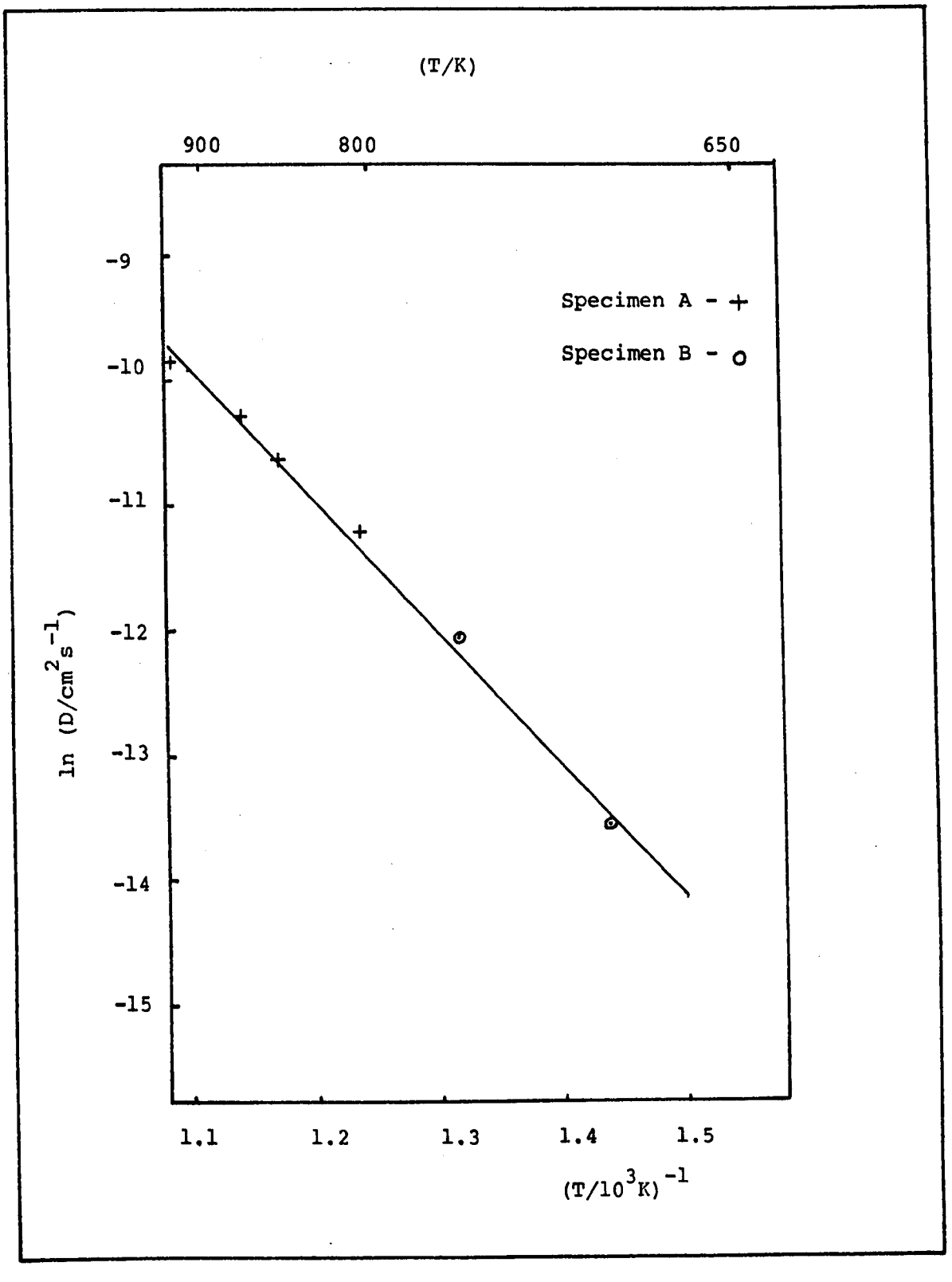

Fig. 5.10 ln D v T^{-1} for deuterium in molybdenum

Table 5.2

The collected diffusion coefficient of deuterium in Molybdenum

(T/K)	$(T/10^{+3}K)^{-1}$	$(D/cm^2s^{-1}$	$\pm(\Delta D/D)$ %	$\ln(D/cm^2s^{-1})$	Specimen	Thickness
922	1.085	$5.25x10^{-5}$	4	- 9.855	A	0.025
875	1.143	$3.35x10^{-5}$	5	-10.304	A	0.025
853	1.172	$2.37x10^{-5}$	4	-10.650	A	0.025
808	1.238	$1.34x10^{-5}$	2	-11.220	A	0.025
759	1.317	$5.64x10^{-6}$	2	-12.086	B	0.025
695	1.439	$1.29x10^{-6}$	3.5	-13.561	B	0.025

and the difference in activation energies is

$$(E_H - E_D) = (0.93 \pm 0.03 - 0.91 \pm 0.03)\,eV$$

$$= (0.02 \pm 0.06)\,eV$$

The observed ratio of D_O^H/D_O^D may be seen to compare favourably with the expected value of $2^{\frac{1}{2}}$, from classical theory, and to be within experimental error of this value. Also it may be seen that there is no significant difference in the isotopic activation energies, so there is no evidence for a variation of isotopic ratio with temperature. Table 5.3 collects the isotopic ratios at the individual temperatures using the data from Tables 5.1 and 5.2.

Table 5.3

Isotopic ratios of diffusion coefficients for molybdenum in the temperature range 695 - 922K

(T/K) :	695	759	808	853	875	922
(D_H/D_D) :	1.16	1.06	1.07	1.16	1.16	1.06

$$\text{Mean of } (D_H/D_D) = 1.11 \pm 0.05$$

$$= (0.78 \pm 0.04)\sqrt{2}$$

The mean value of the isotopic ratio at individual temperatures is significantly lower than (D_O^H/D_O^D) and shows considerable difference from the classical value of $2^{\frac{1}{2}}$. This difference is because D_O's are evaluated using what is effectively an extrapolation; they therefore have a falsely high deviation relative to the set of measurements; thus expect a tighter ratio to be evaluated in the temperature range of the experiment.

5.1.2 Silver

Figure 5.11 shows plots of phase lag, ϕ, versus the square root of frequency, $\nu^{\frac{1}{2}}$, for hydrogen in a silver specimen of 0.06cm thickness. Data taken at two temperatures, 654K and 764K are shown. Injection currents of 3.5mA with modulation amplitudes of 0.75mA were used. Both curves are derived from the one specimen. The detection chamber conditions for these experiments were: 5.2×10^{-7} torr with a modulation amplitude of about 4×10^{-8} torr; 7.1×10^{-7} torr with a modulation amplitude of about 6×10^{-8} torr, respectively.

The curves show the characteristics of diffusion limited permeation, with the high frequency data extrapolating back to an intercept of $-\pi/4$ on the phase axis. The actual values of the intercepts of the two curves shown in Figure 5.11 are, -0.75 ± 0.03 and -0.80 ± 0.05 respectively. As with molybdenum the phase data showed consistency with variations in the mean injection current. That is, the variations did not produce changes in phase which were in excess of expected experimental errors.

Having regularly found curves of the above character it was possible, with confidence, to use equation 4.37 for the evaluation of diffusion coefficients. In Figure 5.12 is shown the collected data for the diffusion of hydrogen in silver. The diffusion coefficients were calculated using a least squares fit on equation 4.37, using all the phase/frequency data. This data was collected using four specimens. The main body of the data came from specimens A and B which were of 0.06cm thickness. Specimen C was 0.05cm thick and specimen D was 0.03cm thick. The collected diffusion coefficient data are given in Table 5.4. A least squares fit to this data gives as the diffusion coefficient of hydrogen in silver:

$$D_H = (1.7 \pm 0.7) \times 10^{-2} \exp\left(-(0.39 \pm 0.02)\ \mathrm{eV}/kT\right)\ \mathrm{cm}^2\mathrm{s}^{-1} \qquad (5.3)$$

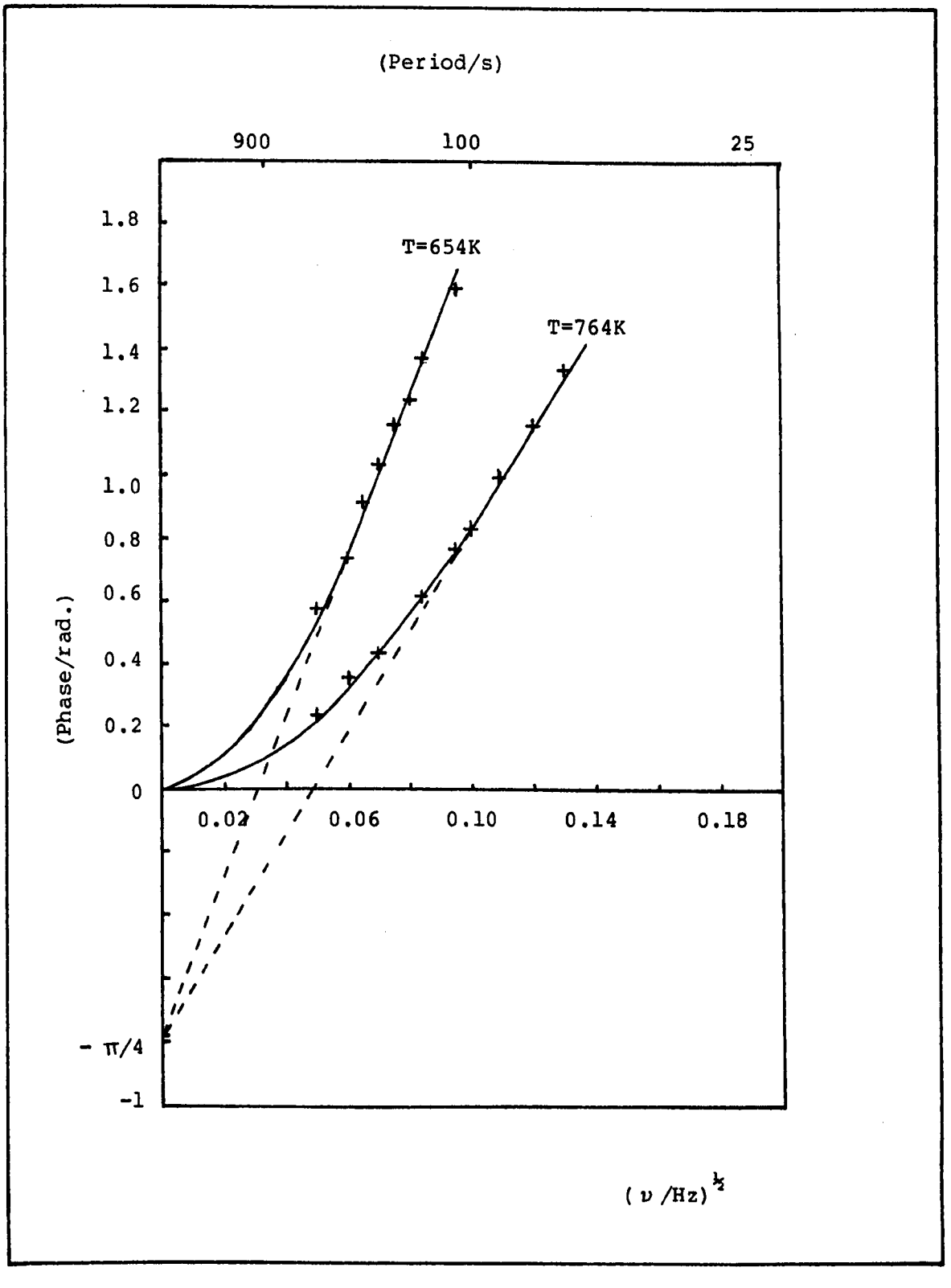

Fig. 5.11 Ø v $\nu^{\frac{1}{2}}$ for hydrogen in 0.06cm thick silver at 654K and 764K.

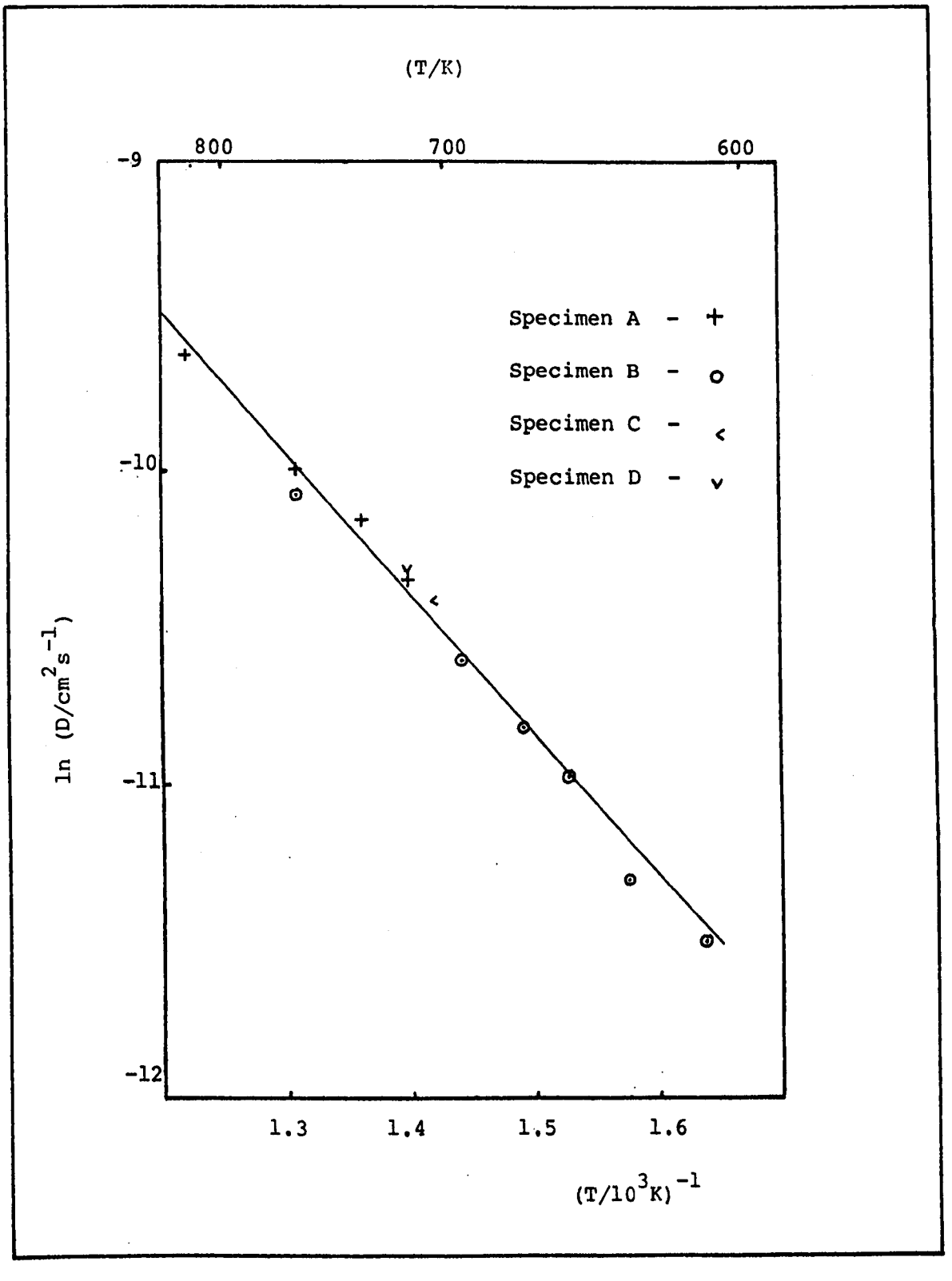

Fig. 5.12 ln D v T^{-1} for hydrogen in silver

Table 5.4

The collected diffusion coefficient of hydrogen in silver

T/K	$(T/10^{+3}K)^{-1}$	(D/cm^2s^{-1})	$\pm(\Delta D/D)$ %	$\ln(D/cm^2s^{-1})$	Specimen	Thickness
717	1.395	$3.21x10^{-5}$	4	-10.347	A	0.06
734	1.362	$3.89x10^{-5}$	3	-10.155	A	0.06
764	1.309	$4.75x10^{-5}$	2.5	- 9.955	A	0.06
821	1.218	$6.58x10^{-5}$	3.5	- 9.629	A	0.06
611	1.637	$1.01x10^{-5}$	7	-11.503	B	0.06
635	1.575	$1.22x10^{-5}$	2	-11.314	B	0.06
654	1.529	$1.71x10^{-5}$	3.5	-10.976	B	0.06
670	1.493	$2.0\ x10^{-5}$	2.5	-10.820	B	0.06
693	1.443	$2.47x10^{-5}$	2.5	-10.609	B	0.06
764	1.309	$4.18x10^{-5}$	2.5	-10.083	B	0.06
705	1.418	$2.98x10^{-5}$	2.5	-10.421	D	0.05
716	1.397	$3.28x10^{-5}$	3	-10.325	C	0.03

A series of experiments were also performed with silver using deuterium as the experimental gas. One of the specimens used in these experiments was specimen D, 0.05cm thick, mentioned above. The other specimen was also of 0.05cm thickness. Experiments were performed over the temperature range $670^{\circ}K$ - $870^{\circ}K$ and amongst these several were performed with conditions identical to those used for hydrogen.

Figure 5.13 shows a plot of phase lag, ϕ, versus the square root of frequency, $\nu^{\frac{1}{2}}$ at, $764^{\circ}K$. The input conditions were as with the hydrogen experiments. The detection chamber conditions were 4.45×10^{-7}torr with a modulation amplitude about 5×10^{-8} torr. Also shown in Figure 5.13, as a dotted curve, is the corresponding hydrogen curve using (L^2/D) from Table 5.4.

Characteristic of the data for deuterium in silver was the extrapolation of the high frequency data to an intercept of $-\pi/4$ on the phase axis. For the curve in Figure 5.13 this intercept was actually -0.80 ± 0.03 radians which comfortably includes $-\pi/4$.

Regular observation of the indicators of "classical" permeation made it possible to confidently evaluate diffusion coefficients using equation 4.37. The resulting collected diffusion data for deuterium in silver is illustrated in Figure 5.14 and tabulated in Table 5.5 . A least squares fit to this data gives as the diffusion coefficient of deuterium in silver:

$$D_D = (9.8 \pm 3.0) \times 10^{-3} \exp(-(0.37 \pm 0.02)\ eV/kT)\ cm^2 s^{-1}. \quad (5.4)$$

Comparing D_H and D_D from equations 5.3 and 5.4 its found that the ratio of the pre-exponential factors is

$$\frac{D_O^H}{D_O^D} = 1.73 \pm 1.2$$

$$= (1.23 \pm 0.86)\sqrt{2}$$

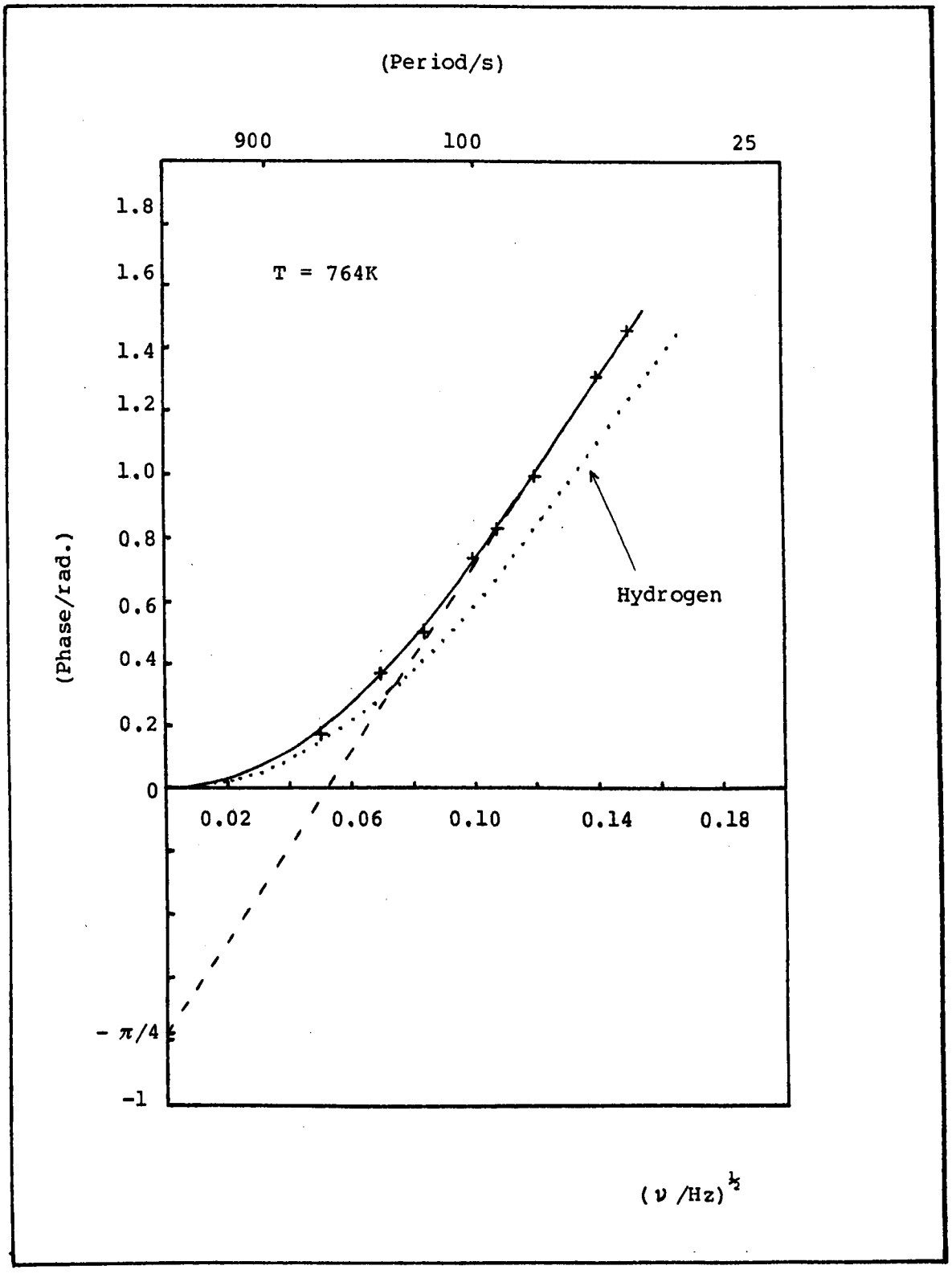

Fig. 5.13 ϕ v $\nu^{\frac{1}{2}}$ for deuterium in 0.05cm thick silver at 764K. Also shown as a dotted line is the hydrogen phase/frequency curve (with L^2/D = 58.1, where the diffusion coefficient from Table5.4 has been used).

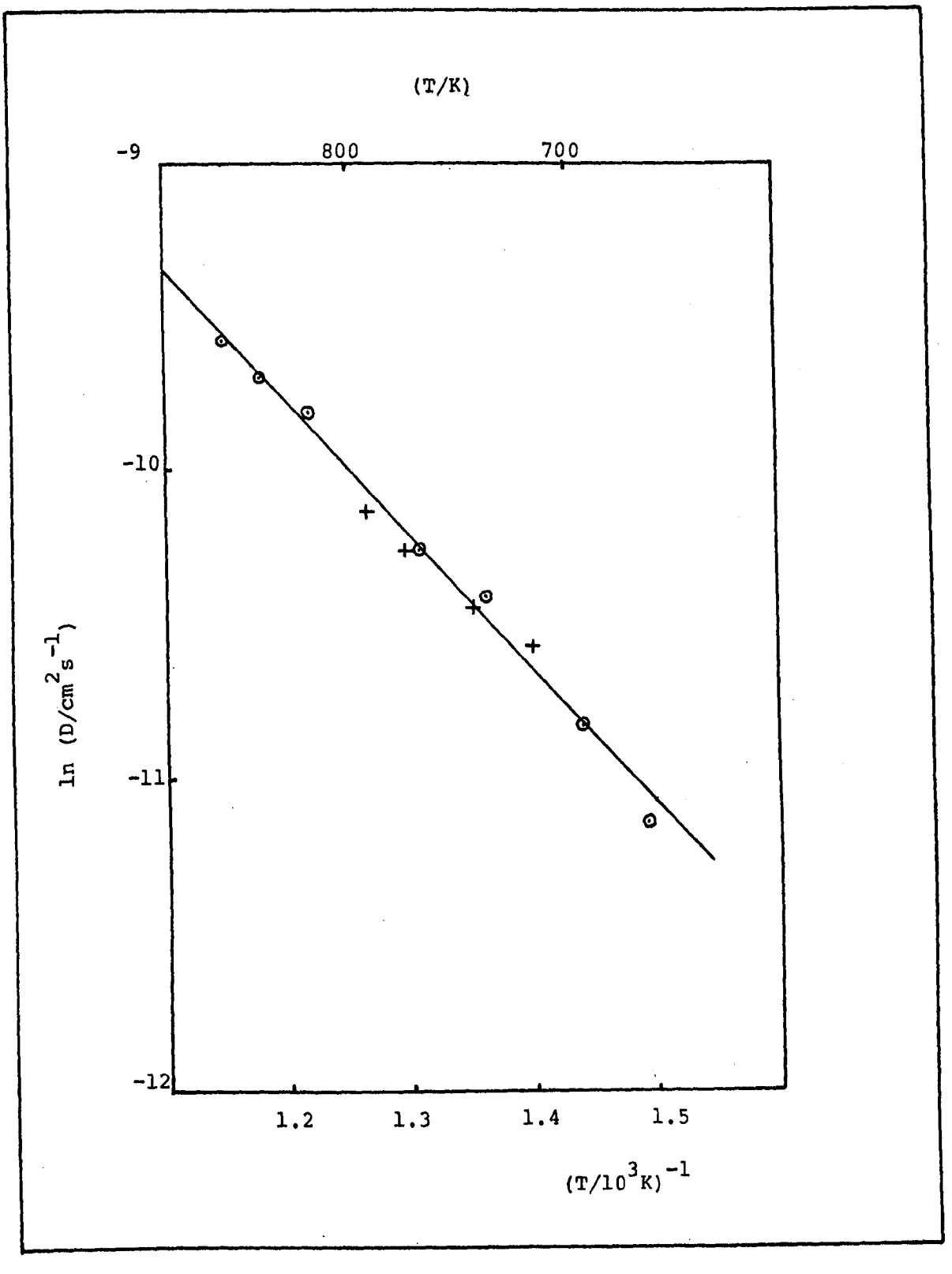

Fig. 5.14 ln D v T^{-1} for deuterium in silver.

Table 5.5

The collected diffusion coefficient of deuterium in silver

T/K	$(T/10^{+3}K)^{-1}$	(D/cm^2s^{-1})	$\pm(\Delta D/D)\%$	$\ln(D/cm^2s^{-1})$	Specimen	Thickness
714	1.401	2.57×10^{-5}	2	-10.569	D	0.05
740	1.351	2.90×10^{-5}	3	-10.448	D	0.05
771	1.297	3.48×10^{-5}	1.5	-10.266	D	0.05
789	1.267	3.95×10^{-5}	1	-10.139	D	0.05
670	1.493	1.45×10^{-5}	1.5	-11.141	E	0.05
694	1.441	1.985×10^{-5}	3	-10.827	E	0.05
734	1.362	2.99×10^{-5}	1	-10.418	E	0.05
764	1.309	3.47×10^{-5}	2	-10.269	E	0.05
821	1.218	5.43×10^{-5}	1.5	- 9.821	E	0.05
849	1.178	6.09×10^{-5}	2.5	- 9.706	E	0.05
871	1.148	6.90×10^{-5}	2.5	- 9.581	E	0.05

and the difference in activation energies is:

$$(E_H - E_D) = (0.39 \pm 0.02 - 0.37 \pm 0.02)\ eV$$
$$= (0.02 \pm 0.04)\ eV$$

The observed ratio of D_O^H/D_O^D is significantly larger than the expected value of $2^{\frac{1}{2}}$ from classical theory. Also there is no significant difference in isotopic activation energies, hence there is no experimental evidence for variation of isotopic ratio with temperature. Table 5.6 collects the isotopic ratios at particular temperatures using the data from Tables 5.4 and 5.5

Table 5.6

Isotopic ratios of diffusion coefficients for silver in the temperature range 670 - 821K.

(T/K):	670	695	715	734	764	764	821
(D_H/D_D):	1.38	1.24	1.23	1.30	1.37	1.20	1.21

Mean value $(D_H/D_D) = 1.28 \pm 0.07$
$= (0.90 \pm 0.05)\sqrt{2}$

The mean value of the isotopic ratios at individual temperatures is significantly lower than the expected value of $2^{\frac{1}{2}}$ from classical theory and is significantly lower than (D_O^H/D_O^D). This latter difference is again due to the method of evaluating the D_O's which is effectively an extrapolation with a high deviation relative to the set of measurements.

5.2 Materials with permeation data broadly conforming to the $\phi_{H>>1}$ expectation

In section 4.3.2 circumstances were identified where $\phi_{Classical}$ ceased to be a valid description of phase/freqeuncy behaviour. Under these

conditions it was supposed that processes at the input and exit played an important part in determining the response time of fluctuations in the detection chamber due to fluctuations at the input. Therefore $\phi_{H >> 1}$ was proposed as a possible description of phase/frequency behaviour.

It was found during the course of experiment that the phase/frequency data of gold and aluminium showed characteristics broadly conforming to those detailed in section 4.3.2. These results are reported here.

5.2.1. Gold

Gold was chosen for experimental work for two reasons; (a) it has a low hydrogen solubility and (b) it shows non-Sievert behaviour at input pressures available for study with the present equipment, (52). Steady-rate experiments for gold, detailed in section 5.3.2 confirm both of these observations.

A series of modulation experiments were performed at four temperatures, in the range 769 - 875K, with hydrogen. Two specimens were used, one 0.025cm thick the other 0.05cm thick, and the experiments were performed at almost identical temperatures in each case.

In all of the experiments the input hydrogen pressure was $\sim$ 1.8torr. The majority of the data was taken with mean discharge currents of 4mA and modulation amplitudes of the discharge current of 0.6mA. In the detection chamber, hydrogen partial pressures were mainly determined by the outgas rate from the hot regions of the stainless steel vacuum chambers. The partial pressure was $\sim 4 \times 10^{-8}$ torr.

Figure 5.15 shows the variation of observed phase, ϕ, with mean discharge current I_m mA. The actual dependent variable was chosen to be

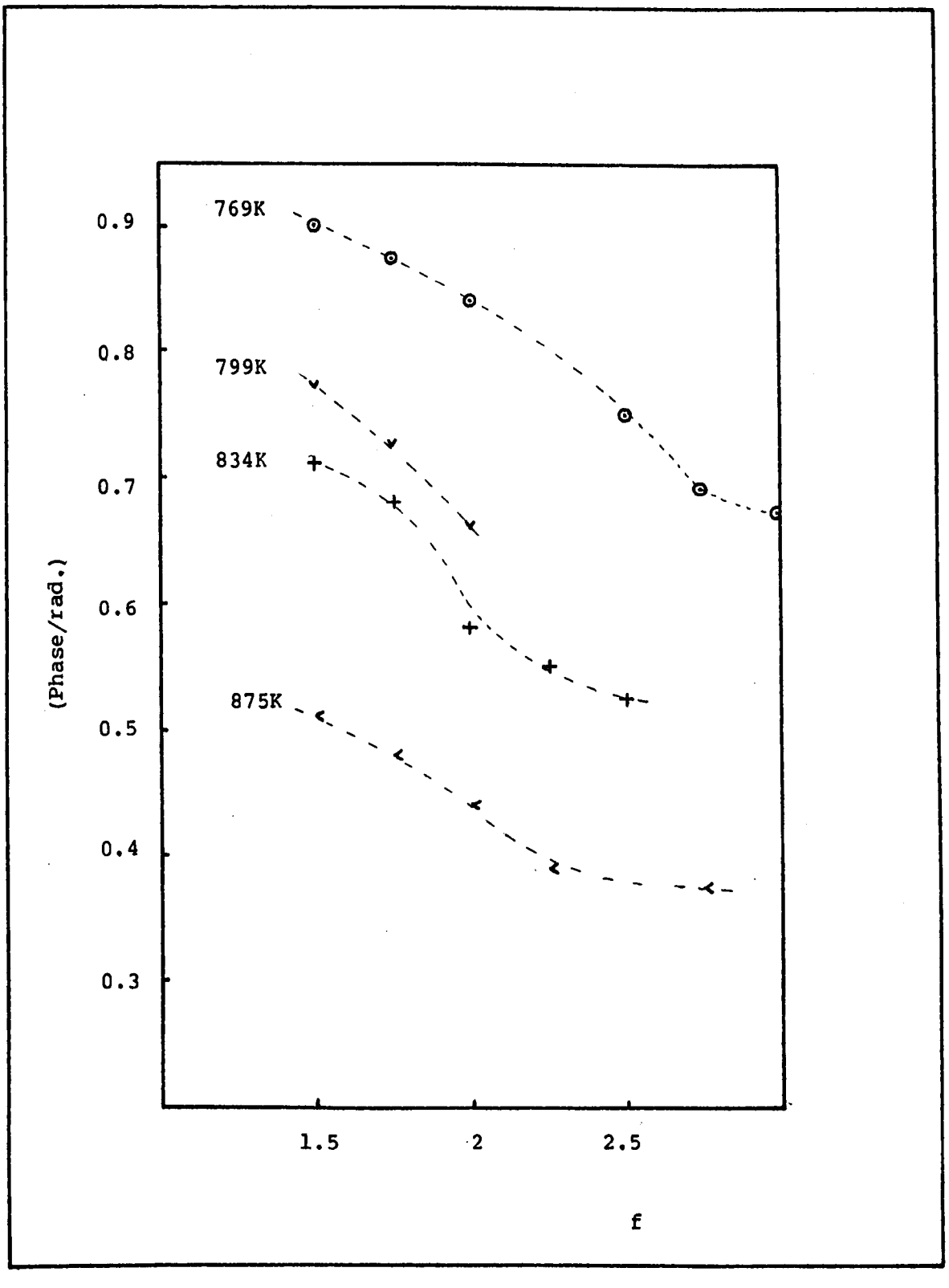

Fig. 5.15 Ø v f, illustrating the mean discharge current dependence of the phase lag through the 0.05cm thick foil at the temperatures: 769K, 799K, 834K and 875K, (See text).

N.B. The broken lines are visual aids only.

$f = (1 + \alpha I_m)$ where α is a factor relating the mean discharge current to the flux that it induces relative to the dissolution flux. From observations made a suitable value is $\alpha \sim 0.25$. All the data shown in the figure were taken at a fixed modulation frequency, $\nu = 10^{-2}$ Hz, and with the 0.05cm thick specimen. Similar behaviour was also found with the 0.025cm thick specimen.

A possible dependence of phase on mean discharge current was described in section 4.3 .2. It was characterised by $\phi_{H >> 1}$.

The Figure 5.16 shows the observed ϕ v $\nu^{\frac{1}{2}}$ results at 769K, for both the 0.025cm thick specimen and the 0.05cm thick specimen. Similar plots are also shown in Figures 5.17 and 5.18 at 799K and 834K. In Figure 5.19 the ϕ v $\nu^{\frac{1}{2}}$ data for the 0.025cm thick specimen at 870K is shown with that of the 0.05cm thick specimen at 875K. If the linear regions of these curves are extrapolated back to the phase axis, it is found that the intercept on the axis is greater than $-\pi/4$ for all the curves. The four intercepts are all close to -0 . 25 radians.

A possible dependence of phase on the square root of frequency with the condition that extrapolated intercepts on the phase axis are more than $-\pi/4$ was found in section 4.3 .2 to be characterised by $\phi_{H >> 1}$.

A second important feature seen in Figures 5.16, 5.17, 5.18 and 5.19 is that the phases are not strongly dependent on the thickness of the specimen.

All the features noted above suggest that processes at the input and exit surfaces of the gold foils are playing a major role in determining the phase lag; ϕ. An attempt was therefore made to analyse the experimental data in terms of the model $\phi_{H >> 1}$.

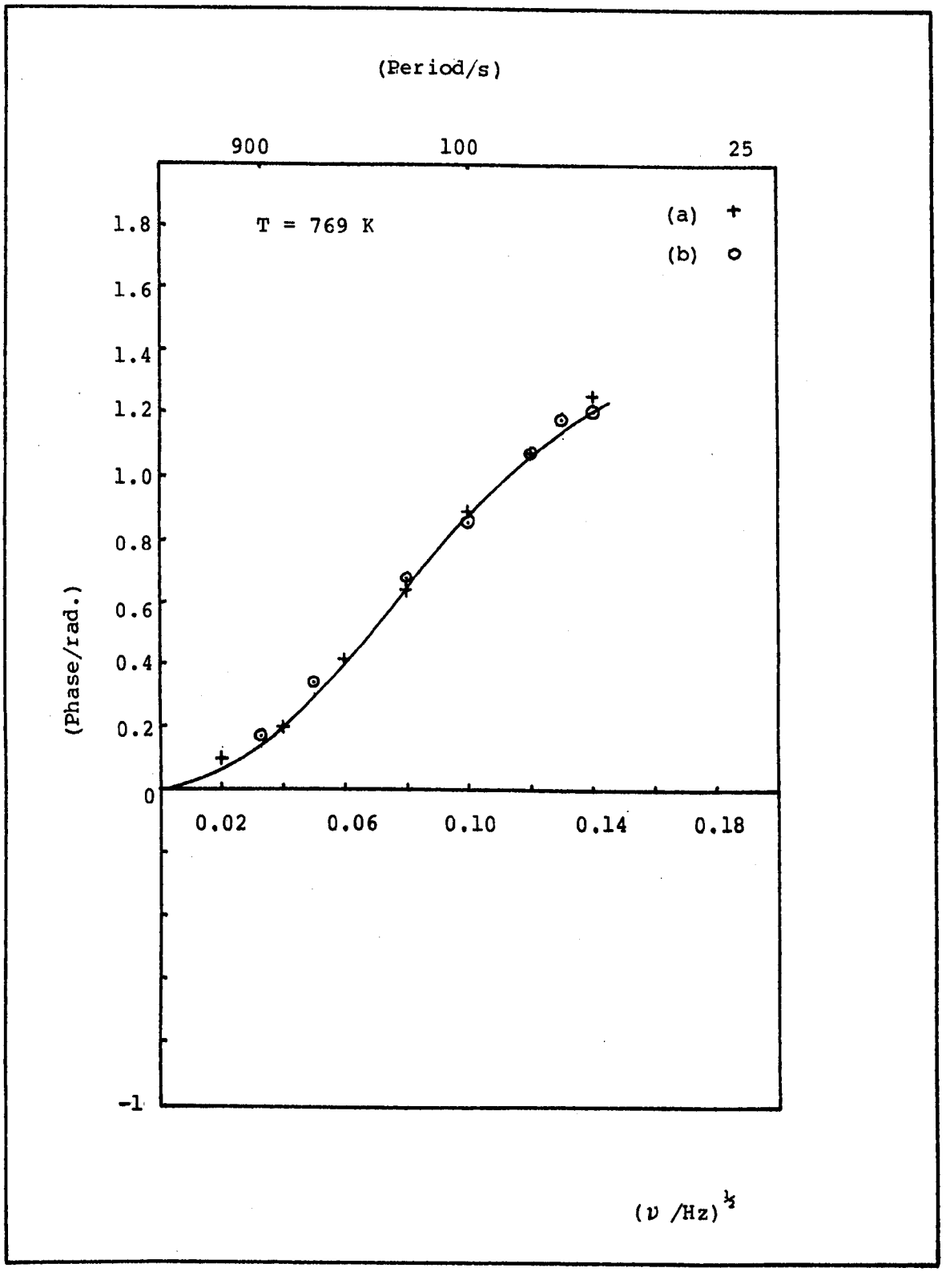

Fig. 5.16 ϕ v $\nu^{\frac{1}{2}}$ for hydrogen in gold at 769K
(a) 0.025cm thick foil
(b) 0.05cm thick foil
The best fit $\phi_{H>>1}$ curve is shown through the data.
(See Table 5.7 for details of D and c_5)

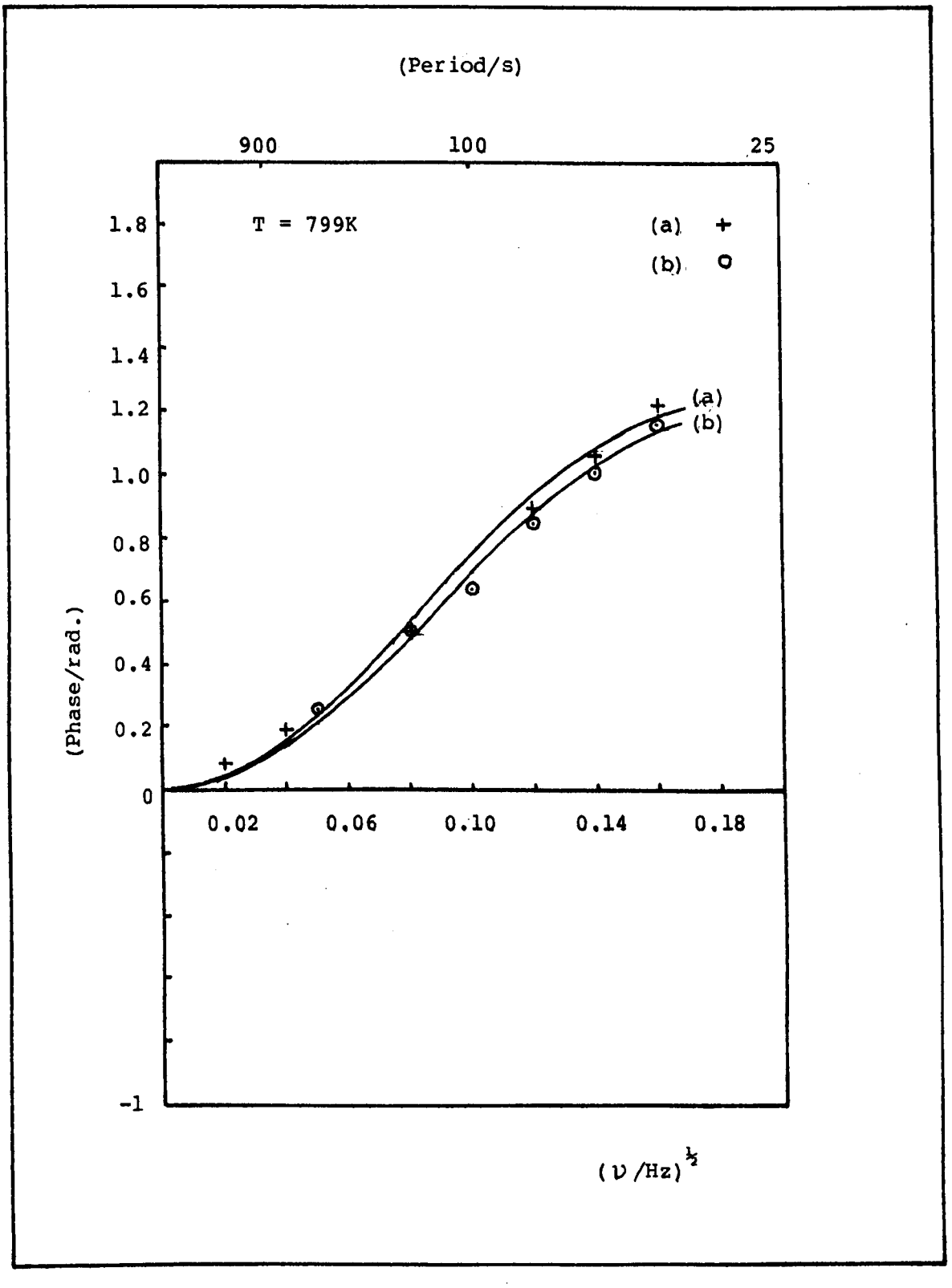

Fig. 5.17 ϕ v $\nu^{\frac{1}{2}}$ for hydrogen in gold at 799K
(a) 0.025cm thick foil
(b) 0.05cm thick foil
The best fit $\phi_{H>>1}$ curves are shown through the data.
(See Table 5.7 for details of D and c_5)

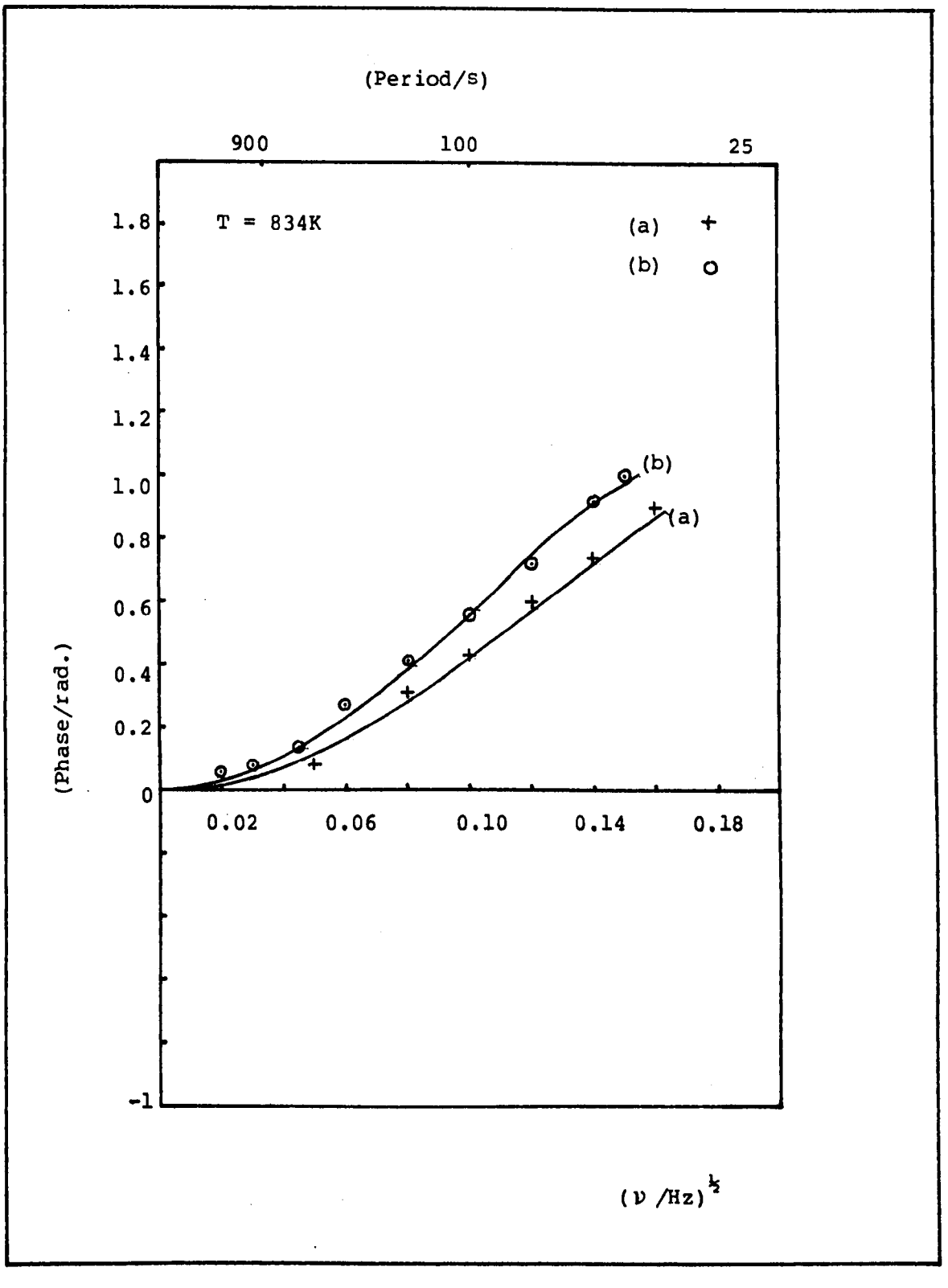

Fig. 5.18 ϕ v $\nu^{\frac{1}{2}}$ for hydrogen in gold at 834K.
(a) 0.025cm thick foil
(b) 0.02cm thick foil
The best fit $\phi_{H>>1}$ curves are shown through the data
(See Table 5.7 for details of D and c_5)

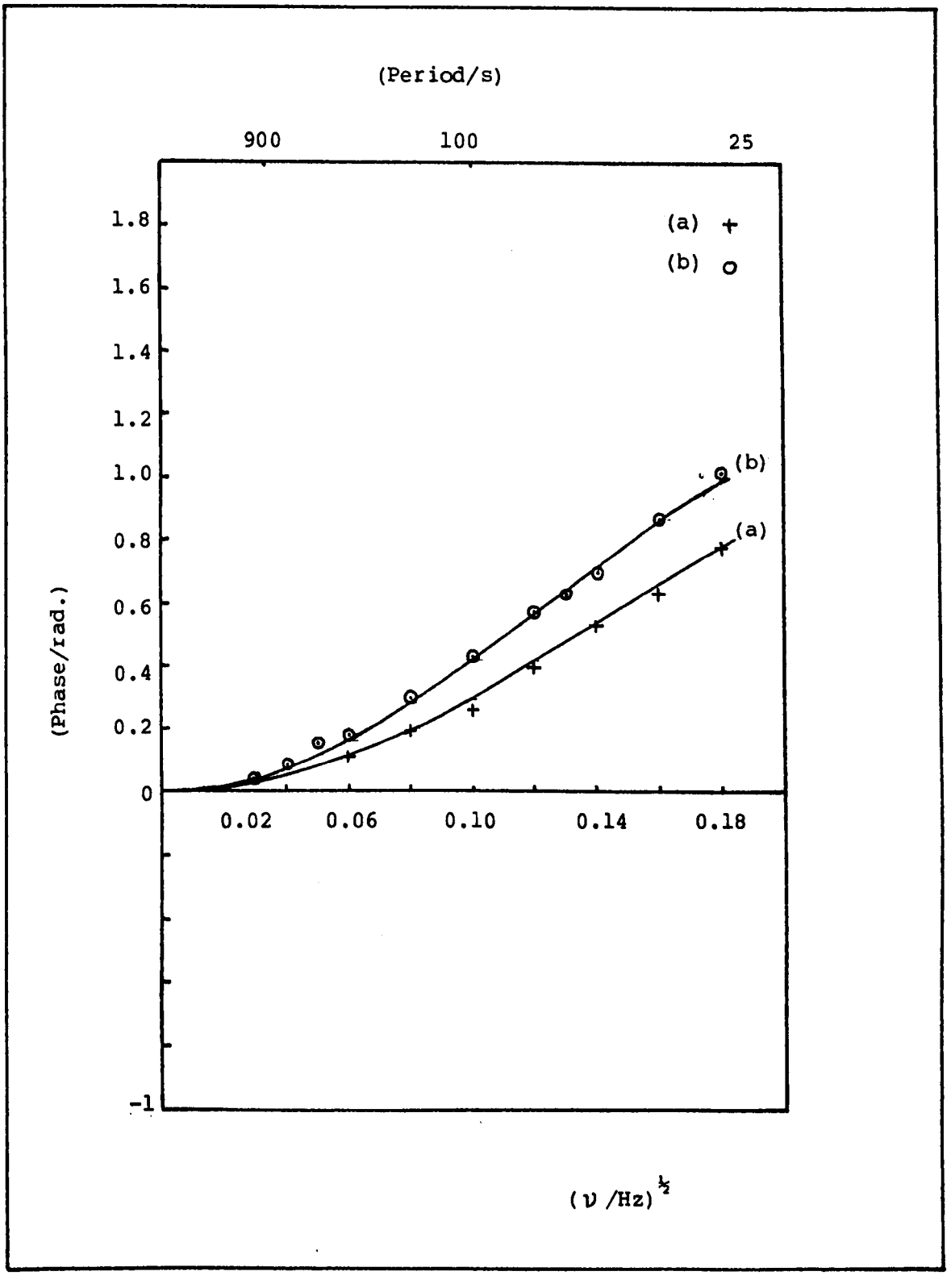

Fig. 5.19 ϕ v $\nu^{\frac{1}{2}}$ for hydrogen in gold.
(a) 0.025cm thick foil at 870 K.
(b) 0.05cm thick foil at 875K
The best fit $\phi_{H>>1}$ curves are shown through the data
(See Table 5.7 for details of D and c_5)

The smooth curves also shown in the ϕ v $\nu^{\frac{1}{2}}$ figures are the best least squares fits of $\phi_{H >> 1}$ to the experimental data. The values of D, c_5 and (c_4/c_5) corresponding to these curves are detailed in Table 5.7. As may be seen from the figures there is good agreement between experiment and theory. Also, as may be seen from Table 5.7, the diffusion coefficients, $D_{0.025}$ and $D_{0.05}$ for the 0.025cm thick and 0.05cm thick specimens, are in good agreement with the phase lag dominated by the magnitude of c_5. It is also gratifying to find that the ratio $(c_5^{0.025}/c_5^{.05})$ is roughly two, which is a not unreasonable factor.

It is interesting to note that the best fit $\phi_{H >> 1}$ curves have $(c_4/c_5) \sim 1$. This suggests that $H_4 \sim H_5$, where

$$H_4 = b\,\bar{N}_i$$

$$H_5 = b\,\bar{N}_e$$

therefore since the parameter b was assumed to be the same at the input and exit surface this, suggests $\bar{N}_i \sim \bar{N}_e$ and that $\bar{N}(0) \sim \bar{N}(L)$. This supposition may be checked using equation 4.25 from which

$$N(L) \sim \frac{(H_2 + H_5)}{H_3\, H_5\, \lambda}\, J(L)$$

Therefore, if $|J(L)| \sim \frac{D}{L}\,(|N(0)| - |N(L)|)$ then

$$\left|\frac{N(L)}{|N(0)|-N(L)|}\right| \sim \frac{(H_2 + H_5)}{H_3\, H_5\, \lambda}\,\frac{D}{L}$$

By definition

$$c_5 = \frac{H_2 + H_5}{H_3\, H_5 \lambda}\,(D/2)^{\frac{1}{2}}$$

Therefore

$$\frac{1}{c_5}\left|\frac{N(L)}{|N(0)|-N(L)}\right| \sim (2D)^{\frac{1}{2}}$$

Hence on substituting for D and c_5 into this equation $|N(L)| \sim |N(0)|$.

This is a surprising result and it is accompanied by surprising

Table 5.7

Hydrogen diffusion coefficients, $D_{0.025}$ and $D_{0.05}$, through 0.025cm thick and 0.05cm thick gold foils.

T/K	$(T/10^3K)^{-1}$	$(D_{0.025}/cm^2s^{-1})$	$(D_{0.05}/cm^2s^{-1})$	$c_5^{0.025}$	$c_5^{0.05}$	(c_4/c_5)	$\ln(D_{0.025}/cm^2s^{-1})$	$\ln(D_{0.05}/cm^2s^{-1})$
769	1.3	2.7×10^{-3}	2.9×10^{-3}	280	150	1	- 5.91	- 5.84
799	1.252	3.3×10^{-3}	3.5×10^{-3}	240	120	1	- 5.71	- 5.65
834	1.199	3.7×10^{-3}	3.7×10^{-3}	120	90	1	- 5.60	- 5.60
870	1.149	3.9×10^{-3}	-	84	-	1	- 5.55	-
875	1.143	-	3.9×10^{-3}	-	63	1	-	- 5.55

diffusion coefficients, some 25-100 larger than values published elswhere (52), (64), (65). However there are some reasons for accepting that such values may be possible since only this will explain the almost identical phase frequency data for the 0.025cm thick and 0.05cm thick specimens.

A final comment concerning the quoted diffusion coefficients is that they were evaluated by making a least squares fit on the experimental data with three floating parameters, c_5, (c_4/c_5) as well as the diffusion coefficient itself. Hence it is expected that the precision of measurement is not as good as the molybdenum and silver results, with possible deviations of $\pm$ 20%.

Table 5.8 details the variation of c_5 with mean discharge current, at the four temperatures studied. This data is plotted in Figure 5.20 as c_5 v $(1 + I_m/4)^{-1}$, where it may be seen that the data is broadly consistent with the expected behaviour of c_5, i.e. approximately proportional to $(\bar{N}(L))^{-1}$.

The diffusion coefficients listed in Table 5.7 are plotted as ln D v T^{-1} in Figure 5.21. A best least squares fit to this data gives

$$D_H = (4.6 \pm 3.5) \times 10^{-2} \exp\left[- (0.18 \pm 0.04)\ eV/kT \right] cm^2 s^{-1} \qquad (5.5)$$

Figure 5.22 shows $\ln[(c_5)^{-1}]$ v T^{-1} plotted for the 0.025cm thick and 0.05cm thick specimens, using the data in Table 5.7. The curves suggest that $(c_5)^{-1}$ has Arrhenius behaviour, however the obvious difference in gradients suggests that the activation energy may be specimen specific rather than a constant parameter of gold. The activation energy for $c_5^{0.025} \sim$ 0.73eV and for $c_5^{0.05} \sim$ 0.45 eV.

Modulation experiments were also performed with deuterium in gold using a second 0.025cm thick specimen. Two sets of data were gathered, at

Table 5.8

Variation of c_5 with mean discharge current

T/K	(mean discharge current/mA) I_m	c_5
769	2mA	180
"	4mA	150
"	8mA	100
799	2mA	135
"	4mA	110
834	2mA	120
"	4mA	90
"	6mA	75
875	2mA	70
"	4mA	63
"	6mA	50

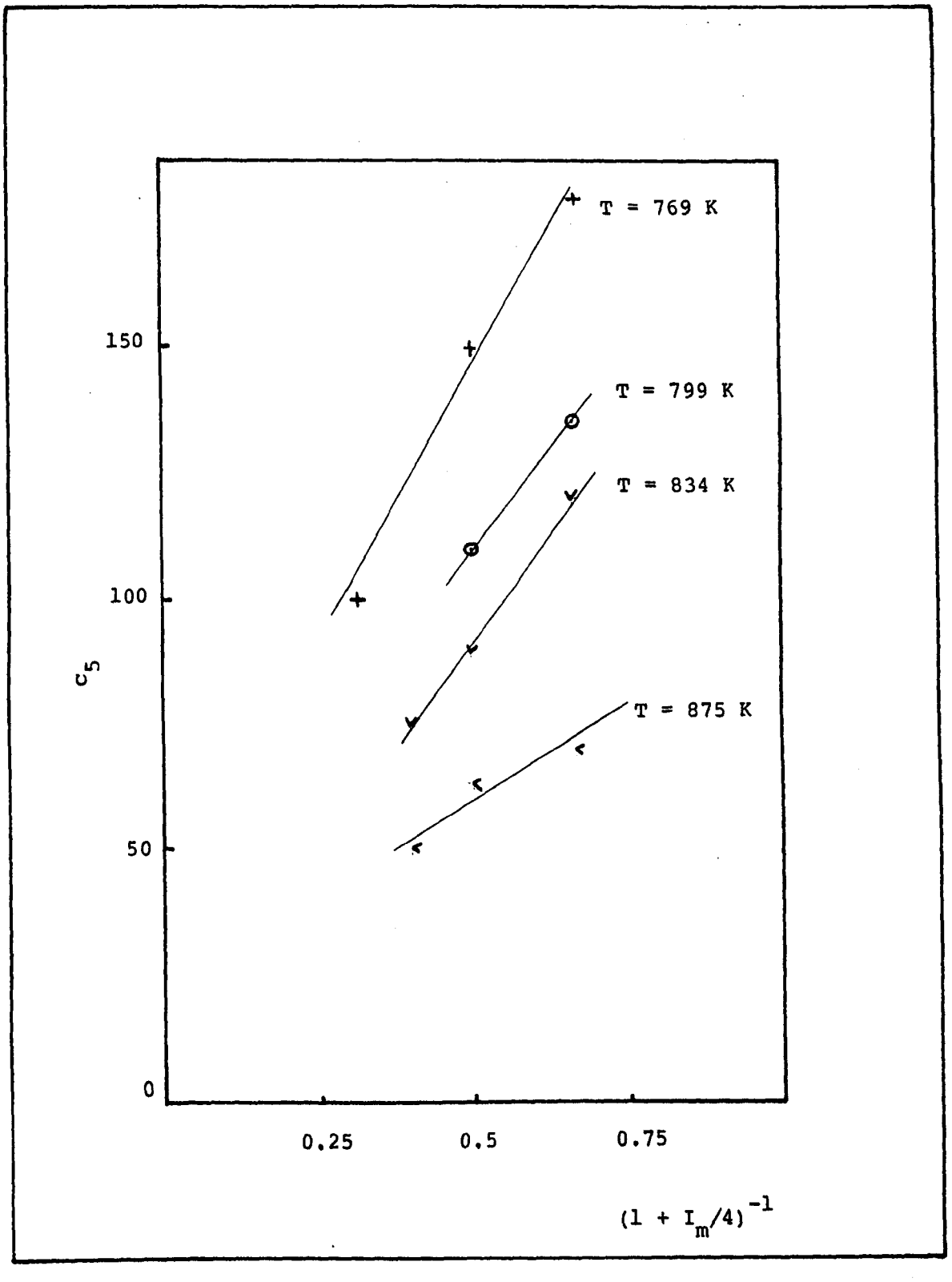

Fig. 5.20 c_5 v $(1 + I_m/4)^{-1}$ (I_mmA is the mean discharge current).

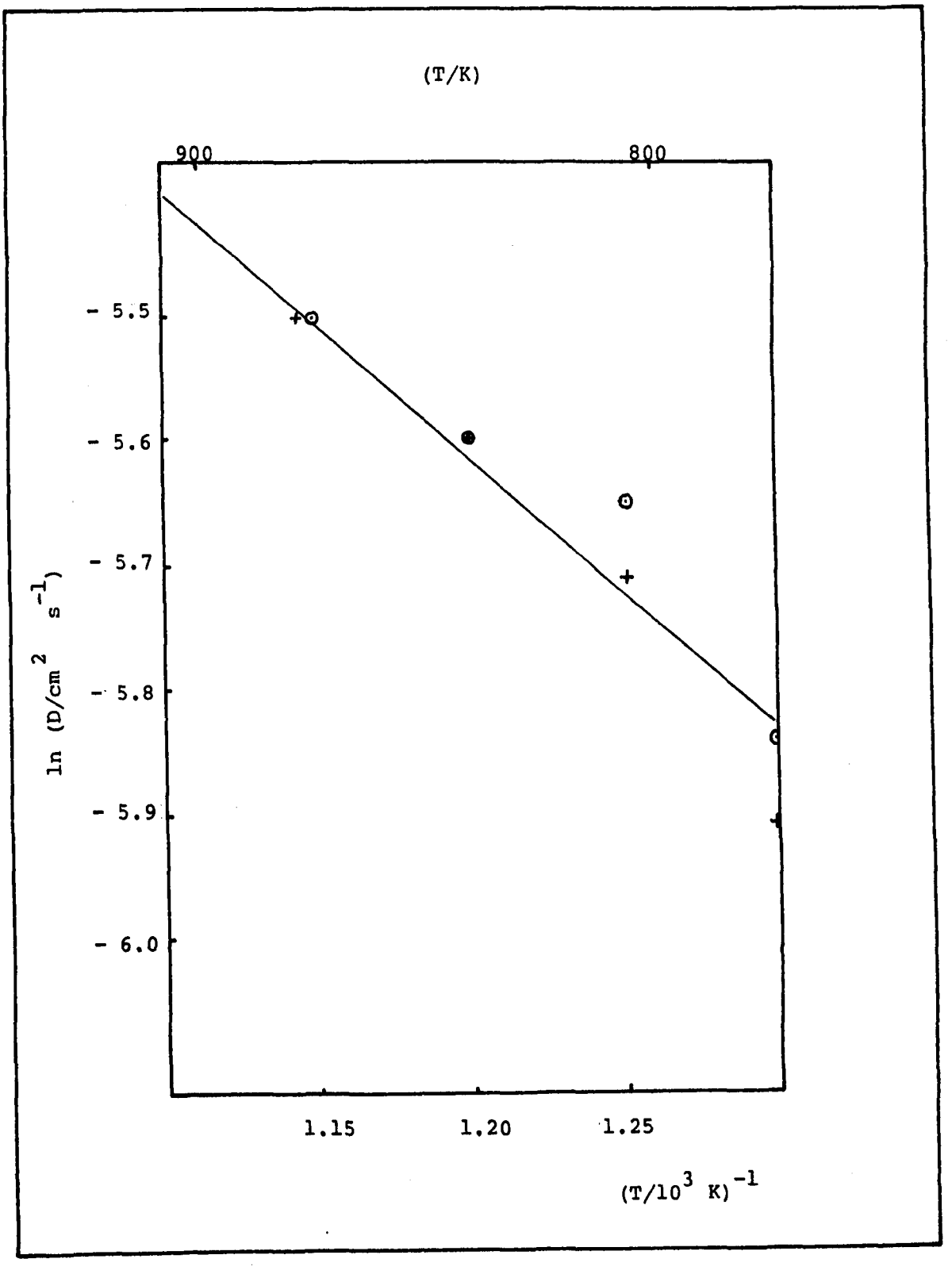

Fig. 5.21 ln D v T^{-1} for hydrogen in gold.

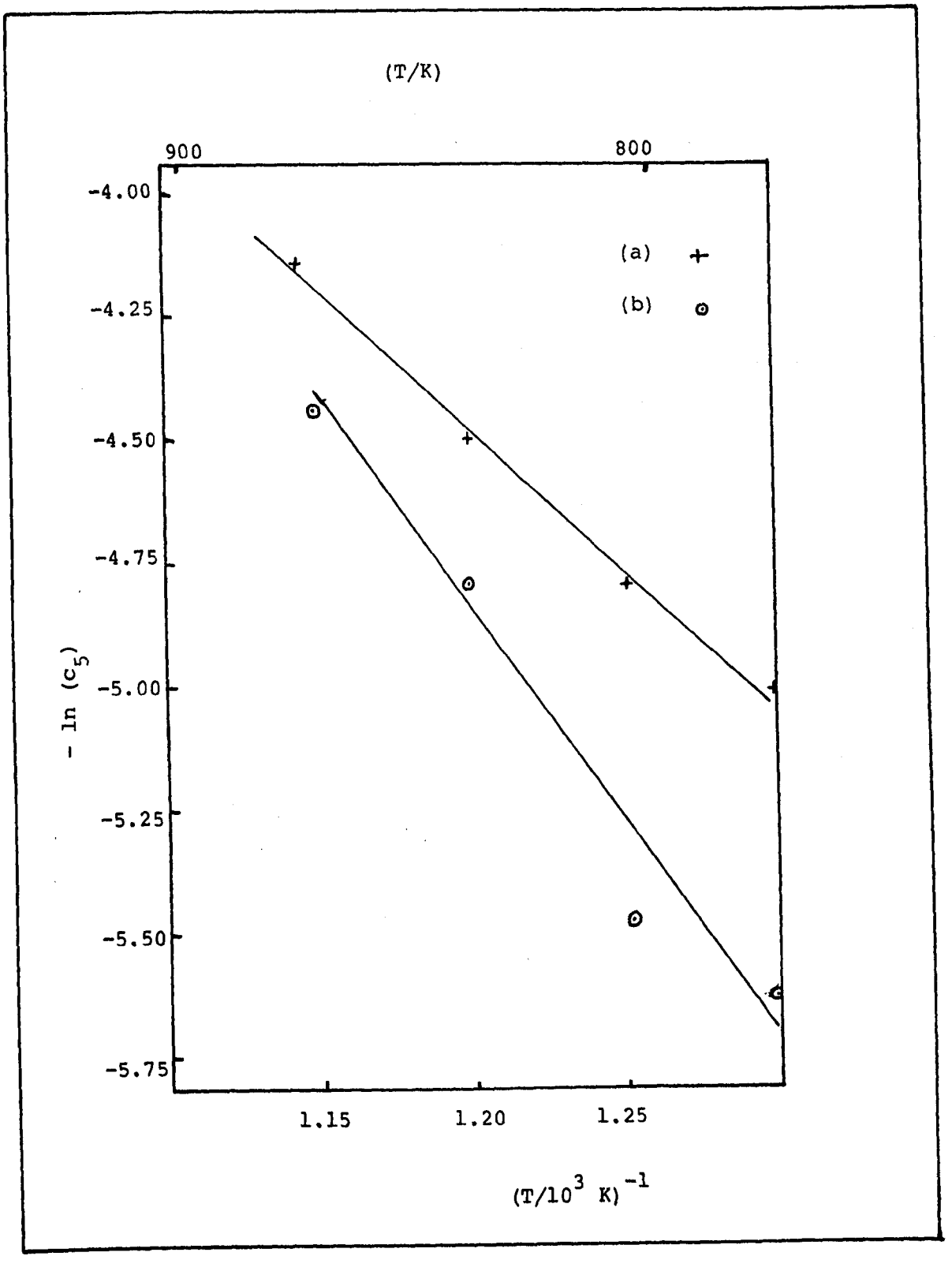

Fig. 5.22 ln (c_5^{-1}) v T^{-1} for hydrogen in gold
a) 0.05cm thick foil
b) 0.025cm thick foil

the temperatures 799K and 901K, these are shown plotted as ϕ v $\nu^{\frac{1}{2}}$ in Figure 5.23. The smooth curves drawn through the experimental data points are the best least squares fits of $\phi_{H \gg 1}$ on the data and in Table 5.9 the parameters, D, c_5 and (c_4/c_5) related to these curves, are summarised.

Table 5.9

Diffusion coefficients of deuterium in gold.

(T/K)	$(T/10^3 K)^{-1}$	$(D/cm^2 s^{-1})$	ln $(D/cm^2 s^{-1})$	c_5	c_4/c_5
799	1.252	2.4×10^{-3}	- 6.03	137	1
901	1.110	3.5×10^{-3}	- 5.65	60	1

In these experiments an attempt was made to drive the phase/frequency curves towards the $\phi_{Classical}$ curves expected at large input gas pressures and mean discharge currents. Gas pressures of $\sim$ 15 torr were used and mean discharge currents of 6mA. At pressures beyond 15 torr non-linearities were observed in the discharge i.e. the modulation was no longer sinusoidal, so the experiment was bound by the equipment limits. As can be seen from the curves in Figure 5.23 the attempt was not successful and extrapolations from the linear parts of the curves have intercepts on the phase axis at phases larger than $-\pi/4$. The actual intercepts are - 0.4 radians and - 0.55 radians at 799K and 901K respectively.

In Figure 5.24 the ln D v T^{-1} for the deuterium data is compared with the hydrogen curve. The deuterium data corresponds to a diffusion coefficient of

$$D_D = 6.8 \times 10^{-2} \exp(-0.23 \text{ eV}/kT) \qquad (5.6)$$

There is not sufficient data to determine the standard deviations of the activation energy and the pre-exponential factor.

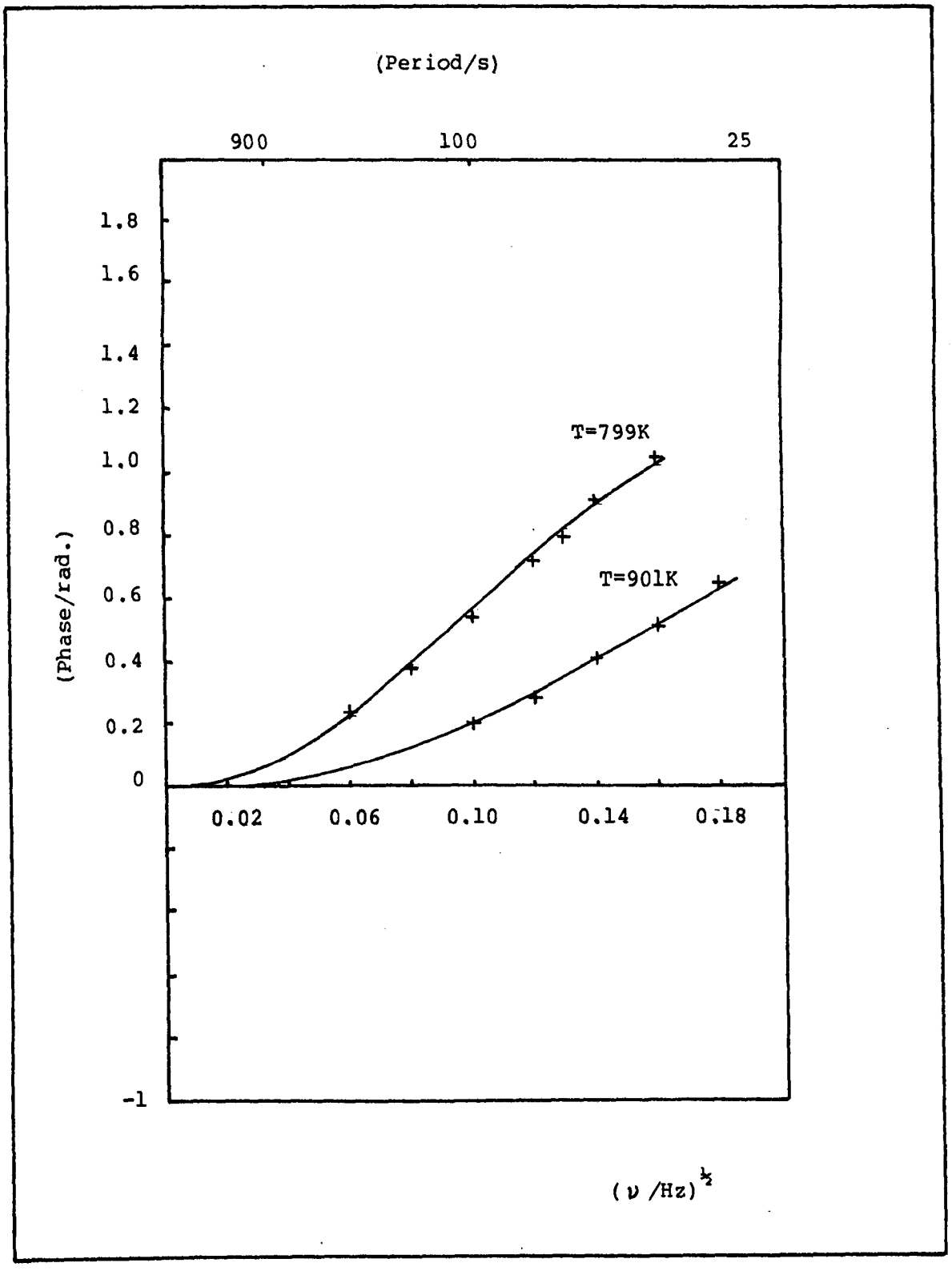

Fig. 5.23 ϕ v $\nu^{\frac{1}{2}}$ for deuterium in 0.025cm thick gold at 799K and 901K. The best fit $\phi_{H>>1}$ curves are shown through the data. (See Table 5.9 for details of D and c_5).

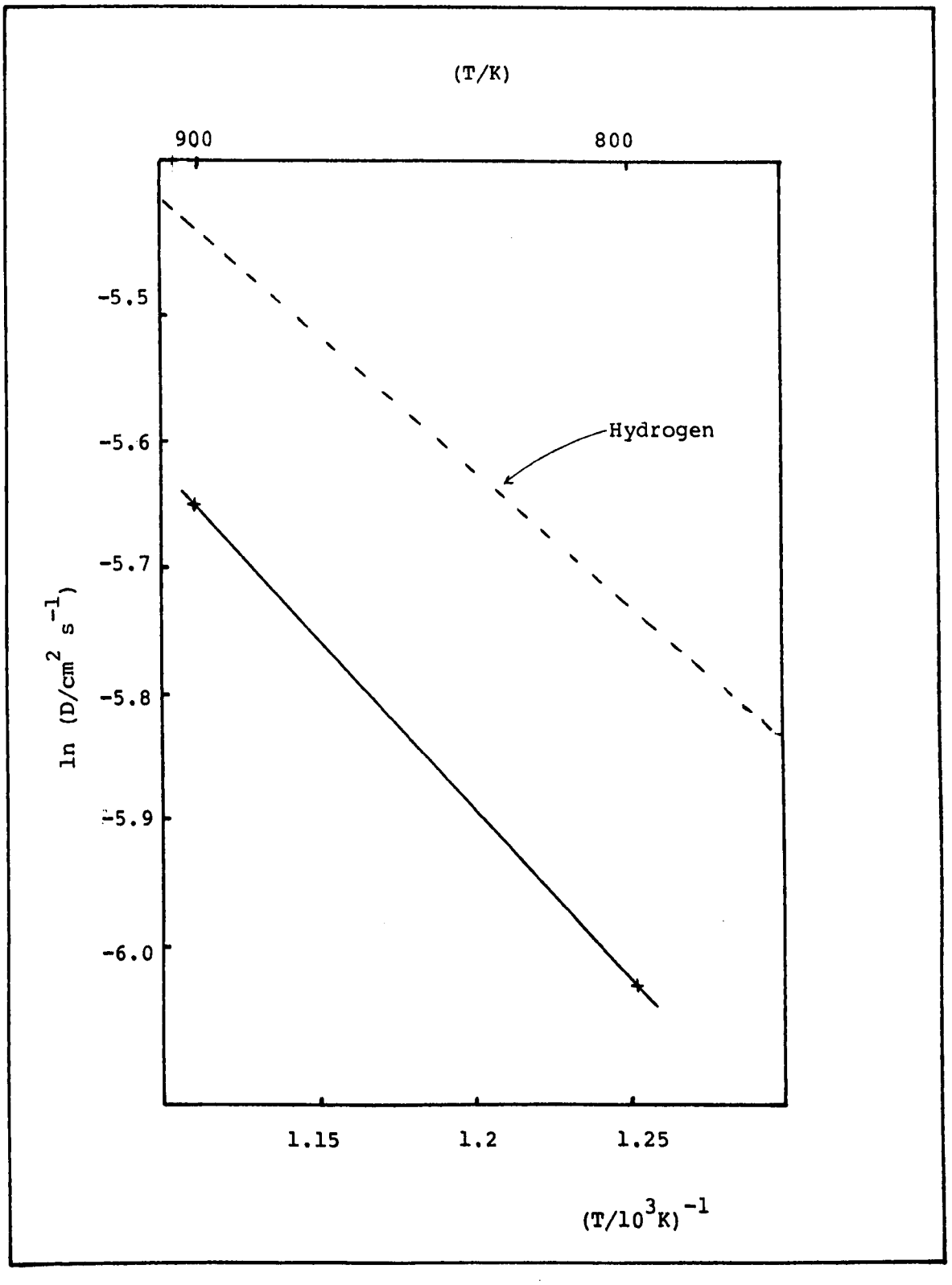

Fig. 5.24 ln D v T^{-1} for deuterium in gold. Also shown as a broken line is the best line through the hydrogen data.

Comparison of equations 5.5 and 5.6 show that

$$(E_H/E_D) = \frac{0.18}{0.23} \sim 0.8$$

and

$$(D_O^H/D_O^D) = \frac{4.6}{6.8} \sim 0.67$$

Once more the ratio of pre-exponential factors suffers from the mode of their derivation, an extrapolation from a short interval of data. If the ratios of the diffusion coefficients themselves at like temperatures are taken then the isotopic ratio is approximately 1.5.

5.2.2 Aluminium.

Aluminium is well known for its tenacious and impervious oxide layer and it was hoped the discharge injection of ions might overcome the difficulties this layer imposes. This hope did not materialize. Instead within minutes of begining an experiment dramatic changes were observed. Phase/frequency plots changed perceptively, even as measurements were being made. This is illustrated in Figure 5.25.

For this reason no serious attempt has been made in analysing the data. However, as illustrated in Figure 5.26, the phase/frequency plots are dependent on the mean discharge current and comparison of these curves with Figure 4.9 , the example of $\phi_{H \gg 1}$ v $\nu^{\frac{1}{2}}$ when c_5 is large, shows identical characteristics. When, in $\phi_{H \gg 1}$, c_5 is large this implies that the input and exit processes are dominating permeation, which is consistent with the supposition of an impervious oxide layer.

In conclusion from the observations made with aluminium and gold, an acceptable level of consistency between theory and experiment was found. On critical inspection of this consistency the author admits that it is mainly circumstantial. One critical test failed, that of driving the hydrogen/gold

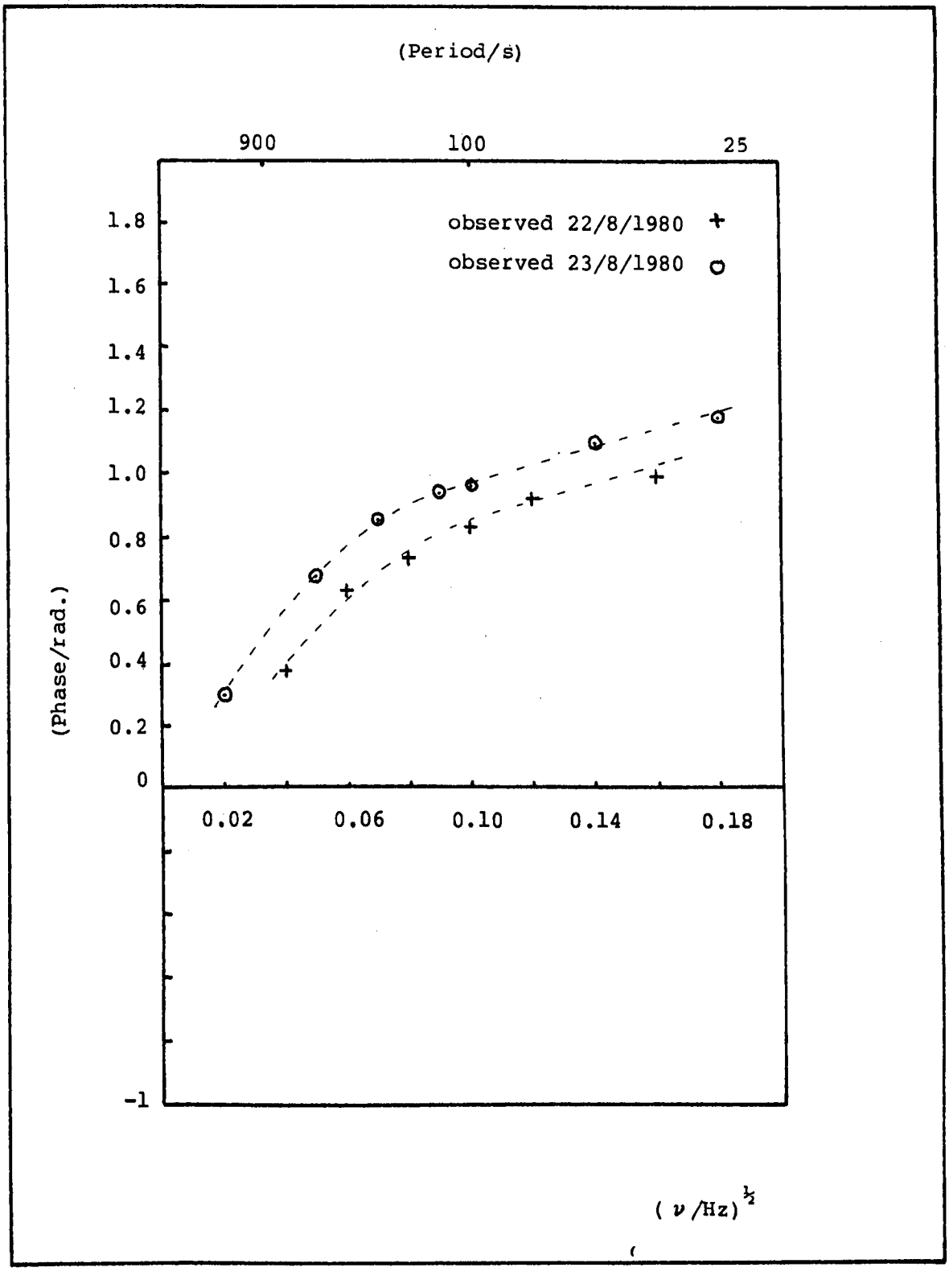

Fig. 5.25 ϕ v $\nu^{\frac{1}{2}}$ for hydrogen in 0.025cm thick aluminium at 700K. The data was gathered on two consecutive days using identical input conditions.

N.B. The broken lines are visual aids only.

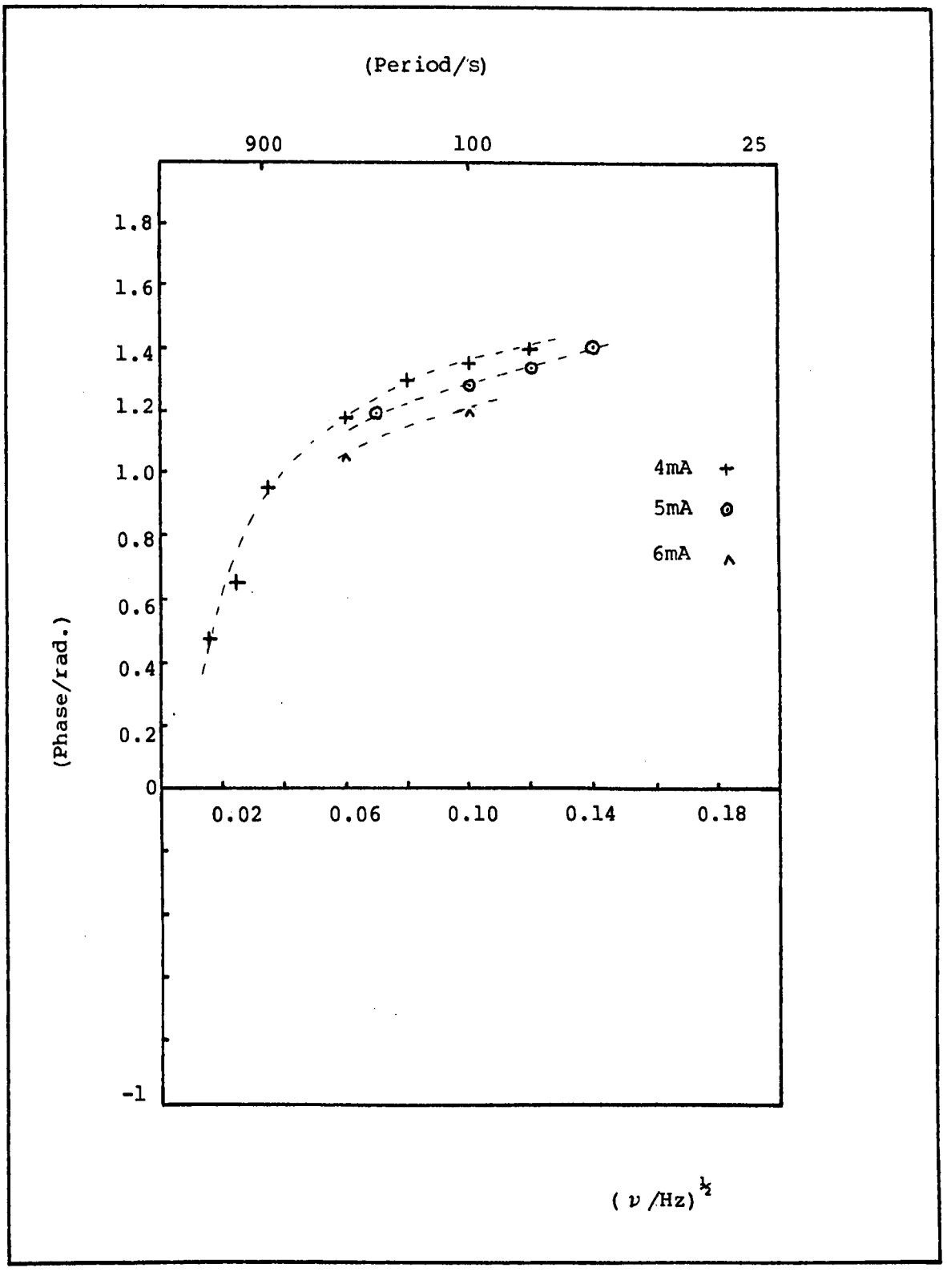

Fig. 5.26 ϕ v $\nu^{\frac{1}{2}}$ for hydrogen in 0.025cm thick aluminium at 750K. Data is illustrated for the three mean discharge currents; 4mA; 5mA; 6mA, demonstrating phase dependence on mean discharge current.

N.B. The broken lines are visual aids only.

and hydrogen/aluminium system into the $\phi_{Classical}$ regime. This would have given strong support for the suggested analysis. However, as will be discussed in section 5.3 where it is shown that, the expected input conditions required to drive the hydrogen/gold system to the $\phi_{Classical}$ regime are beyond the limits of the present experiment.

5.3 Steady rate permeation

The main body of experimental data was obtained by the modified time lag technique. However, during the course of study, ancillary measurements and separate specific experiments also provided data relating to the steady rate permeation of hydrogen through molybdenum and gold.

5.3.1 Molybdenum

In Figure 5.27 is plotted the logarithm of the permeation coefficient, lnP, versus T^{-1} for hydrogen in molybdenum. The same data is also presented in Table 5.10, it relates to the two specimens reported in section 5.1.1 and covers the temperature range 695-922K. These measurements were made with input pressures of 1.8torr.

To evaluate P the specimen surface area was taken as $9.5cm^2$ and the pump rate as 50 ls^{-1}. A least squares fit to the data corresponds to

$$P=(6.36 \pm 3.0)\times10^{-7} \exp\left[-(0.98 \pm 0.06)eV/kT\right] \text{ Mole } cm^{-1}s^{-1}torr^{-\frac{1}{2}} \qquad (5.7)$$

Figure 5.28 shows ln P versus T^{-1} for deuterium in molybdenum for the temperature range 695-922K with the same specimens as above. The input pressures were again 1.8torr. The data of Figure 5.28 is detailed in Table 5.11. A least squares fit on these results corresponds to

$$P=(1.10 \pm 2.0)\times10^{-6} \exp\left[-(1.03 \pm 0.05)eV/kT\right] \text{ Mole } cm^{-1}s^{-1}torr^{-\frac{1}{2}} \qquad (5.8)$$

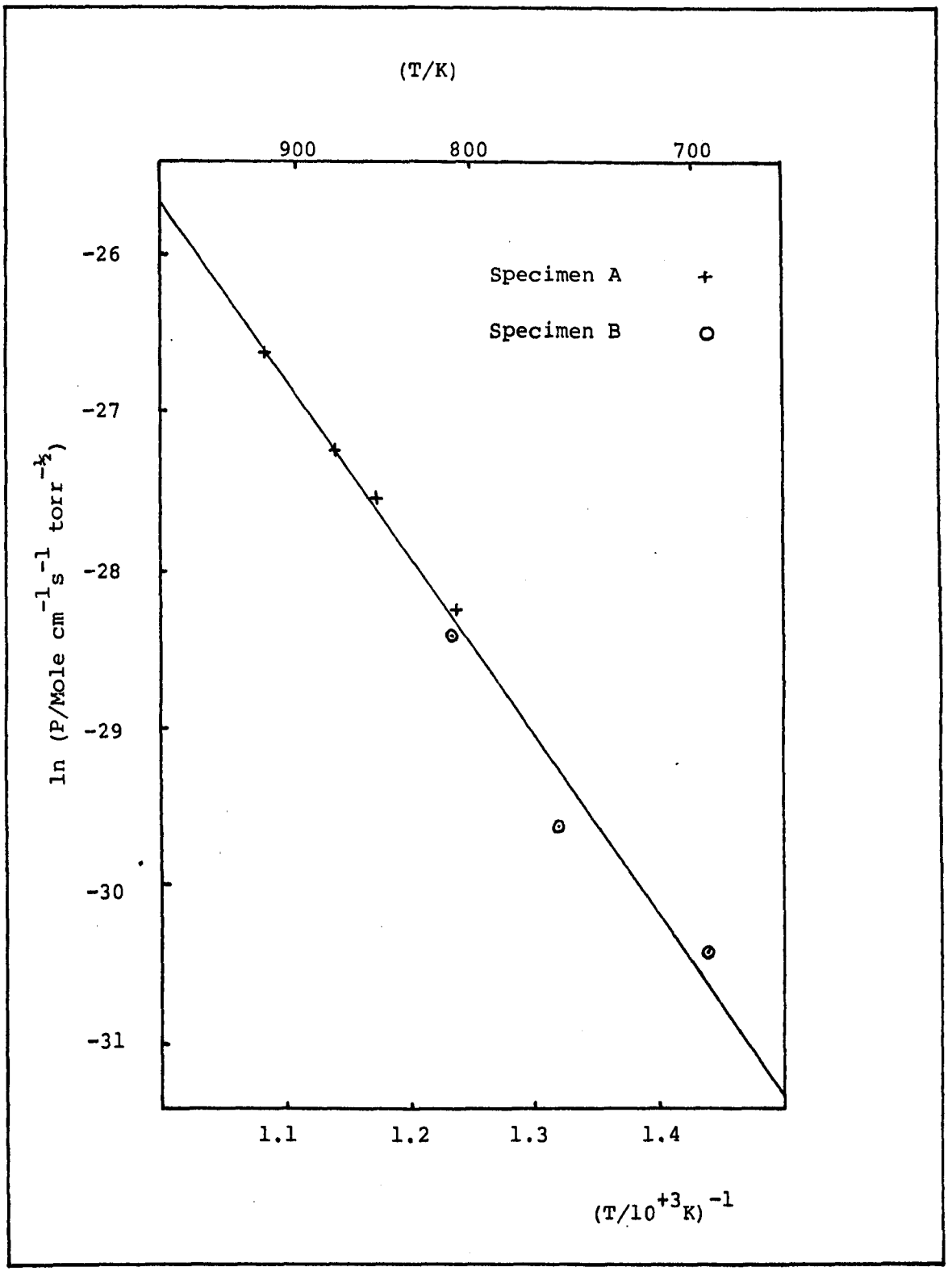

Fig. 5.27 ln P v T^{-1} for hydrogen in molybdenum.

Table 5.10

Permeation coefficients for hydrogen in molybdenum

Specimen	$(T/10^{+3}K)^{-1}$	$(P/\text{mole cm}^{-1}\ \text{s}^{-1}\ \text{torr}^{-\frac{1}{2}})$	ln P
A	1.238	5.43×10^{-13}	-28.24
A	1.175	1.09×10^{-12}	-27.54
A	1.143	1.46×10^{-12}	-27.25
A	1.085	2.72×10^{-12}	-26.63
B	1.439	6.14×10^{-14}	-30.42
B	1.318	1.38×10^{-13}	-29.61
B	1.235	4.51×10^{-13}	-28.43

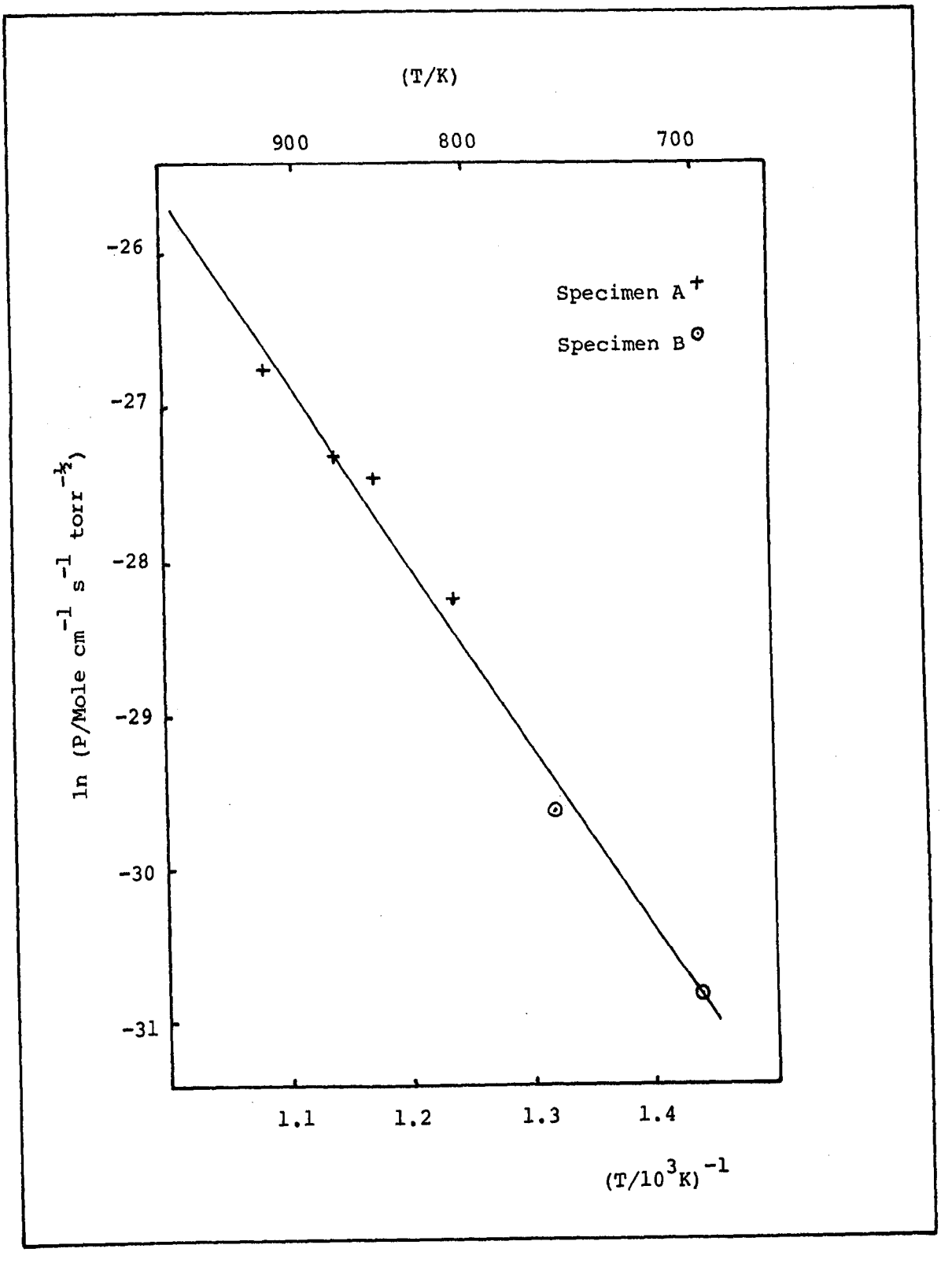

Fig. 5.28 ln P v T^{-1} for deuterium in molybdenum

Table 5.11

Permeation coefficients for deuterium in molybdenum

Specimen	$(T/10^{+3}K)^{-1}$	$(P$ /mole cm^{-1} s^{-1} $torr^{-\frac{1}{2}})$	ln P
A	1.238	5.43×10^{-13}	-28.24
A	1.175	1.17×10^{-12}	-27.47
A	1.143	1.36×10^{-12}	-27.32
A	1.085	2.34×10^{-12}	-26.78
B	1.439	4.07×10^{-14}	-30.83
B	1.318	1.36×10^{-13}	-29.63

5.3.2 Gold

There is evidence, from the phase/frequency results reported above, that the supposition of a front surface concentration in equilibrium with the gas and $N^*(0,t)$ much greater than $N^*(L,t)$ did not hold for hydrogen permeation in gold. For this reason a study was also made into steady rate permeation.

Table 5.12 details the observed fluxes, J, of hydrogen through the 0.05cm thick gold specimen for which data has been reported in section 5.2.1. The specimen surface area was $9.5cm^2$ and the pump speed was taken to be $50.1s^{-1}$. The listed results cover the temperature range 769 - 951K, with input pressures, p, in the range 0.1 - 10 torr at each temperature. In Figure 5.29 these fluxes are shown plotted as ln (J/mole $cm^{-2}s^{-1}$) versus ln (p/torr).

As may be seen, the characteristic features of these curves are that they are linear and that they have gradients, $g \sim 0.65$, over the interval of flux measured. It is interesting to note that this value for g, is significantly different from the value that would be found with Sieverts supposition, equation 2.18, ($g_{Sievert} = 0.5$). From section 4.4, this implies that the mean output surface concentration, $\bar{N}(L)$, cannot be neglected with respect to the mean input surface concentration, $\bar{N}(0)$.

Using equation 4.56, an estimate can be made for the characteristic flux, j, of hydrogen in gold. Substituting into this equation g=0.63 gives

$$y^{\frac{1}{2}} = \left(\frac{J}{j}\right)^{\frac{1}{2}} = 1.91 \qquad (5.9)$$

The mean value of J over the interval measured is $\sim 2.25 \times 10^{12}$ molecules cm^{-2} s^{-1}, therefore on substitution into equation 5.9

$$j \sim 6 \times 10^{11} \text{ molecules } cm^{-2} s^{-1}$$

Table 5.12

Steady rate flux for hydrogen through 0.05cm thick gold

T/K	$(T/10^{+3}K)^{-1}$	Input pressure (p/torr)	ln p	Flux (J/Mole $cm^{-2}s^{-1}$)	ln J
950	1.052	0.15	-1.9	2.25×10^{-12}	-26.82
"	"	0.40	-0.92	4.92×10^{-12}	-26.04
"	"	1.50	0.41	1.10×10^{-11}	-25.23
"	"	2.0	0.69	1.38×10^{-11}	-25.01
"	"	5.0	1.61	2.25×10^{-11}	-24.52
900	1.112	0.11	-2.21	1.41×10^{-12}	-27.29
"	"	0.50	-0.69	3.85×10^{-12}	-26.28
"	"	1.50	0.41	7.14×10^{-12}	-25.67
"	"	5.10	1.63	1.32×10^{-11}	-25.05
835	1.198	0.70	-0.36	8.99×10^{-13}	-27.74
"	"	3.45	1.24	2.44×10^{-12}	-26.74
"	"	5.0	1.61	3.06×10^{-12}	-26.51
799	1.252	1.50	0.41	9.89×10^{-13}	-27.64
"	"	2.50	0.92	1.26×10^{-12}	-27.39
"	"	5.0	1.61	1.97×10^{-12}	-26.95
"	"	7.20	1.97	2.56×10^{-12}	-26.69
769	1.300	3.5	1.25	6.18×10^{-13}	-28.11
"	"	4.9	1.59	7.59×10^{-13}	-27.91
"	"	8.0	2.08	1.15×10^{-12}	-27.49

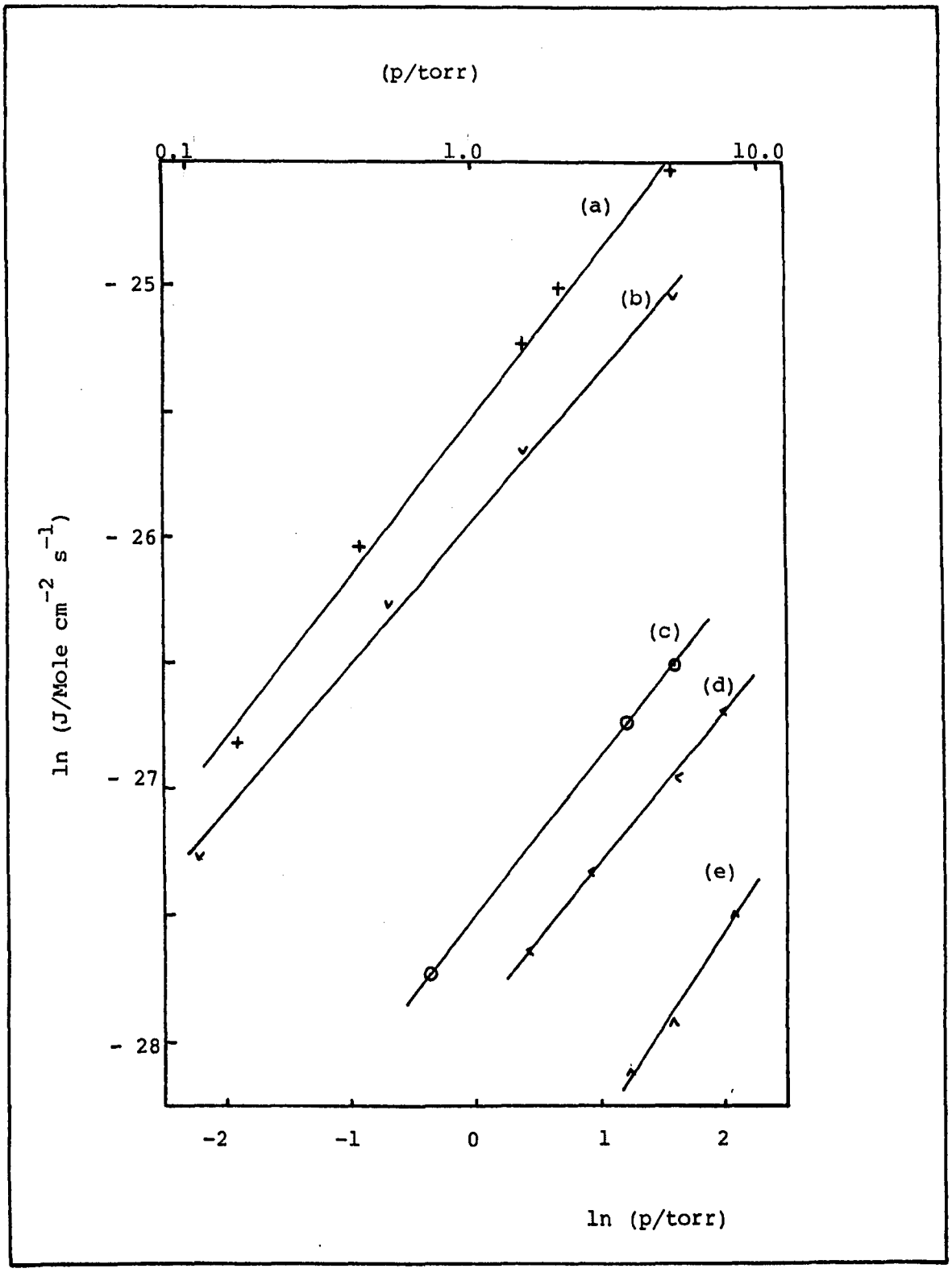

Fig. 5.29 ln J v ln p for hydrogen in gold.
a) T=950K; g=0.66
b) T=900K; g=0.62
c) T=835K; g=0.64
d) T=799K; g=0.62
e) T=769K; g=0.71

Table 5.13 details the hydrogen permeation coefficients, P , for temperatures in the range 719 - 951K in gold. This data was evaluated by finding the flux at the input pressure p = 5 torr from the curves in Figure 5.29. These results are plotted as ln P versus T^{-1} in Figure 5.30 and least squares fit to the data gives

$$P_m = (1.0 \pm 0.95) \times 10^{-6} \exp\left[-(1.18 \pm 0.05)\,eV/kT\right] \text{ Mole cm}^{-1}\, s^{-1} \text{torr}^{-\frac{1}{2}} \qquad (5.10)$$

A similar investigation was made for deuterium in gold. Table 5.14 details the steady rate flux, J, at 835K for the input pressures; 1.5torr; 3.5ton 5.0 torr and 10.0 torr through a 0.025cm thick foil. The specimen surface area was $9.5cm^2$ and the pumping rate was taken as 50 ls^{-1}. These results are shown plotted as ln J versus ln p in Figure 5.31. The gradient is $g \sim 0.7$, for this curve. Substituting this value for g in equation 4.56 and letting the mean value of J over the interval be $J = 5 \times 10^{12}$ molecules $cm^{-2}s^{-1}$, gives the characteristic flux

$$j \sim 5 \times 10^{12} \text{ molecules cm}^{-2}\text{s}^{-1}$$

The estimates made for j for hydrogen and deuterium are both of order 10^{12} molecules $cm^{-2}s^{-1}$, this flux characterizes permeation in gold for these gases. It is worth estimating the experimental conditions that might be required for gold to show Sievert behaviour. For this purpose suppose g = 0.51 in equation 4.56 then

$$J/j \sim 650$$

Comparing this value with the previous values (~ 1), it may be seen that to observe Sievert type permeation, fluxes of more than $\sim 10^{15}$ molecules $cm^{-2}s^{-1}$. Such fluxes would produce, under the present experimental conditions, detection chamber pressures $\sim 10^{-5}$torr which is within the upper limit of detection for the present equipment. Again using equation 4.56 the required input pressures would be $\sim$ 50 atmospheres at T $\sim$ 800K, which is well beyond the upper limit for input pressures with the present equipment.

Table 5.13

Permeation coefficients for hydrogen in gold

$(T/10^{+3}K)^{-1}$	(P /mole $cm^{-1}s^{-1}torr^{-\frac{1}{2}}$)	ln P
1.052	5.33×10^{-13}	-28.26
1.112	3.08×10^{-13}	-28.81
1.198	7.22×10^{-14}	-30.26
1.252	4.51×10^{-14}	-30.73
1.300	1.78×10^{-14}	-31.66

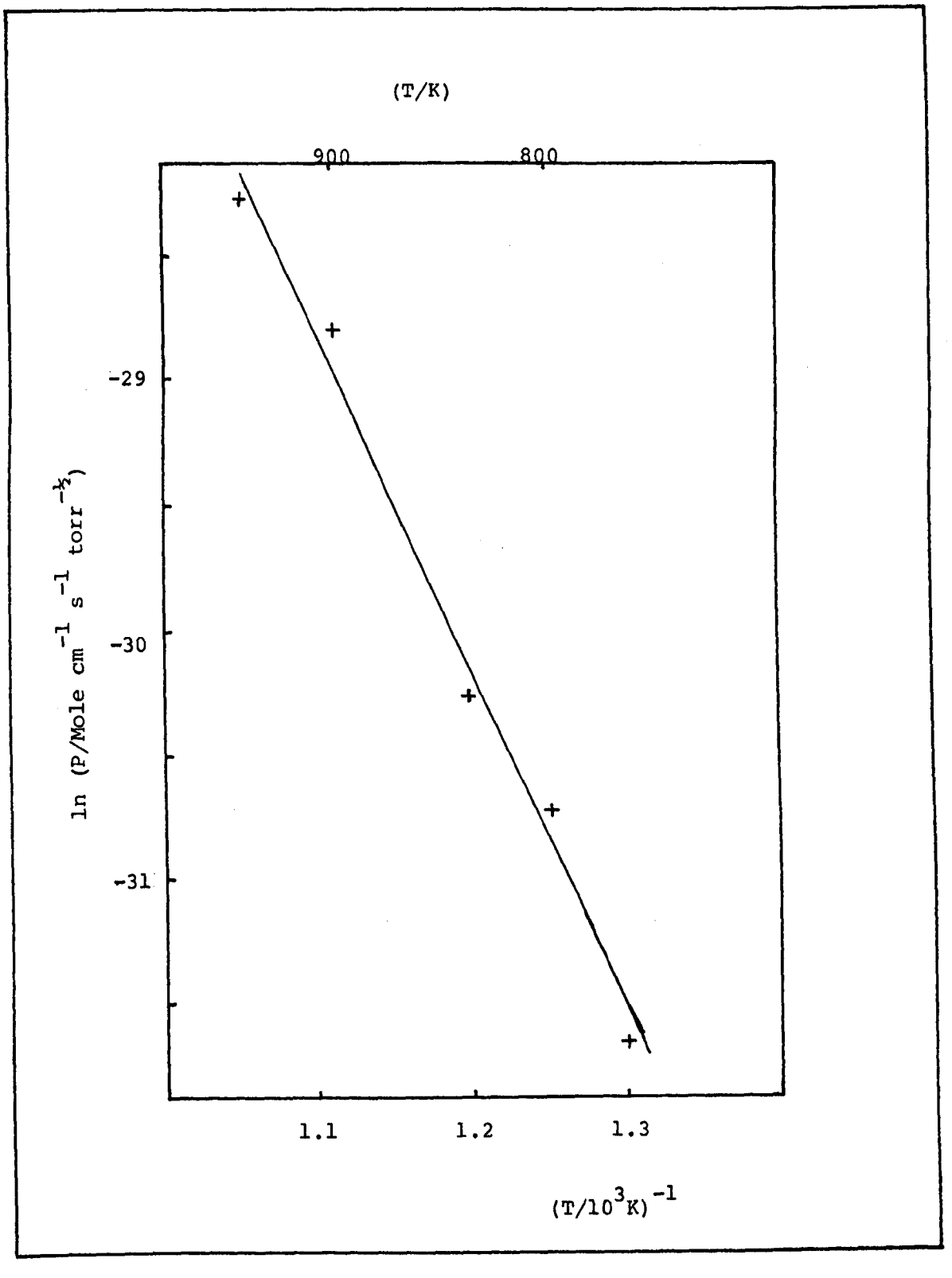

Fig. 5.30 ln P v T^{-1} for hydrogen in gold.

Table 5.14

Steady rate flux for deuterium through 0.025cm thick gold

$(T/10^{+3}K)^{-1}$	Input pressure (p/torr)	ln p	flux ($J/mole\ cm^{-2}s^{-1}$)	ln J
1.198	1.5	0.41	6.37×10^{-12}	-25.78
"	3.5	1.25	9.79×10^{-12}	-25.35
"	5	1.61	1.03×10^{-11}	-25.30
"	10	2.30	2×10^{-11}	-24.64

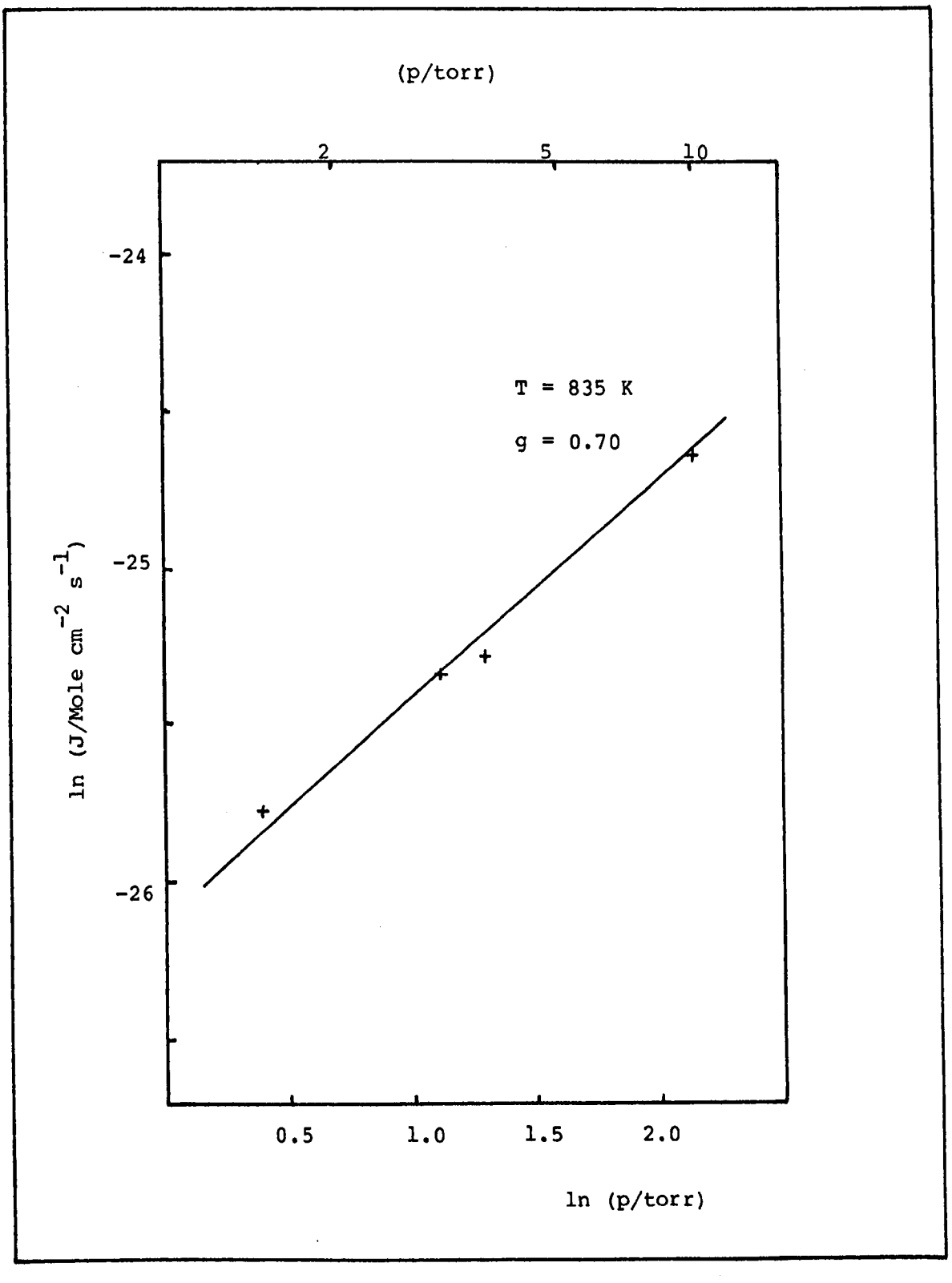

Fig. 5.31 ln J v ln p for deuterium in gold at T = 834K

Table 5.15 lists the permeation coefficients, P , for deuterium in gold for temperatures in the range 729 - 888K. This data is plotted as ln P versus T^{-1} in Figure 5.32 and a least squares fit to the data gives

$$P = (5.4 \pm 2.5) \times 10^{-3} \exp\left[-(1.77 \pm 0.02)\,eV/kT\right] \text{ Mole cm}^{-1}\text{s}^{-1}\text{torr}^{-\frac{1}{2}} \quad (5.11)$$

5.4 Helium

It did not prove possible to pass helium through silver, gold or aluminium using the discharge injection technique which had been successful in the work with the hydrogen isotopes. A more elaborate injection device was built, a saddle field ion gun, which gave precisely known injection currents and ion energies, but it too failed to give measureable helium flow into the detection chamber. This section relates the attempts made to find helium diffusion coefficients.

5.4.1 Early work

The possible use of a glow discharge to inject gas at a metal surface had been investigated previously (42), and some preliminary data, suggesting that flow did take place through silver, gathered.

In this work such results were not found to be reproducible. This failure to observe flow could have been due to insufficient injection of ions by the discharge or very low helium mobility in metals.

If Ficks first law is used with $\Delta N(0)$ the modulation amplitude of the volume concentration just inside the input surface, then

$$\Delta J \sim \frac{D}{L} \Delta N(0) \quad (5.12)$$

Therefore, if Δp is the detection chamber partial pressure modulation amplitude and S is the pump speed, then from equation 5.12

Table 5.15

Permeation coefficients for deuterium in gold.

$(T/10^{+3}K)^{-1}$	$(P$ /Mole $cm^{-1}s^{-1}torr^{-\frac{1}{2}})$	ln P
1.126	4.21×10^{-13}	-28.50
1.198	1.58×10^{-13}	-29.48
1.239	4.44×10^{-14}	-30.75
1.271	2.78×10^{-14}	-31.21
1.319	7.10×10^{-15}	-32.58
1.372	3.51×10^{-15}	-33.28

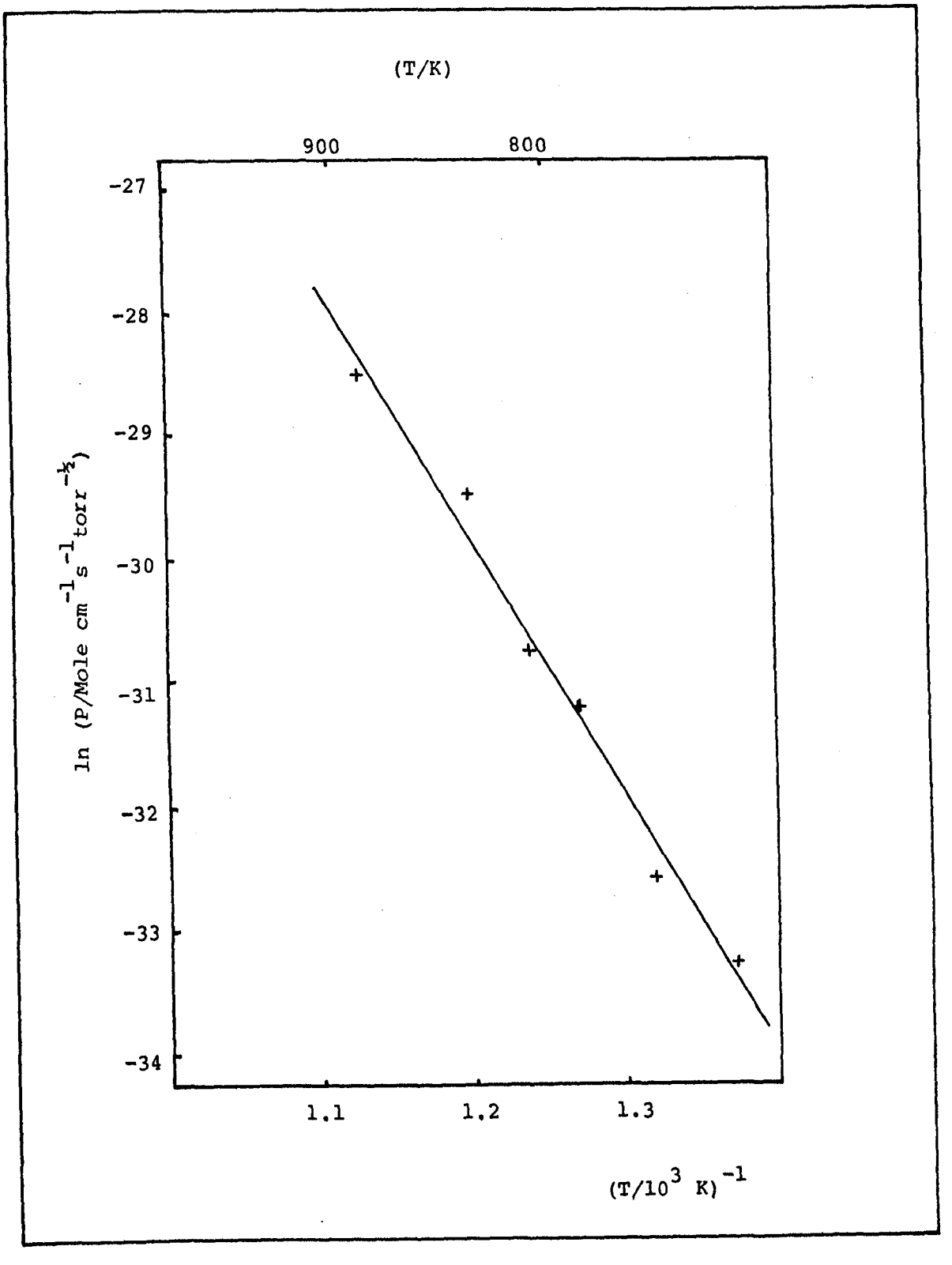

Fig. 5.32 ln P v T^{-1} for deuterium in gold.

$$S_H \Delta p_H \sim \frac{D_H}{L} \Delta N_H(0) \qquad (5.13)$$

and

$$S_{He} \Delta p_{He} \sim \frac{D_{He}}{L} \Delta N_{He}(0) \qquad (5.14)$$

for hydrogen and helium respectively. From these equations it follows that

$$D_{He} \sim \left(\frac{D_H}{p_H}\right)\left(\frac{S_{He}}{S_H}\right)\left(\frac{\Delta N_H(0)}{\Delta N_{He}(0)}\right) \Delta p_{He} \qquad (5.15)$$

From the hydrogen experiments reported earlier $(D_H/\Delta p_H) \sim 10^2$, from the pump specifications $S_H \sim 6S_{He}$ and since no detectable pressure modulations were observed $\Delta p_{He} \lesssim 5 \times 10^{-11}$torr the minimum detectable partial pressure. Therefore

$$D_{He} \lesssim 10^{-9} \left(\frac{\Delta N_H(0)}{\Delta N_{He}(0)}\right) cm^2 s^{-1}$$

from which, if discharge injection was equally efficient with hydrogen and helium then it follows $D_{He} \lesssim 10^{-9}$ $cm^2 s^{-1}$. If discharge injection was less efficient then D_{He} could have had some higher value and flow would still have not been detected.

5.4.2 Ion gun experiments.

The use of an ion gun gave sure and measurable injection currents. The requirements on gun design;the specific gun design and its performance have already been reported in section 3.2.

Experiments with the ion gun are interesting from the point of view that helium concentrations are not in equilibrium with some input gas pressure Instead the input concentration of helium is entirely determined by the equilibrium established between the diffusion fluxes, to the x = 0 and x = L boundaries, and the injection current. From the model developed in chapter 4. this suggests the flux through the membrane is independent of the diffusion coefficient. An analogy may make this clear; consider a conveyor belt with

sand falling on it at a constant rate, then no matter how fast the conveyor belt is driven the rate of sand transport will be the rate at which the sand falls.

Since there is no knowledge of the input concentration in this experiment the conveyor belt supposition will be made to estimate expected detection chamber helium partial pressure modulation amplitudes.

From probability theory, specifically the theory of Markov chains, a particle starting from a point X in the interval (0,L) and making unit jumps of length d in a random walk fashion, has a probability (X/L) of reaching x = L and (L-X)/L of reaching x = 0. Therefore if particles are injected into the metal a mean distance X, at the rate n $cm^{-2}s^{-1}$ then the expected flux to the exit surface at x = L, is

$$J \sim \frac{X}{L} n$$

$$\therefore \quad \Delta J \sim \frac{X}{L} \Delta n \qquad (5.16)$$

where ΔJ and Δn are the modulation amplitudes of the flux and injection current respectively. If the pump speed for helium is S_{He} and the modulation amplitude of the detection chamber partial pressure is Δp_{He} then

$$\alpha S_{He} \Delta p_{He} = Z \frac{X}{L} \frac{\Delta n}{Z} \qquad (5.17)$$

Where α is a conversion factor from (pressure x volume) to numbers of atoms and when using the units torr litres at ambient temperatures $\alpha \sim 3.5 \times 10^{19}$ molecules $torr^{-1}\ l.^{-1}$.

In the present experiment the net injection current used was $\sim 50\mu A$ or $\sim 4 \times 10^{14}$ atoms s^{-1}, the mean penetration of ions into the metal surface was $\sim$ 300 lattice separations, $S_{He} \sim 8$ l. $s.^{-1}$, and specimen thicknesses were 0.025cm. Hence it was expected that $\Delta p_{He} \sim 2 \times 10^{-10}$ torr, which is well within the available detection limit for partial pressures.

In performing these experiments a modification of the method described in sections 3.3 and 3.5 for data gathering and experimental operation had to be made. This was because the ion gun was found to interfere with the running of the signal averager which was replaced by an integrating voltmeter with print out capability.

Intergration times of 1800s (½hr) were chosen, at the end of which the voltmeter would print a number which was proportional to the mean input voltage measured over the time interval. This voltage was in turn proportional to the mean detection chamber partial pressure for helium.

Figure 5.33 shows the results over a twenty four hour interval for an experiment using a 0.03cm thick silver foil at ~ 900K. The plot shows a decay of pressure from ~ 1.6×10^{-8}torr to ~ 1×10^{-8}torr and a number of features of ~ 10^{-9} torr amplitude. These features raised hopes that these signals, monitored on mass 4 with the mass spectrometer, were due to helium flow. However there were a number of reasons for doubt:

1) the injection current modulation frequency had a period of 6 hrs. which is not matched by the intervals between successive peaks or successive troughs in Figure 5.33.
2) the features in the figure were found to have 24 hr. periodicy.
3) the expected helium diffusion coefficients were of order the self diffusion coefficient of silver, hence it was expected several days would have to elapse before signals were observed. Behaviour of the type illustrated in Figure 5.33 was found even after the first day.

Because of these inconsistencies the experiment was reperformed but this time the detection chamber was pumped by an U.H.V. diffusion pump, rather than the triode pump used before, with interesting results. First the

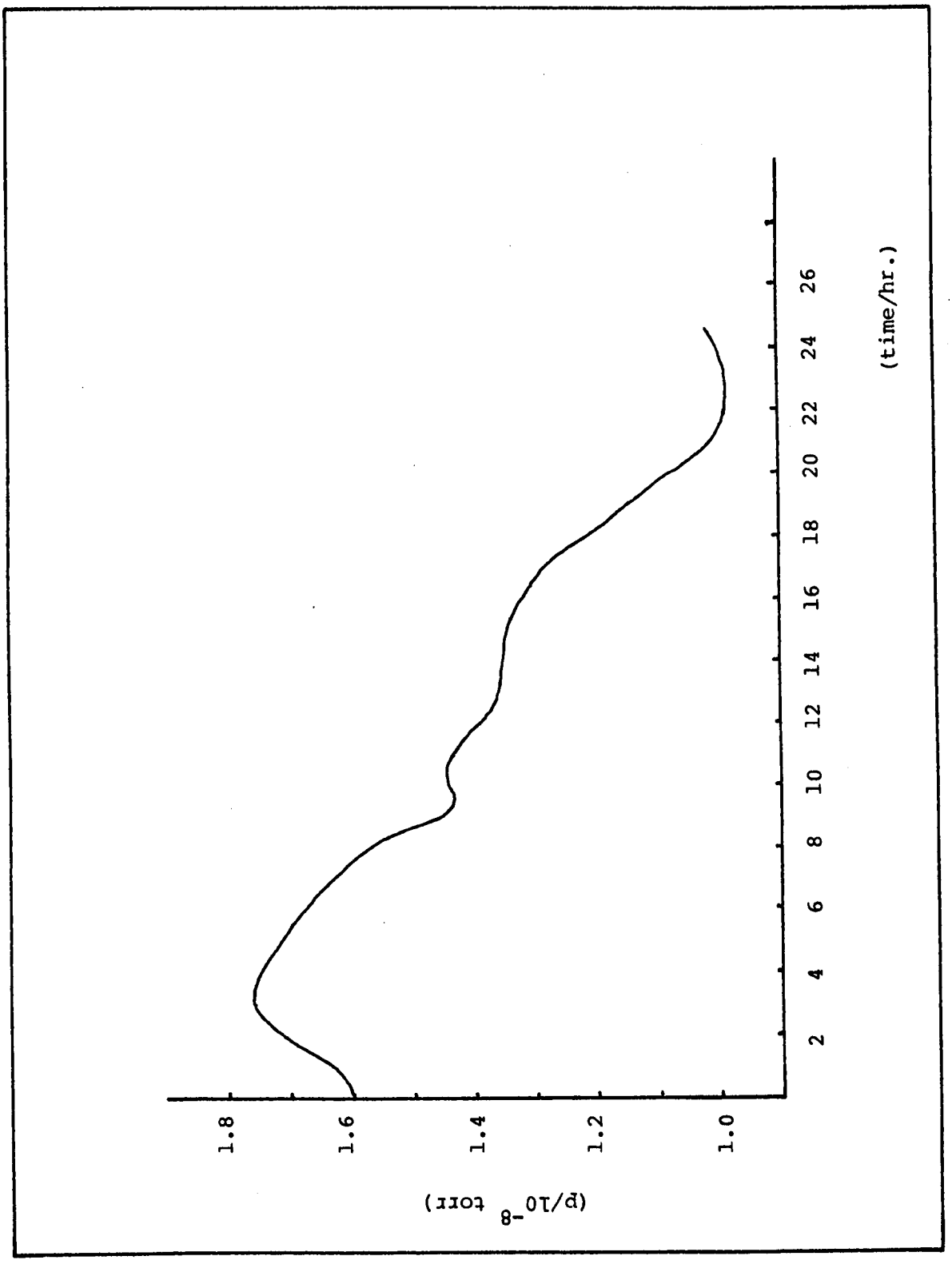

Fig. 5.33 Plot of detection chamber pressure p versus time, over 24 hrs, showing drift and fluctuations. See text.

mean detection chamber partial pressure with mass 4 dropped from $\sim 5 \times 10^{-9}$ torr to $\sim 3 \times 10^{-11}$ torr, the minimum detection limit, yet the difference in pump speed was only by a factor ~ 10. Evenso, since absolute pressures cannot be determined accurately at such low levels, a modulation experiment was performed over several days, no signal was observed.

From these results the conclusion drawn was that the behaviour illustrated in Figure 5.33 was entirely due to the "memory effect" of the triode pump. Such effects had already been observed in some early experiments. The memory effect arises from the pumping action of triode pumps. Gas atoms in the pump are ionized and accelerated, by an electric field of $\sim$ 5kV/cm, at the anode where they are embedded in its surface. The surface is continuously renewed by sputtering from the titanium cathodes. During this process some of the previously embedded atoms may be released. One of the major gases pumped during previous experiments is deuterium which also registers as mass 4 on the mass spectrometer. Hence the observed signals were probably deuterium liberated as hydrogen, from outgassing at the chamber tubulation, was being pumped. The 24 hr periodicy was probably daily temperature instabilities of the electronics.

Helium experiments were not immediately abandoned, gold and aluminium foils were also used. Helium diffusion coefficients had already been determined in aluminium (12), and it was known $D_{He} \sim 10^{-9}$ $cm^2 s^{-1}$ at 850K, which seemed measurable with the present equipment. However, no signals were observed with either metal. In the case of aluminium on inspection of the specimen surface, after removal from the vacuum rig, it was found to have suffered severe damage at the input with signs of oxidation and large numbers of macroscopic bubbles covering the surface. It was supposed that this damage prevented signals from being observed.

In conclusion, since helium modulation amplitudes of sufficient

strength to be detected were expected, the lack of signal suggests an insufficient elapsed time was allowed for transmission through the solid. This offers a means of estimating an upper limit for the helium diffusion coefficient in silver, gold and aluminium based on the characteristic time for diffusion through a foil

$$\tau = \frac{L^2}{D}$$

where L is the specimen thickness. Experimental durations, T, were approximately 5×10^5 s, therefore

$$T \lesssim \tau = \frac{L^2}{D}$$

$$D \lesssim \frac{L^2}{T}$$

$$D \lesssim \frac{(3\times10^{-2})^2}{5 \times 10^5} \sim 10^{-9}\ cm^2 s^{-1}$$

Thus the experiment would have detected signals if the diffusion coefficient had been greater than about $10^{-9}\ cm^2 s^{-1}$.

SUMMARY

This completes the report of experimental results for hydrogen deuterium and helium. It was found that with helium the experiments were one sided and it was only possible to quote a single limit for the helium diffusion coefficient in silver and gold for temperatures $\lesssim$ 900K, $D_{He} \lesssim 10^{-9}$ $cm^2 s^{-1}$. For hydrogen and deuterium materials were found for which the response time of fluctuations in the election chamber due to fluctuations at the input corresponded to $\phi_{Classical}$ as given by equation 4.37. This supposes that the diffusion flux plays a minor role in maintaining equilibrium at the input and exit of the metal foil, thus the input concentration $N^*(0,t)$ is supposed in continuous equilibrium with the gas and $N^*(L,t) << N^*(0,t)$. These materials were molybdenum and silver.

A different situation was found with gold and aluminium for which the phase/frequency data showed characteristics associated with $\phi_{H >> 1}$ (given by equation 4.42) The most notable characteristic was the dependence of the phase on the mean discharge current.

For the metals molybdenum, silver and gold diffusion coefficients were evaluated by making least squares fits of the theoretical curves on the experimental data with good agreement in every case. From the temperature dependences of the diffusion coefficients, the activation energies were determined and found to be $\sim$ 0.2eV, $\sim$ 0.39eV and $\sim$ 0.92eV for gold, silver and molybdenum respectively.

From the hydrogen and duterium diffusion coefficients, the isotopic ratios in molybdenum, silver and gold were determined as $\sim$ 1.1, $\sim$ 1.3 and $\sim$ 1.5 respectively.

CHAPTER SIX

DISCUSSION

In this chapter the main concerns are:

1) to confirm the experimental technique by comparison of data with that reported elsewhere.

2) to relate the new data reported in chapter five to current theories of diffusion.

6.1. Molybdenum

The permeability, P, and the diffusion coefficient D, of hydrogen and deuterium in molybdenum were found in sections 5.1.1. and 5.3.1. to be represented by the quations.

$$D_H = 7.8 \exp(-0.93eV/kT)\ cm^2\ s^{-1} \quad (5.1)$$

$$P_H = 6.36x10^{-7} \exp(-0.98eV/kT)\ Mole\ cm^{-1}s^{-1}torr^{-\frac{1}{2}} \quad (5.7)$$

$$D_D = 5.3 \exp(-0.91\ eV/kT)\ cm^2 s^{-1} \quad (5.2)$$

$$P_D = 1.10x10^{-6} \exp(-1.03\ eV/kT)\ Mole\ cm^{-1}\ s^{-1}torr^{-\frac{1}{2}} \quad (5.8)$$

The results are here compared with other data reported in the literature.

6.1.1 Hydrogen permeability.

In Figure 6.1 the permeability of hydrogen in molybdenum as given by equation 5.7 is compared with values obtained from elsewhere, (53), (54), (55), (56), and (57). As can be seen the results of this work are a little high relative to the available comparisons. All curves are consistent to within a factor 1.5 and there is not much scatter in the activation energies.

Data attributed to other authors may require some interpretation for experimental conditions were not identical to those in the present work.

1) Reuben (57) was engaged in work not unlike that described here. The two experiments differed in that he used input pressure modulation rather than the discharge injection method. For

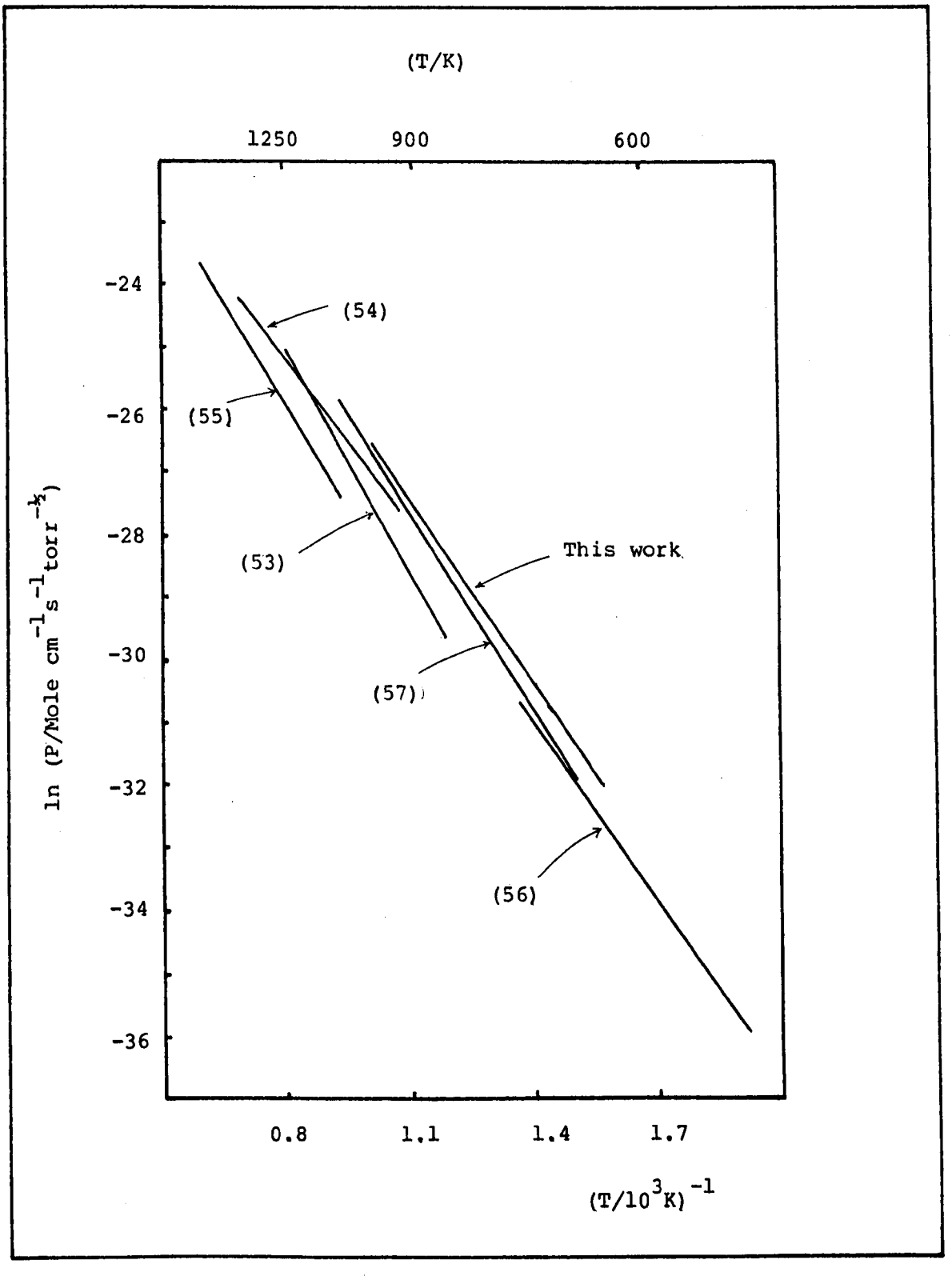

Fig. 6.1. Permeabilities for hydrogen in molybdenum.

(53) Hill
(54) Huffine and Williams
(55) Fraunfelder
(56) Jones et. al.
(57) Reuben

1) this reason his work is the most closely related to the present work. That there is good agreement between the two sets of results confirms that little specimen degradation was induced at that stage by the discharge. The actual measurement of permeabilities was made over nearly identical conditions of pressure and temperature.

2) The permeability attributed to Hill(53) was obtained by multiplying his reported solubility and diffusion coefficients. Hill used a desorption technique for measuring diffusion rates and the material was charged at between 1580-2000K. His data is thus extrapolated over a wide range to make the present comparison. This could explain the deviation between the curves.

3) Huffine and Williams (54) made measurements at 810 torr input pressures; in the present work the input pressure was $\sim$ 2 torr. It is not expected that this should make a significant difference since molybdenum was found to conform with, what has been described here as, Sievert or classical behaviour. Huffine and Williams's measurements were made over a higher temperature range than that of the present work, and so the present extrapolation may be unjust.

4) Fraunfelder (55) investigated a wide range of input pressures between 2×10^{-6} and 200 torr and found deviations from Sievert behaviour at pressures around 10^{-2} torr. These effects were supposed associated with the extent of pre-dissociation of gas at the relatively high temperatures used. Again there is no obvious reason for the difference between Fraunfelder's and the present results, but, as with Hill, the data was taken at relatively high temperatures and show a high activation energy which extrapolates badly into the data of all authors who have worked at lower temperatures.

6.1.2 Deuterium permeability.

The permeability of deuterium in molybdenum, given by equation 5.8, is shown compared with the permeabilities reported by (58) and (59) in Figure 6.2. There is substantial agreement between the data of the present work and that reported by the other authors. Again however experimental conditions were not identical:

1) Guthrie et.al. (58), made measurements over the input pressure range 1-2000 torr.
2) Caskey et.al. (59), made measurements at an input pressure of about 1000 torr.

Deuterium, as with hydrogen, showed classical behaviour in molybdenum so the difference in input pressure conditions between the present work and (58) and (59) is not believed to be important.

6.1.3. Hydrogen diffusivity.

In contrast to the good consistency, amongst authors, for hydrogen permeabilities in molybdenum, there is a large scatter for hydrogen diffusivity data. This is illustrated by Figure 6.3, which shows the diffusivity as given by equation 5.1, compared with diffusivities reported by others,(53), (56), (57), (60) and (61). The inconsistency amongst authors may be due to the differences in experimental conditions:

1) Reuben (57) again found data in good agreement with that reported here. There is a small difference in activation energy however, Reubens lower value represents a best line through a curved plot. An activation energy based on his low temperature data alone would give a value closer to that reported here.
2) Jones et. al. (56), also measured diffusivities with a response time method, but compared to the present work they found a low activation energy. There is no obvious reason for this.

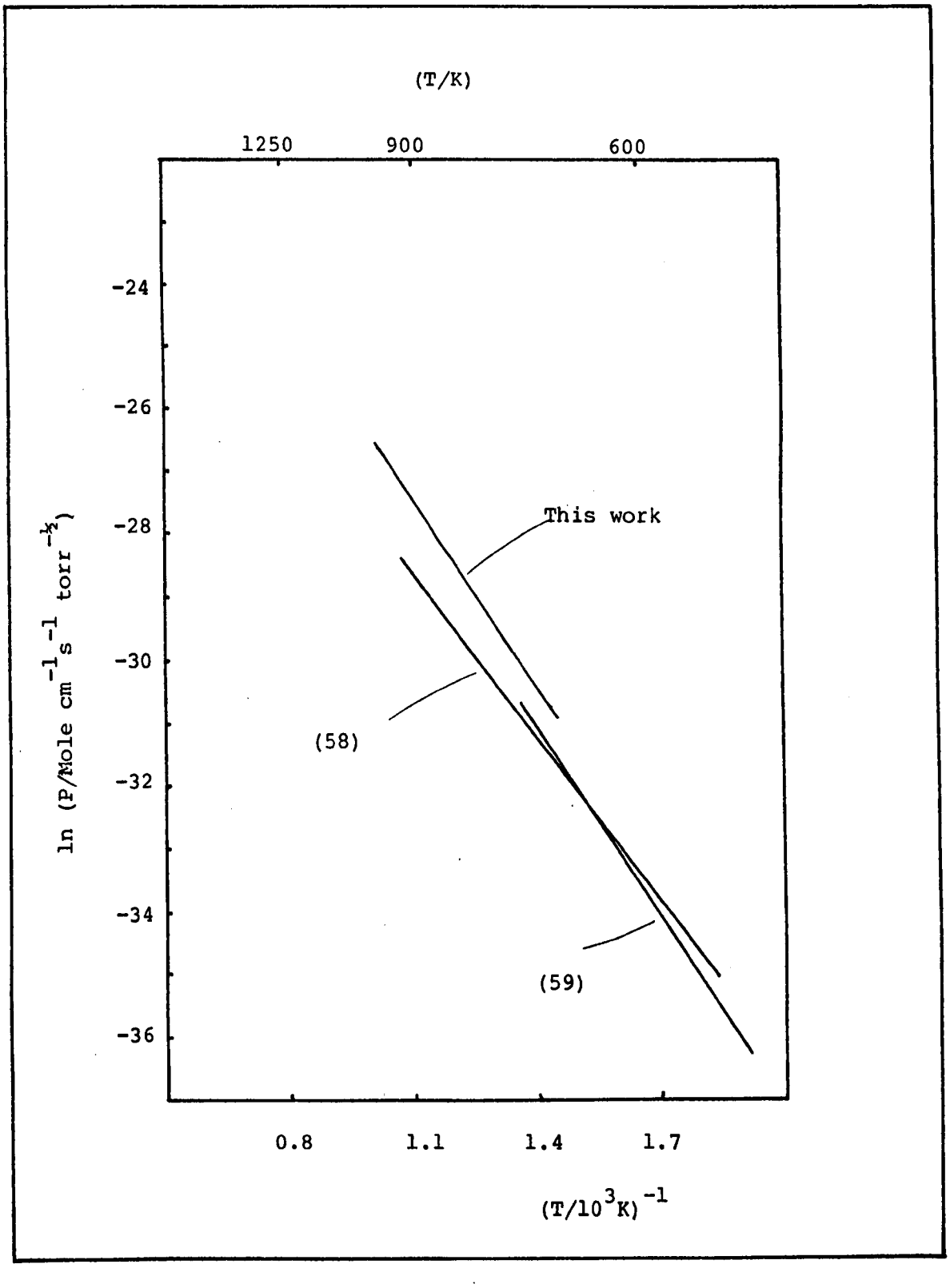

Fig. 6.2 Permeabilities for deuterium in molybdenum.

(58) Guthrie et. al
(59) Caskey et. al.

3) Hill (53), used a desorption technique and also found a lower activation energy.

4) Ryabchikov (60), used a desorption technique. His results are drawn as a dotted line because they are extrapolated from outside the temperature range shown. Ryabchikov found a similar value for the activation energy to that reported here, but a lower pre-exponential factor, by a factor of ~ 50.

5) The experiments of Zakharov et. al. (61), are particularly interesting because they also used discharge injection. Their work covered a similar range of temperature and discharge potential, but used current density of $5mA/cm^2$ as opposed to the $0.3mA/cm^2$ used here. Zakharov et.al. reported the diffusion coefficients shown in Figure 6.3 which go down to a temperature $\sim 625K$. Below a temperature $\sim 725K$ however they found that the flow through their thinner specimens (0.01cm and 0.05cm) were not, diffusion controlled; they interpreted this as due to surface degradation. In the present work specimen thickness of 0.025cm were used.

In the present work there was definite evidence for specimen degradation, perhaps of a kind similar to that reported by Zakharov et. al. After about twenty four hours of experimentation specimens showed a major drop in permeation; a factor ~ 10. This change did not seem to be temperature specific, with one specimen it occurred at $\sim$ 800K with the second at $\sim$ 650K. The phase/frequency plots took a non-classical form. In general, phase lags were increased relative to what might have been expected from data gathered at the beginning of experimentation. Whatever new processes were involved, therefore, their effect was to slow the passage of the diffusing gas.

From inspection of Figure 6.3 it may be seen that Zakharov et. al. have reported two sets of diffusivities, one for hydrogen and the other for

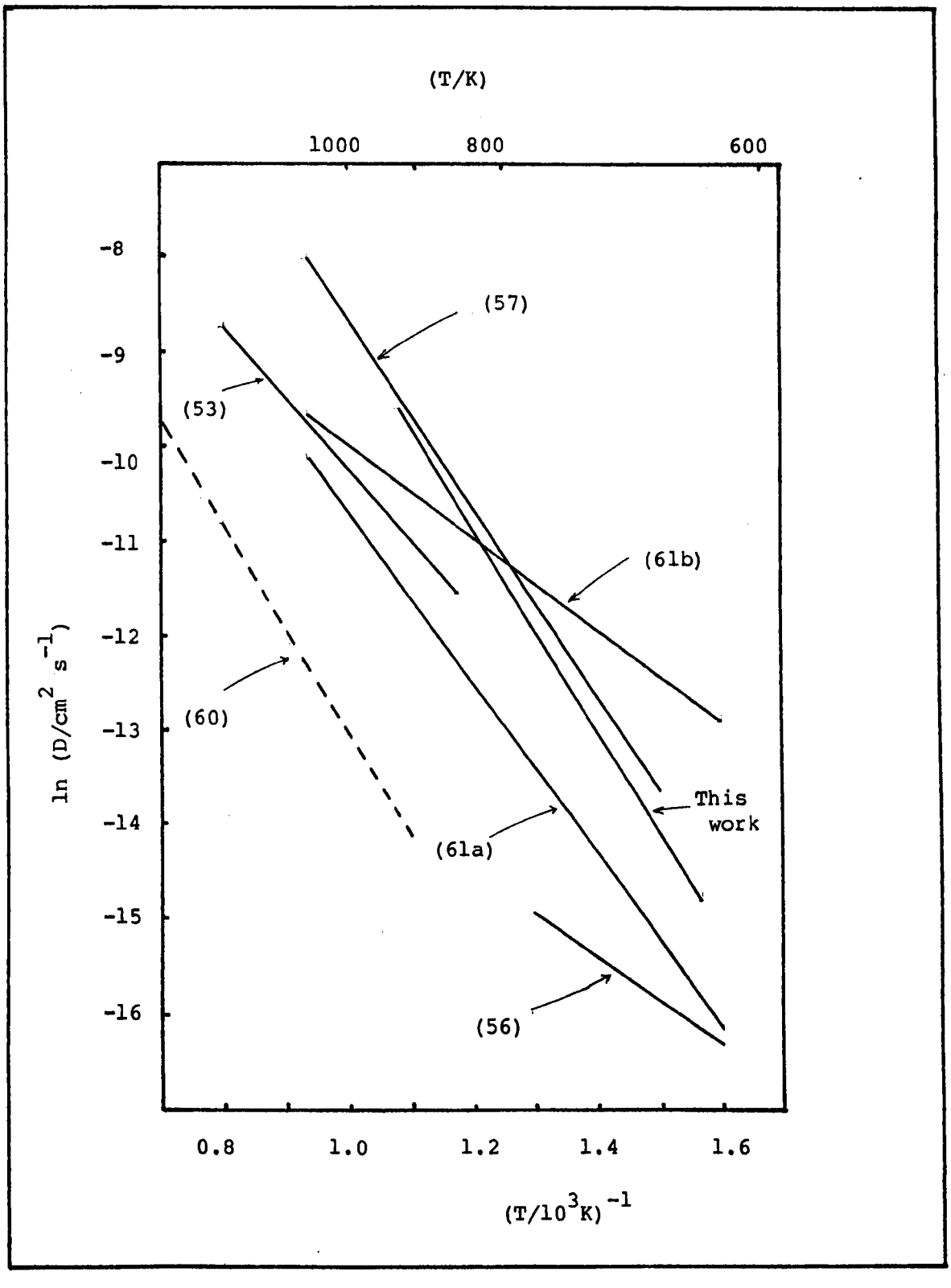

Fig. 6.3 Diffusivities for hydrogen in molybdenum

(53) Hill
(56) Jones et. al.
(57) Reuben
(60) Ryabchikov
(61a) Zakharov et. al. for hydrogen
(61b) Zakharov et. al. for complex

the hydrogen/defect complexes believed formed at the surface. These curves show that the complexes are attributed a higher diffusion coefficient over the measured temperature range. This conclusion is not consistent with the observations reported here. It is, in any case, a surprising interpretation since it calls for a structured and more massive entity than the hydrogen atom to have a larger diffusion coefficient.

6.1.4. Deuterium diffusivity.

As with deuterium permeabilities, there are at the time of writing few available deuterium diffusivities reported by other authors. In Figure 6.4 the present data, described by equation 5.2 is compared with the diffusivities reported by Caskey et. al. (59). Also shown in the figure as a dotted line is the hydrogen diffusivity given by equation 5.1.

It should be noted that Caskey et. al. report two sets of data one relating, in effect, to the absorption of gas, the other to the desorption of gas. In their work the rate of rise in gas flow to the detection chamber consequent on a step rise in input pressure was first measured. The input pressure was then sharply reduced and the consequent fall in flow measured. Caskey et. al. did not find it possible to derive a single diffusion coefficient from their measurements. The coefficient derived from a pressure fall was greater than the coefficient from a rise. These authors propose an explanation of these differences involving trapping of hydrogen in molybdenum.

An alternative explanation could, in the light of Fraunfelders (55) observations of low pressure non-Sievert permeation, be proposed in terms of the behaviour of fluxes at the input and the exit of a foil. However, a detailed calculation would be required, which cannot be made here.

In any case, trapping effects of the kind reported by Caskey et. al.

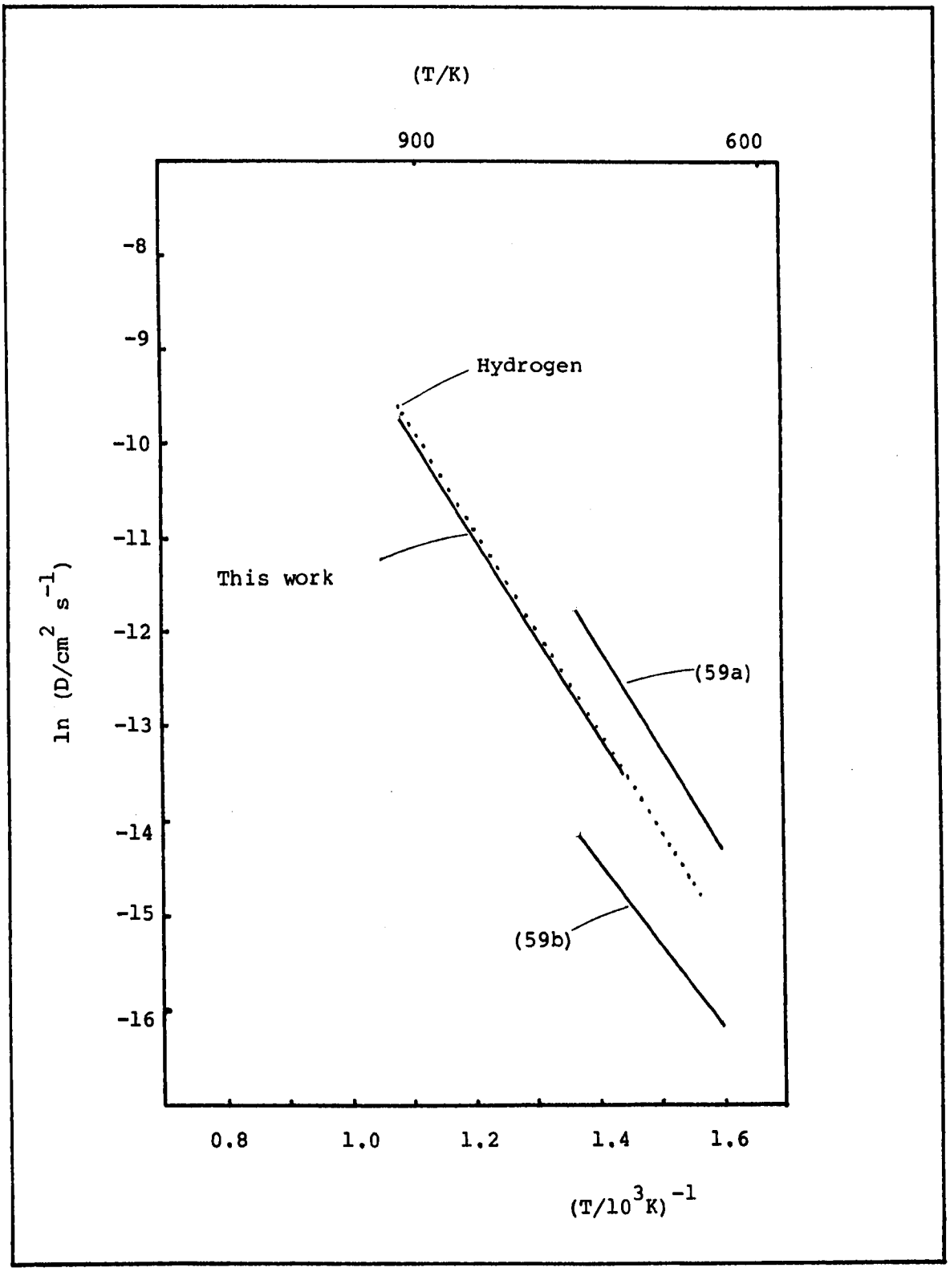

Fig. 6.4 Diffusivities of deuterium in molybdenum

(59a) Caskey et. al. desoption method
(59b) Caskey et. al. absorption method

should certainly have been detected in the present work where it is anticipated on the basis of the analysis by Cummings (51), it would have been detected, very sensitively, as an increase in the harmonic content of the output pressure. No such effects were observed for the measurements reported.

6.1.5. Comparison of hydrogen and deuterium diffusivity in molybdenum with theory.

In general the diffusivity activation energies reported here and elsewhere, and consequently the derived pre-exponential factors, have given values for molybdenum large relative to those observed for other hydrogen/metal systems.

The presently reported activation energies for the diffusivity are smaller than those for the permeability of hydrogen and deuterium in molybdenum. This is consistent with the definition of permeability, and a rising solubility with temperature.

It was pointed out in section 2.2 that no predictive theories are currently available giving diffusion parameters in terms of fundamental hydrogen/metal constants. The only useful relationship was equation 2.7 for the pre-exponential factor. If the interstitial void radius in molybdenum is $\sim$0.04nm then using the observed activation energy and the harmonic approximation the characteristic frequency of hydrogen in an interstitial site is $\sim 5.3 \times 10^{13}$ Hz. If the lattice separation is assumed to be 0.27nm then from equation 2.7 the pre-exponential factor $\sim 10^{-2}$ $cm^2 s^{-1}$. This is orders of magnitude too small compared to the observed value.

A second useful theory, though not predictive, was outlined in section 2.2.2 relating to the isotopic ratios of the permeation constants. Models of this type were developed independently by Ebisuzaki (18) and

Le Claire (17) and could explain, in terms of a quantum correction, deviations of isotopic ratio from the classically expected value of $2^{\frac{1}{2}}$.

The quantum correction may be shown to be approximately dependent on two parameters ν_1 and ν'_1 the frequencies associated with the normal and transition state vibration modes in the harmonic approximation. By matching theory with observed isotopic ratio temperature dependence for solubility and diffusivity, ν_1 and ν'_1 may be evaluated. Due to the absence of solubility data from the present study, ν_1 was assigned the value 5.3×10^{13}Hz, estimated earlier. The parameter ν'_1 was then determined by matching the data in Table 5.3 to the relationship.

$$\frac{D_H}{D_D} = \sqrt{2}\left[\frac{f(x_1)}{f(\sqrt{2}\,x_1/2)}\right]^3\left[\frac{f(\sqrt{2}\,x_1/2)}{f(x_1)}\right]^2 \qquad (6.1)$$

where $f(x) = \sinh(x)/x$ and $x=h\nu/2kT$. From this $\nu'_1 \sim 8.3\times10^{13}$Hz, giving the ratio $\nu'_1:\nu_1 \sim 1.6$

At the time of writing no other Ebisuzaki parameters were available for molybdenum, however this ratio is typical relative to the ratios found for other metals (18) and (52).

6.2 Silver

The diffusion coefficients of hydrogen and deuterium in silver were found in section 5.1.2 to be given by

$$D_H = 1.7\times10^{-2}\exp(-0.39\text{eV}/kT)\ \text{cm}^2\,\text{s}^{-1} \qquad (5.3)$$

$$D_D = 9.8\times10^{-3}\exp(-0.37\text{eV}/kT)\ \text{cm}^2\,\text{s}^{-1} \qquad (5.4)$$

These results are here compared with other data reported in the literature.

6.2.1 Hydrogen diffusivity.

As silver is not of major technological importance there have been few studies made for the permeation of hydrogen in this metal. Some work has been done by Eichanauer et. al. (62) and Katsuta and McLellan (63). In Figure 6.5 the data by these authors is compared with the diffusivity found in the present work and given by equation 5.3. The experimental conditions used by the earlier authors were:

1) Eichanauer et. al. (62) used a desorption technique and measurements were made over a temperature range almost identical with that for the present work. Their results are approximately a factor three lower than those of this work and have a lower activation energy $\sim$ 0.33eV.

2) Katsuta and McLellan (63), made a more recent study and used a permeation technique with time lag analysis. These authors made measurements over a temperature range lying above that shown in the figure so the curve representing their data is shown as a dotted line. Comparison of their pre-exponential factor with that reported here shows it a factor 1.5 lower. In fact extrapolation of the present data into their temperature range passes through the main body of data reported by these authors. This a consequence of the higher activation energy found in the present work. Comparison of activation energies shows they are within experimental error. Hence there is a good agreement between the two studies.

Katsuta and McLellan propose that the difference between their work and that of Eichanauer et. al. may be due to the improved purity of modern specimens. In the present work silver was found to behave classically, in the sense described in chapter four, but it is not possible to estimate to what extent impurities might change this. However, it was observed that silver

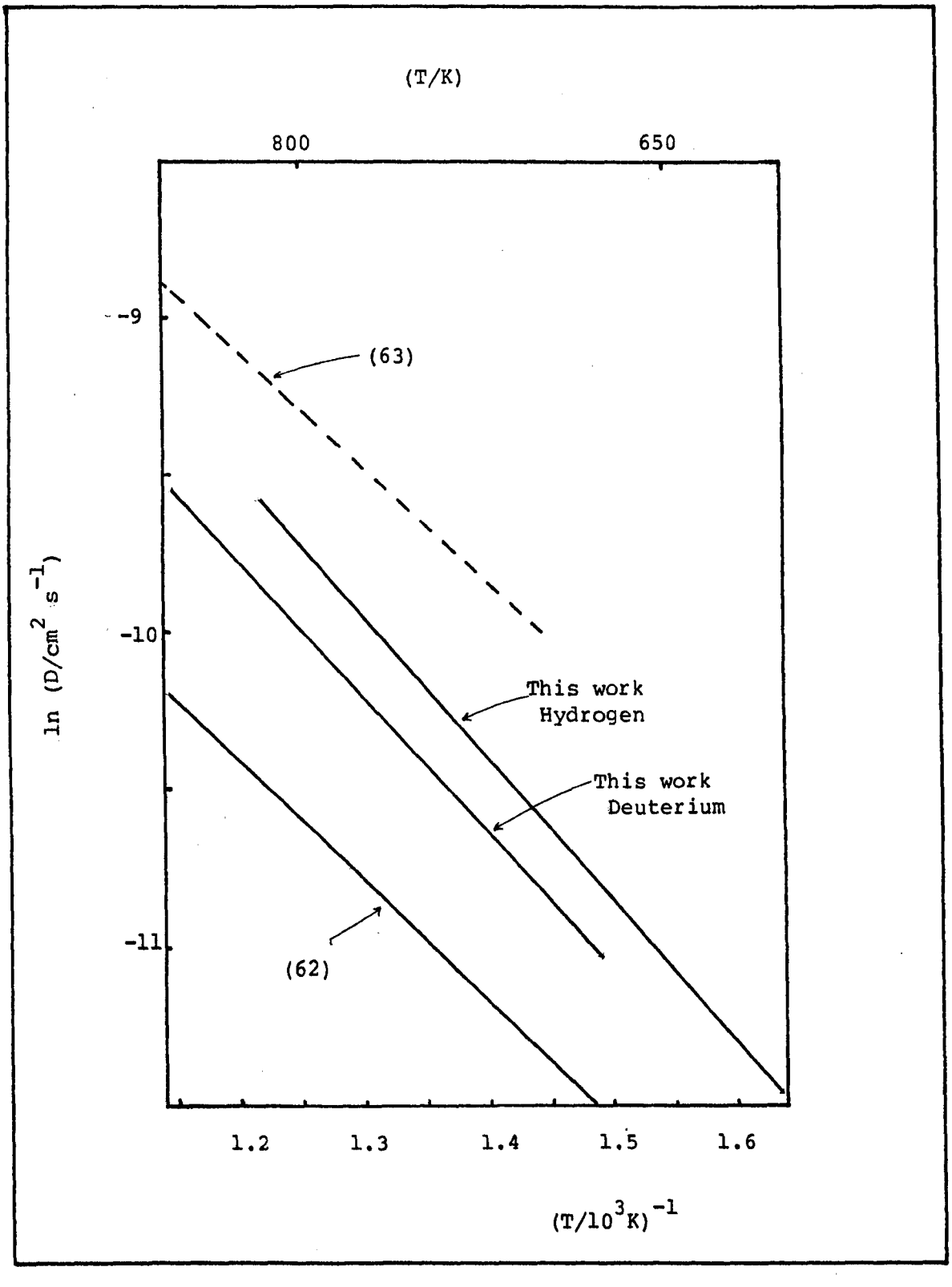

Fig. 6.5 Diffusivities for hydrogen and deuterium in silver

(62) Eichanauer et. al.
(63) Katsuta and McLellan

may develope a surface oxide if due care is not taken and this may introduce non-classical behaviour.

6.2.2 Deuterium diffusivity.

The diffusion coefficient of deuterium in silver as given by equation 5.4 is also plotted in Figure 6.5. As far as could be established at the time of writing these results were unique.

6.2.3. Comparison of hydrogen and deuterium diffusivity in silver with theory.

The activation energies and pre-exponential factors derived for the diffusivities in silver are fairly typical of hydrogen/metal systems. Equation 2.7 may be used to estimate the pre-exponential factor expected by classical theory. For this purpose suppose the interstitial void radius be 0.06nm. Then, using the harmonic approximation and the observed activation energy as an estimate for the potential well depth, the characterizing frequency for hydrogen in an interstitial site has the value, $\nu \sim 2.3\times10^{13}$ Hz. If the lattice separation is assumed to be 0.29nm, the pre-exponential factor $\sim 5\times10^{-3}$ $cm^2 s^{-1}$. This is only a factor two smaller than the value found from experiment.

Again using equation 6.1, the Ebisuzaki parameters corresponding to the isotopic ratios detailed in Table 5.6 for silver may be derived by matching theoretical expectation with experimental results. Since no solubility results were available in this work, the characterizing frequency calculated earlier will be assigned as the normal state frequency, $\nu_1 \sim 2.3\times10^{13}$Hz. With this, the transition state frequency is found to be $\nu_1' \sim 3.6\times10^{13}$Hz. Therefore, the ratio of the Ebisuzaki parameters $\nu_1' : \nu_1 \sim 1.6$, again a typical value.

6.3 Gold

In sections 5.2.1 and 5.3.2 were reported the studies made for

hydrogen and deuterium diffusivity and permeability in gold. The interpretations of the observed data were represented by the equations

$$D_H = 4.1\times10^{-2} \exp(-0.18\text{eV/kT}) \ \text{cm}^2\ \text{s}^{-1} \quad (5.5)$$

$$P_H = 1.10^{-6} \exp(-1.18\ \text{eV/kT}) \ \text{Mole cm}^{-1}\ \text{s}^{-1}\text{torr}^{-\frac{1}{2}} \quad (5.10)$$

$$D_D = 6.8\times10^{-2} \exp(-0.23\text{eV/kT}) \ \text{cm}^2\ \text{s}^{-1} \quad (5.6)$$

$$P_H = 5.4\times10^{-3} \exp(-1.77\text{eV/kT}) \ \text{Mole cm}^{-1}\ \text{s}^{-1}\ \text{torr}^{-\frac{1}{2}} \quad (5.11)$$

As with silver there are few reported permeation constants for hydrogen isotopes in gold from elsewhere, (38), (52), (64), (65). The main reason for this, is the low absorption of hydrogen in gold which makes measurement very difficult.

6.3.1 Hydrogen permeabilities

In the present work, steady rate permeation experiments were performed (a) to determine the dependence of the steady rate flux on input pressure at constant temperature, (b) to determine the dependence of the steady rate flux, hence the permeability, on temperature. Similar experiments have been reported by Chung (52). From his experiments on the pressure dependence he found that fluxes were proportional to $p^{0.7}$. The present author found the flux proportional to $p^{0.65}$ with measurements over a similar pressure range, but a wider range of temperatures. Although there is not precise agreement both experiments suggest that gold shows non-Sievert behaviour. This, in the present authors opinion, is a vital facet in the interpretation of diffusivity

In Figure 6.6 the permeability in gold from Chung is compared with that from the present work given by equation 5.10. As may be seen there is good agreement and the activation energies are almost identical, Chung finds it to be 1.17eV.

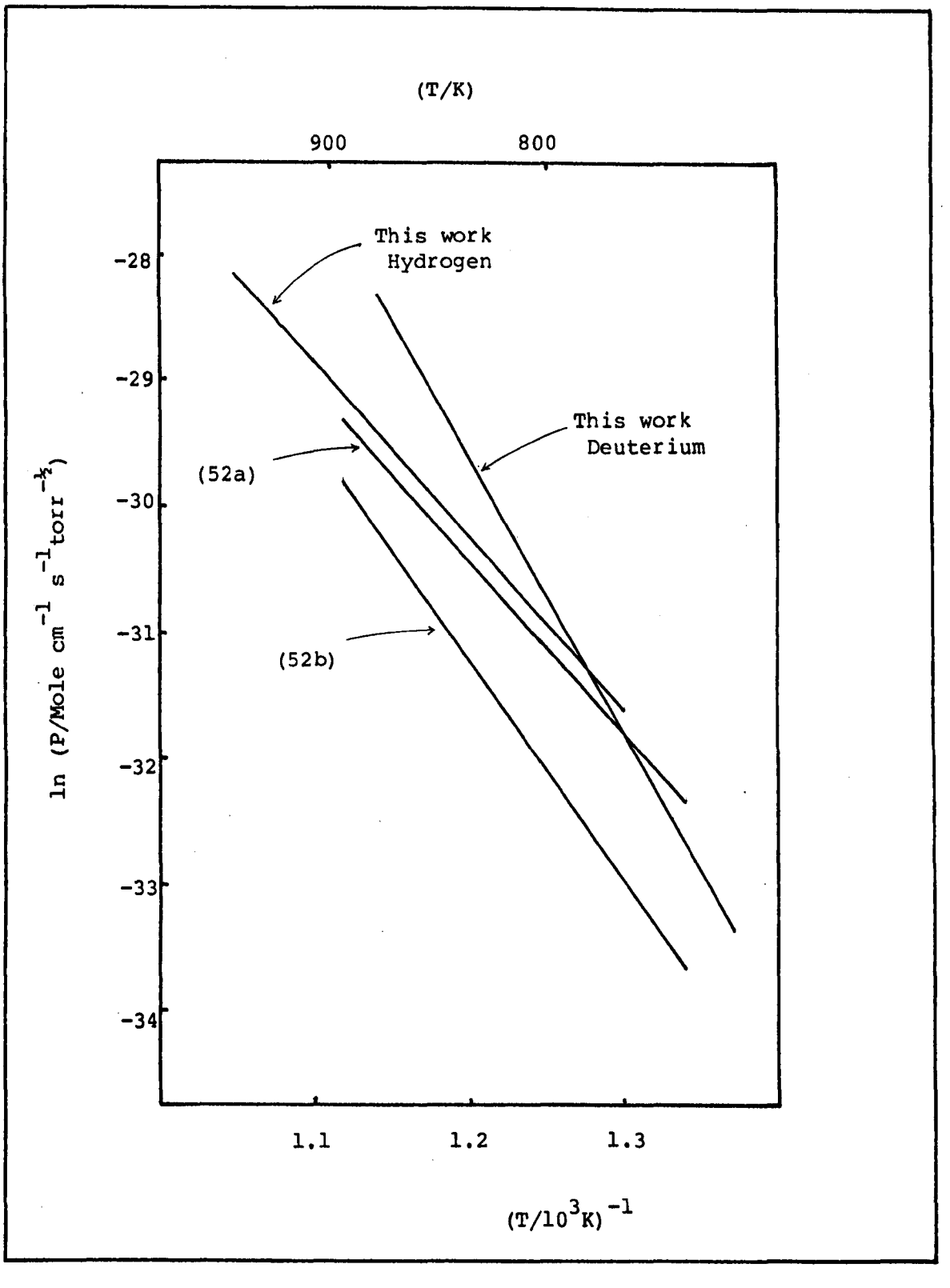

Fig. 6.6 Permeabilities for hydrogen and deuterium in gold

(52a) Chung. Hydrogen
(52b) Chung. Deuterium

6.3.2. Deuterium permeability

Experiments similar to those performed with hydrogen were also performed with deuterium. For the pressure dependence Chung found fluxes proportional to $p^{0.75}$, whereas the present author found them proportional to $p^{0.70}$. Once more agreement is not precise but both studies agree that gold also shows non-Sievert behaviour with deuterium.

Also shown in Figure 6.6 are the permeabilities in gold, as determined by Chung compared with the new data represented by equation 5.11. Agreement is not as good as with hydrogen and Chung found the activation energy to be 1.51eV. In the study reported here for deuterium a 0.025cm thick specimen was used, whereas the specimen used for hydrogen was 0.05cm. Chung's experiments were all performed with 0.05cm thick specimens. The difference in thickness may be significant as the characteristic flux depends on it. Also note that the dimensions of P include $torr^{-\frac{1}{2}}$ which supposes Sievert behaviour.

6.3.3. Hydrogen diffusivity.

In Figure 6.7 the new diffusivity data, represented by equation 5.5 is compared with the results of other authors Chung (52), Eichanauer and Leibscher (64) and Kurakin et. al. (65). It is clear from inspection of the figure that there is general agreement over the activation energy, which is $\sim$ 0.2eV.

There is also agreement amongst previous studies for the pre-exponential factor. Chung (52) and Eichanaur and Leibscher (64) found almost identical values; Kurakin et. al. found a value about three times larger then theirs. In contrast the present author found a pre-exponential factor, one to two orders of magnitude larger.

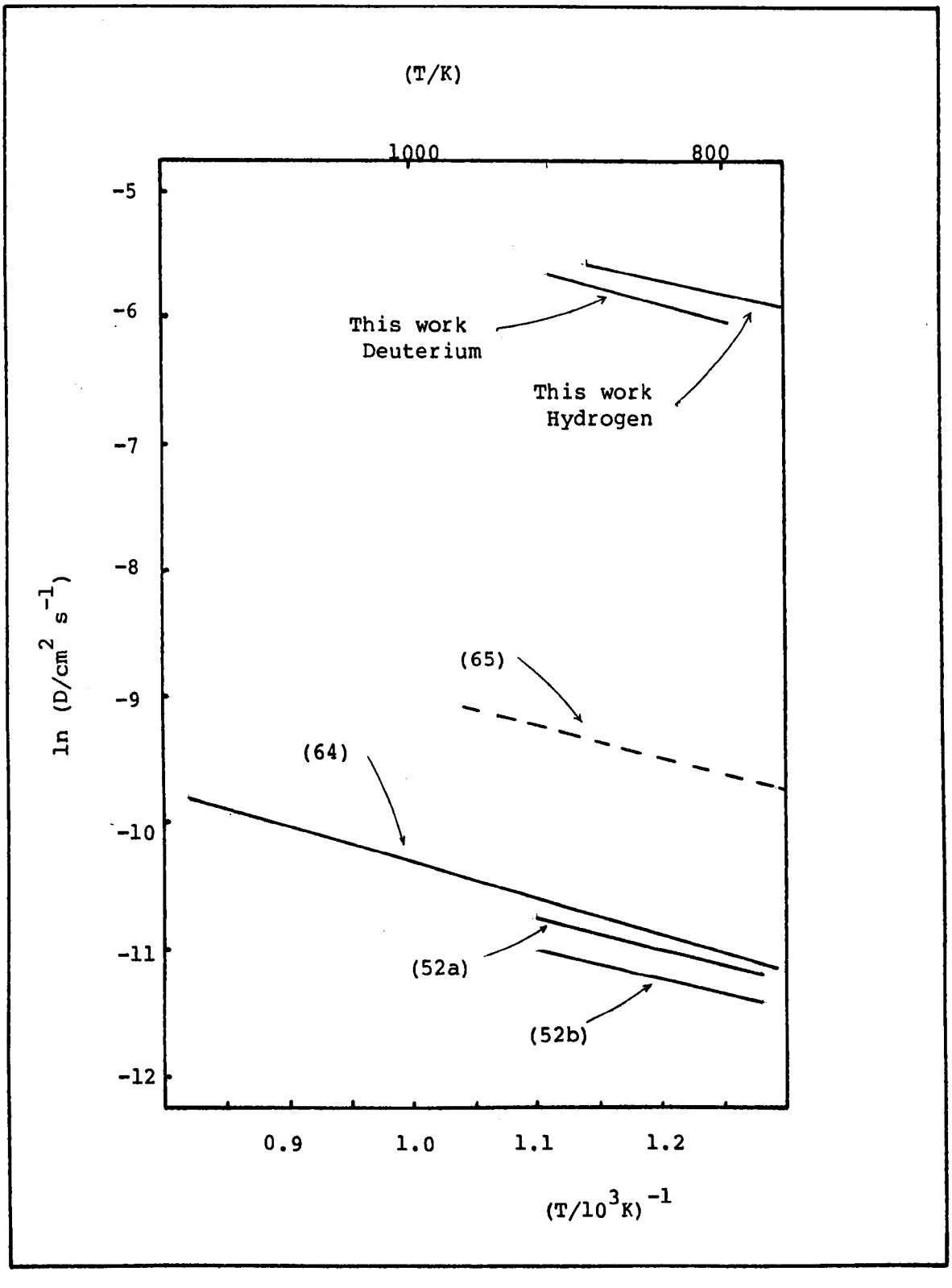

Fig. 6.7 Diffusivities of hydrogen and deuterium in gold.

(52a) Chung. Hydrogen
(52b) Chung. Deuterium
(64) Eichanauer et. al.
(65) Kurakin et. al.

This value of 4×10^{-2} $cm^2 s^{-1}$, although differing from previous studies in gold, is fairly typical of hydrogen/metal pre-exponential factors. Values reported by the other authors are in fact significantly lower than the main body of pre-exponential factors found with other metals. In the opinion of the present author this difference is due to the inadequate attention given, in previous studies, to the processes working at the input and exit surfaces of the experimental foils.

1) Eichanauer and Leibscher (64) used a desorption technique, normally a sound method, and worked in the temperature range 770-1200K. Theirs, however, was an early work and they made no allowance for the non-Sievert behaviour of gold.

2) Chung (52), as discussed in sections 6.3.1 and 6.3.2 was aware of the non-classical permeation shown by gold. He used a permeation method with a step function input and time-lag analysis, but made no modification to the analysis to take account of phase boundary processes.

3) Kurakin et. al. (65), used a method similar to that of Chung. These authors were specifically interested in measuring diffusion coefficients in metals of low absorption, and in their paper make it clear that they were aware of the importance of phase boundary processes. The main body of the work reported was actually with copper, which apparently showed similar behaviour to gold.

These authors point out that for the normal type of time lag analysis to be valid , thick specimens or high input pressures or both are required, but that these conditions may not be suitable for experiment. Rather than modify the analysis, they proposed the use of a hot tungsten filament to atomize hydrogen in the gaseous phase and hence to increase the adsorption activity.

For their work with copper Kurakin et. al. provided evidence

showing the success of this method, but for gold, in the temperature range 500-700K, no details were given.

The present work is in seeming contradiction to Kurakin et. al. A glow discharge generates a gas phase with energetic ions and hydrogen atoms. According to Kurakin et. al. it should thus greatly increase gas flow so measurements of the present type should have been particularly easy. This was not found to be so.

The interpretation of data given in section 5.2.1. gives diffusion coefficients well separated from those reported elsewhere (52), (64) and (65). The origins of this difference lie in the suppositions from which the present analysis is derived, for they permit non-equilibrium hydrogen concentrations at the input and exit surfaces of the specimen foils whereas in all previous analyses the supposition of equilibrium concentrations is central to the analysis.

Before deciding between the interpretations an interesting check is to see whether the basic data are fundamentally incompatible. This can be done by using $\phi_{Classical}$ defined in equation 4.37 and noting that it as a linear asymptote against $\upsilon^{\frac{1}{2}}$, of gradient $(\pi L^2/D)^{\frac{1}{2}}$. If, instead of attempting a least squares fit which shows a systematic variation, a diffusion coefficient is derived from the gradient of the line passing through $-\pi/4$ on the phase axis and the high frequency data, values like those in Table 6.1 result. In general these pseudo-diffusion coefficients are close to the values found elsewhere so it seems the data are indeed compatable.

Table 6.1

pseudo-diffusion coefficients, D^*, in gold

T/K	D^*/cm^2s^{-1}
769	$3.5x10^{-5}$
799	$4.5x10^{-5}$
834	$5.0x10^{-5}$
875	$7.5x10^{-5}$

In question then is whether the present data are good enough to justify the suggested change in interpretation. As mentioned in the chapter three the equipment was expected to allow measurement of phase to within $\pm$ 0.02 radians and this was realised for the main body of data collected. This accuracy was exemplified by repeatably reproducible extrapolation to the phase axis intercept of $-\pi/4$ of the high frequency data with molybdenum and silver. Although with gold the conditions were not identical, fluxes through the specimen being smaller than for the other metals, the phase measurements made over the experimental temperature range are believed to be of the same quality. This is because the amplitude of pressure fluctuations was well inside the detection limit and the Fourier spectrum of these fluctuations had small harmonic content, after signal averaging. Therefore the present author believes the data is good enough to resolve the alternative analyses.

To illustrate the differences between the classical model and the model proposed here, Figure 6.8 shows: (a) the relative phases of J(0), N(0), J(L), N(L) and the driving fluctuation in the classical regime. N(0) is locked in phase with the driving fluctuation. When the modulation frequencies are small, both J(0) and J(L) are very nearly in phase with N(0), but as the frequencies get larger its found J(0) can lead N(0) by a maximum of $\pi/4$ and

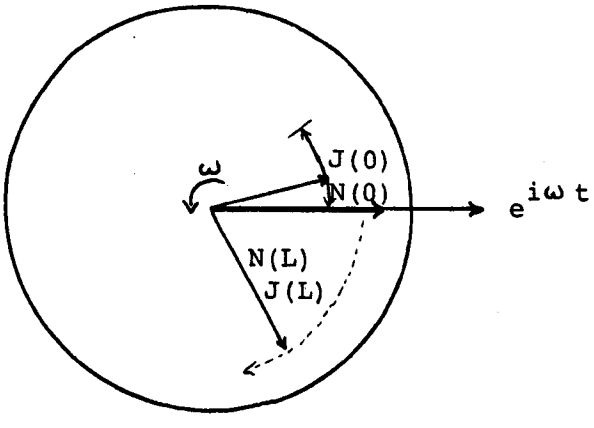

(a)

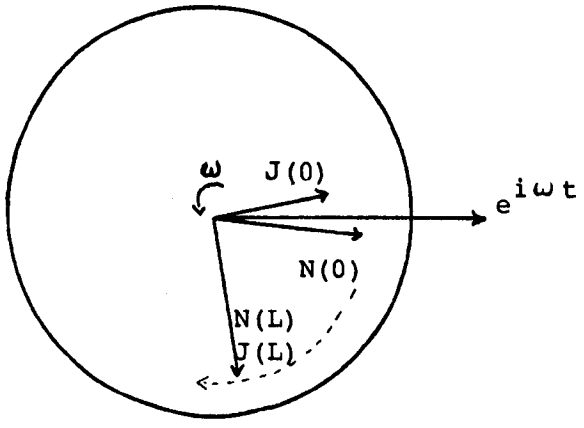

(b)

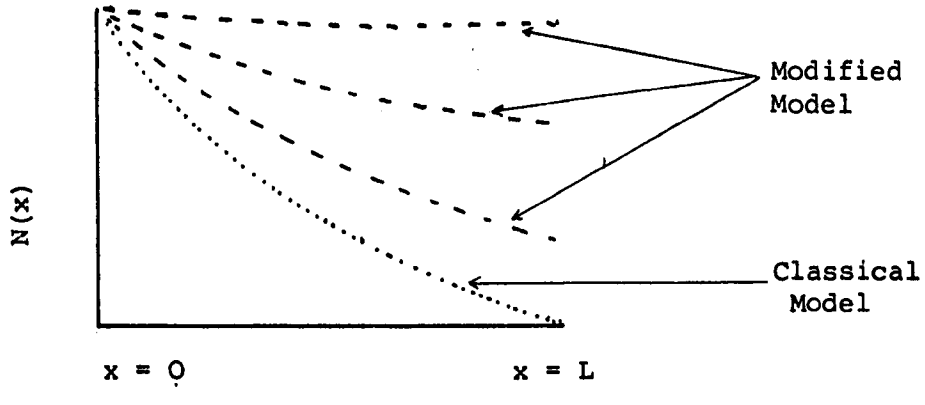

(c)

Fig. 6.8 Comparison of relative phases and amplitudes of the classical and modified models

(a) Relative phases of N(0), J(0) N(L) and J(L) with classical model

(b) Relative phases of N(0), J(0), N(L) and J(L) with modified model

(c) Gas concentrations across the foil.

J(L) lags behind N(0): (b) the relative phases of J(0), N(0), J(L), N(L) and the driving fluctuation, for the new model at some intermediate frequency. The vectors of J(0) and N(0) now lie either side of the vector of the driving fluctuation and J(L) lags behind N(0) with a phase that is greater than for the classical regime because of the reflection at the exit surface allowed by the new model. In this way the phase lag between the driving fluctuation and J(L), in the new model, may be larger than the phase expected by the classical model for identical values of the ratio (L^2/D). At very large frequencies the new model allows J(0) to be in phase with the driving fluctuation and N(0) then lags behind them, which is what might be expected: (c) the spatial variation of concentration for the classical regime compared with the variation expected by the new model. The new model allows reflection at the back surface hence it is possible $|N(L)| \sim |N(0)|$.

In conclusion there is agreement amongst all authors that surface processes play an important role in hydrogen diffusion in gold. In question is whether the coefficients reported here are acceptable. An experiment that could resolve the issue would use a surface independent technique, such as N.M.R. This has been tried by Weaver (38). Normally due to the low solubility of hydrogen in gold such an experiment would be impossible, but Weaver induced large hydrogen concentrations ($\sim$ 30 atomic per cent) in gold films by forming them by sputtering in a hydrogen atmosphere. Unfortunately he concluded from his results that hydrogen was present in gold as microbubbles and so the data cannot be interpreted as diffusion rates.

6.3.4 Deuterium diffusivity.

Shown in Figure 6.7 besides the hydrogen data are the deuterium diffusivities from the present work, represented by equation 5.6 The values of the coefficients for deuterium are lower than those for hydrogen by a factor of about 1.5, hence they are much larger than the values found by Chung (52)..

It is interesting to note that the present deuterium experiments used input pressures of about 15 torr and mean discharge currents of about 6mA, both close to the maximum limits allowed by the equipment. These values are larger than those used in the hydrogen experiments. The result was that the phase/frequency data for instance at 799K, for deuterium lie below those for hydrogen. Classically this would have to interpreted as a deuterium diffusion coefficient that is larger than that for hydrogen. This would be an unusual conclusion and is due to the classical analysis not allowing phase dependence on surface concentrations. The other comments made in section 6.3.3. also apply here.

6.4. Aluminium

The chemical affinity of aluminium for oxygen is well known (66) and has made estimation of gaseous permeabilities in aluminium difficult. To the author's knowledge a glow discharge injection method has not been used before. It was hoped this method would overcome the problems associated with the impermeable surface oxide layer.

This hope was not realised. It was found, when the aluminium surface was relatively new, that permeation through a 0.025cm thick foil was large relative to foils of gold and molybdenum at similar temperatures. However the surface rapidly deteriorated - hours - and the flux through the specimen dropped by orders of magnitude until it was comparable with those through gold under similar conditions of temperature and pressure. It proved impossible to make useful diffusion coefficient measurements. However, typical plots of observed phase/frequency data were shown in section 5.2.2 because they seemed to conform with $\phi_{H >> 1}$ behaviour, represented by equation 4.42, when c_5 is large.

Further study may be valuable; since the present experiment gave

data which if it had been reproducible may have been analysed; improvements in partial pressures might give sufficient experimental time to allow the necessary reproducibility.

6.5. Helium

Measurement of helium diffusion coefficients proved impossible. Several experiments using variations of injection method were performed, but on no occasion was a flux, induced by these methods, detected.

Detection sensitivity for these experiments was good, particularly since signal averaging was used, and net fluxes of about 10^{-10} torr litres s^{-1} or about $5x10^{9}$ molecules s^{-1} into the detection chamber could have been observed.

An approximate expectation value for the partial pressure modulation amplitude was derived in section 5.4.2, using favourable assumptions. This amplitude was found to be well inside the equipment detection limits. That such fluctuations were not observed was seen as due to the small diffusion coefficient of helium in the materials studied. This allows an upper limit of 10^{-9} cm^2 s^{-1} at temperatures below $\sim$ 900K to be assigned for the helium diffusion coefficient. This is in general agreement with the LeClaire and Lazarus theories which suggests that helium diffuses at about the rate expected for substitutional impurities.

6.6. General discussion of hydrogen and deuterium diffusivities in molybdenum, silver, and gold.

The experimental work reported in this thesis was designed to identify and if possible to quantify the parameters governing the permeation of hydrogen through a number of metal foils.

In the experiments with molybdenum and silver the characteristics of the phase/frequency plots identified these systems as being unperturbed by the processes at phase boundaries. Hence diffusion through these metals could be adequately described by a single parameter, the diffusion coefficient.

In contrast the phase/frequency plots for gold did not show the strong characteristics of classical permeation and it was supposed that processes at the phase boundaries of this metal strongly control permeation through it. The steady rate permeation studies also conform to this view. In gold it was found that three parameters were needed to represent the diffusion results, these were the diffusion coefficient and two functions of the surface rate constants, c_4 and c_5, specific to the input and exit surfaces respectively.

Although the phase/frequency plots for gold conform with the description $\phi_{H >> 1}$, equation 4.42, to a high level of consistency, there is not the same confidence in the diffusion coefficients quoted for gold as was for molybdenum and silver. This is because unlike $\phi_{Classical}$, given by equation 4.37, $\phi_{H >> 1}$ does not have strong characteristics. Also with three floating parameters, $\phi_{H >> 1}$ v $\nu^{\frac{1}{2}}$ plots are less stringently defined.

Such doubts would not exist if it had been possible to drive gold, through use of large input pressures and/or large mean discharge currents, to the classical limit. As discussed in section 5.3.2, the required input conditions are such that, certainly with the present equipment, experiments of this class are impossible with gold. However, it may be possible to drive metals which at input pressures greater than a few torr show classical behaviour, to show phase boundary process dependence by reducing input pressures until fluxes through the foil tend to the characterizing flux defined in section 4.4.

Using the measured hydrogen and deuterium diffusivities in the metals studied, comparison was made with current theory for diffusion.

Specifically the isotope ratios were analysed using Ebisuzaki's theory, equation 6.1, and Ebisuzaki parameters, ν_1 and ν_1', the vibrational frequencies of the normal and transition state modes in the harmonic approximation derived. For molybdenum and silver it was found $(\nu'_1/\nu_1) \sim 1.6$. This is close to the value found by Ebisuzaki et. al. in nickel, $(\nu'_1, \nu_1) \sim 1.7$. Are such values of this ratio reasonable ?.

Figure 6.9 sketches the normal and transition states under the assumption of harmonic potentials. The vibrational frequencies associated

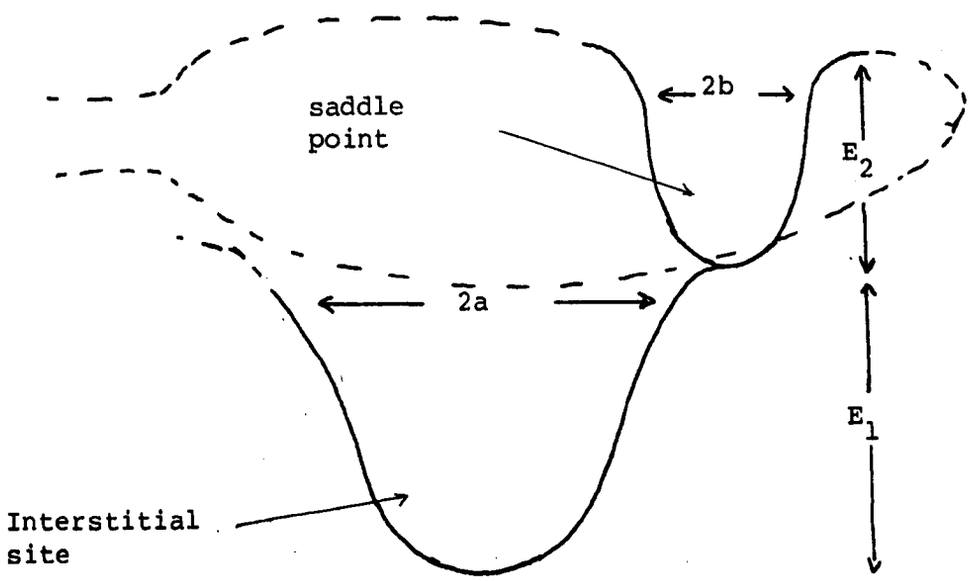

Fig. 6.9. Sketch of interstitial site and saddle point potential.

with the normal and transition states are then

$$\nu_1 \sim \alpha \frac{E_1^{\frac{1}{2}}}{a} \tag{6.2}$$

$$\nu_1' \sim \alpha \frac{E_2^{\frac{1}{2}}}{b} \tag{6.3}$$

where α is a constant of proportionality, 2a and 2b are the widths of the interstitial and transition state respectively. Therefore:

$$\left(\frac{E_2}{E_1}\right)^{\frac{1}{2}} \sim \left(\frac{b}{a}\right)\left(\frac{\nu_1'}{\nu_1}\right) \tag{6.4.}$$

Figure 6.10 illustrates equation 6.4 with plots of (E_2/E_1) versus (b/a) for several values of (ν_1'/ν_1). It is important to note that the range of (b/a) is limited and hence for a particular value of the ratio of the Ebisuzaki parameters a limit is set for (E_2/E_1). So the question posed above may be answered by determining the allowed range of (E_1+E_2), the total depth of the interstitial potential well, for $(\nu_1'/\nu_1) \sim 1.6$. The upper limit of this range should be order 1eV if it is to be acceptable.

For the sake of argument, since b < a, let

$$0.2 \lesssim (b/a) \lesssim 0.5$$

then for

$$(\nu_1'/\nu_1) \sim 1.6$$

$$0.1 \lesssim (E_1+E_2) \lesssim 0.5$$

Under these conditons, the upper limit of the total well depth for silver is ~ 0.6eV and for molybdenum is ~ 1.5eV. Such values seem acceptable, hence the present ratio of Ebisuzaki parameters is not unreasonable.

An interesting point, arising from the above discussion, is that E_2 can be so small that, for a given value of ν_1', the number of allowed harmonic transition state energy levels may be no more than one. If this were so, equation 6.1 would cease to be a good approximation for the isotopic ratio, hence perhaps greater care should be excercised when drawing conclusions from the Ebisuzaki theory.

6.7 Some Ideas

The following proposition of a model for the frequency of the basic diffusion jump process, Γ, is made with the hope that interest may be raised in models involving energy bands.

In a periodic potential it is found that particle states may be described by functions that extend over the entire lattice, Bloch functions.

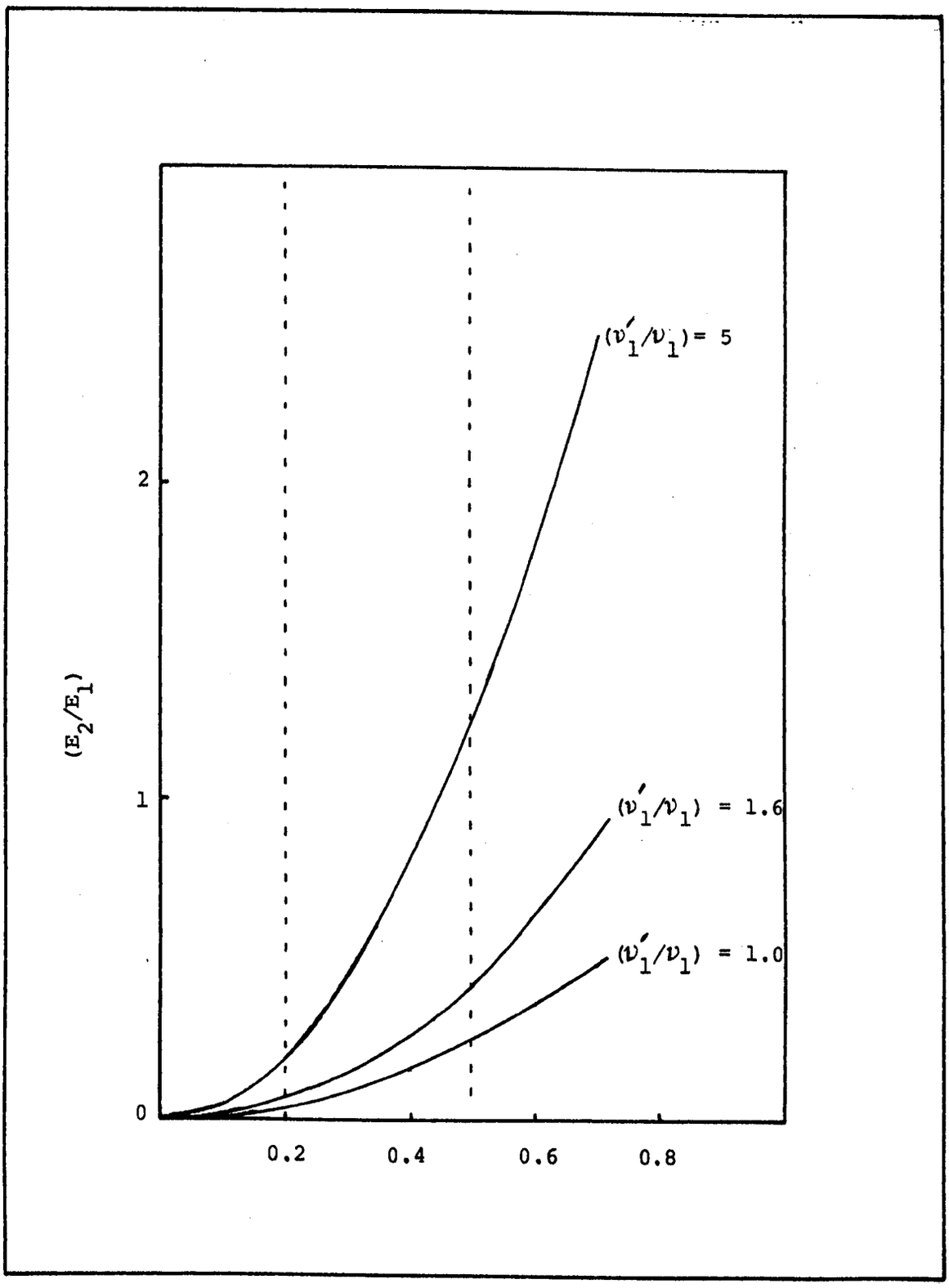

Fig. 6.10 (E_2/E_1) v (b/a). (See text)

The energies of these states are not as discrete levels, but form bands. In this band description, particles are associated with wavepackets which are the sum of Bloch functions. These wave packets generally develop with time in two ways; (a) they travel through the lattice with a group velocity given by

$$v = \hbar^{-1} \frac{dE}{dk} \qquad (6.5)$$

where E is the energy and k is a wavevector associated with the lattice; (b) the wavepacket may change shape, as the relative phases of the Bloch functions change.

It is supposed here that the basic jump process is from a localised, narrow, ground state band in the initial potential well to a transition state band and wavepacket localised over the initial well which develops with time, becoming delocalised and overlapping with the neighbouring well. The particle then decays from the delocalised transition state to the localised, ground state of the final well.

The development of the wavepacket is supposed to be a translational displacement and is sketched in Figure 6.11

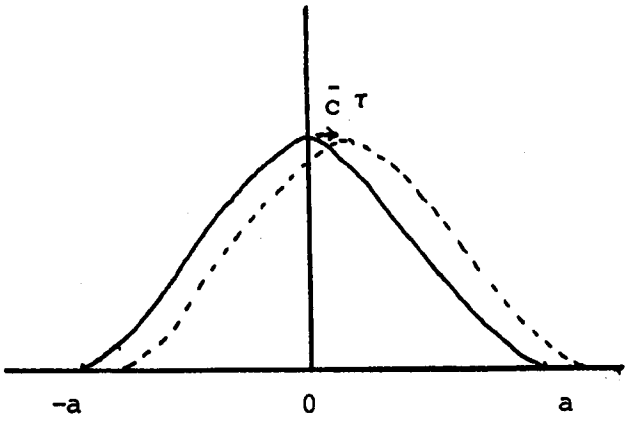

Fig. 6.11 Sketch of wavepacket.

The wavepacket will be represented by F(x), $\bar{c}$ is its group velocity and τ is the wavepackets mean lifetime before decaying via some interaction into a ground state.

The probability of transition from the wavepacket into the ground state of the final well is

$$p = 1 - \int_{-a}^{a} |F(x)|^2 \, dV$$

As an approximation, treat $|F(x)|^2$ as a cone. Then, with γ as some constant

$$p \sim \gamma \int_{a-\bar{c}\tau}^{a} r^2 (a-r)\, dr$$

$$p \sim \gamma \left[r^3 \left(\frac{a}{3} - \frac{r}{4} \right) \right]_{a-\bar{c}\tau}^{a}$$

$$p \sim \gamma \left[\frac{a^4}{12} - (a - \bar{c}\tau)^3 \left(\frac{a}{12} + \frac{\bar{c}\tau}{4} \right) \right]$$

if $\bar{c} \ll a$

$$p \sim \gamma \frac{a^3}{4} \bar{c}\tau$$

$$p \sim \frac{(a^3 \bar{c}\tau / 4)}{(a^4 / 6)} = 1.5 \frac{\bar{c}\tau}{a}$$

where $= (a^4 / 6)$

The jump frequency Γ is then $\sim p/T$ where T is the ground state lifetime and

$$T \sim \tau \exp (E/kT)$$

where E is the energy of the transition state above the ground state, Therefore:

$$\Gamma \sim 1.5 \frac{\bar{c}}{a} \exp (-E/kT)$$

Therefore the diffusion coefficient

$$D \sim \bar{c}\, a \exp (-E/kT) \qquad (6.6)$$

Equation 6.6 may be useful because the group velocity may be easier to derive, in terms of fundamental crystal parameters, than the interaction matrix elements.

Equation 6.6. defines the diffusion pre-exponential factor to be $\bar{c}a$, is this acceptable ? A simple order of magnitude calculation may help.

Suppose $E = \left(\frac{E_o}{k_o} \right) k$

where k_o is the maximum allowed lattice wavevector and is equal to (π/a) E_o is a constant parameter. Then

$$E_o = \frac{\pi \bar{c} \hbar}{a} \text{ Joules}$$

$$= \frac{\pi \bar{c} \hbar}{ae} \text{ eV}$$

$$E_o \sim 2 \times 10^{-5} \bar{c} \text{ eV}$$

From the magnitude of typical experimental pre-exponential factors, it is expected that $\bar{c} \sim 5 \times 10^5 \text{cm s}^{-1} = 5 \times 10^3 \text{ m s}^{-1}$, therefore $E_o \sim 0.1\text{eV}$. E_o is expected to be related to the potential well depth, hence a value of $\sim 0.1\text{eV}$ is reasonable. For any given periodic lattice the band shape will depend on many factors and $\bar{c}$ may vary widely, hence explaining the broad range of pre-exponential factors. More detailed calculations may even give isotopic ratios.

SUMMARY

Molybdenum was used mainly to confirm the experimental technique and to explore the possibility of surface hold up. It was found that the present permeation data for hydrogen and deuterium were in general line with the work of others. The diffusion coefficients were found to be some what high, relative to most others, but very close to a companion experiment using pressure modulation.

In the region of $p \sim 2$ torr, $650K \lesssim T \lesssim 950K$, the diffusion process assumes classical form. This was repeatedly verified and there was no evidence for trapping. However, there was evidence of specimen degradation after prolonged injection by the discharge method.

The isotopic ratio for diffusion was determined and found to be $(D_H/D_D) \sim 1.1$ and constant over the experimental range.

Silver diffusion coefficients with hydrogen and deuterium were determined. The observed data conformed with classical diffusion with no surface holdups, and diffusivities were about what was found elsewhere.

The isotopic ratio was found to be $(D_H/D_D) \sim 1.3$ and showed zero temperature variation over the experimental range.

With gold there was general agreement with others on permeabilities for both hydrogen and deuterium, but with an isotopic ratio marginally larger then reported in the single other study. Pressure behaviour was non-Sievert in character and there was evidence to suggest that the equilibrium hypothesis may not hold: suspicious of surface effects.

When the classical analysis was applied to the gold phase/frequency

data diffusion coefficients similar to those found elsewhere were found, but the data deviated systematically from the phase versus frequency relationship required by the model: deviation was clearly in excess of the noise level for the equipment.

Use of an alternative model incorporating surface rate constants gave preferred fit to the data. Diffusion coefficients were now larger than those reported elsewhere (factor of 30-200), but the activation energies were comparable with others. Also such coefficients were closer to the general range of pre-exponential factors, observed with other metals.

Due to difficulties no data are reported on helium in any of the metals used and hydrogen and deuterium in aluminium.

An interesting alternative to the current theories for the basic jump process was proposed, based on the band model. This simple example shows that such models may be compatible with observed data.

REFERENCES

1) J. Volkl and G. Alefeld, Diffusion in Solids,Recent developments. Eds A.S. Nowick, J.J. Burton. Academic Press, New York, 231 (1975).

2) Y. Adda, J. Phillibert, La Diffusion dans la Solid,Biblioteque des Sciences et Techniques Nucleaire.

3) W. Jost and A. Widman, Z. Phys Chem B, 29, 247 (1935)

4) J. Cermak and A. Kufudakis, Mem. Sci. Rev. Met., 63, 767, (1966)

5) R.M. Barrer, Trans. Faraday Soc., 38, 78, (1942)

6) W. Eichanauer, W. Loser and H. Witte, Z. Metallk., 56, 287, (1965)

7) L. Katz, M. Guinan and R.L. Borg, Phys. Rev. B4,330, (1971)

8) H. Steeb and H. Kronmuller, Phys. Status Solidi, A16, K175, (1973)

9) A.D. Le Claire and A.H. Rowe, A.E.R.E. (Harwell), M R 1417,(1957)

10) J.M. Tobin, Acta. Met., 5, 398, 1957; Ibid., 7, 704, (1959)

11) H.R. Glyde and K.I. Mayne, Phil. Mag., 919, (1965)

12) H.R. Glyde and K.I. Mayne, Phil. Mag., 997, (1965)

13) S. Glasstone, K.J. Laidler, H. Eyring, The Theory of Rate Processes, New York McGraw - Hill Book Co., (1941)

14) J.C. Fisher, J.H. Hollomon, JUNIOR MEMBER AIME and D. Turnbull, Met. Tech, TP 2344, (1948)

15) C. Wert and C. Zener, Phys. Rev., 76, 1169, (1949)

16) C.H. Vineyard, J. Phys. Chem. Solids, 3, 121 (1957)

17) A.D. Le Claire, Phil. Mag., 14, 1721, (1966)

18) Y. Ebisuzaki, W.J. Kass and M.O'Keefe, J. Chem. Phys., 46, No.4,1373,(1967)

19) J.A. Sussman, Ann.Phys., t.6. No.2, 135, (1971)

20) C.P.Flynn and A.M. Stoneham, Phys. Rev. B, 1, No.10, 3966, (1970)

21) J.H.Weiner, J. Chem. Phys., 69 (S), 2492, (1978)

22) D. Lazarus, Phys. Rev., 43, 973, (1954)

23) A.D. LeClaire, Phil. Mag., 7, 141,(1962)

24) L.W. Barr and A.D. LeClaire, Proceedings of the British Ceramic Society No.1, July, (1964)

25) R.M. Cotts, Ber. Bunsenges, Phys. Chem., 76, 760, (1972)

26) T. Springer, Springer tracts in Modern Physics, Vol.64, Springer-Verlag, Berlin and New York

27) J.L. Snoek, Physica, 8, 711, (1941)

28) R.E. Norberg, Phys. Rev., 86, 745, (1952)

29) D. Zamir and R.M. Cotts, Phys.Rev. A, 134,666, (1964)

30) H. Lutgeimeier, R.R. Arons and H.G. Bohn, J. Magn. Resonance, 8, 74, (1972)

31) A. Zeilinger and W.A. Pochman, J. Appl. Phys., 47, No.12, 5478 (1976)

32) H. Wipf, Thesis, Tech. Univ. Munchen Germany; Jul-Ber. Jul 876FF (1972)

33) D.G. Westlake, S.T. Ockers and D.W. Regan, J. of the-less-common metals, 49, 341, (1976)

34) J. Volk, Ber.Bunseger. Phys. Chem., 76, 797, (1972)

35) R.M. Barrer, Trans. Faraday Soc., 35, 628 (1939)

36) R. Wagner and R. Sizman, Z. Agnew. Phys. 18, 193, (1964)

37) N.J. Freeman, I.D. Latimer, Can. J. Phys., 46, 467, (1968)

38) H.T. Weaver, J. Appl. Phys., 42, No.6, 2356, (1971)

39) R.S. Barnes and D.J. Mazey , Proc. Roy. Soc. A., 47, 275, (1963)

40) C.E. Ellis, Acta Met., 11; 87, 1963

41) P.G. Shewmon, Trans. AIME, 206, 918, (1956)

42) K.M. Chui, Private Communication.

43) H. Verbeek, W. Eckstein and R.S. Bhattacharya, J. Appl. Phys. 81(3), 1783, (1980)

44) O. Kubaschewski and E.L. Evans, Metallurgical Thermochemistry, Butterworth-Springer (1951)

45) J. Crank, The Mathematics of Diffusion, 2nd Ed., Clarendon Press, Oxford.

46) C.J. Smithels and C.E. Ranseley, Proc. Roy. Soc., A150, 172, (1935)

47) J. Wang, Proc. Camb. Phil. Soc., 32, 657, (1936)

48) J.D. Fast, Phillips Techn. Rev., 6, 365, (1941)

49) J.D. Fast, Phillips Techn. Rev., 16, 341, (1955)

50) A.McNabb and P.K. Foster, Trans. Met. Soc. AIME, 227, 618 (1963)

51) D.L. Cummings, Private Communications.

52) C .K. Chung, Thesis, Open University, (1975)

53) M.L. Hill, J. Metals, 12, 725, (1960)

54) C.L. Huffine and J.M. Williams, Corrosion, 16, 740, (1960)

55) R. Fraunfelder, J. Chem. Phys., 48, 3955, (1968)

56) P.M.S. Jones, R. Gibson, J.A. Evans, A.W.R.E. Report No. 0-16/66 (1966)

57) R.L. Reuben, Thesis, Open University (1981)

58) J.W. Guthrie , L.C. Beavis, D.R. Begeal and W.G. Perkins, J.Nucl. Mater., 53, 313, (1974)

59) G.R. Caskey, M.R. Lowthan and R.G. Derrick, J. Nucl.Mater, 55, 279, (1975)

60) L.N. Ryabchikov, Ukr. Fiz.Zh., 9, 293, (1964)

61) A.P. Zakharov, A.E. Gorodetsky and V.M. Shaparov, Z. Phys. Chem., 117, 245, (1979)

62) W. Eichanauer, H. Kunzig, A. Pebler, Z. Metallk., 48, 373, (1958)

63) H. Katsuta, R.B. McLellan, Scripta METALLURGICA, 13, 65, (1979)

64) W. Eichanauer, D. Leibscher, Z. Naturforsch, 17a, 355, (1962)

65) V.A. Kurakin, A.A. Kurdyumov, V.N Lyasnikov, M.I. Patapov, Sov. Phys. Solid State, 21(4), 616, (1974)

66) H. Morrison, D.A. Blackburn, K.M. Chui, Private Comminication.